

**GEOLOGICA ULTRAIECTINA**

Mededelingen van de  
Faculteit Geowetenschappen  
Universiteit Utrecht

No.253

**Late Pliocene millennial to Milankovitch-scale  
climate variability: A case study of Marine Isotope  
Stages 101-95 in the Mediterranean and adjacent  
North Atlantic**

**Julia Becker**

ISBN: 90-5744-116-0

**Late Pliocene millennial to Milankovitch-scale  
climate variability: A case study of Marine Isotope  
Stages 101-95 in the Mediterranean and adjacent  
North Atlantic**

**Laat Pliocene klimaatvariabiliteit op millennia tot  
Milankovitch tijdschalen: Een onderzoek van Mariene  
Isotopen Stadia 101-95 in de Middellandse Zee en de  
aangrenzende Noordelijke Atlantische Oceaan**

(met een samenvatting in het Nederlands)

**Proefschrift**

ter verkrijging van de graad van doctor aan de Universiteit Utrecht  
op gezag van de Rector Magnificus, Prof. Dr. W.H. Gispen,  
ingevolge het besluit van het College voor Promoties  
in het openbaar te verdedigen op 14 november 2005  
des middags te 12:45 uur

door

**Julia Becker**

geboren op 14 november 1973 te München, Duitsland

Promotor:

Prof. Dr. J.E. Meulenkamp

Royal Netherlands Institute for Sea Research

Den Burg, Texel, The Netherlands

Co-promotoren:

Dr. F.J. Hilgen

Department of Earth Sciences

Utrecht University

Utrecht, The Netherlands

Dr. L.J. Lourens

Department of Earth Sciences

Utrecht University

Utrecht, The Netherlands

This research was carried out at the faculty of Geosciences, Universiteit Utrecht, Budapestlaan 4, 3584 CD Utrecht. [www.geo.uu.nl](http://www.geo.uu.nl). This research was carried out within the framework of the PIONEER programme of F.J. Hilgen, which is financially supported by the Netherlands Organization for Scientific Research (NWO).

Le greynour bien que nature  
Fist a lo hume en ce folz monde  
Fu le don dont pris faconde  
Prist en ly sens et mesure

E pourtant quant unz n'a cure  
Proassembler de sciences parfonde  
Tretout cilz du pris en fonde  
Metre ye n'ai en cuer ardure

Mes il est grant desparanche  
Quand hom pans' en sa fumea  
Plus estre qu'en apparanche

Onques d'avoir renomea  
En tres bons soit en speranche  
S'il no im prent assoufisanche

*Matteo Perusio* [1380-1410]

Ms: Mod. Est.  $\alpha$ 5,24

The highest good that Nature has given to man in his mad world was the gift of sense and of measurement through which he could acquire eloquence. And yet, when one is not concerned with using profound knowledge to reach a universal truth, then my heart is not moved. Surely, a man demeans himself when with his clouded vision he fancies his renown to be greater than it really is. He must never wish for the fame of the great when he has not yet attained perfection.



## Contents

|  |            |
|--|------------|
| <b>CHAPTER 1</b>   | <b>9</b>   |
| <i>Introduction and summary of investigation</i>   |            |
| <b>CHAPTER 2</b>   | <b>25</b>  |
| <i>Late Pliocene climate variability on Milankovitch to millennial time scales: A high-resolution study of MIS100 from the Mediterranean</i>   |            |
| Julia Becker, Lucas J. Lourens, Frederik J. Hilgen, Erwin van der Laan, Tanja J. Kouwenhoven and Gert-Jan Reichert, in press. <i>Palaeogeography, Palaeoclimatology, Palaeoecology</i> . |            |
| <b>CHAPTER 3</b>   | <b>51</b>  |
| <i>High-frequency climate linkages between the North Atlantic and the Mediterranean during Marine Oxygen Isotope Stage 100 (MIS100)</i>  |            |
| Becker, J., L.J. Lourens and M.E. Raymo, submitted to <i>Paleoceanography</i> .  |            |
| <b>CHAPTER 4</b>   | <b>69</b>  |
| <i>Redox conditions and dust deposition at San Nicola during MIS100: results from trace element and grain size analysis</i>  |            |
| <b>CHAPTER 5</b>   | <b>87</b>  |
| <i>Cycle geometry of MIS100-96 in relation to orbital forcing</i>  |            |
| in cooperation with L.J. Lourens, R. Bintanja and R.S.W. van de Wal  |            |
| <b>CHAPTER 6</b>   | <b>105</b> |
| <i>Evaluation of African aridity and North Atlantic Dansgaard-Oeschger cycles during Pliocene MIS101-95</i>  |            |
| <b>References</b>  | <b>134</b> |
| <b>Samenvatting</b>  | <b>149</b> |
| <b>Acknowledgements</b>  | <b>162</b> |
| <b>Curriculum Vitae</b>  | <b>164</b> |





# CHAPTER 1

## Introduction and summary of investigation

### 1.1. Milankovitch theory of ice-ages

The Milankovitch theory of the ice ages holds that astronomical perturbations in the Earth's orbit and axis are responsible for glaciations by influencing climate through changes in the seasonal and latitudinal distribution of incoming solar radiation; this theory is now generally accepted by the geological community. It was *Adh mar* [1842] who first suggested that ice ages might be astronomically controlled, only 5 years after *Agassiz* presented his Ice Age theory in [1838]. In [1864] *Croll* elaborated the initial theory and formulated the relationship between astronomically variables and ice ages. Using formulas of the French astronomer *Leverrier*, he calculated curves for past changes in eccentricity<sup>1</sup> and precession<sup>2</sup> and suggested that cold winters were critical for the initiation of an ice age. However, he also remarked that astronomical forcing is too small to directly control glacial cycles and suggested that an internal amplifying mechanism within the climate system is needed as positive feedback. Sixty ears after *Croll*, *K ppen and Wegener* [1924] presented an alternative ice age theory, based on solar irradiance curves calculated by the Serbian astronomer *Milankovitch*. In contrast to *Croll*, who assumed that winter insolation is critical for glaciation, they assumed that low summer insolation would initiate ice growth. In [1941] *Milankovitch* further elaborated this early work and calculated the incoming solar radiation on top of the atmosphere of different latitudes taking into account the changes in precession, obliquity<sup>3</sup> and eccentricity. He stated that summer insolation at 65 N triggered the ice ages and predicted that ice age cycles are dominated by the 41-kyr cyclicality.

With the advance of magnetostratigraphy, and radio- and stable isotope analysis in the 60's, acceptance of the Milankovitch theory was pushed forward. In addition, new coring techniques resulted in the recovery of long and continuous cores. The break-

---

<sup>1</sup> Eccentricity is a measure of the degree of elongation of the Earth's orbit and varies between nearly zero (circular orbit) and 0.06 (slightly elliptical) with main periods of 400,000 and around 100,000 years

<sup>2</sup> Axial precession is the slow movement of the rotation axis around a circular path with one revolution completed every 26,000 years. Due to the opposite movement of the eccentric orbit itself, the precession of the equinoxes also called climatic precession completes one full cycle in about 21,000 years. Climatic precession is modulated by eccentricity.

<sup>3</sup> Obliquity describes the angle between the Earth's axis of rotation and the orbital plane and varies between 22  and 25  with a main period of 41,000 years.

through in accepting the Milankovitch theory came from the finding of spectral peaks in ice volume proxy ( $\delta^{18}\text{O}$ ) records that matched exactly with the predicted Milankovitch frequencies, indicating a clear relationship between glacial-interglacial driven ice volume changes and the astronomical parameters [Hays *et al.*, 1976]. Comparison with simple ice sheet model indicated that there is a connection between ice volume and orbital obliquity and precession, thereby confirming that glacial-interglacial variations are driven by orbital forcing with fixed leads and lags [Imbrie and Imbrie 1980; Imbrie *et al.*, 1984]. This recognition led to the construction of an astronomically tuned timescale (SPECMAP) for the past  $\sim 800$  kyr, which has been used as a template for dating deep marine late Pleistocene oxygen isotope records ever since [Imbrie *et al.*, 1984].

In contrast to what was predicted by *Milankovitch*,  $\delta^{18}\text{O}$  records of the late Pleistocene proved to be dominated by a 100 kyr ice age cycle, suggesting a relation of global climate change with eccentricity. It is generally accepted that the amount of the global annual insolation perturbation associated with the (100 kyr) eccentricity cycle is insufficient to cause a climate change on ice-age magnitude and, hence, that it is more likely that the strong 100-kyr eccentricity cycle observed in the  $\delta^{18}\text{O}$  spectrum arises from a nonlinear transfer of power from the precession band [Imbrie *et al.*, 1984; Hagelberg *et al.*, 1991]. Alternative models propose that the glacial-interglacial fluctuations are a consequence of nonlinear internal interactions in a highly complex system [Saltzman and Sutera 1984] and that ice volume fluctuations are modulated rather than driven by orbital variations. Finally, it has been proposed that the 100-kyr cycle is related to changes in orbital inclination rather than to changes in eccentricity [Muller and MacDonald 1995]. Evidently, the quasi periodic fluctuations within the various components of the climate system such as variations in  $\text{CO}_2$ , ocean circulation, surface and deep water temperature are phase-locked to insolation changes due to the 100-kyr cycle.

In contrast, climate records of the late Pliocene and early Pleistocene are dominated by the obliquity cycle and it is generally accepted that glacial-interglacial cycles during the past 1–3 Ma are related to orbital obliquity [Shackleton *et al.*, 1984; Ruddiman *et al.*, 1986; Raymo *et al.*, 1989] in agreement with *Milankovitch*'s predictions. However, it should be realised that the insolation curves of *Milankovitch* were calculated for the caloric half-year; this strengthens the obliquity signal relative to the same signal in peak summer (21 June – June/July) insolation curves [Berger *et al.*, 1999; Raymo and Nisancioglu 2003].

## 1.2. Mediterranean sapropels

Although the Milankovitch theory is widely used to explain ice ages and associated climate changes at mid- to high-latitudes, it was shown that perturbations in the Earth orbit and rotational axis also exert a strong effect on low-latitude climate. However,

low-latitude insolation is dominated by precession in contrast to the obliquity-dominated insolation received at high-latitudes. For instance, low-latitude climate systems such as the monsoon are controlled by the seasonal distribution of incoming insolation received at low-latitudes, especially during summer.

A classical example of precession-dominated climate variability is the Mediterranean sapropel record [Hilgen 1991]. The regular and cyclic occurrence of sapropels (organic carbon rich intervals) has been associated with changes in river-runoff and circum-Mediterranean humidity [Rohling and Hilgen 1991], linked to intensified African monsoon circulation at times of minimum precession [Rossignol-Strick 1983; 1985]. Microfossil assemblages, pollen and stable isotope data have indicated that the principal climate variability in the precession band is related to changes in warm-wet and cold-dry conditions [Cita *et al.*, 1977; Vergnaud-Grazzini *et al.*, 1977; Rossignol-Strick 1983; 1997; Kallel *et al.*, 2000]. Still, the precise mechanism behind sapropel formation in the Mediterranean is not fully understood. An ongoing point of discussion is whether the high  $C_{org}$  concentrations observed in sapropels are primarily caused by enhanced preservation of organic matter during anoxic bottom water conditions or by increased surface water productivity and subsequent export of organic material to the deep sea. Clearly, sapropel formation is the result from the interplay of several processes of varying importance.

The occurrence of sapropels is related to periods of intensified monsoonal circulation associated with large precessional amplitudes. Since precession is modulated by orbital eccentricity, sapropels occur in clusters associated with eccentricity maxima. Furthermore, alterations of thinner and thicker sapropels within a sapropel cluster indicate additional modulation by orbital obliquity [Lourens *et al.*, 1996]. This modulation is still not fully understood but preliminary modelling studies indicate that obliquity might influence or modulate [Tuenter *pers. comm.*] the African monsoon system and thus (indirectly) influence the runoff into the Mediterranean.

Next to the precession-related occurrence of sapropels, obliquity-related variability in sea surface temperatures (SST) and ice volume is evidenced in planktonic foraminiferal assemblages and  $\delta^{18}O$  throughout the past 1-3 Ma. These variations can be correlated to changes in ice volume and temperature known from North Atlantic records [Zachariasse *et al.*, 1990; Lourens *et al.*, 1992], implying a close relationship between Mediterranean and North Atlantic climate on a glacial-interglacial timescale throughout the late Pliocene and early Pleistocene. Thus, the Mediterranean climate record reveals variations that can be attributed to two different climate systems, namely the high-latitude North Atlantic and the low-latitude monsoonal system. The different spectral characteristics of the records further indicate that these climate systems were at least partially decoupled from one another.

### 1.3. Phase lags

It is generally assumed that sapropels lag the precession parameter by 3 kyr. This lag is based on the age difference between the AMS  $^{14}\text{C}$ -dated midpoint of the youngest Holocene sapropel, S1 ( $\sim 8.5$  kyr), and the correlative summer insolation maximum at 11.5 kyr *Lourens et al.* [1996] suggested that this lag could be related to a  $\sim 3$  kyr time lag of maximum summer temperature ( $T_{\text{max}}$ ) in northern Africa with respect to the precession parameter, as indicated by the outcome of an Energy Balance Model [*Short and Mengel* 1986]. More recent modelling experiments revealed that  $T_{\text{max}}$  at low-latitudes ( $15^{\circ}\text{N}$ ) lags indeed the precession parameter, but that no time lag was observed between the African-Indian monsoon annual precipitation and the precession parameter [*Tuenter et al.*, 2003]. This implies that either sapropel formation in the Mediterranean is not (only) linked to changes in African-Indian monsoon precipitation or that the time lag estimate for the S1 is an exception, being influenced by the deglaciation and Younger Dryas.

By adopting an in phase relationship between circum Mediterranean humidity and insolation *Lourens et al.* [2001] showed that the obliquity-related time lag for the Mediterranean humidity proxy Ti/Al is in the same order of that for precession, i.e.  $150 \pm 300$  years. This observation is confirmed by the modelling work of *Tuenter et al.* [2005], who observed an in phase relationship between the annual precipitation in the African-Indian monsoon and the obliquity parameter. These outcomes differ significantly from the results of *Clemens et al.* [1996], who observed phase lags between the Asian monsoon and the precession and obliquity parameters of 6 kyr and 13.4 kyr, respectively, during the late Pleistocene. These phase relations are very different to those observed from the ice volume records [*Imbrie and Imbrie* 1980], suggesting that parts of the low-latitude climate system are decoupled from the high latitude glacial history. Finally, they suggested that these phase relations are not constant but varied over time in response to the global distribution of the polar ice cap(s).

### 1.4. Sub-Milankovitch variations

The recovery of the long ice cores from the Greenland ice sheet indicated that the Earth's climate and system was extremely unstable throughout the past 150 kyr undergoing rapid changes in the order of a few thousand years [*Dansgaard et al.*, 1984]. Distinct oscillations in air temperature above Greenland, termed Dansgaard-Oeschger (D-O) cycles, culminated in large-scale ice rafting events known as Heinrich (H) events [*Heinrich* 1988; *Bond* 1992; *Broecker* 1992; *Bond et al.*, 1993; *Dansgaard et al.*, 1993; *Bond et al.*, 1999]. These oscillations that are associated with a major reorganisation of North Atlantic SST and the global thermohaline circulation are recorded in sedimentary records throughout the North Atlantic and the leading hypothesis links the cold phases of the D-O cycles and H events to a collapse of the ice sheets, resulting in the injection of large volumes of meltwater to source regions of North Atlantic Deep Water

(NADW) formation. Subsequently, lowered surface water salinities lead to a reduction of the deep convection and hence a slowdown of the global thermohaline circulation (THC) [Broecker 1997].

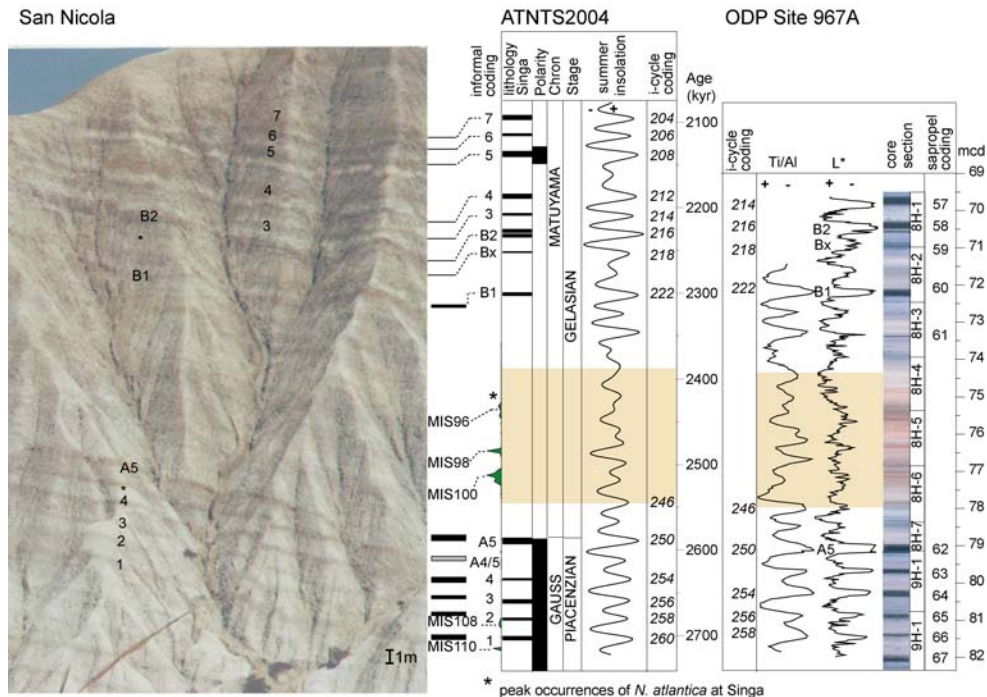
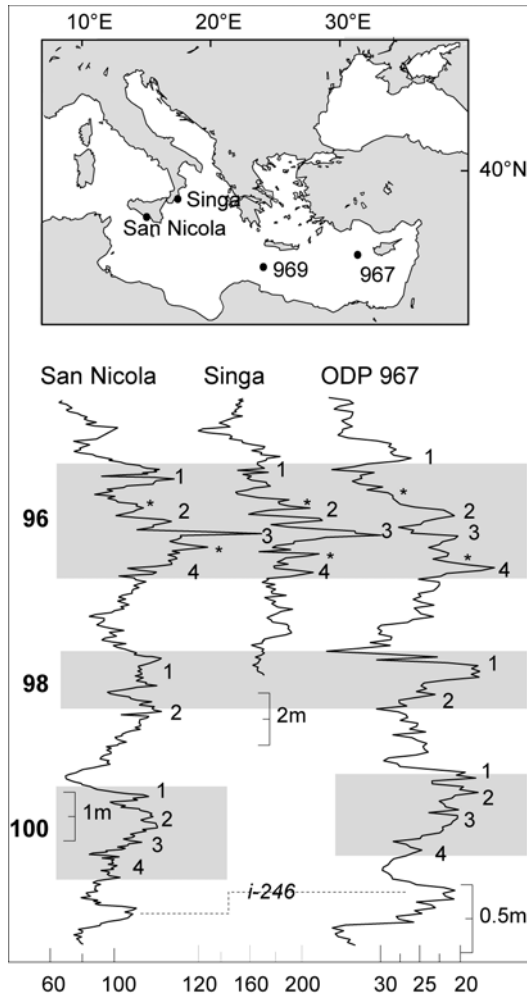


Figure 1.0: Lithology of Monte San Nicola section (SN) in comparison with the ATNTS2004 and lithology of ODP Site 967. For a detailed description of the section see *Rio et al.* [1994]. Individual sapropels of sapropel clusters A and B [coding after *Verhallen 1987; Zijderveld et al., 1991*] are labelled in the photograph of SN. Thick black and grey bars at the right hand side of the photograph indicate stratigraphic positions (scale bar lower right corner) of sapropels based on field observations, while the thin bars indicate positions of sapropels as assumed from the photograph. Stipple lines indicate correlation to the lithology of the Monte de Singa section that was incorporated in the ATNTS2004 [*Lourens et al., 2004*]. Additionally, marine isotope stages (MIS) 110, 108 and 100-96 are indicated in the lithology of SN and by peak occurrences of *Neogloboquadrina atlantica* (green shaded) at Singa [*Lourens et al., 1992*]. The ATNTS2004 shows the sapropel occurrences, polarity, chrons and stages in relation to the  $La04_{(1,1)}$  65°N summer insolation curve. Insolation maxima correlating to sapropels are labelled according to the i-cycle coding and ages (kyr) are indicated on the right axis [*Lourens et al., 1996*]. The yellow shaded area indicates the interval of MIS101-95 at Singa and Site 967, respectively. Ti/Al, colour reflectance and lithology of ODP Leg 160 Site 967 (composite) are plotted versus meter composite depth (mcd), after *Sakamoto et al.* [1998]. I-cycle codes are indicated on the left and sapropel codes of *Kroon et al.* [1998] on the right. Sapropels A5, B1, Bx and B2 are indicated in addition.



**Figure 1.2: Upper part: Location map of the Mediterranean sections. Lower part: Magnetic susceptibility (SI) of San Nicola and Singa (preliminary data) and colour reflectance ( $L^*$ ) of ODP Site 967 versus depth (see scale bars). Shaded intervals mark MIS100, 98 and 96 and labels indicate dark intervals during glacials. Italic label indicates the ghost sapropel at i-246.**

However, climate fluctuations associated with the D-O cycles and H events are not restricted to the North Atlantic region but have been found in climate archives all over the world [Leuschner and Sirocko 2000; Voelker *et al.*, 2002]. The forcing mechanism behind the high-frequency climate variations is uncertain and the debate generally distinguishes between internal forcing mechanisms, such as ice sheet oscillations forced by the interaction of large ice sheets with the underlying bedrock [MacAyeal 1993; Alley and MacAyeal 1994], and external forcing mechanisms, such as variations in solar output [Van Geel *et al.*, 1999; Perry and Hsu 2000; Bond *et al.*, 2001], periodic tidal motions of

the Earth and Moon [Keeling and Whorf 2000] amplified in the presence of large ice sheets, non-linear response as harmonics or combination tones of the main orbital cycles [Pestiaux *et al.*, 1988; Hagelberg *et al.*, 1994; Ortiz *et al.*, 1999], or simply the twice-yearly overhead passage of the sun across the equator [Short and Mengel 1986; Short *et al.*, 1991]. Especially the latter two forcing mechanism suggests that millennial-scale climate variability could be driven by low-latitude rather than by high-latitude climate; the processes involved include strong atmosphere-ocean feedbacks, such as changes in the equatorial wind system equivalent to long-term changes in El Niño - Southern Oscillation (ENSO), changes in the intensity of the Inter Tropical Convergence Zone (ITCZ) or monsoon variability [Stott *et al.*, 2002].

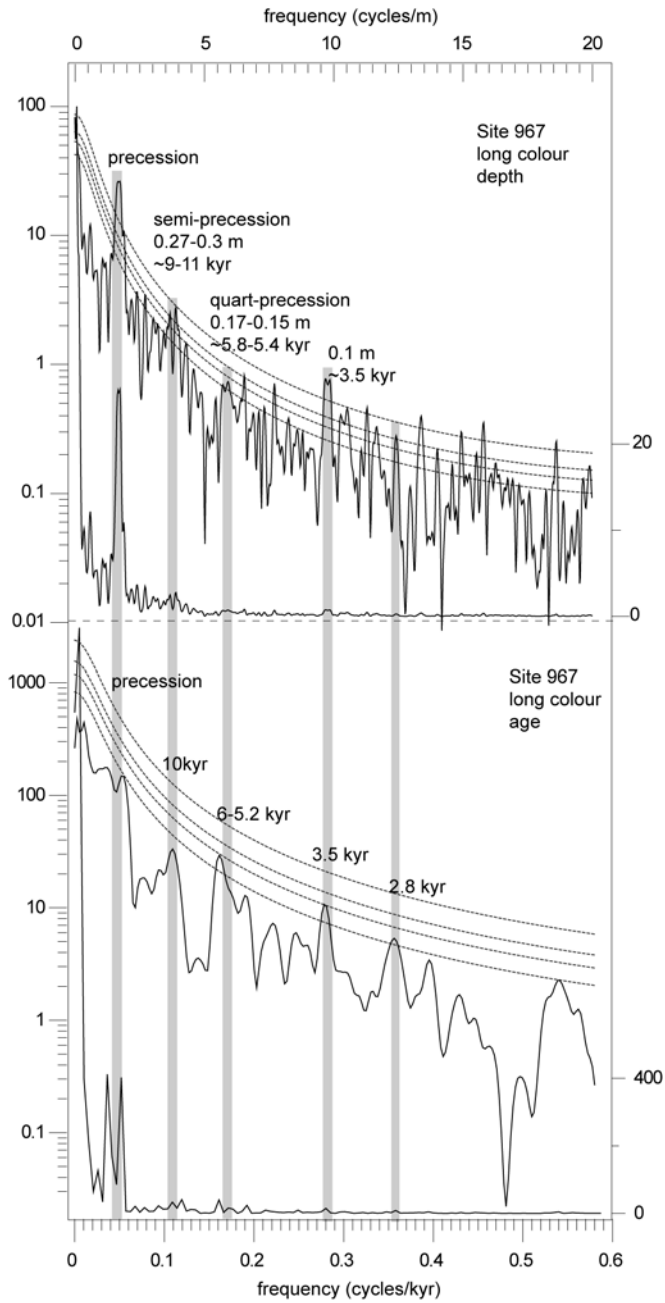


Figure 1.3: Frequency analysis of ODP Site 967 colour reflectance a) in the depth (70-83 mcd) and b) in the time (2.2-2.7 Ma) domain. Shaded intervals/labels mark important frequencies/periods and stipple lines indicate 80%, 90%, 95% and 99% significance levels.

## The Plio-Pleistocene climate record

Most of these studies concentrated on the time interval in which ice-age cycles were dominated by the 100 kyr pacing, and then in particular on the last 150,000 years. Since the origin of these 100-kyr ice-age cycles is still hotly debated, it is probably more straightforward to study the relationship between millennial-scale climate variability and primary Milankovitch forcing during the obliquity-controlled ice ages of the late Pliocene or early Pleistocene. The presence of D-O and H-like fluctuations at times without major Northern Hemisphere ice sheets during the smaller obliquity-dominated glacial cycles of the late Pliocene - middle Pleistocene [Raymo *et al.*, 1998; McIntyre *et al.*, 2001], or climate fluctuations with similar spacing as D-O and H-oscillations at

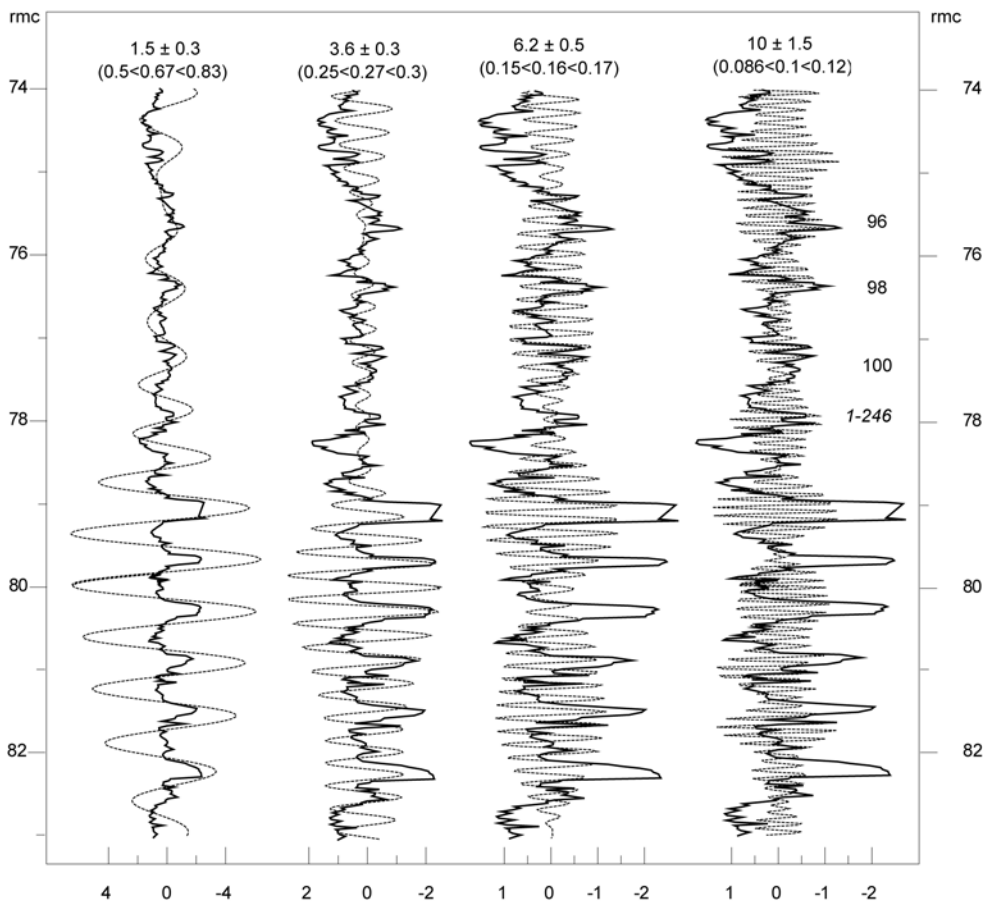


Figure 1.4: Normalised colour reflectance ( $L^*$ ) data of Site 967 with superimposed filter (stippled line) versus depth. Numbers indicate central frequency and bandwidth (1/m) and corresponding periodicity (kyr; in brackets) of the applied filter.



times before 2.7 Ma [Ortiz *et al.*, 1999; Kleiven *et al.*, 2002; Steenbrink *et al.*, 2003] indicate that such high-frequency climate fluctuations are consistently present in Earth's climate history. Yet, interpretation of these records is not always straightforward, either because of the poor stratigraphic control or the lack of detailed correlations with the open ocean record.

Late Pliocene to early Pleistocene Mediterranean successions are well suited to study millennial-scale climate variations since they contain both obliquity-controlled glacial-interglacial cycles and precession-related sapropels; the latter allow astronomical tuning, thus providing an excellent age control. Furthermore, variations on a D-O and H-scale are observed in the glacial-interglacial cycles of the central Mediterranean marine land-based sections (field observations) and in eastern Mediterranean ODP Leg 160 records throughout the past 2-3 Ma [Shipboard data Sakamoto *et al.*, 1998] (Figure 1.1). Fast variations in the sedimentary properties<sup>4</sup> can be correlated basin-wide, suggesting a common (climate) mechanism operating on Milankovitch to sub-Milankovitch timescales (Figure 1.2). Preliminary spectral analysis<sup>5</sup> of the long Site 967 colour record (69.64-89.73 rncd; Shipboard data) indicates cyclic colour changes with wavelengths of ~60 cm, 27-30 cm, 17-15 cm and ~10 cm, being significant above the 90% level (Figure 1.3a). Clearly, the variation at 60 cm is related to the occurrence of sapropels at Site 967 (Figure 1.1) and, hence, corresponds to the precession frequency. Subsequently, frequencies in the depth domain translate into periodicities in the time domain at semi-precession (30 cm), quart-precession (15 cm) and some periodicity ~3.5 kyr (10 cm). Filter outputs<sup>6</sup> of these frequencies generally show larger amplitudes in sapropel intervals (Figure 1.4). Variations at a semi-precession period are not very clear in these intervals and might present an artefact due to small colour variations in between sapropels or shoulders on top of sapropels. Variations with wavelengths of 15cm (corresponding to the quart precession) and 10 cm are present in the entire record. These 10 and 15 cm cycles make up most of the sub-Milankovitch scale colour changes observed in the glacials. In sapropel intervals, two 15 cm or three 10 cm cycles fit into a single sapropel. Frequency analysis in the time domain of the Site 967 colour variations [age model of Lourens *et al.*, 2001], confirms that changes in sediment colour occur with periods of 21 kyr, (10 kyr), 6-5 kyr and 3.5 kyr above the 80% confidence limit (Figure 1.3b).

Preliminary frequency analysis on the magnetic susceptibility record of San Nicola indicates concentration of variance with wavelengths of 357, 175, 102, 45, 30 and 26

<sup>4</sup> ODP Site 967 shipboard colour reflectance data and preliminary magnetic susceptibility data of SN and Singa. See *Chapter 6* for a more detailed description of methods and data.

<sup>5</sup> Frequency analysis is carried out using the REDFIT computational program of Schulz and Mudelsee [2002].

<sup>6</sup> Filtering was carried out using a Gaussian filter with central frequency provided by Paillard *et al.*, [1996].

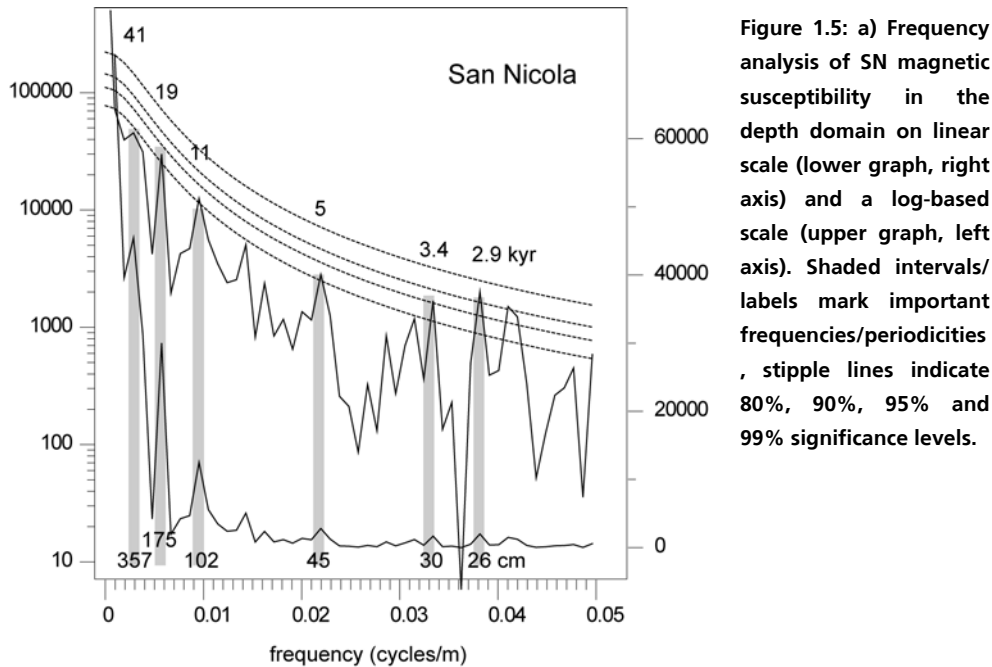


Figure 1.5: a) Frequency analysis of SN magnetic susceptibility in the depth domain on linear scale (lower graph, right axis) and a log-based scale (upper graph, left axis). Shaded intervals/labels mark important frequencies/periodicities, stipple lines indicate 80%, 90%, 95% and 99% significance levels.

cm above the 80% significance level (Figure 1.5). Filtering of the low frequency signal centred at 0.0028 cycles/cm (i.e. with a period of 357 cm) indicates that this frequency corresponds to the obliquity cycle (Figure 1.6). Subsequently, the observed variations in the depth domain translate into periodicities in the time domain of 41, 19, 11, 5, 3.4 and 2.9 kyr, with wavelengths around 30 cm ( $\sim 3$  kyr) corresponding to the smallest-scale (low amplitude) changes in the magnetic susceptibility record of San Nicola.

### 1.5. Marine oxygen isotope stages 101-95

Visual inspection of Monte San Nicola (SN) and Site 967 indicates that the interval between the A and B sapropel clusters (i.e.  $\sim 2.5$  Ma) is perfectly suitable for high-resolution studies of climate variations at Milankovitch to sub-Milankovitch time scales (Figure 1.1). Precession amplitude is low in this time interval due to a minimum in the 400-kyr eccentricity and, consequently, sediments in the central and eastern Mediterranean reflect obliquity-related glacial-interglacial variations rather than precession cycles. Earlier studies indicated that these dark-light alternations on a metre scale in-between the A<sub>5</sub> sapropel (base Gelasian) and the B sapropel cluster reflect glacial cycles MIS<sub>100</sub>, MIS<sub>98</sub> and MIS<sub>96</sub> [Zachariasse *et al.*, 1990], three of the most prominent glacial cycles that occurred shortly after the onset of major Northern Hemisphere glaciations [Ruddiman *et al.*, 1986; Raymo *et al.*, 1989]. Within the dark glacial stages, light-coloured centimetre-thick bands are visible indicating variability at sub-orbital scale superimposed on the obliquity related variation. Evidence for

occasional massive discharge of icebergs during these first full glacial cycles with a similar spacing as Mediterranean colour reflectance variations comes from the colour variations in the core photographs of North Atlantic DSDP sites (Figure 1.7) and ice rafted debris (IRD) records [Raymo *et al.*, 1992; Carter and Raymo 1999]. Rapid changes in the size of the continental ice-sheets at that time are confirmed by major shifts in benthic foraminiferal oxygen isotope records [Raymo *et al.*, 1989; Raymo *et al.*, 1992].

Additionally, the colour reflectance data of ODP Site 967 indicates further, that MIS100, 98 and 96 are not equally thick but show an alternating thick, thin, thick pattern. This alternation points towards a modulation of the obliquity-related glacial

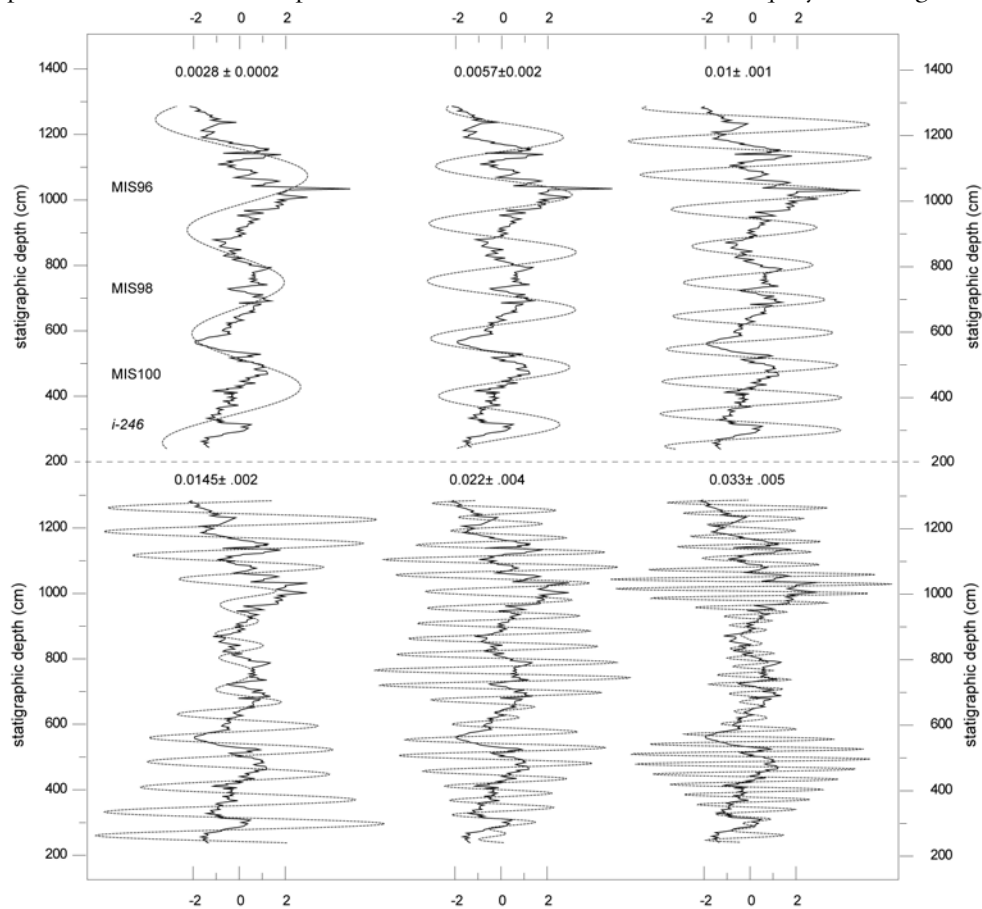
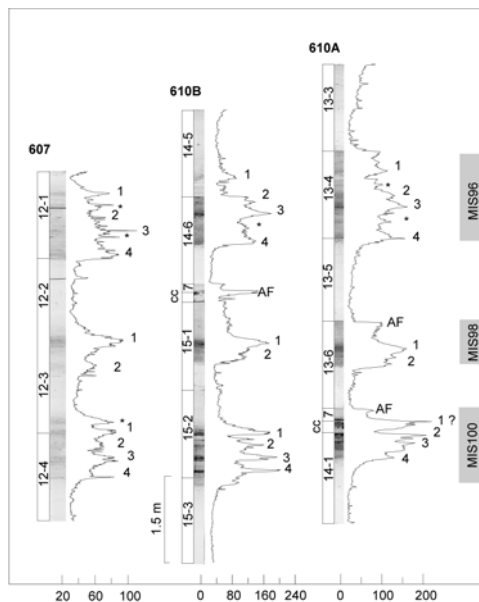


Figure 1.6: Normalised magnetic susceptibility data of San Nicola with superimposed filter (stippled line) versus depth. All data are plotted on the same scales. Numbers indicate central frequency and bandwidth (1/m) and corresponding periodicity (kyr; in brackets) of the applied filter.

signature, possibly by the (400-kyr) eccentricity signal. Additionally, sub-Milankovitch variability is more clearly observed in the thick stages MIS100 and MIS96.

## 1.6. Summary of investigations

The selected time interval and sections should shed new light on the following fundamental research questions: Are sub-Milankovitch frequencies present in the late Pliocene with frequencies similar to those observed in the late Pleistocene and, if so, is the climate mechanism comparable (*Chapter 2*)? What is the relationship of these signals with high latitude and low latitude climate (*Chapters 3 and 4*)? Are the phase relations of the different climate components with respect to the primary forcing frequencies



**Figure 1.7:** Core photographs and greyscale measurements of DSDP Leg 94 Site 607, 610B and 610A. Core sections are indicated alongside core photographs and labelled (vertical labels: core-section; CC: core catcher). The length of the individual core sections is 150 cm (see scale bar Site 610B). Horizontal labels on the greyscale graphs indicate dark intervals during glacials. AF: artefact related to cracks (dark) or bad illumination. Positions of MIS100-96 are indicated on the right (grey-shaded).

(obliquity and precession) constant within the studied interval and are they comparable with those of the Pleistocene (*Chapter 5*)? What is the role of sub-Milankovitch variability on the time lags of climate change on Milankovitch scales? And, finally, is it possible to couple the observed sub-Milankovitch variations with primary Milankovitch frequencies (*Chapter 6*)?

To answer these questions, the interval of MIS101-99 was studied at high resolution (~400 years) in the marine land-based section of Monte San Nicola (Sicily/Italy) and ODP Leg 160 Site 967 by means of foraminiferal assemblages, stable isotopes (ice volume) and  $\text{CaCO}_3$ . This study was carried out to get first insight into Mediterranean climate variability operating on a Milankovitch to sub-Milankovitch time scale in the late Pliocene (*Chapter 2*). Obliquity-controlled glacial variability is clearly reflected in the oxygen isotope records of planktonic and benthic foraminifera, which depict a saw-

tooth asymmetry with superimposed stadial-interstadial variability in MIS100: in total two stadials (100.3 and 100.5) and three interstadials (100.2, 100.4 and 100.6) are recognised. Both  $\delta^{18}\text{O}$  and SST lag orbital obliquity by  $\sim 6$  kyr. Sea surface temperature (SST) estimates derived from changes in planktonic foraminiferal assemblages also indicate cooling cycles with saw-tooth asymmetry, confirming stadial-interstadial type of climate variability similar in duration and nature as the open ocean Bond-cycles of the late Pleistocene. Furthermore, the abundance pattern of *Neogloboquadrina atlantica*, a cold water planktonic foraminifer, indicates episodes of low SST with an even shorter duration (1.5–3 kyr) during MIS100. Cold episodes are associated with high abundances of the benthic foraminifer *Trifarina angulosa* indicating that these episodes were characterised by increased deep ventilation caused by intensive mixing and deep convection. This scenario is analogous with observations in the western Mediterranean during the late Pleistocene [Cacho *et al.*, 1999; 2001] and a similar mechanism has been proposed: Low SST associated with increased deep water formation during stadials are related to a) a direct influence of cold Atlantic surface waters entering the Mediterranean, and b) a more indirect connection with the Atlantic system, which probably extended further into the Mediterranean due to weakened monsoonal circulation at times of minimum (400-kyr) eccentricity. Discrepant conditions are found during cycle i-244, when a low salinity surface layer associated with a deep chlorophyll maximum (DCM) points to the influence of precession-related climate variability.

The absence of high-frequency variations in the  $\delta^{18}\text{O}$  of Site 967 suggests that the eastern part of the Mediterranean was either decoupled from or not sensitive to North Atlantic climate forcing. However, colour reflectance records show similar millennial-scale variability in the eastern and the central Mediterranean. Comparison of these variations with the Ti/Al (a proxy for circum-Mediterranean humidity/aridity) record of ODP Site 969 [data Wehausen 1999] indicates a relationship between sedimentary properties (colour reflection,  $\text{CaCO}_3$ ), African dust deposition (Ti/Al) and cold intervals ( $\delta^{18}\text{O}$ ), suggesting a linkage between high- and low-latitude climate. The proxy data of the Mediterranean indicate that high-frequency climate change is highly complex due to the interaction of climate variations on different timescales.

The relationship between high-frequency climate changes observed in the Mediterranean during MIS101–95 and high latitude climate variability are investigated in **Chapter 3**. This is done by comparing the Mediterranean  $\delta^{18}\text{O}$  and *N. atlantica* records with high resolution  $\delta^{18}\text{O}$ ,  $\delta^{13}\text{C}$ , *N. atlantica* and ice rafted debris (IRD) records from Atlantic DSDP Leg 94 Site 607 and ODP Leg 162 Site 981. For this purpose, the highly accurate timescale of Site 967 is exported to the Atlantic using the benthic oxygen isotope record for correlation. The comparison reveals that millennial-scale cooling cycles in the Mediterranean are also found in the Atlantic, where they are

accompanied by episodes of intensive ice rafting. Depleted  $\delta^{13}\text{C}$  during IRD episodes indicates a coupling of changes in the global thermohaline circulation with North Atlantic ice rafting history, as observed during late Pleistocene HE and D-O events.

Again, an exception occurs during MIS100.3 (i-244) when sea surface water warming at Site 607 evidenced by the presence of *Globorotalia menardii*, a sub-tropical planktonic foraminifera, is accompanied by a restart in deep water circulation. It remains unclear whether the associated depletion in benthic  $\delta^{18}\text{O}$  indicates a warming of the deeper water as well. In the studied time interval, two additional influxes of *G. menardii* are closely related to precession minima as well, pointing to the interference of precession-related (low?) climate variability and obliquity-controlled glacial-interglacial cycles. Nonetheless, the results unambiguously demonstrate that the Bond cycles and associated Heinrich events are an intrinsic part of the climate system throughout the late Pliocene and Pleistocene notwithstanding the transition from dominant 41-kyr to 100-kyr controlled glacial cycles.

The role of precession-related climate variability in the Mediterranean and the possible relationship between a low latitude (dust) climate component and high latitude climate change during MIS100 is further evaluated in *Chapter 4*. For this purpose, bulk sediment geochemical and grain size data are produced with the same temporal resolution as the SST and  $\delta^{18}\text{O}$  records.

The chemical data indicate that environmental conditions during MIS100 were too weak for sapropel formation, which is in agreement with the reduced precession amplitude at that time as a consequence of minimum eccentricity. However, the development of a DCM during i-244 as proposed in *Chapter 2* is to be expected. The chemical data further indicates that sediments at San Nicola present a two component mixing system with biogenic carbonates and aluminosilicates as end members. The relative contribution of these two components changes predominantly at glacial-interglacial (obliquity) scale. Superimposed on the glacial-interglacial variability are precession-related variations in dust deposition and basin-wide short-term (1.5-4.5 kyr) variations in dust and  $\text{CaCO}_3$ , which are probably related to episodes of enhanced dust delivery from the African continent amplified during maximum precession and minimum obliquity. These dust episodes in the Mediterranean are time equivalent to north Atlantic IRD events, suggesting a relationship between low-latitude dust variability and high-latitude ice rafting during MIS100.

In *Chapter 5* phase relations between benthic  $\delta^{18}\text{O}$  and obliquity are separately investigated for the glacial stages MIS100, MIS98 and MIS96. For this purpose, the  $\delta^{18}\text{O}_{\text{benthos}}$  of Site 967 was extended throughout MIS95 and subsequently decomposed into an ice volume and a Northern Hemisphere annual air temperature component by using the coupled model of Northern Hemisphere ice sheets and ocean temperatures

developed by *Bintanja et al.* [2005]. This model allows to accurately extract the ice volume and temperature component from the  $\delta^{18}\text{O}$  at a given time interval. Advantage of using Site 967 is that its timescale is independent of glacial-interglacial variability; the age model has been developed by correlating the Ti/Al record to the  $\text{LaO}_{4(i,1)}$  summer insolation time series at  $65^\circ\text{N}$  assuming an in phase relationship [*Lourens et al.*, 2001].

The modelling results show global sea level changes in the order of 60-70 m during MIS101-95, indicating that the deep water temperature component has been underestimated in earlier studies of sea level estimates for the late Pliocene. During glacials, Northern Hemisphere annual air temperatures are reduced by  $\sim 12^\circ\text{C}$  as compared to interglacials showing superimposed (stadial-interstadial) variations of up to  $4-6^\circ\text{C}$  (MIS96). Spectral analysis of the  $\delta^{18}\text{O}$  and its derivatives global ice volume and Northern Hemisphere annual air temperature reveals strong peaks at  $\sim 80$ , 41 and 28 kyr and, remarkably, no variance in the precession band. Filtered 41-kyr components of the different proxies show a 5-8 kyr lag with respect to obliquity. However, the time lag increases during MIS100 and MIS96 and decreases during MIS98 by  $\sim 5$  kyr, respectively, if the 80-kyr and 28-kyr components are included in the reconstructed signals. Evidence for nonlinear interactions between obliquity and eccentricity to explain the 80-kyr and 28-kyr components is ambiguous. Instead, the 80 kyr (and 28 kyr) is probably caused by the nonlinear behaviour of ice sheets to obliquity forcing by internal dynamics. In particular the existence of a significant large ice cap during MIS99 may largely explain the occurrence of these frequencies as sidebands.

In *Chapter 6* spectral analysis is applied to the different records (SST and ice volume and African dust) of Mediterranean climate. Oxygen isotope and sediment property data of San Nicola and Site 967 record climate relationships during MIS98 and MIS96 that are comparable to those observed during MIS100 (*Chapters 2, 3 and 4*), i.e. low latitude dust episodes as recorded by the colour reflectance (CR) and magnetic susceptibility (MS) can be linked with cooling cycles in the Mediterranean and the North Atlantic, and with North Atlantic ice rafting history. Spectral analysis indicates however, that these climate systems might have operated on slightly different time scales: On a Milankovitch-scale, spectra of the oxygen isotope records are dominated by 80, 41 and 28 kyr periodicities, which is in agreement with global ice volume and Northern Hemisphere annual air temperature in that interval (*Chapter 5*). Only the spectra of  $\delta^{18}\text{O}_{\text{G.ruber}}$  indicate variance at the precession period, reflecting a local sea surface salinity/temperature component. The CR and MS spectra indicate a much stronger precession component but they differ significantly from one site to the other. These differences may be explained by the shortness of the records and, probably more importantly, differences in the glacial-interglacial signature of the individual sites and the strength of the precessional signal. Spectra of these records are more similar in the sub-Milankovitch range, showing concentration of variance around 6-7 kyr close to periodicities resulting from harmonics and combinations tones of the primary

precession components. Comparison with the power spectrum of a curve constructed by taking the difference between the strongest temperature maximum ( $T_{\max}$ ) and the strongest minimum ( $T_{\min}$ ) in the annual cycle at the equator indicates that differential heating related to the orbital configuration may explain the observed climate variability recorded by the MS and CR at SN and Site 967. Such a model would be in agreement with a (stationary) periodic climate signal as observed in the sediment property records of SN and Site 967. However, a link with primary precession may be considered less likely in view of the reduced precessional amplitude as a consequence of minimum eccentricity at that time.

On the contrary, spacing of  $\delta^{18}\text{O}$  subcycles, which represent the most prominent feature on a sub-Milankovitch scale in the  $\delta^{18}\text{O}$  record of the investigated time interval (see also *Chapter 2*), vary from one glacial to the other between 7 and 9 kyr, with the length of the cycles being related to the length of the glacial. Wavelet analysis indicates that both intensities and frequencies of the climate signal change through time, explaining the relatively broad peak in the power spectrum around 7-9 kyr. Such a non-stationary behaviour points towards nonlinear components either in the recording mechanism, the climate response or the forcing itself. Such nonlinear components could arise from frequency modulation of the primary eccentricity, obliquity and precession cycle or from internal ice sheet dynamics. An example of frequency modulation is presented for the Northern Hemisphere annual air temperature ( $T_{\text{air}}$ ), a derivative of the  $\delta^{18}\text{O}_{\text{benthos}}$  of Site 967, which shows the presence of a 8 kyr or  $\sim 12$  kyr component being modulated by a  $\sim 70$  kyr periodicity. This example is more in agreement with the model proposed by *McIntyre and Molino* [1996], who related zonal wind-driven divergence in the equatorial Atlantic with a periodicity of  $\sim 8.4$  kyr to nonlinear interaction between precession and an anomalous short eccentricity periodicity. However, our data also clearly indicate that more work has to be done to unravel the enigmas of sub-Milankovitch variability in the climate system.



## CHAPTER 2

### Late Pliocene climate variability on Milankovitch to millennial time scales: A high-resolution study of MIS100 from the Mediterranean

#### Abstract

Astronomically tuned high-resolution climatic proxy records across marine oxygen isotope stage 100 (MIS100) from the Italian Monte San Nicola section and ODP Leg 160 Hole 967A are presented. These records reveal a complex pattern of climate fluctuations on both Milankovitch and sub-Milankovitch timescales that oppose or reinforce one another. Planktonic and benthic foraminiferal  $\delta^{18}\text{O}$  records of San Nicola depict distinct stadial and interstadial phases superimposed on the saw-tooth pattern of this glacial stage. The duration of the stadial-interstadial alterations closely resembles that of the late Pleistocene Bond cycles. In addition, both isotopic and foraminiferal records of San Nicola reflect rapid changes on timescales comparable to that of the Dansgaard-Oeschger (D-O) cycles of the late Pleistocene. During stadial intervals winter surface cooling and deep convection in the Mediterranean appeared to be more intense, probably as a consequence of very cold winds entering the Mediterranean from the Atlantic or the European continent.

The high-frequency climate variability is less clear at Site 967, indicating that the eastern Mediterranean was probably less sensitive to surface water cooling and the influence of the Atlantic climate system. Concomitant changes in the colour reflectance of ODP Site 967 and the calcium carbonate record of San Nicola probably indicate that part of the high-frequency climate variability (3-5 kyr) in the eastern Mediterranean is related to changes in Saharan dust supply. Evidently enhanced dust deposition in the Mediterranean correlates with the cold intervals of the millennial-scale D-O oscillations suggesting that the Atlantic pressure system may have played a critical role in varying the wind strength and/or aridification of northern Africa.

## 2.1. Introduction

Much work has been done in describing and modelling natural variability of the Earth's climate system. While it has been demonstrated that variations in the Earth's climate system at Milankovitch timescales (20 to 400-kyr) are caused by variations in the solar insolation and, hence, are orbitally induced, the origin of climate variability at sub-Milankovitch timescales (periods <20-kyr) is still under debate. Possible forcing mechanisms that have been proposed for these high-frequency climate variations include non-linear response to harmonics or combination tones of the main orbital cycles [Pestiaux, *et al.*, 1988; Hagelberg, *et al.*, 1994; Ortiz, *et al.*, 1999], twice-yearly overhead passage of the sun across the equator [Short and Mengel, 1986; Short, *et al.*, 1991], variation in solar output [Van Geel, *et al.*, 1999; Perry and Hsu, 2000; Bond, *et al.*, 2001] or periodic motion of the Earth and Moon [Keeling and Whorf, 2000].

From sedimentary and ice-core data it became evident that the Earth's climate system is extremely instable, especially during the last glacial. Rapid cold-warm fluctuations in North Atlantic sea surface and Greenland air temperature are associated with fluctuations in global thermohaline circulation and occasionally with ice rafting events from Northern Hemisphere ice sheets [Heinrich, 1988; Bond, 1992; Bond, *et al.*, 1993; Dansgaard, *et al.*, 1993; Bond, *et al.*, 1999]. The occurrence of high-amplitude millennial-scale climate variations during full glacial conditions in contrast to relatively low-amplitude millennial-scale variability during interglacial times (e.g., Holocene) suggests that Northern Hemisphere ice sheets are important. However, the role of large ice sheets is still controversial, because some models propose ice sheets to be the trigger for tropical climate variability [MacAyeal, 1993], whereas others argue that rapid oscillations of the northern climate are a response to rather than the cause of low latitude climate variability [McIntyre and Molino, 1996; Curry and Oppo, 1997]. Proposed mechanisms are those including changes in the equatorial wind system equivalent to long-term changes in El Niño - Southern Oscillation (ENSO) and changes in the intensity of the Inter Tropical Convergence Zone (ITCZ) and monsoon variability [Stott, *et al.*, 2002]. Moreover, older records show that high-frequency variability is a significant component of high-latitude and low-latitude climate prior to the onset of Northern Hemisphere glaciations [Ortiz, *et al.*, 1999; Steenbrink, *et al.*, 2003]. Although the interpretation of these records is not straightforward they strengthen the idea that high-frequency components are persistent in the Earth's climate and independent from the large ice sheets of the late Pleistocene. But it is generally accepted that northern Hemisphere ice sheets (or possibly even southern Hemisphere ice sheets) act as amplifiers [Raymo, *et al.*, 1992; McIntyre, *et al.*, 2001] or a resonating system [Wara, *et al.*, 2000].

Most studies on millennial-scale climate variability have focussed on the late Pleistocene time interval when glacial-interglacial alternations were primarily paced by the 100-kyr periodicity [Imbrie, *et al.*, 1993], of which the origin has been intensively debated [Le

Treut and Ghil, 1983; Imbrie, *et al.*, 1984; Saltzman and Sutera, 1984; Imbrie, *et al.*, 1992; Liu, 1992, 1995; Clemens and Tiedemann, 1997; Rial, 1999; Shackleton, 2000]. In contrast, it is generally accepted that the glacial-interglacial cycles of the late Pliocene and early Pleistocene are controlled by the obliquity cycle [Shackleton, *et al.*, 1984; Ruddiman, *et al.*, 1986; Raymo, *et al.*, 1989]. Hence studying these glacial-interglacial cycles in high resolution may shed new light upon the relation between millennial-scale and astronomically-driven climate cycles. Here, we present a high-resolution multi-proxy study of the late Pliocene marine oxygen isotope stage 100 (MIS100) from the Mediterranean to unravel millennial-scale climate variability in a region that is well

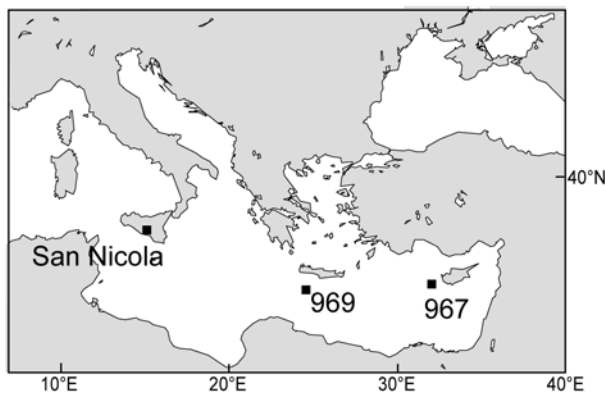


**Figure 2.1:** Location map.

known to be dominated by the Earth's precession and obliquity cycles throughout the late Neogene [i.e. Lourens, *et al.*, 1992; Hilgen, *et al.*, 1995; Lourens, *et al.*, 1996]. MIS100 was chosen as case study, because in the first place it revealed characteristic high-frequency changes in sediment colour in both the land-based marine succession Monte San Nicola (Sicily, Italy) and ODP Site 967 (Figures 2.1 and 2.2). Secondly, both sequences have been astronomically calibrated, independent of global ice volume chronologies [Lourens, *et al.*, 2001; Lourens, *et al.*, 2004]. Finally, MIS100 is one of the first pronounced obliquity-controlled glacial periods at the onset of Northern Hemisphere glaciations [Shackleton, *et al.*, 1984; Raymo, *et al.*, 1989]. Evidence for occasional massive discharge of icebergs during these first full glacial cycles comes from ice rafted debris (IRD) records in DSDP/ODP cores from the North Atlantic [Raymo, *et al.*, 1992; Carter and Raymo, 1999]. Rapid changes in the size of the continental ice-sheets at that time are confirmed by major shifts in benthic foraminiferal oxygen isotope records [Raymo, *et al.*, 1989; Raymo, *et al.*, 1992].

## 2.2. Material and Methods

Monte San Nicola is situated 10 km north of the coastal town Gela in southern Sicily (Italy) (for detailed location map and description see [Rio, *et al.*, 1994]). A succession of ~160 m of rhythmically bedded marly limestones and marls from the Trubi and Monte Narbone Formation are well exposed. The sapropels of the O, A, B and C clusters [Verhallen, 1987; Zijdeveld, *et al.*, 1991] are visible in the section (Figure 2.2). The sedimentary sequence was estimated to be deposited at a water depth of 800-1000 m

[Bonaduce and Sprovieri, 1984; Rio, et al., 1994] with an average sedimentation rate of ~8 cm/kyr [Sprovieri, et al., 1986]. The section presents the Gelasian stratotype [Rio, et al., 1994] with the base of the Gelasian being defined at the top of the A<sub>5</sub> sapropel (Figure 2.2).

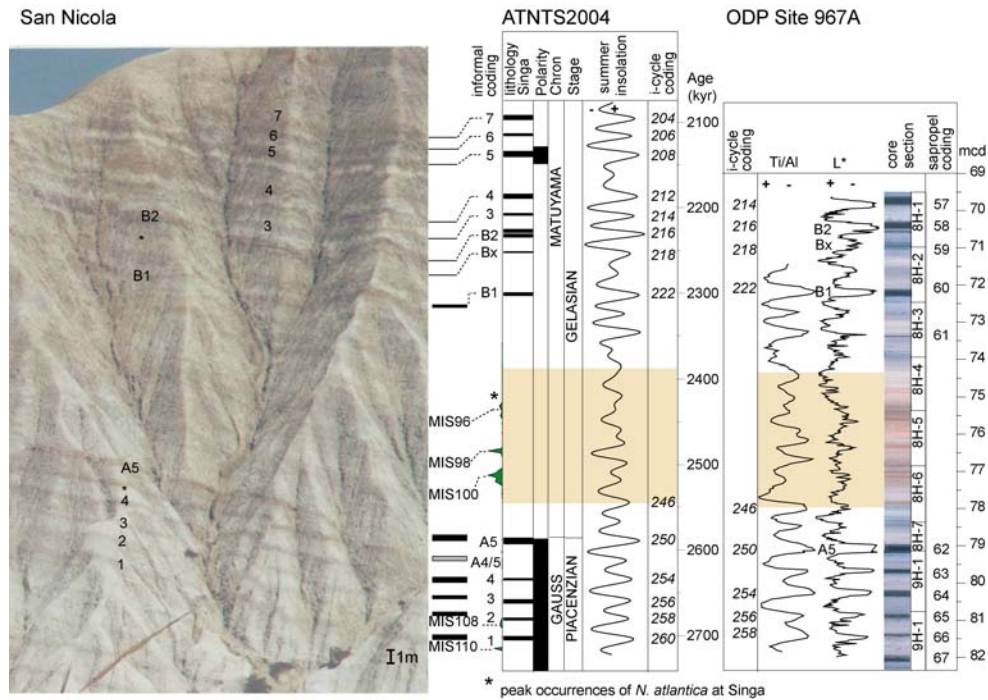


Figure 2.2: Lithology of Monte San Nicola section in comparison with the ATNTS2004 and lithology of ODP Site 967. Individual sapropels of sapropel clusters A and B (informal coding after Verhallen, [1987]; Zijderveld et al. [1991]) are labelled in the photograph of SN. Thick black and grey bars at the right hand side of the photograph indicate stratigraphic positions (scale bar lower right corner) of sapropels as recorded in the field and thin bars indicate positions of sapropels as assumed from the photograph. Stipple lines indicate correlation to the lithology of the Monte de Singa section as incorporated in the ATNTS2004 [Lourens, et al., 2004]. Additionally, marine isotope stages (MIS) 110, 108 and 100-96 are indicated in the lithology of SN and by peak occurrences of *Neogloboquadrina atlantica* (green shaded) at Singa [Lourens, et al., 1992]. The ATNTS2004 shows the sapropel occurrences, polarity, chrons, stages in relation to the La04<sub>(1,1)</sub> 65°N summer insolation curve. Insolation maxima correlating to sapropels are labelled according to the i-cycle coding after Hilgen [1991a] and ages (kyr) are indicated on the right axis. The yellow shaded area indicates the interval of MIS101-95. Ti/Al, colour reflectance and lithology of ODP Leg 160 Site 967 (composite) are plotted versus meter composite depth (mcd), after Sakamoto et al. [1998]. I-cycle codes are indicated on the left and sapropel codes of Kroon et al. [1998] on the right. Sapropels A5, B1, Bx and B2 are indicated in addition. The grey shaded area indicates the interval of MIS101-95.

Monte San Nicola has been used to establish the astronomically calibrated (polarity) timescale by Hilgen [Hilgen, 1991b; 1991a]. The position of marine oxygen isotope stages (MIS) 96-100 is well constrained in this section [Sprovieri, 1993]. These stages are visible as grey-white alternations on a metre scale in-between the A<sub>5</sub> sapropel and the B sapropel group with grey layers reflecting glacial stages 100, 98 and 96 (Figure 2.2). Light-coloured decimetre thick bands are visible within the dark glacial stages. The base of MIS<sub>101</sub> is characterised by a dark layer which is a not fully developed sapropel (ghost sapropel) corresponding to i-cycle 246 [Lourens, *et al.*, 1996].

The MIS<sub>101</sub> to MIS<sub>99</sub> interval was sampled every 3 cm. The sampling trajectory was chosen carefully to ensure a continuous and undisturbed record. The weathered surface was cleaned and only 'fresh' material was sampled. Generally, two cores of 2.5 cm diameter were drilled per sample level using an electric water-cooled drill. Samples for foraminiferal counts and stable isotope analysis were dried at 50 °C in an oven and were washed through 63, 125 and 600 µm sieves. Samples for geochemical analysis were dried and homogenised in an agate mortar.

ODP Leg 160 Site 967 (34°04'N, 32°43'E) was drilled in the eastern Mediterranean near the Eratosthenes seamount at a water depth of 2554 m. The palaeodepth was estimated to be 1800-2500 m [Emeis, *et al.*, 1998]. Three holes were drilled in order to gain a continuous succession. A composite depth profile was constructed by correlating colour reflectance records between different holes [Sakamoto, *et al.*, 1998]. The top 125 m consist of lower Pliocene to Holocene hemipelagic sediments containing 80 sapropels. Sapropels occur in clusters and correlate to the large-scale sapropel groups O, A, B and C as exposed in the land-based marine successions of the Vrica, Singa, Punta Piccola and San Nicola sections [Kroon, *et al.*, 1998; Lourens, *et al.*, 1998]. The interval between the A<sub>5</sub> sapropel and the B sapropel group is marked by a reddish colour and glacial stages 100, 98 and 96 are visibly darker in the core (Figure 2.2). Hole A on Site 967 was sampled every centimetre in the interval 8H4-6 (hereafter referred to as Site 967). Core photographs and colour reflectance data of all holes (A-C) were used to check the stratigraphic completeness and un-disturbance of the core section. Additionally, colour reflectance was measured on the half core every centimetre and on the individual samples using a hand-held Minolta CM 503i spectrophotometer. Samples for foraminiferal stable isotope analysis were freeze-dried and washed through 63, 125 and 600 µm sieves.

For stable isotope analysis of the San Nicola samples about 20 specimens of the benthic foraminifer *Uvigerina peregrina* and 50 specimens of the planktonic foraminifer *Globigerinoides ruber* were hand picked from a split of the >212 µm size fraction in the size range 300-400 µm. The analysis was carried out at Utrecht University stable isotope facility where an ISOCARB common bath carbonate preparation device linked on-line to a VG SIRA24 mass spectrometer is operated. Isotope values were calibrated to the PeeDeeBelemnite (PDB) scale. Analytical precision was determined by replicate

analyses and by comparison to the international (IAEA-CO1) and in house carbonate standard (NAXOS). Replicate analyses showed standard deviations of  $< 0.06\text{‰}$  and  $< 0.1\text{‰}$  for  $\delta^{13}\text{C}$  and  $\delta^{18}\text{O}$ , respectively.

For benthic stable isotope analysis of Site 967 3-5 specimens of *Cibicidoides kullenbergi* were hand picked from the  $>212\ \mu\text{m}$  fraction in the size range  $300\text{--}400\ \mu\text{m}$ . Measurements were carried out at Bremen University stable isotope facilities where a CARBO-KIEL automated carbonate preparation device linked on-line to a FINNIGAN MAT 251 mass spectrometer is operated. Replicate analyses and calibration to the international carbonate standard NBS19 and in-house standard (shk\_br; carrara) revealed an analytical precision better than  $0.03\text{‰}$  and  $0.05\text{‰}$  for  $\delta^{13}\text{C}$  and  $\delta^{18}\text{O}$ , respectively. The  $\delta^{18}\text{O}$  results of *Cibicidoides kullenbergi* were adjusted by adding  $0.64\text{‰}$  to be in equilibrium with *Uvigerina* and ambient sea water [Shackleton, 1974].

Carbon weight percentages were measured before and after removal of carbonates with  $1\ \text{M HCl}$  on a Fisons Instruments NCS NA 1500 analyser (Utrecht University) using dry-combustion at  $1030\ \text{f}\text{f}\text{C}$ . Relative standard deviations in duplicate measurements are below  $3\text{‰}$  for carbon and  $4\text{‰}$  for nitrogen. Carbonate weight percentages were calculated by converting all inorganic carbon into carbonate.

Quantitative foraminiferal analysis was carried out on the San Nicola samples by counting approximately 200 specimens per sample from splits of the  $>125\ \mu\text{m}$  size fraction. Splits were obtained using an Otto micro-splitter. All specimens were picked, mounted on Chapman slides and identified. The juvenile forms of the planktonic species *Globigerina falconensis* and *Globigerina bulloides* were counted together because of their close morphological similarity. The adult forms are predominantly specimens of *G. falconensis* and very few specimens of *G. bulloides* and, therefore, plotted together. Sinistrally and dextrally coiled forms of the *Neogloboquadrina* sp. group were counted separately. In the benthic foraminiferal group of the non-costate buliminids *Bulimina aculeata* s.s., *Bulimina marginata* s.s. and intermediate morphotypes are counted together. Groups like miliolids, discorbids, nodosariidae and *Elphidium* spp. are not specified any further.

### 2.2.1. Age model

The studied interval of ODP Site 967 has been astronomically dated by correlating the Ti/Al to the  $\text{La}_{90-93(1,0.3)}\ 65^\circ\text{N}$  summer insolation curve [Lourens, et al., 2001]. The Ti/Al ratio has been interpreted in terms of changes in the relative contribution of aeolian versus fluvial material. For statistical purposes Lourens et al. [2001] assumed an in-phase relationship between Ti/Al and  $65^\circ\text{N}$  summer insolation. Therefore, ages of i-cycle 246 and 244 differ by 3 kyr from the lagged ages given by Lourens et al. [1996]. Here, we apply a new astronomical solution,  $\text{La}_{04(1,1)}$  with present-day values for the Earth's tidal dissipation and dynamical ellipticity [Laskar, et al., 2004] in stead of the

older La90–93 solution [Laskar, *et al.*, 1993], although both solutions reveal the same ages within the studied interval.

The age model for San Nicola is based on the graphical correlation between the benthic oxygen isotope record of San Nicola and Site 967 (Figure 2.3a). Tie-points

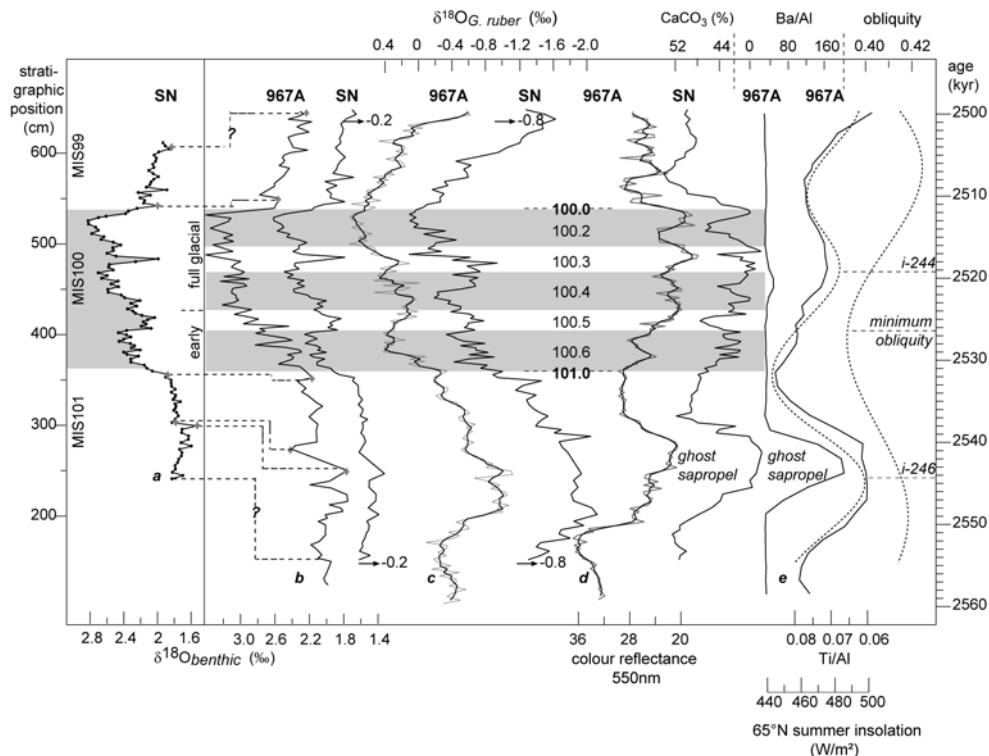


**Figure 2.3:** a) graphical correlation of the  $\delta^{18}\text{O}_{\text{benthos}}$  record of San Nicola (versus depth) with the  $\delta^{18}\text{O}_{\text{benthos}}$  of ODP Site 967A (versus age). Crosses and stippled lines indicate tie points used for age calibration. Ages are interpolated linearly in between tie points. b)  $\delta^{18}\text{O}_{\text{benthos}}$  of San Nicola versus age plotted on the same (inversed) x-axis as  $\delta^{18}\text{O}_{\text{benthos}}$  of Site 967. Shaded areas indicate stadials with even labels referring to stadials and odd labels referring to interstadials, respectively. Marine oxygen isotope stage 100 extends from 2531.5 kyr to 2511.5 kyr. The distribution into an early and full glacial phase is indicated on the right age-axis. c)  $\delta^{18}\text{O}_{\text{plankton}}$  curves of ODP Site 967A and San Nicola plotted on common axes (inverse x-axis). Note that the San Nicola curve is shifted 0.8‰ towards lighter values for clarity. A three point moving average (dark line) overlies the  $\delta^{18}\text{O}_{\text{plankton}}$  of site 967A d) ODP Site 967A 550nm colour reflectance (dark line) with superimposed three point moving average and San Nicola bulk sediment  $\text{CaCO}_3$  weight percentage. Low values in the colour reflectance and  $\text{CaCO}_3$  weight percentage respectively mark the position of the ghost sapropel. e) ODP Site 967A Ba/Al, Ti/Al (inversed) [data Lourens, *et al.*, 2001] and La04<sub>(1,1)</sub> 65°N summer insolation (stippled-line) and obliquity. I-cycles i-246 and i-244 (i-cycle notation after Lourens *et al.* [1996]) are indicated on the left age-axis.

were set at the MIS101/MIS100 and MIS100/MIS99 transitions and within MIS99 and MIS101. Ages in between the tie-points are interpolated linearly resulting in a duration of ~20 kyr for MIS100 and average sedimentation rates of ~6 cm/kyr and ~8.6 cm/kyr equivalent to a time resolution of ~500 yr and ~350 yr in the interglacials and the glacial of San Nicola, respectively. Sedimentation rate at Site 967 is on average 2.5 cm/kyr, resulting in a sample resolution of ~400 yr.

## 2.3. Results

### 2.3.1. Oxygen isotopes

San Nicola  $\delta^{18}\text{O}$  values for *U. peregrina* ( $\delta^{18}\text{O}_{\text{benthos}}$ ) and *G. ruber* ( $\delta^{18}\text{O}_{\text{G.ruber}}$ ) are highest during MIS100 with maximum values being 2.8‰ and 0.8‰, respectively (Figure 2.3b,c). Lowest values (-1.2‰ for  $\delta^{18}\text{O}_{\text{G.ruber}}$  and 1.6‰ for  $\delta^{18}\text{O}_{\text{benthos}}$ ) are reached during the ghost sapropel. Average interglacial  $\delta^{18}\text{O}_{\text{benthos}}$  values (MIS99 and MIS101 averaged) are 1.8‰ resulting in a glacial-interglacial (G-I) difference (maximum-average interglacial) of ~1.0‰ for  $\delta^{18}\text{O}_{\text{benthos}}$ . Interglacial  $\delta^{18}\text{O}_{\text{G.ruber}}$  values are ~ -0.6‰ during MIS101 except for the ghost sapropel and decrease from maximum glacial values of -1.2‰ to minimum interglacial values of -0.6‰ during MIS99. The  $\delta^{18}\text{O}_{\text{G.ruber}}$  values decrease later and slower than  $\delta^{18}\text{O}_{\text{benthos}}$  values (Figure 2.3b). At the MIS100/MIS99 transition  $\delta^{18}\text{O}_{\text{benthos}}$  is already  $\sim\frac{3}{4}$  the interglacial value, whereas  $\delta^{18}\text{O}_{\text{G.ruber}}$  is still at one third the interglacial value. Assuming a minimum interglacial  $\delta^{18}\text{O}_{\text{G.ruber}}$  value of ~-0.6‰, a value that is reached at the beginning of MIS101, before the MIS101/100 transition and at the top of the record in MIS99 results in a G-I difference (maximum glacial-assumed interglacial) of ~1.4‰ for  $\delta^{18}\text{O}_{\text{G.ruber}}$ .

Benthic oxygen isotope values of Site 967 are generally ~0.5‰ heavier than at San Nicola, except during the onset of MIS100, averaging to 2.2‰ in the interglacial and ~3.2‰ in the glacial. This implies that the glacial-interglacial  $\delta^{18}\text{O}_{\text{benthos}}$  difference of Site 967 is like at San Nicola 1.0‰. This is in close agreement with G-I amplitudes of North Atlantic records [Ruddiman, et al., 1986; Raymo, et al., 1989; Lisiecki and Raymo, 2005]. Lowest  $\delta^{18}\text{O}_{\text{G.ruber}}$  values (-1.0‰) of Site 967 are associated with the ghost sapropel, being ~-0.3‰ before and after the sapropel, a value that is also reached at the top of MIS99 and during the following interglacials (unpublished data). Therefore, interglacial  $\delta^{18}\text{O}_{\text{G.ruber}}$  values of Site 967 are assumed to be in the range of -0.3‰ and thus heavier by 0.3‰ than interglacial  $\delta^{18}\text{O}_{\text{G.ruber}}$  values of San Nicola. This results in a G-I (maximum glacial-assumed interglacial)  $\delta^{18}\text{O}_{\text{G.ruber}}$  difference of ~1.1‰ for Site 967 compared to 1.4‰ for at San Nicola. Furthermore,  $\delta^{18}\text{O}_{\text{G.ruber}}$  values of Site 967 decrease also much slower after the MIS100/99 transition than associated  $\delta^{18}\text{O}_{\text{benthos}}$ . Planktonic and benthic oxygen isotope records of both sites show a remarkable good correlation (Table 1.1) revealing an overall distinct saw-tooth pattern characterised by a gradual increase during the early glacial towards maximum values during full glacial conditions and a sudden decrease at the termination. A time lag of ~8 kyr can be



observed between the midpoint of MIS100 (~2.519 Ma) and the minimum in obliquity at 2.527 Ma (Figure 2.3e).

The  $\delta^{18}\text{O}_{\text{benthos}}$  record of San Nicola is furthermore characterised by three sub-cycles. Each sub-cycle shows a saw-tooth pattern, starting with a gradual increase in isotope values that takes about 4-5 kyr followed by a sudden decrease to lighter values. Values remain low for another 2-3 kyr so that the average duration of each sub-cycle is 6-8 kyr. We labelled the San Nicola sub-stages according to the nomenclature established for late Pleistocene glacials where even numbers refer to stadial phases and odd numbers refer to interstadial phases [Imbrie, *et al.*, 1984; Martinson, *et al.*, 1987]. San Nicola sub-stages are also observed in the  $\delta^{18}\text{O}_{\text{G.ruber}}$ , but are generally noisier. Benthic and planktonic  $\delta^{18}\text{O}$  values correlate except for the stadial MIS100.4 where the relation is partly inverted. Sub-stages have amplitudes of about 0.4-0.5‰. Partitioning into an early and a full glacial is also evident in the  $\delta^{18}\text{O}_{\text{benthos}}$  of Site 967, but sub-stages as defined in San Nicola are not clear. Millennial-scale (2-3 kyr) variations in the order of 0.2-0.4‰ can be recognised in both  $\delta^{18}\text{O}_{\text{benthos}}$  records.

### 2.3.2. Calcium carbonate

$\text{CaCO}_3$  weight percentages of SN are maximal (50%) in the interglacials except during the ghost sapropel and low in the glacial and the ghost sapropel (minimal 36%) with values fluctuating between 36-44% during MIS100 (Figure 2.3d). Total organic carbon weight percentages (not shown) are 0.6% in the ghost sapropel and ~0.16% in the remaining part of the record. Maximum colour reflectance (550nm) values (36%) at Site 967 are reached at the beginning of MIS101, minimum values (20%) during the ghost sapropel and MIS100 and intermediate values (28-24%) in the rest of the interval.

The  $\text{CaCO}_3$  of San Nicola and the CR of Site 967 show an overall similar pattern during MIS101-99. Correlation during MIS100 is modest ( $r=0.36$ , Table 1) as we abstained from inserting additional age control points within MIS100. It was shown, that the colour reflectance of Site 967 is associated with the calcium carbonate content of the bulk sediment [Wehausen and Brumsack, 1999] so that dark intervals (MIS100 and ghost sapropel) correlate with low carbonate percentages and light intervals

**Table 2.1: correlation coefficients between selected parameters of SN and Site 967.**

| r  | Site 967<br>$\delta^{18}\text{O}_{\text{benthos}}$ | SN<br>$\delta^{18}\text{O}_{\text{G.ruber}}$ | SN<br>$\delta^{18}\text{O}_{\text{benthos}}$ | SN<br>$\text{CaCO}_3$ |
|--|--|--|--|-----------------------|
| Site 967<br>$\delta^{18}\text{O}_{\text{G.ruber}}$ | 0.85<br>(0.58) <sub>1</sub>                        | 0.94<br>(0.76)                               | 0.88<br>(0.67)                               | n.s.<br>(-0.37)       |
| Site 967<br>$\delta^{18}\text{O}_{\text{benthos}}$ |  | 0.86<br>(0.55)                               | 0.91<br>(0.63)                               | -0.29<br>(-0.42)      |
| N<br>$\delta^{18}\text{O}_{\text{G.ruber}}$        |  |  | 0.88<br>(0.61)                               | n.s.<br>(-0.30)       |
| SN<br>$\delta^{18}\text{O}_{\text{benthos}}$       |  |  |  | -0.26<br>(-0.44)      |
| Site 967<br>CR                                     | -0.58<br>(-0.85)                                   | -0.37<br>(-0.47)                             | -0.49<br>(-0.53)                             | 0.64<br>(0.36)        |

<sup>1)</sup> numbers in brackets are coefficients for MIS100 only

(interglacials) with high carbonate percentages. This indicates that sedimentary calcium carbonate content varied with a similar pattern at both Sites during MIS100.

### 2.3.3. Planktonic foraminifers

The interglacial stages 101 and 99 are characterised by high percentages of *G. ruber*, *Globorotalia puncticulata*, *Globigerinoides obliquus* and *Globorotalia crassaformis* (Figure 2.4). All these species are indicative of warm water and oligotrophic conditions [Bé and Hutson, 1977; Hemleben, et al., 1989; Hilbrecht, 1996] with the exception of *G. puncticulata*, which is assumed to be a mixed layer species that proliferates in temperate regions during winter similar to its living relative *Globorotalia inflata* [Bé and Hutson, 1977; Rohling, et al., 2004]. However, the occurrence of *G. puncticulata* in association with the warm water species *G. ruber* and *G. obliquus* suggests that *G. puncticulata* thrive under slightly higher temperatures than modern *G. inflata* as suggested by Kennett and Srinivasan [1983] and Loubere and Moss [1986].

The warm water species are almost totally absent during the glacial. MIS100 is characterised by the occurrence of *Globorotalia scitula* and *Neogloboquadrina atlantica* with maximum relative abundance being 8% and 29%, respectively, during the full glacial. *G. scitula* and *N. atlantica* are generally associated with cool water [Bé and Hutson, 1977;

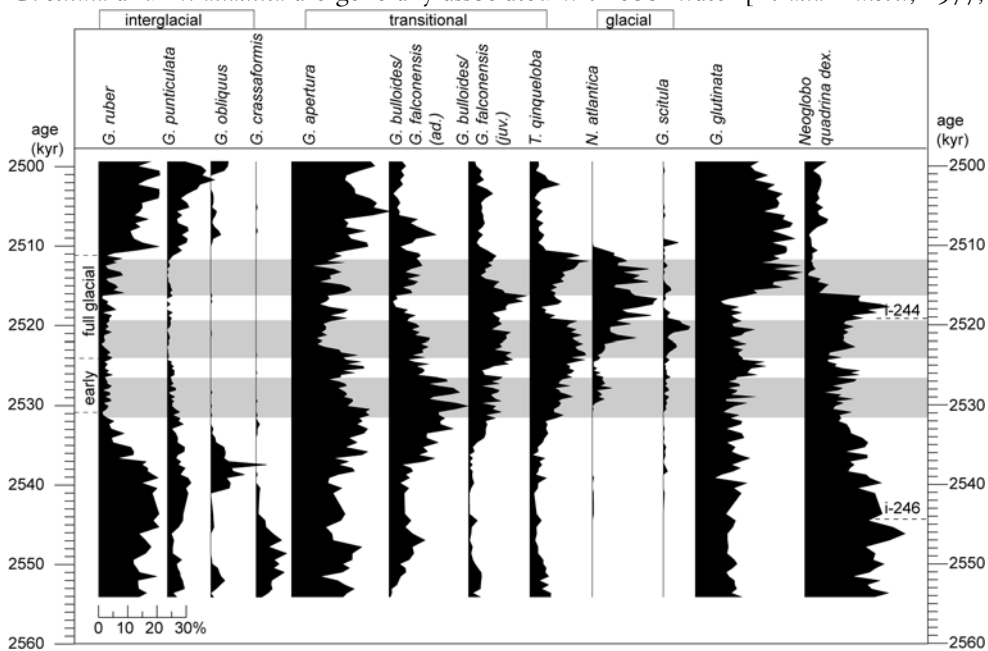
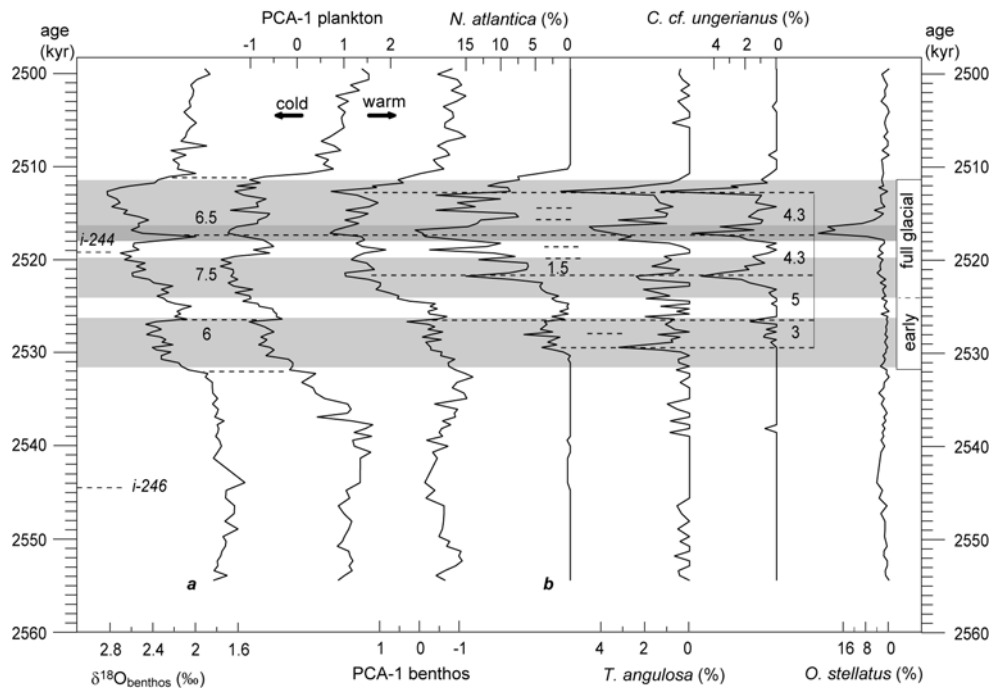


Figure 2.4: Relative abundance of the most important planktonic foraminiferal species in the San Nicola MIS100 record versus age. The three different assemblages are indicated on top of the figure. Glacial intervals are marked on the right age-axis.

*Hemleben, et al.*, 1989; *Zachariasse, et al.*, 1990]. *G. scitula* is wide-spread in the Mediterranean throughout the Plio-Pleistocene during glacial times [*Zachariasse, et al.*, 1990; *Lourens, et al.*, 1992; *Rohling, et al.*, 1993]. *N. atlantica* is an extinct species that is endemic to high latitudes in late Miocene to Pliocene times [*Poore and Berggren*, 1975; *Meggers and Baumann*, 1997]. Morphological studies and biometric measurements indicate that the test size of *N. atlantica* decreased with the late Neogene global temperature decline [*Meggers and Baumann*, 1997]. Typical sinistrally-coiled *N. atlantica* invaded the Mediterranean first during MIS110 [*Lourens, et al.*, 1996] and successively during the following glacial periods associated with MIS108 to MIS96 [*Zachariasse, et al.*, 1990] after which it became extinct. Since the appearance of *N. atlantica* is exclusively related to glacial periods this species is clearly associated with surface water cooling in the Pliocene Mediterranean [*Zachariasse, et al.*, 1990].

The transition between the interglacial and glacial fauna assemblages is marked by high relative abundances (30%) of *Globoturbotalita apertura*, *Globigerina bulloides/falconensis* and *Turbotalita quinqueloba*. These latter two species are cool water species that proliferate in the Mediterranean winter mixed layer [*Rohling, et al.*, 1993; *Rohling, et al.*, 2004]. *G. apertura* probably occurred in warm to temperate waters similar to its living successor *G. rubescens*. *G. apertura* dominates the Mediterranean faunal assemblage of the early Late Pliocene but becomes less important towards the end of the Pliocene [*Lourens, et al.*, 1992]. *Lourens et al* [1992] inferred a similar habitat as *G. ruber* but a presumably larger temperature tolerance for *G. apertura* might be suggested from the slightly different abundance pattern during MIS100. The relative increase in the temperate to cool water species indicates a gradual cooling of the sea surface layer across the glacial boundaries.

The distribution pattern of *Neogloboquadrina* sp. (dex) and *Globigerinita glutinata* seems not related to the glacial-interglacial variability. The distribution of these species shows opposite patterns in accordance with similar observations at the nearby Singa section (Calabria, Italy) for the late Pliocene time interval [*Lourens, et al.*, 1992]. Relative abundance of *G. glutinata* is around 15% in the interglacial and the early and middle glacial and rises to 30% at the MIS100.2/MIS100.3 transition. Vice versa, relative abundance of *N. sp. (dex)* is around 30% in the interglacial and early to middle glacial and decreases to 15% at the MIS100.2/MIS100.3 transition. *G. glutinata* lives in the upper 200 m of the Mediterranean water column and is probably more prolific during spring [*Rohling, et al.*, 2004]. Compared to other species *G. glutinata* has a different feeding strategy as it feeds mainly on diatoms associated with a later stage in productivity blooms [*Hemleben, et al.*, 1989; *Hilbrecht*, 1996]. In the Atlantic, high abundance of *G. glutinata* is related to the entrainment of nutrients into the deeper layers by storms [*Schiebel, et al.*, 2001]. *Neogloboquadrina* sp. (dex) is observed to be abundant in deep chlorophyll maxima (DCM) and, therefore, is assumed to proliferate under high-productivity surface water masses and/or stratified surface water conditions



**Figure 2.5: a) San Nicola  $\delta^{18}\text{O}_{\text{benthos}}$ ,  $\delta^{18}\text{O}_{\text{plankton}}$  and  $\text{PCA1}_{\text{plankton}}$  and  $\text{PCA1}_{\text{benthos}}$  (inverse x-axis). b) Relative abundance of *Neogloboquadrina atlantica*, *Trifarina angulosa*, *Cibicides cf. ungerianus*, *Oridordalis stellatus*. Notice that fauna abundances are plotted on inverse x-axes in order to**

[Thunell and Williams, 1989]. In the Mediterranean high abundance of *N. sp.* (dex) is often associated with sapropel layers [Rohling and Gieskes, 1989] and with high abundance of *G. ruber*, indicating intensive surface water stratification during relatively warm summers and a seasonal DCM [Lourens, et al., 1992; Negri, et al., 1999].

We applied a standardised principle component analysis (PCA; SPSS standard software) to further unravel the observed changes in the planktonic foraminiferal abundance patterns. The first two components ( $\text{PCA-1}_{\text{plankton}}$  and  $\text{PCA-2}_{\text{plankton}}$ , respectively) explain  $\sim 52\%$  of the total variance in the planktonic foraminiferal data. Positive scores are recorded for the glacial interval and are related to the cold-water assemblage, including the species *T. quinqueloba*, *G. bulloides/falconensis* (juv), *N. atlantica* and *G. scitula*, whereas negative scores are linked to the warm-water and oligotrophic assemblage, consisting of *G. ruber*, *G. punctulata*, *G. obliquus* and *G. apertura*.  $\text{PCA-1}_{\text{plankton}}$  is, therefore, interpreted to reflect primarily glacial-interglacial changes in annual sea surface temperature ( $\text{SST}_{\text{annual}}$ ). This interpretation is strengthened by the good correlation ( $r = -0.86$ ) between  $\text{PCA-1}_{\text{plankton}}$  and  $\delta^{18}\text{O}_{\text{benthos}}$ , which both depict the glacial-interglacial transitions as well as the characteristic sawtooth pattern simultaneously (Figure 2.5; Table 2). Also on sub-Milankovitch scales  $\text{PCA-1}_{\text{plankton}}$  strongly co-varies with the  $\delta^{18}\text{O}_{\text{benthos}}$  record as evidenced by concomitant changes associated with the sub-stages of MIS100 and the millennial-scale changes within the

sub-stages. These shorter events correlate with rapid changes in the abundance of *N. atlantica* (notice the high degree of correlation ( $r=0.89$ ) between *N. atlantica* and  $\text{PCA1}_{\text{plankton}}$ ). One marked exception is observed during MIS100.3 during which the relative warm SST conditions are interrupted by a short cooling event that corresponds with the most depleted  $\delta^{18}\text{O}_{\text{benthos}}$  values within MIS100 (shaded interval in Figure 2.5).

$\text{PCA-2}_{\text{plankton}}$  is almost exclusively based on the distribution of dextral-coiled *N. sp.* (dex) (positive loadings) versus *G. glutinata* (negative loadings). This component seems to be closely related to the first principal component derived from the total faunal counts of the Singa section (Lourens et al., 1992), which has been interpreted as reflecting primarily changes in sea surface productivity (SSP) conditions. In addition, the trend in  $\text{PCA-2}_{\text{plankton}}$  (Figure 2.6) probably reflects the relative decrease in *N. sp.* (dex) associated with the 400-kyr eccentricity minimum between the A and B-sapropel cluster [Lourens, et al., 1992]. Maximum  $\text{PCA-2}_{\text{plankton}}$  values are observed during i-246 and i-244 (Figure 2.6).

**Table 2.2: correlation coefficients between selected parameters of SN and Site 967.**

| r  | PCA1<br>benthos             | PCA1<br>plankton | <i>N.</i><br><i>atlantica</i> | <i>C. kullen</i><br><i>bergi</i> |
|--|-----------------------------|------------------|-------------------------------|----------------------------------|
| Site 967<br>$\delta^{18}\text{O}_{\text{G.ruber}}$ | 0.56<br>(0.65) <sub>1</sub> | -0.74<br>(0.42)  | 0.61<br>(0.67)                | 0.57<br>(0.55)                   |
| Site 967<br>$\delta^{18}\text{O}_{\text{benthos}}$ | 0.80<br>(0.85)              | -0.85<br>(-0.69) | 0.77<br>(0.70)                | 0.71<br>(0.69)                   |
| SN<br>$\delta^{18}\text{O}_{\text{G.ruber}}$       | 0.60<br>(0.63)              | -0.80<br>(-0.52) | 0.62<br>(0.59)                | 0.59<br>(0.48)                   |
| SN<br>$\delta^{18}\text{O}_{\text{benthos}}$       | 0.76<br>(0.76)              | -0.86<br>(-0.61) | 0.76<br>(0.66)                | 0.70<br>(0.64)                   |
| PCA1<br>benthos                                    |                             | -0.77<br>(-0.76) | 0.89<br>(0.83)                | 0.80<br>(0.83)                   |
| PCA1<br>plankton                                   |                             |                  | -0.74<br>(-0.52)              | -0.67<br>(-0.47)                 |

1) numbers in brackets are coefficients for MIS100 only.

#### 2.3.4. Benthic foraminifers

The glacial-interglacial variability as reflected in the benthic foraminiferal  $\delta^{18}\text{O}$  is less clear in the benthic composition. In contrast, variation at precessional frequency is clearly visible in the benthic associations and partly interferes with the glacial-interglacial signal. We performed a standardised principal component analysis (PCA; SPSS standard software). For this we reduced the data set by omitting single occurrences, ill-defined taxonomic groups and taxa with relative abundance <1.5%. Unrotated factor scores are plotted in Figure 2.5.

The first principal component (PCA-1<sub>benthos</sub>) explains 18% of the total variance in the data set. Positive scores on the first component are recorded for the full glacial and are related to the relative abundance of *Cibicidoides kullenbergi*, *Globocassidulina subglobosa*, *C. cf. ungerianus*, *Trifarina angulosa*, *Bolivina pseudoplicata* and *Globobulimina* spp (factor loading >0.6) in association with *Gyroidina orbicularis* and *Oridorsalis stellatus* (factor loading >0.5). These taxa have a more or less cosmopolitan distribution but some are

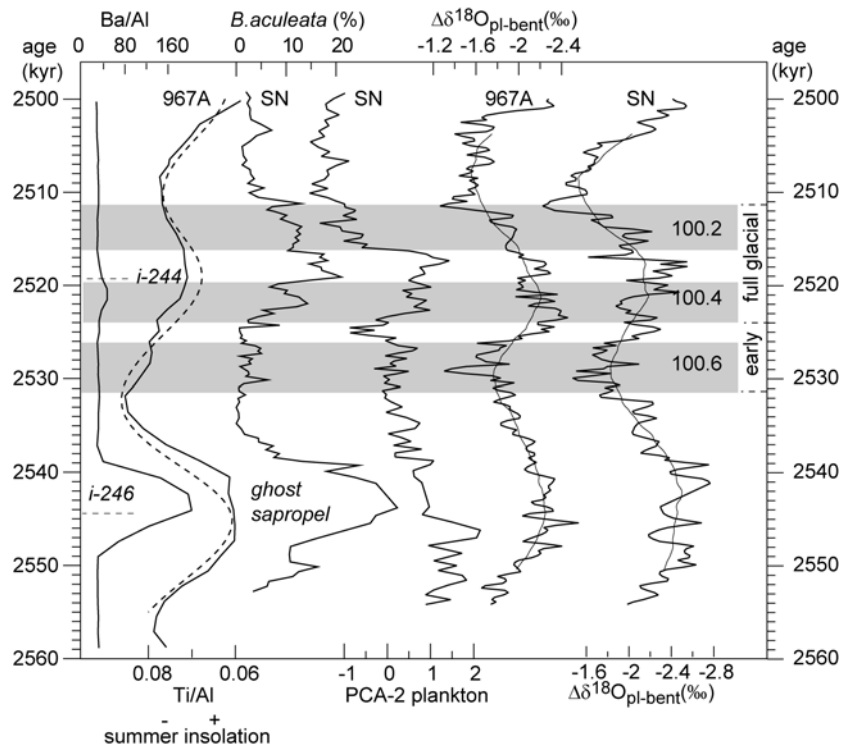


**Figure 2.6:** ODP Site 967A  $\Delta\delta^{18}\text{O}_{\text{plankton-benthos}}$  (overlain by moving average), San Nicola  $\Delta\delta^{18}\text{O}_{\text{plankton-benthos}}$  (overlain by moving average) and PCA2<sub>plankton</sub> in relation to ODP Site 967A Ba/Al, Ti/Al (inverse axis) and La04<sub>(1,1)</sub> 65°N summer insolation. Labelling according to Figure 2.3.

more commonly associated with relatively cool waters. *T. angulosa* has been used as an indicator for cold bottom waters in the Pliocene Mediterranean [Zachariasse, *et al.*, 1990] and is indigenous to North Atlantic high latitudes in Miocene to recent time [Mackensen, *et al.*, 1985; Qvale, 1986]. It predominantly occurs in outer shelf to upper slope, well-oxygenated environments [Murray, 1991; Mackensen, *et al.*, 1995; Harloff and Mackensen, 1997]. Hayward *et al.* [2002] and Murray [1991] further proposed a relation of *T. angulosa* with low temperatures. *Cibicidoides kullenbergi* is commonly reported as a surface dweller and associated with well-aerated bottom waters and low organic flux

[Lutze and Colbourn, 1984; Corliss, 1985; Fariduddin and Loubere, 1997; Schmiedl, et al., 1997]. Its recent distribution appears to be associated with cooler water-masses off West Africa [Lutze and Colbourn, 1984] and Schmiedl et al. [1997] stress its co-occurrence with North Atlantic Deep Water (NADW). From a perspective of trophic and oxygenation state of bottom waters, the behaviour of *Trifarina angulosa* and *Bolivina pseudoplicata* is quoted by Verhallen [1991] as intermediate between opportunistic and equilibrium. For *T. angulosa* a relation with high [Gupta, 1997; Harloff and Mackensen, 1997] as well as with low organic flux rates [Mackensen, et al., 1995] is documented. *Gyroidina orbicularis* is mentioned as an opportunistic taxon requiring ventilated bottom waters [Jorissen, et al., 1992]. Ecological preferences of *Oridorisalis* spp. are under debate. *O. umbonatus* is considered an opportunistic taxon, related to elevated organic flux by Sarnthein and Altenbach [1995], Miao and Thunell [1996] and Kuhnt et al. [1999]. At similar latitudes it is found to be abundant in the glacial as well as in the interglacial [Jian, et al., 1999].

Negative scores on the PCA-I<sub>benthos</sub> are related to the relative abundances of costate buliminids, *Bolivina spathulata*, *Uvigerina peregrina* and *Siphonina reticulata*. The first three species are indicative for slightly depleted bottom water oxygenation and relatively high and continuous organic matter supply [Verhallen, 1991; Schmiedl, et al., 2003]. Rathburn and Corliss [1994] report *Siphonina* from thermospheric (>10°C) waters in the Sulu Sea. Positive PCA-I<sub>benthos</sub> scores are interpreted to represent well-ventilated, possibly cooler bottom waters during the full glacial with an intermittent organic matter supply to the sea floor.

The distribution pattern of the non-costate buliminids is related to precessional cyclicity. These taxa abound during precession minima i-246 (the ghost-sapropel) and to a lesser extent i-244 (Figure 2.6). Non-costate buliminids are mentioned in relation to fine-grained substrates and elevated productivity and/or lowered bottom-water oxygenation [Mackensen, et al., 1993; Fariduddin and Loubere, 1997; Gupta, 1997; Jannink, et al., 1998; Jian, et al., 1999; Hayward, et al., 2002].

## 2.4. Discussion

### 2.4.1. Milankovitch-scale climate variability

#### 2.4.2. Sea surface temperatures

The  $\delta^{18}\text{O}_{\text{benthos}}$  glacial-interglacial differences at San Nicola and Site 967 are in good agreement with open ocean benthic isotope records [Raymo, et al., 1989; Shackleton, et al., 1995] and are, therefore, interpreted to represent dominantly obliquity-controlled variations in global ice volume. The ice volume effect during MIS100 was estimated to be  $\sim 0.8\text{‰}$  [Raymo, et al., 1989; Raymo, et al., 1992], which is in agreement with the rapid deglaciation in our Mediterranean  $\delta^{18}\text{O}_{\text{benthos}}$  records at the MIS100/99 transition and leaves only a minor temperature and/or salinity-related component for the Mediterranean  $\delta^{18}\text{O}_{\text{benthos}}$  records of  $\sim 0.2\text{‰}$ . Modelling experiments suggest that the

evaporation/precipitation (E-P) balance did not change significantly during glacial times [Bigg, 1995], therefore excluding a significant salinity effect on the  $\delta^{18}\text{O}_{\text{benthos}}$  record. However, it remains uncertain to infer regional  $\delta^{18}\text{O}_{\text{sw}}$  (sw: sea water) from a purely E-P basis, because on a local scale the degree of mixing in intermediate waters to a few hundred metres below the sea surface may alter the  $\delta^{18}\text{O}_{\text{sw}}$  significantly [Bigg, 1995]. Additionally, the  $\delta^{18}\text{O}$  measured on specific foraminifera species might be biased towards a very specific growth season or optimum temperature at which the species calcify. Furthermore, the  $\delta^{18}\text{O}_{\text{sw}}$  of the inflowing Atlantic surface water and sea level-related difference in the sill depth of Gibraltar and Sicily may have influenced the  $\delta^{18}\text{O}_{\text{sw}}$  of the Mediterranean even if the E-P balance remained similar. The good correlation between the  $\delta^{18}\text{O}_{\text{benthos}}$  and  $\text{PCA-I}_{\text{plankton}}$  may indicate that at least part of the (glacial-bound) reduced  $\text{SST}_{\text{annual}}$  conditions at glacial times has been exported towards deeper waters. Based on the empirical temperature- $\delta^{18}\text{O}$  relationship of  $1^\circ\text{C}/0.25\text{‰}$  [Shackleton, 1967; O'Neil, et al., 1969], the MIS100-bound temperature decrease should have been less than  $1^\circ\text{C}$  for the deeper waters.

The  $\delta^{18}\text{O}_{\text{G.ruber}}$  glacial-interglacial amplitude is larger (by  $\sim 0.4\text{‰}$  at San Nicola and  $0.1\text{‰}$  at Site 967) than that of the  $\delta^{18}\text{O}_{\text{benthos}}$  and indicates that planktonic  $\delta^{18}\text{O}$  records are additionally affected by small changes in temperature and/or salinity. Preliminary  $U_{37}^{K'}$  data indicate that average  $\text{SST}_{\text{annual}}$  at San Nicola was  $\sim 6^\circ\text{C}$  lower during MIS100 than during the adjacent interglacial stages (Menzel pers. comm., 2004). This is in agreement with SST reconstruction from the last glacial maximum (LGM) in the western and eastern Mediterranean Sea [Kallel, et al., 1997b; Cacho, et al., 1999; Paterne, et al., 1999] but disagrees with the observed  $\delta^{18}\text{O}_{\text{G.ruber}}$  glacial-interglacial amplitude during MIS100. However, the  $\Delta T_{\text{glacial-interglacial}}$  component of the  $\delta^{18}\text{O}_{\text{G.ruber}}$  might be underestimated because *G. ruber* is known to calcify at optimum temperatures during the summer season [Schmidt and Mulitza, 2002]. This could have biased the oxygen isotope signal towards warmer SST, since only the warmest summers are recorded by *G. ruber* and colder summers are 'skipped'. As a result the  $\Delta T_{\text{annual}}$  should have probably been larger, implying that the  $\Delta T_{\text{annual}}$  recorded by the alkenones is not necessarily larger than the  $\Delta T_{\text{summer}}$  recorded by *G. ruber*.

We subtracted the  $\delta^{18}\text{O}_{\text{benthos}}$  values of Site 967 from both  $\delta^{18}\text{O}_{\text{G.ruber}}$  records to reconstruct this additional (combined temperature and salinity) effect. For this purpose all  $\delta^{18}\text{O}$  records were interpolated at 250-year steps. We used the  $\delta^{18}\text{O}_{\text{benthos}}$  of site 967 as reference because this site is deeper and, therefore, assumed to reflect ice volume changes more appropriate. Remarkably, the resulting  $\Delta\delta^{18}\text{O}_{\text{G.ruber-benthos}}$  records of both San Nicola and Site 967 closely follow the precession-dominated summer insolation pattern and much less the obliquity-controlled  $\text{PCA-I}_{\text{plankton}}$  and SST (Figure 2.6). It appears that the amplified  $\delta^{18}\text{O}_{\text{G.ruber}}$  values are not controlled by the glacial-interglacial  $\text{SST}_{\text{annual}}$  variability, but reflect merely the influence of precession-bound surface water salinity (SSS) and/or SST changes. Evidently, periods of maximum absolute



$\Delta\delta^{18}\text{O}_{\text{G.ruber-benthos}}$  values correspond with the summer insolation maxima i-244 and i-246 reflecting a more stratified water column at times of high seasonality.

The fact that precession exerts the main control on eastern Mediterranean climate and hydrography during the Plio-Pleistocene has been extensively shown by studies on Mediterranean marine cores and land-based marine successions [Lourens, *et al.*, 1992; Hilgen, *et al.*, 1993; 1998]. Microfossil assemblages, pollen and stable isotope data have indicated that the principal climate variability in the precession frequency band is related to changes in warm-wet and cold-dry conditions [Cita, *et al.*, 1977; Vergnaud-Grazzini, *et al.*, 1977; Rossignol-Strick, 1983; Kallel, *et al.*, 1997a; Kallel, *et al.*, 2000]. The most characteristic sedimentary expression of the precession-controlled climate variability is the regular and cyclic occurrence of sapropels, which has often been associated with changes in river-runoff and circum-Mediterranean humidity [Rohling and Hilgen, 1991]. These conditions are generally linked to an intensified African monsoon circulation causing a low salinity surface water lens in the eastern Mediterranean and hence stagnant bottom waters during minimum precession [Rossignol-Strick, 1983, 1985]. The existence of a low salinity surface water lens is evidenced by very depleted  $\delta^{18}\text{O}_{\text{plankton}}$  values of in particular *G. ruber* [Vergnaud-Grazzini, *et al.*, 1977; Rossignol-Strick, *et al.*, 1982; Kallel, *et al.*, 1997a; Emeis, *et al.*, 2003; Rohling, *et al.*, 2004]. Such a low salinity lens may in turn have induced a shoaling of the pycnocline into the nutricline and resulted in the development of a deep chlorophyll maximum (DCM) [Rohling and Hilgen, 1991].

In the interval of MIS101-99 no sapropels are deposited at San Nicola and Site 967, but the existence of a ghost sapropel and the minima in Ti/Al [Lourens, *et al.*, 2001] and maxima in absolute  $\Delta\delta^{18}\text{O}_{\text{G.ruber-benthos}}$  during summer insolation maxima i-244 and i-246 indicate that climate conditions were not much different from those leading to sapropel formation. The elevated Ba/Al contents at ODP Site 967 [Wehausen and Brumsack, 1999] and the high PCA-2<sub>plankton</sub> values at San Nicola furthermore point to enhanced primary productivity during i-244 and i-246 possibly as a result of a distinct (seasonal) DCM. Such an increase in SSP conditions may have increased the oxygen consumption rate in the bottom water as indicated by the relative abundance of non-costate buliminids in the benthic foraminiferal assemblages (Figure 2.6).

### 2.4.3. Response times

The obliquity-forced SST and  $\delta^{18}\text{O}_{\text{benthos}}$  are in phase with one another and lag obliquity by  $\sim 8$  kyr (Figures 2.3 and 2.5). This estimate is in very good agreement with the outcome of simple ice sheet models applied to explain the late Pleistocene glacial cyclicity [Imbrie and Imbrie, 1980; Imbrie, *et al.*, 1984]. A similar time lag was applied for the construction of astronomical time scales based on tuning open ocean benthic isotope records of Pliocene and early Pleistocene age to the obliquity time series [Raymo, *et al.*, 1989; Ruddiman, *et al.*, 1989; Shackleton, *et al.*, 1990]. The obliquity-

related time lag, however, may have been variable through time because of changes in the response time of the climate system related to the size of the ice sheets [Oerlemans and van der Veen, 1984]. A reduced ice sheet during the Pliocene would result in a smaller time constant and a reduction of the obliquity lag [Chen, et al., 1995]. Despite the different size in ice sheet and the different duration of the glacials in late Pliocene compared to late Pleistocene, the behaviour of the ice sheet to obliquity forcing was probably the same. The saw-tooth structure of the San Nicola and Site 967  $\delta^{18}\text{O}_{\text{benthos}}$  records confirms the asymmetric ice sheet development (slow growing and fast waning) predicted in models for late Pleistocene ice sheet behaviour [Imbrie, et al., 1984; MacAyeal, 1993].

Small uncertainties in the astronomical solution and in the adopted precession-related response time of the climate system may significantly alter the outcome of the obliquity-related lag [Lourens, et al., 1996; 2001]. However, for the investigated time interval the theoretical changes in tidal dissipation and dynamical ellipticity will change the obliquity-related time lag one kyr at most [Lourens, et al., 2001]. More important is the uncertainty in the response time of the climate system to precession forcing. In our age model the time lag with respect to precession forcing was set to zero assuming an immediate response of Ti/Al to African aridity changes. This assumption differs from that of Lourens et al. [1996] who incorporated a time lag of 3 kyr based on the age difference between the AMS  $^{14}\text{C}$ -dated midpoint of the youngest Holocene sapropel, S1 (~8.5 kyr), and the correlative summer insolation maximum at 11.5 kyr. Lourens et al. [1996] suggested that this lag could be related to the modelled ~3 kyr time lag of the maximum summer temperature ( $T_{\text{max}}$ ) in northern Africa with respect to the precession parameter [Short and Mengel, 1986] applying an Energy Balance Model. Short and Mengel [1986] argued that  $T_{\text{max}}$  may be an indication of the moisture availability to the monsoon area during the rainy season, which could therefore explain the observed lag between a monsoon trigger of sapropel formation and precession. Recently Tuenter et al. [2003] carried out transient runs with an intermediate complexity climate model (CLIMBER2.3) to test the scenario of Short and Mengel [1986]. These experiments revealed that  $T_{\text{max}}$  at low-latitudes (15°N) indeed lags the precession parameter, but that no time lag was observed between the African-Indian monsoon annual precipitation and the precession parameter. This implies that either sapropel formation in the Mediterranean is not (only) linked to changes in African-Indian monsoon annual precipitation but probably influenced by the Atlantic system or that the time lag estimate of the S1 is an exception. The latter option however seems unlikely because the timing based on  $^{230}\text{Th}$ -U (TIMS) of peak hydrological conditions associated with sapropels S1-S5 as evidenced from speleothems (Soreq cave, Israel) also points to a significant lag of 3-5 kyr [Bar-Matthews, et al., 2000]. This estimate clearly falls in the range of the lag adopted by Lourens et al. (1996) and the 5-kyr time lag modelled for the precession-bound ice sheet response time of the late Pleistocene glacial cycles [Imbrie and Imbrie, 1980; Imbrie, et al., 1984]. Presumably, the slow changes in ice

volume may have an effect on the time lag between precession and the peak humid climate conditions associated with sapropel midpoints of the late Pleistocene. Application of a 3-5 kyr lag instead of the zero lag used in the present study will increase the obliquity-related time lag to  $\sim 11-13$  kyr for MIS100. This large lag cannot be simply explained in terms of ice sheet dynamics and is, therefore, highly unlikely. Moreover, the role of precession-related high-latitude variability in global ice volume during the late Pliocene to early Pleistocene is not evident [Raymo, *et al.*, 1989; Ruddiman, *et al.*, 1989]. All this suggests that during the late Pliocene the response time for the precession-related dry-wet oscillations of circum-Mediterranean climate are most likely in phase with the precessional forcing and, hence, could be primarily driven by changes in the intensity of the African-Indian monsoon.

## 2.5. Sub-Milankovitch scale climate variability

### 2.5.1. Changes on a stadial-interstadial time scale

The registration of sub-Milankovitch scale climate variability is most evident from the rapid decreases in the  $\delta^{18}\text{O}_{\text{benthos}}$  of San Nicola and concomitant  $\text{SST}_{\text{annual}}$  changes associated with the sub-stages of MIS100. Episodes of relatively warmer SST conditions interrupt the overall colder glacial conditions and coincide with interstadials MIS100.3 and MIS100.5. Each of these warm phases is preceded by a gradual cooling trend during the stadials MIS100.2, MIS100.4, and MIS100.6. The sawtooth pattern in combination with the average duration of  $\sim 6-8$  kyr shows strong similarities with the so-called Bond-cycles during the late Pleistocene [Bond, 1992; Bond, *et al.*, 1993; Bond and Lotti, 1995] and hence may indicate a direct coupling between North Atlantic and Mediterranean high-frequency climate changes. This interpretation is confirmed by North Atlantic sedimentary records, which indicate ice rafting events during MIS100 that have a similar temporal spacing (5-7 kyr) as the San Nicola  $\delta^{18}\text{O}_{\text{benthos}}$  and  $\text{SST}_{\text{annual}}$  sub-stages (Chapter 3).

The remarkable absence of distinct sub-Milankovitch scale cycles in the  $\delta^{18}\text{O}_{\text{benthos}}$  of Site 967 indicates that the inferred climate changes were most likely not accompanied by significant changes in global ice volume. Moreover, amplitudes of sub-cycle changes in the San Nicola  $\delta^{18}\text{O}_{\text{benthos}}$  record are of almost the same magnitude as glacial-interglacial variations, which would imply melting of large parts of land-based ice sheets within a few hundred years. Although fast waning of ice-sheets is in accordance with current ice sheet models, ice sheet growth requires more time [MacAyeal, 1993] than the San Nicola benthic oxygen isotope record indicates. This is illustrated at the beginning of MIS100 where San Nicola  $\delta^{18}\text{O}_{\text{benthos}}$  increases by 0.4‰ within 2 kyr, while it takes  $\sim 6$  kyr to reach the same change in the  $\delta^{18}\text{O}_{\text{benthos}}$  of Site 967 (Figure 2.3). An increase of 0.4‰ is half the total ice volume-estimate for MIS100 implying an ice sheet accumulation to half its size within 2 kyr. This is clearly not in agreement with ice sheet models and indicates that the sub-cycles in the San Nicola  $\delta^{18}\text{O}_{\text{benthos}}$  record

are most likely caused by other mechanisms. These mechanisms may be directly linked to changes in the properties and volume of the inflowing North Atlantic surface waters and/or indirectly by changes in the intensity and position of atmospheric pressure gradients in the North Atlantic region.

North Atlantic surface waters may show depleted  $\delta^{18}\text{O}$  values because of the large input of isotopic light melt water as consequence of massive iceberg melting in the North Atlantic. The  $\delta^{18}\text{O}$  of *Neogloboquadrina pachyderma* during Heinrich event 4 (H4) for example shows a maximum drop of 2‰ right in the centre of maximum iceberg discharge but decreases quickly at greater distances (i.e., off Portugal, amplitudes were much smaller than 0.5‰) [Cortijo, et al., 1997]. The San Nicola  $\delta^{18}\text{O}$  records show changes in the order of 0.4–0.8‰ during the sub-stages of MIS100, which require even more extreme iceberg melting events than during H4. It seems, therefore, unlikely that the strong depletion in the San Nicola  $\delta^{18}\text{O}$  records originate from the inflow of low salinity Atlantic surface water alone.

### 2.5.2. Changes in Mediterranean thermohaline circulation

The strong similarity of the San Nicola  $\delta^{18}\text{O}_{\text{benthos}}$  sub-stages with the  $\delta^{18}\text{O}_{\text{G.rubber}}$  ( $r=0.88$ , Table 1) and SST record ( $r=-0.86$ , Table 1) suggests a coupling to surface water cooling events. In the present-day Mediterranean, deep and intermediate water is formed above all during boreal winter, when latent heat loss and surface cooling are strongest and initiate thermocline deepening and, subsequently, deep mixing [Pinardi and Masetti, 2000]. Temperature of the surface water during winter, therefore, determines the temperature of deep and intermediate water and, hence, influences the oxygen isotope composition of benthic foraminifers.

The peak abundances of *N. atlantica*, *C. cf. ungerianus*, and *T. angulosa* indicate a high-frequency component that is superimposed on the obliquity-controlled ice volume/temperature signal and occurs simultaneously in the surface and deeper waters (Figure 2.5). The fast fluctuations in the abundance of *C. cf. ungerianus* and *T. angulosa* could also indicate a response to a more pulsating export production and convective overturning regime during MIS100. Although, *N. atlantica* is assumed to be related to temperature, peak abundances in *N. atlantica* could also be related to productivity-related nutrient pumping from a seasonal DCM. However, little is known about the feeding strategy of *N. atlantica*. As *N. atlantica* is probably ancestral to the modern *Neogloboquadrinids* it could have had a similar feeding strategy as *Neogloboquadrina* relying on high phytoplankton productivity. At San Nicola highest relative abundances in *N. atlantica* are accompanied by high abundances of *Neogloboquadrina* with exception of MIS100.4 (Figure 2.4). In any case, the concomitant peak abundances of these species may indicate that winter cooling and deep mixing were at a maximum. Such a scenario would be in analogy with late Pleistocene peak abundances of left-coiling *N. pachyderma* found in cores from the Gulf of Lions during Heinrich events [Rohling, et

*al.*, 1998]. Within MIS100, the severe winter cooling conditions coincide with the stadial phases and with interstadial MIS100.3. The latter exception closely matches with the interval of strongly depleted  $\delta^{18}\text{O}_{\text{benthos}}$  values associated with MIS100.3 at San Nicola. At Site 967, this interval is characterised by heavy  $\delta^{18}\text{O}_{\text{benthos}}$  values, which approximate the values recorded during the last phase of MIS100.4, which may point to full glacial conditions as well. Despite this uncertainty, it is obvious that the strong winter cooling events take place during the most extreme glacial conditions of MIS100. These events occur rather regularly with average spacing of  $\sim 1.5\text{--}4.5$  kyr (Figure 2.5), which is similar to the spacing of variations found in the late Pleistocene oxygen isotope and  $U_{37}^{K'}$  records of the western Mediterranean Sea [Cacho, *et al.*, 2000; Cacho, *et al.*, 2002]. These events have been unambiguously correlated to the Dansgaard-Oeschger cycles and Heinrich events in the Greenland ice cores and North Atlantic sediments. Cacho and co-workers argued that the variability in the oxygen isotope and  $U_{37}^{K'}$  records of the western Mediterranean Sea reflects changes in surface water-cooling and deep-water formation as an immediate response to the North Atlantic climate changes. This is partly caused by the direct inflow of cold Atlantic surface waters but most importantly by an indirect atmospheric connection.

Pollen data showed that with the extension of glaciers and sea ice in the Northern Hemisphere, polar air masses expanded southward and cooled the European continent during MIS100 [Willis, *et al.*, 1999] and subsequent glacial stages [Combourieu-Nebout, 1991]. This southward expansion of polar air masses may have set the stage for more frequent and intense cold air outbreaks over the central Mediterranean (San Nicola) and more frequent Atlantic depressions entering the Mediterranean. To resume, we hypothesize that both cooler Atlantic surface water and cooler and more frequent Atlantic depressions caused intensified surface water-cooling and deep convection during stadial phases MIS100.2, MIS100.4 and MIS100.6. The strength of winter mixing depends, however, not only on winter conditions but also on the internal structure of the water column before winter cooling. A weaker stratification would facilitate winter mixing while summer stratification isolates the deeper water from surface processes [Pinardi and Masetti, 2000]. Changes in these water column properties may explain the high frequency alternations of peak occurrences of *N. atlantica* and *G. scitula* (Figure 2.4). During interstadial MIS100.5 the intensified winter cooling and deep mixing ceased and the climate state returned to the background MIS101/MIS100 transition as indicated by the intermediate  $\delta^{18}\text{O}_{\text{benthos}}$  values at San Nicola and Site 967 and the drop in *N. atlantica* percentages.

### 2.5.3. Exceptional interstadial MIS100.3

It seems highly unlikely that the strong depletion in the  $\delta^{18}\text{O}_{\text{benthos}}$  record of San Nicola during interstadial MIS100.3 also reflects more interglacial climate conditions with a generally warmer atmosphere and a weaker wind field preventing severe winter cooling and deep convection. Such a scenario is in particular rejected by the highest abundance

of *N. atlantica* within MIS100 and the peak occurrences of *C. cf. ungerianus*, and *T. angulosa*, indicating that winter cooling and deep mixing were at their maximum. Moreover very depleted  $\delta^{18}\text{O}_{\text{G.ruber}}$  values during MIS100.4 and early MIS100.3 in combination with high SSP, low  $\text{SST}_{\text{annual}}$  and low  $U_{37}^{K'}$  point towards a low salinity surface layer related to precessional forcing of insolation cycle i-244. A sharp decrease in the  $\delta^{18}\text{O}_{\text{G.ruber}}$  during the middle of MIS100 coincides with the strong depletion in the  $\delta^{18}\text{O}_{\text{benthos}}$  record of San Nicola, indicating the transfer of depleted surface water  $\delta^{18}\text{O}$  towards deeper waters by intensified winter mixing. A similar mechanism has been proposed for the interruption of the sapropel S1 [de Rijk, et al., 1999] and S5 [Rohling, et al., 2004]. The prominent peak of *Oridorsalis stellatus* (Figure 2.5b) probably confirms this mechanism. *O. stellatus* is an opportunistic benthic foraminifer and among the first taxa to re-colonise the benthic realm after the Messinian salinity crisis [Sprovieri and Hasegawa, 1990] and thought to be tolerant to salinity changes [Seidenkrantz, et al., 2000]. The development of a low-salinity surface water layer in contrast to severe winter mixing illustrates that different climate mechanisms interfere (a combination of Milankovitch and sub-Milankovitch related processes) making MIS100.3 an exceptional interval.

The absence of MIS100.3 and to a lesser extent MIS100.5 in the  $\delta^{18}\text{O}_{\text{benthos}}$  of Site 967 suggests that the eastern Mediterranean was not sensitive to winter mixing during MIS100 or that deeper waters at Site 967 were not coupled to surface water. Similar to the western Mediterranean, present-day deep-water formation in the eastern Mediterranean basin is related to winter surface cooling by cold air outbreaks from the European continent and subsequent vertical convection. Additional mixing with high saline intermediate water results in a cold saline deep water mass [Pinardi and Masetti, 2000]. If deep-water circulation during MIS100 was similar to today either winter cooling in the eastern Mediterranean was not efficient or intermediate-water not saline enough. From the  $\delta^{18}\text{O}_{\text{G.ruber}}$  it can be argued that surface waters at Site 967 were significantly different from the central Mediterranean during MIS100 and were probably not affected by the North Atlantic pressure system on sub-Milankovitch time-scales.

#### 2.5.4. High latitude versus low latitude climate variability

Evidence for concomitant high-frequency climate variability in the eastern and western Mediterranean comes from sedimentary colour reflectance and magnetic susceptibility data of different ODP Leg 160 and 161 sites (Shipboard data, ODP Leg 160 and 161

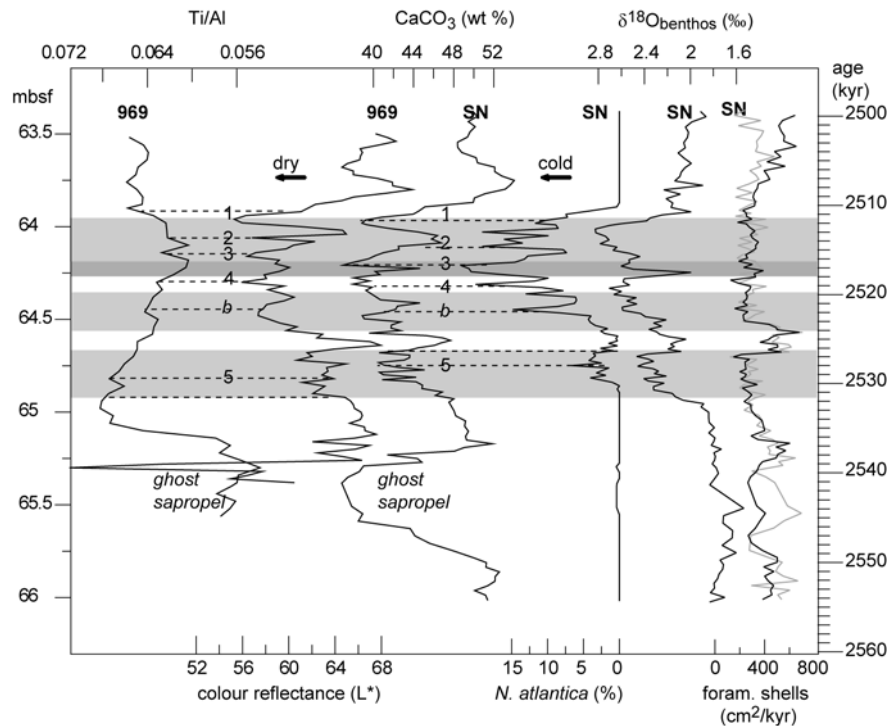


**Figure 2.7:** ODP Site 969D Ti/Al [data *Wehausen, 1999*] and colour reflectance ( $L^*$ ) versus depth (mbsf). Horizontal stippled lines and numbers indicate intervals with high Ti/Al and low colour reflectance values. Site 967  $\text{CaCO}_3$ , *N. atlantica*,  $\delta^{18}\text{O}_{\text{benthos}}$  and planktonic (black line) and benthic (grey line; benthic fluxes are multiplied by a factor 10 to match with x-axis) foraminiferal fluxes versus age. Notice inverted x-axes for  $\text{CaCO}_3$ , *N. atlantica* and  $\delta^{18}\text{O}_{\text{benthos}}$ . Horizontal stipple lines and labels indicate intervals with low  $\text{CaCO}_3$  and cold Dansgaard-Oeschger phases. Further labelling according to Figure 2.3.

data bases). Variations in calcium carbonate and colour reflectance also co-occur in San Nicola and Site 967 (Figure 2.3d) and to a higher degree in San Nicola and ODP Site 969D (Figure 2.7, for location of Site 969 see Figure 2.1) reflecting basin-wide changes in the bulk composition of the sediment. Although the mechanisms behind these changes are not fully understood, these changes are primarily driven by (i) carbonate productivity, (ii) dilution of carbonates by aluminosilicates or (iii) dissolution of carbonates with (i) and (ii) being the most important factors for Pliocene carbonate cycles on Sicily [*Van Os, et al., 1994*] and for ODP Site 967 and Site 969 [*Wehausen,*

1999]. Low carbonate productivity during MIS100 is evidenced by low foraminiferal fluxes at San Nicola but variability in these fluxes is too small to explain the observed changes in the sediment properties except for interstadial MIS100.5 (Figure 2.7). Also changes in the fluxes of calcareous nannoplankton would be unlikely to be large enough to cause these changes in  $\text{CaCO}_3$ , so that dilution of carbonates by aluminosilicates during times of lowered carbonate productivity seems to be the most important mechanism with either wind-blown or fluvial transported material as major aluminosilicate source. A synchronous basin-wide variation in terrestrial sediment supply would favour wind-blown rather than fluvial transported material.

The most important dust source for the present day Mediterranean is the African continent, especially the Sahara and its peripheral regions [Guerzoni and Roy, 1996]. Although dust is exported to the Mediterranean all year round, major dust storms across the Mediterranean occur during spring and summer, when atmospheric depression systems lie over the Saharan region [Dulac, et al., 1996]. Deposition of Saharan dust in the Mediterranean is estimated to several million tons  $\text{km}^{-2} \text{y}^{-1}$  with a strong year-to-year variability [Prospero, 1996] being sensitive to even minor changes in the source region climate and the dust transport path. Particularly changes in the atmospheric vertical stability and the precipitation regime affect the rate at which dust is lifted and deposited and changes in the storm tracks can modify the seasonality of dust storm events [Giorgi, 1996].

Clay mineral analyses and geochemical data of Mediterranean sediments indicate an increase in the relative contribution of Sahara dust during insolation minima, which is commonly interpreted to be linked to low African monsoon activity and drought in North Africa during precession maxima [Foucault and Mélières, 1995; Wehausen and Brumsack, 1999; Foucault and Mélières, 2000; Lourens, et al., 2001]. As indicated by the Ti/Al record of Site 967, dust supply during MIS99-101 was similarly related to African aridity and strength of Saharan depressions and varied in phase with summer insolation. However, short-term fluctuations are evident in the Ti/Al of Site 969D (data Wehausen, [1999]) (Figure 2.7). High Ti/Al values correlate with dark sediments and thus low  $\text{CaCO}_3$  values indicating peak dust episodes during intervals with low  $\text{CaCO}_3$ . Comparison with the  $\text{CaCO}_3$ , *N.atlantica* and  $\delta^{18}\text{O}_{\text{benthos}}$  record of San Nicola indicates further that these dust episodes during MIS100 are contemporaneous with vigorous surface water cooling and deep convection in the central Mediterranean during the cold intervals of the D-O cycles (Figure 2.7).

Such a relationship has been observed in the Mediterranean paleoclimate record of the past 50 kyr [Allen, et al., 1999; Moreno, et al., 2001; Combourieu-Nebout, et al., 2002; Sanchez-Goni, et al., 2002; Moreno, et al., 2004]. These studies attribute dry phases with increased dust transport from the Sahara to the western and central Mediterranean to a strengthening and a northward displacement of the North-Westerlies during stadial intervals similar to present day high NAO (North Atlantic Oscillation) index years.



During these times, prolonged winter anticyclones stability over central and northern Europe may have resulted in a strong flow over the Mediterranean region and very cold and dry Mediterranean winters and may have favoured the dryness in Mediterranean during stadial phases in addition to a more vigorous atmospheric circulation over the western and central Mediterranean region.

Although this interpretation renders no explanation for the difference in seasonality and the exact phasing of spring/summer dust plumes and winter water column instability it is in agreement with general circulation models that suggest that Atlantic SST could influence African climate by strengthening the subtropical pressure cell and effecting both dust source area aridity and intensity of the dust transporting trades [*deMenocal and Rind, 1993*]. During minimum eccentricity forcing and thus minimum insolation amplitude, the African continent would be most sensitive for high latitude forcing (*deMenocal and Rind, 1993*).

## 2.6. Conclusions

Obliquity related changes in SST and global ice volume at San Nicola and Site 967 during MIS101-99 are in phase with one another and lag obliquity by ~8 kyr. This time lag is in agreement with open ocean Pleistocene records and ice sheet models. Precession-related variability is evident in the fauna and oxygen isotope data indicating that dry-wet oscillations within MIS100 were not so much different from the climate changes linked to sapropel formation. These dry-wet oscillations are in phase with precession and most likely driven by changes in the African-Indian monsoon although the simultaneous influence from the Atlantic system may have played a role [*Tuenter, et al., 2003*].

The absence of sapropels in San Nicola and ODP Site 967 and Site 969 during MIS100 indicates a weakened monsoonal circulation related to the 400-kyr eccentricity minimum. Consequently, the atmospheric connection to the North Atlantic pressure system was probably extended allowing Atlantic depressions to enter further into the Mediterranean and more indirectly initiating downwind cooling from the Alps. Therefore, stadial-interstadial climate changes in the western and central Mediterranean are probably directly related to changes in the strength of the North Atlantic atmospheric wind field. Stadial phases are associated with short-time sea surface cooling events causing intensive stirring and deep convection. These cooling events are very similar to the Dansgaard-Oeschger and Heinrich events that occurred during the late Pleistocene in the western Mediterranean. The absence of such high-frequency climate variations in the eastern Mediterranean suggests that this part of the Mediterranean was either decoupled from or not sensitive to North Atlantic climate forcing.

Episodes of Mediterranean-wide increase in the Sahara dust deposition is evidenced by the sedimentary calcium carbonate of San Nicola and Ti/Al of Site 969D during the cold intervals of the D-O and HE-like events. Although the origin of this high-

frequency component is clearly the African continent, the similarity with high latitude climate features suggests a linkage between high and low latitude climate possibly through the North Atlantic pressure system. The data further indicate, that high-frequency climate change is highly complex in the Mediterranean due to the interference of climate variations forced by the primary Milankovitch frequencies.

## **CHAPTER 3**

### **High-frequency climate linkages between the North Atlantic and the Mediterranean during Marine Oxygen Isotope Stage 100 (MIS100)**

#### **Abstract**

High-resolution records of Mediterranean and North Atlantic deep-sea sediments indicate that rapid changes in hydrology and climate occurred during marine oxygen isotope stage 100 (MIS100) at ~2.52 Ma, which exhibit characteristics similar to late Pleistocene Dansgaard-Oeschger, Bond cycles and Heinrich events. As in the late Pleistocene, North Atlantic oceanographic and atmospheric changes were probably transmitted into the Mediterranean by 1) surface water inflow and 2) Atlantic-Mediterranean atmospheric pressure gradients. Our data suggest that the mechanism(s) responsible for sub-Milankovitch and millennial scale climate oscillations were the same over at least the past 2.6 Ma, notwithstanding the transition from the late Pliocene 41-kyr dominated glacial cycles to the 100-kyr cycles of the late Pleistocene.

### 3.1. Introduction

Northern Hemisphere ice sheets are unstable and have oscillated on Milankovitch to millennial time scales throughout the late Pliocene and Pleistocene. Millennial-scale changes are most prominently reflected in North Atlantic sea surface and Greenland air temperature proxy records. These records reveal distinct oscillations on time scales of 1–3 kyr during the last glacial maximum, termed Dansgaard-Oeschger (D-O) cycles, which culminated in large-scale ice rafting events known as Heinrich (H) events [Heinrich 1988; Bond 1992; Broecker 1992; Bond *et al.*, 1993; Dansgaard *et al.*, 1993; Bond *et al.*, 1999]. Climate fluctuations associated with D-O cycles and H events are found in climate archives all over the world [Leuschner and Sirocko 2000; Voelker *et al.*, 2002]. The leading hypothesis links the cold phases of the D-O cycles and H events to a collapse of the Northern Hemisphere ice sheets, resulting in the injection of large volumes of meltwater to the source regions of North Atlantic Deep Water (NADW) formation. Subsequently, lowered surface water salinities lead to a reduction of the deep convection and hence a slowdown of the global thermohaline circulation (THC) [Broecker 1997] accounting for lower temperatures at high latitudes. The forcing of H events is controversial. Some authors relate H events to internal ice sheet oscillations forced by the interaction of large ice sheets with underlying bedrock [MacAyeal 1993; Alley and MacAyeal 1994]. However, the presence of D-O and H-like fluctuations at times without large Northern Hemisphere ice sheets (e.g., during the ‘stable’ Holocene; [Marchitto *et al.*, 1998], during the smaller obliquity-dominated glacial cycles of the late Pliocene – middle Pleistocene [Raymo *et al.*, 1998; McIntyre *et al.*, 2001], or before 2.7 Ma [Ortiz *et al.*, 1999; Kleiven *et al.*, 2002] argue against this binge-purge hypothesis. It was therefore supposed that the D-O climate perturbations are persistent in the Earth’s climate, probably triggered by changes in solar activity [Bond *et al.*, 2001] and amplified in the presence of large ice sheets [Raymo *et al.*, 1992; Wara *et al.*, 2000; McIntyre *et al.*, 2001]. Furthermore, modeling experiments [Clement *et al.*, 1999; Schmittner and Clement 2002] and tropical paleoclimate records [Peterson *et al.*, 2000; Dannenmann *et al.*, 2003] suggest that millennial-scale climate variability could be driven by low-latitude rather than high-latitude forcing mechanisms, including strong atmosphere–ocean feedbacks, such as changes in the equatorial wind system equivalent to long-term changes in El Niño - Southern Oscillation (ENSO), changes in the intensity of the Inter Tropical Convergence Zone (ITCZ) or monsoon variability [Stott *et al.*, 2002].

A key region to study the influence of D-O cycles and H events at mid to low-latitudes is the Mediterranean. Proxy data from the western Mediterranean reveal distinct short-term changes in sea surface temperature (SST) and deep water formation that are closely related to the D-O cycles and H events of the past 50 kyr [Rohling *et al.*, 1998; Asioli *et al.*, 1999; Cacho *et al.*, 1999; Cacho *et al.*, 2000]. These rapid changes in Mediterranean hydrography and THC are partly attributed to the direct influence of the in-flowing Atlantic surface waters as well as by an atmospheric connection with the

North Atlantic climate system, both of which were controlled by the rapid oscillations in the Arctic-Greenland ice cap. Mediterranean pollen and African dust records, on the other hand, suggest a link between Mediterranean continental aridity and dust transport from the African continent and thus a low-latitude climate connection [Cacho *et al.*, 2000; Cacho *et al.*, 2001; Combourieu-Nebout *et al.*, 2002; Sanchez-Goni *et al.*, 2002; Moreno *et al.*, 2004].

Similar rapid changes in Mediterranean SST, THC and African dust supply were evidenced within marine oxygen isotope stage 100 (MIS100; ~2.52 Ma) of the marine successions of the Monte San Nicola (SN) section (Sicily, Italy) and Ocean Drilling Program (ODP) Site 967 (eastern Mediterranean) and a comparable climate mechanism was inferred (Chapter 2). In particular, rapid fluctuations of the abundance of the planktonic foraminifer *Neogloboquadrina atlantica* and  $\delta^{18}\text{O}$  are very similar to those observed in late Pleistocene records, suggesting that D-O and H-like climate variability occurred in the central Mediterranean during MIS100. Here, we present new proxy data from North Atlantic ODP Site 981 and Deep Sea Drilling Program (DSDP) Site 607 at the northern and southern boundary of the North Atlantic ice-rafting belt, respectively [Ruddiman *et al.*, 1989]. These records were used to evaluate North

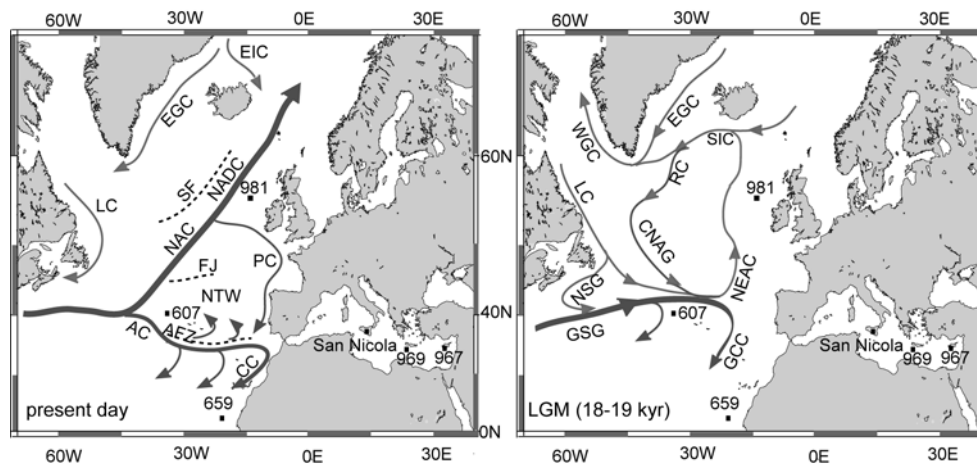


Figure 3.1: Location map of ODP Site 981, DSDP Site 607, Monte San Nicola section and ODP Site 967. Arrows indicate North Atlantic surface water masses: a) AC – Azores current; CC – Canary current; NTW – North Atlantic transitional waters; NAC – North Atlantic current; PC – Portugeses current; EIC – East Island current; EGC - East Greenland current; LC – Labrador current. Dashed lines indicate frontal zones: AFZ – Azores Frontal Zone; SF – Subpolar Front; FJ – Frontal Jets. b) reconstruction of North Atlantic surface circulation during the LGM (18-19 kyr) redrawn from Robinson *et al.*, [1995]: GSG – Glacial subtropical gyre; GCC – Glacial Canary current; NSG – Nova Scotia Current; LC – Labrador Current; CNAG – Central North Atlantic gyre; NEAC – North East Atlantic current; RC – Reykjaenes current; EGC – East Greenland current; WGC – West Greenland current; SIC – South Iceland current.

Atlantic ice-rafting history and open ocean climate variability and to unravel the origin of the rapid climate and paleoceanographic fluctuations in the Mediterranean during MIS100.

### 3.2. Materials and Methods

DSDP Leg 94 Site 607 (32°58'W 41°00'N) is situated on the western flank of the Mid-Atlantic-Ridge at a depth of 3427 m. Surface waters are under the influence of the North Atlantic drift on the northern limb of the sub-tropical gyre (Figure 3.1). During past glacial stages, this site was positioned on the southern margin of the IRD belt and was sensitive to both the extent of global ice volume and the strong meridional heat transfer from the equatorial region [Ruddiman *et al.*, 1986]. Today, deep water at this site is predominantly North Atlantic Deep Water (NADW), whereas during glacial periods of the late Pliocene and Pleistocene benthic foraminiferal  $\delta^{13}\text{C}$  values indicate the presence of a lower  $\delta^{13}\text{C}$  water mass [Raymo *et al.*, 1989; Raymo *et al.*, 2004].

ODP Leg 162 Site 981 (55°28'N, 14°39'W) is located east of the Rockall Bank on the Feni Drift at a depth of 2173 m. At present, deep water at this site is a combination of lower NADW, re-circulated from the southern part of the North Atlantic, and a small component of water overflowing the Wyville-Thompson Ridge (Wyville-Thompson Ridge Overflow Water; WTRO) [Schmitz and McCartney 1993]. Similar to Site 607, benthic foraminiferal  $\delta^{13}\text{C}$  values indicate the presence of a low  $\delta^{13}\text{C}$  water mass during glacial periods, possibly modified WTRO [Raymo *et al.*, 2004].

MIS95-101 were originally defined at Site 607 [Raymo *et al.*, 1989] and can be easily recognized in Site 981 based on paleomagnetic, calcareous nannofossil and planktonic foraminiferal datums [Channell and Lehman 1999; Flower 1999]. MIS100 appears as a dark interval in the cores and is characterized by distinct short-term color changes (Figures 3.2 and 3.3). MIS100 of Site 607 was sampled in a continuous interval of core sections 607-12H-3-71 cm to 12H-4-149 cm (106.90-109.18 mcd) with 10 cc samples being taken every 2 cm from this interval. Dry bulk density was calculated by weighing samples before and after drying at 50°C. Sub-samples for stable isotope measurements and lithic components counting were taken from the dried samples and washed through 37, 63, 125 and 600  $\mu\text{m}$  meshes each fraction as weighed.

MIS100 of Site 981 was sampled following the composite depth profile (Scientific Shipboard Party, [Jansen *et al.*, 1996a; 1996b]) every 5 cm in the interval 981C-17H-4-46 cm to 17H-5-115 cm and 981B-18H-3-52 cm to 135 cm (169.94-174.53 mcd) with an overlap of 30 cm between Hole C and B. Samples were freeze-dried and washed through 63, 150 and 60  $\mu\text{m}$  meshes and the residuals of each fraction weighed.

The planktonic foraminiferal stable isotope measurements of Site 607 were carried out on about 30 specimens of the species *Globigerinoides ruber* (white) that were hand-picked from a split of the >212  $\mu\text{m}$  size fraction. The analysis was done at the Department of Earth Sciences (Utrecht University), where an ISOCARB common bath carbonate

preparation device is linked to a VG SIRA24 mass spectrometer. Isotope values were calibrated to the Pee Dee Belemnite (PDB) scale using an in-house carbonate standard (NAXOS). Analytical precision was determined by replicate analyses and by comparison to the international IAEA-CO1 and NBS19 standard. Replicate analyses showed standard deviations of  $\pm 0.06\%$  and  $\pm 0.1\%$  for  $\delta^{13}\text{C}$  and  $\delta^{18}\text{O}$ , respectively.

The benthic foraminiferal stable isotope analyses of Sites 607 and 981, were carried out on 2-4 specimens of the species *Cibicidoides wuellerstorfi* that were hand-picked from the  $>212\ \mu\text{m}$  fraction. Stable isotope measurements were done at the faculty of Earth and Life Sciences (Amsterdam Free University) where a CARBO-KIEL automated carbonate preparation device is linked to a FINNIGAN MAT 251 mass spectrometer. Replicate analysis and calibration to the international carbonate standard NBS19 and in-house standard revealed analytical precision better than  $\pm 0.05\%$  and  $\pm 0.1\%$  for  $\delta^{13}\text{C}$  and  $\delta^{18}\text{O}$ , respectively. *Cibicidoides wuellerstorfi* oxygen isotope values have been adjusted by  $+0.64\%$  in order to be in equilibrium with ambient sea water [Shackleton and Opdyke 1976; Shackleton and Hall 1984].

Lithic grains were counted in the fraction  $125\text{-}600\ \mu\text{m}$  and  $150\text{-}600\ \mu\text{m}$  in Sites 607 and 981, respectively. Dark and light particles at Site 607 were counted separately; the “dark” particles include sharp-edged rock fragments, single mineral grains and transparent rounded quartz grains. The “light” grains are soft carbonate agglomerates containing occasional foraminifera. Lithic particles at Site 981 include sharp-edged rock fragments, single mineral grains, transparent quartz grains and traces of carbonates, hematite-coated grains and volcanic components.

Grayscale measurements were carried out on digital scans of the Site 607 black and white core photographs using the Scion Image 4.0 freeware image analysis software. Artificial color changes related to small cracks in the sediment and other disturbances were manually removed from the color profile. The color reflectance of Site 981 was measured at Bremen core repository on the archive-half of core 981C-17H-4-46 cm to 17H-5-115 cm and 981B-18H-3-52 cm to 135 cm (169.94-174.53 mcd) every centimeter following the composite depth profile (Scientific Shipboard Party, [Jansen et al., 1996a;1996b]) using a hand-held Minolta CM 503i spectrophotometer.

Lastly, foraminifers were counted at Site 607 in the interval between 12H-3-87 cm and 12H-4-85 cm (107.06-108.54 mcd) with samples every 4 cm on average (32 samples in total). Faunal samples were split using an “Otto micro-splitter” until a total number of 200 to 300 planktonic foraminifers per sample was obtained. Only the temperature-sensitive species *Neogloboquadrina atlantica* (s), *Neogloboquadrina pachyderma* (d) and *Globigerinoides ruber* (white) were counted with respect to the total number of foraminifers per split. *N. pachyderma* was distinguished from *N. atlantica* by the typical flat initial spiral of the oldest chambers and the usually thicker wall structure. Moreover, *N. pachyderma* is predominantly dextral-coiled, while *N. atlantica* has an often extra-umbilical aperture and is predominantly sinistral-coiled (~95%).

### 3.3. Results

#### 3.3.1. Stable isotopes

The oxygen isotope values of *Cibicoides wuellerstorfi* ( $\delta^{18}\text{O}_{\text{benthos}}$ ) at Site 607 vary from  $\sim 3.3\text{‰}$  during MIS99 and MIS101 to maximum values of  $\sim 4.5\text{‰}$  during MIS100, a glacial-interglacial (G-I) difference of  $\sim 1.2\text{‰}$  (Figure 3.2). Three stadial intervals can be distinguished within MIS100 and labeled according to the Mediterranean benthic isotope chronology of this stage MIS100.6, MIS100.4 and MIS100.2 (Chapter 2). Whereas stadial MIS100.6 is only reflected by a small shoulder in the transition, stadials MIS100.4 and MIS100.2 reflect full glacial conditions. During interstadial MIS100.3,  $\delta^{18}\text{O}_{\text{benthos}}$  values decrease from the full glacial value of  $\sim 4.5\text{‰}$  to  $\sim 4.2\text{‰}$ . At Site 981,

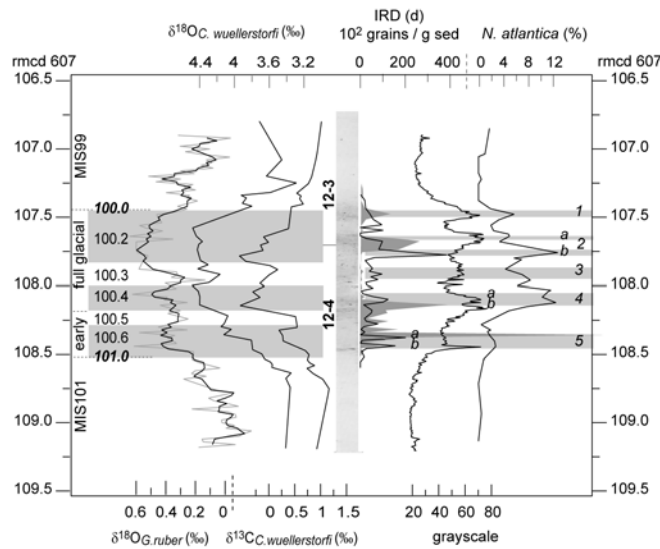


**Figure 3.2:** a) Planktonic and benthic oxygen isotope data and benthic carbon isotope data of DSDP Site 607 plotted versus revised meter composite depth (rmcd). Note that  $\delta^{18}\text{O}$  curves are plotted inversely. The  $\delta^{18}\text{O}_{\text{G.ruber}}$  curve (gray line) is overlain by a three point moving average (dark line). Stadial and interstadial phases within MIS100 are shaded and labeled by even numbers with early and full glacial phases being indicated on the left hand axis. b) Black and white core photograph of core 12-3 (7-150 cm) and 12-4, dark (dark line) and light (filled gray line) lithic particle counts, grayscale measurements and *N. atlantica* percentages. Intervals with high amount of IRD are shaded and labeled from 1-5.

interglacial ( $\sim 3.4\text{‰}$ ) and glacial ( $\sim 4.8\text{‰}$ )  $\delta^{18}\text{O}_{\text{benthos}}$  values are slightly heavier by  $\sim 0.2\text{‰}$  and  $\sim 0.4\text{‰}$  than at Site 607 (Figure 3.3), with G-I of  $\sim 1.4\text{‰}$ . Only stadials MIS100.4 and MIS100.3 are clearly defined in Site 981, and intervening interstadial MIS100.3 is marked by a severe drop in  $\delta^{18}\text{O}_{\text{benthos}}$  values by  $\sim 0.6\text{‰}$  (from  $\sim 4.8\text{‰}$  to  $\sim 4.2\text{‰}$ ). This interval falls into the 30 cm overlap between Hole C and B of Site 981.

The planktonic oxygen isotope ( $\delta^{18}\text{O}_{\text{G.ruber}}$ ) values of Site 607 are  $\sim 0\text{‰}$  in the interglacial and  $\sim 0.6\text{‰}$  in the glacial (Figure 3.2). Superimposed on the long-term glacial-interglacial change, oxygen isotope values fluctuate by  $\sim 0.4\text{‰}$ ,



indicating short-term changes in temperature and/or salinity within both the glacial and interglacial periods.

The benthic carbon isotope record ( $\delta^{13}\text{C}_{\text{benthos}}$ ) of Site 607 depicts a strong negative correlation to the  $\delta^{18}\text{O}_{\text{benthos}}$ . Interglacial  $\delta^{13}\text{C}_{\text{benthos}}$  values average 1‰ while glacial values vary between  $\sim 0.5\text{‰}$  and  $\sim -0.5\text{‰}$  exhibiting lowest  $\delta^{13}\text{C}_{\text{benthos}}$  values during the three stadial periods (Figure 3.2). The  $\delta^{13}\text{C}_{\text{benthos}}$  values of Site 981 are on average 0.2‰ more negative than at Site 607 being 0.8‰ in the interglacial and between  $\sim 0.4\text{‰}$  and  $-0.75\text{‰}$  in the glacial (Figure 3.3). The  $\delta^{13}\text{C}_{\text{benthos}}$  record of Site 981 shows more frequent and higher

amplitude variability during MIS100 (and MIS101 and MIS99) than that of Site 607, although it contains only four more data points within MIS100 ( $\sim 31$  at Site 981 versus 27 at Site 607). Clearly, at least five episodes with negative  $\delta^{13}\text{C}$  excursions occur during MIS100 and one at the MIS100/MIS99 and MIS101/MIS100 transitions (Figure 3.3): one of these depletions occurs at the base of MIS100, one in MIS100.4, one in MIS100.3, and two occur within MIS100.2. The smaller fluctuations in  $\delta^{13}\text{C}_{\text{benthos}}$  during MIS100.3 are related to small differences in  $\delta^{13}\text{C}_{\text{benthos}}$  values between samples from Hole C and B of Site 981.

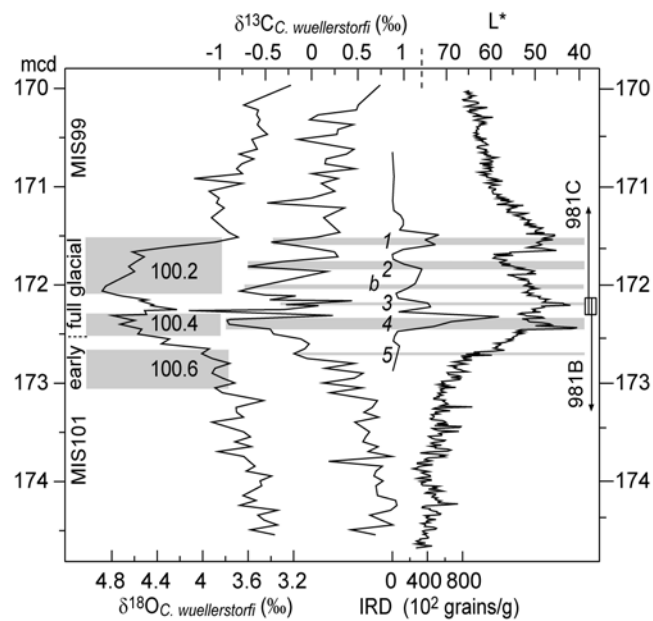


**Figure 3.3:** a) Benthic oxygen, carbon isotope, IRD and color reflectance ( $L^*$ ) data of ODP Site 981 plotted versus meter composite depth (mcd). Note that  $L^*$  and  $\delta^{18}\text{O}$  are plotted inversely.  $\delta^{18}\text{O}$  is plotted on the same scale as in Figure 3.2a. The early and full glacial phases are indicated on the left hand axis, light shaded areas and labels indicate stadials and intervals of low  $\delta^{13}\text{C}_{\text{benthos}}$  are shaded dark. The overlap between Holes C and B of Site 981 is indicated on the right axis.

### 3.3.2. Colour reflectance, lithic grain and faunal counts

The grayscale record of Site 607 shows five intervals (1-5) in MIS100 that exhibit a darker sedimentary color (Figure 3.2). These dark-colored intervals contain high concentrations of lithic particles  $>150\ \mu\text{m}$ . Comparison of dark (black line) and light

(grey shaded) particle numbers with the grayscale record reveals that both signals contribute to the lightness variations, although they do not peak simultaneously. One distinctive dark lithic particle abundance increase occurs below the second youngest dark layer, which is not reflected in the grayscale (labeled as 2b). We interpreted the darker layers and associated enhanced lithic components at Site 607 as representing the episodic input of ice rafted debris (IRD), although it is yet not clear whether the light-colored fragments are also IRD, because the softness and agglomeration character as well as the inclusion of small foraminifers may indicate that these particles are either a product of biological (fecal) pellets or of in-situ calcium carbonate dissolution. In particular, high numbers of light-colored particles correlate with the most severe  $\delta^{13}\text{C}$  depletions, which may indicate carbonate dissolution due to the presence of more corrosive bottom waters. The foraminiferal tests, however, do not show any sign of carbonate dissolution, which could indicate that the light-colored particles are the result of the agglomeration of fine carbonate particles by burrowing organisms.

Concentrating on the dark lithic group, which is clearly related to IRD reveals that the darker intervals of in particular events 5, 4 and 2 consist of multiple ice rafting episodes (Figure 3.2). This interpretation is strengthened by the peak occurrences of *Neogloboquadrina atlantica*, coincident with these five main and 3 minor IRD events. *N. atlantica* is an extinct species that was endemic to high-latitude North Atlantic cold surface water environments during late Miocene to Pliocene [Poore and Berggren 1975; Raymo et al., 1986; Meggers and Baumann 1997]. Biometric data shows that in the North Atlantic *N. atlantica* adapted selectively to the global late Neogene cooling and, therefore, was suggested to be temperature-sensitive [Meggers and Baumann 1997]. Although *N. atlantica* was classified as a subpolar species it might present a cold water end-member for the late Pliocene similar to its modern relative *Neogloboquadrina pachyderma* (sinistral) [Raymo et al., 1986; Meggers and Baumann 1997].

Similar, dark IRD-rich horizons at Site 981 coincide with the six episodes of low  $\delta^{13}\text{C}_{\text{benthos}}$  values (Figure 3.3). The second and third youngest depletion in  $\delta^{13}\text{C}_{\text{benthos}}$  are characterized by one single IRD event, probably due to the poor sample resolution (15 cm) in this interval. In addition, the IRD variability at Site 981 seems less frequent than at Site 607, which is due to the lower resolution of lithic counts at Site 981 (half that of Site 607).

### 3.3.3. Correlation between Atlantic and Mediterranean $\delta^{18}\text{O}$ records

For the studied interval of Sites 981 and 607 a time scale was constructed using the visual correlation between  $\delta^{18}\text{O}_{\text{benthos}}$  records of these sites and that of the Mediterranean SN section. This resulted in an astronomically-tuned age model for all

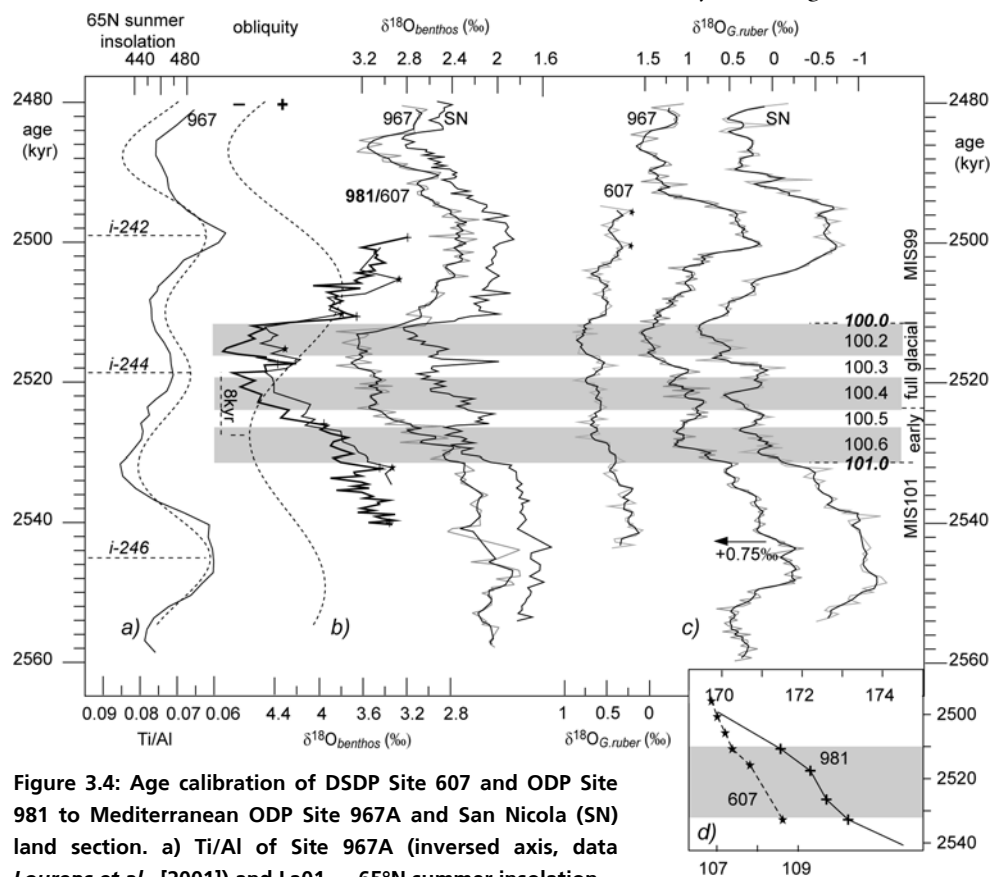


**Figure 3.4:** Age calibration of DSDP Site 607 and ODP Site 981 to Mediterranean ODP Site 967A and San Nicola (SN) land section. a) Ti/Al of Site 967A (inversed axis, data Lourens *et al.*, [2001]) and La01(1,1) 65°N summer insolation (stippled line). The *i*-cycles on the left age axis indicate numbering of insolation maxima according to Lourens *et al.*, [1996]. b)  $\delta^{18}\text{O}_{\text{benthos}}$  of Site 981 (thick line), Site 607, Site 967A (gray line overlain by 3pt moving average) and SN in relation to La04(1,1) obliquity (stippled line). All  $\delta^{18}\text{O}_{\text{benthos}}$  data are plotted on the same scale (inverse axis). Stars (Site 607) and crosses (Site 981) indicate age calibration points. Arrows indicate equivalent age points in SN and Site 967. c)  $\delta^{18}\text{O}_{\text{G.ruber}}$  of Site 607, Site 967A and SN each overlain by a 3pt moving average. Notice that the  $\delta^{18}\text{O}_{\text{G.ruber}}$  of Site 967 has been shifted by 0.75‰ towards heavier values and notice different scale for  $\delta^{18}\text{O}_{\text{G.ruber}}$  of Site 607. Shaded areas and even labels indicate stadials according to Chapter 2. The early and late glacial are indicated on the left age axis. d) Age-depth (kyr-mcd) relation for Site 607 (stars) and Site 981 (crosses). Ages are linearly interpolated between calibration points. The shaded interval indicates MIS100.

sites, because SN was tied to Site 967 (*Chapter 2*), which in turn has been tied directly to the La2001<sub>(t,1)</sub> astronomical solution by tuning the Ti/Al record to the 65°N summer insolation curve [Lourens *et al.*, 2001]. Six tie-points were set to calibrate Site 607 to the  $\delta^{18}\text{O}_{\text{benthos}}$  of SN (Figure 3.4): one at each glacial-interglacial transition, one within MIS100.3, one just above MIS100.0 and two, which tie the  $\delta^{18}\text{O}_{G.\text{ruber}}$  record of Site 607 to the  $\delta^{18}\text{O}_{G.\text{ruber}}$  of SN. Linear interpolation was applied between the age points resulting in average sedimentation rates of 4.7 cm/kyr in MIS99, 6 cm/kyr in MIS100 and 3.4 cm/kyr in MIS101.

Four tie-points were used to correlate Site 981 to SN, with linear interpolation applied in between: one at each glacial-interglacial transition, one in MIS100.4 and one in MIS100.3. This results in an average sedimentation rate of 8.7 cm/kyr during MIS100. Ages for interglacial MIS99 and MIS101 were calculated assuming average sedimentation rates of 13.7 cm/kyr and 17.3 cm/kyr, respectively. These sedimentation rates were achieved by comparing our high-resolution  $\delta^{18}\text{O}_{\text{benthos}}$  data of Site 981 with lower-resolution (unpublished)  $\delta^{18}\text{O}_{\text{benthos}}$  data of MIS104-95 from the same site and tying minimum  $\delta^{18}\text{O}_{\text{benthos}}$  during MIS101 and MIS99 to minimum  $\delta^{18}\text{O}_{\text{benthos}}$  values of Site 967 during these interglacials, respectively.

The Mediterranean and Atlantic benthic oxygen isotope records display the typical asymmetric structure of a slow glacial build-up and a rapid termination (Figure 3.4) that was observed for other late Pliocene and Pleistocene glacial cycles [Raymo 1992]. Small offsets in the  $\delta^{18}\text{O}_{\text{benthos}}$  values between the various sites probably indicate differences in ambient bottom water temperature and salinity with SN being the warmest and shallowest site. The sharp decrease in  $\delta^{18}\text{O}_{\text{benthos}}$  associated with the MIS100/MIS99 transition corresponds with a 0.8‰ drop in all four  $\delta^{18}\text{O}_{\text{benthos}}$  records reflecting global ice volume change. The well defined MIS100.3 (interstadial phase) and MIS100.4 and MIS100.2 (stadial phases) of SN are clearly expressed in Sites 607 and 981, but not in Site 967, while MIS100.6 and MIS100.5 are not well expressed in either the Atlantic or Site 967  $\delta^{18}\text{O}_{\text{benthos}}$  records.

The  $\delta^{18}\text{O}_{G.\text{ruber}}$  records of Site 607, Site 967 and SN show very similar patterns. Stadial and interstadial phases as defined in the Mediterranean  $\delta^{18}\text{O}$  record are clearly reflected in the  $\delta^{18}\text{O}_{G.\text{ruber}}$  record of Site 607, although the amplitude of changes at Site 607 are half that of the Mediterranean records. This difference may be due to the low temperature tolerance of *G. ruber*, which calcifies at optimum temperature [Schmidt and Mulitza 2002] and, therefore, could have biased the  $\delta^{18}\text{O}_{G.\text{ruber}}$  record towards warmer temperature.

### 3.3.4. Timing of stadial-interstadial alternations and IRD events

The new time scale for Sites 981 and 607 reveals that each stadial-interstadial couplet had a duration of 6–8 kyr (Figure 3.4). The mechanism causing this regular alternation of stronger and weaker glacial conditions seems to have affected SST and/or sea surface salinity (SSS) conditions at Site 607 during interglacial periods as well, as evidenced by changes in the  $\delta^{18}\text{O}_{\text{G.rubber}}$  record of this site with approximately the same rate of recurrence.

The relative abundance pattern of *N. atlantica* at Site 607 and SN are in general similar,

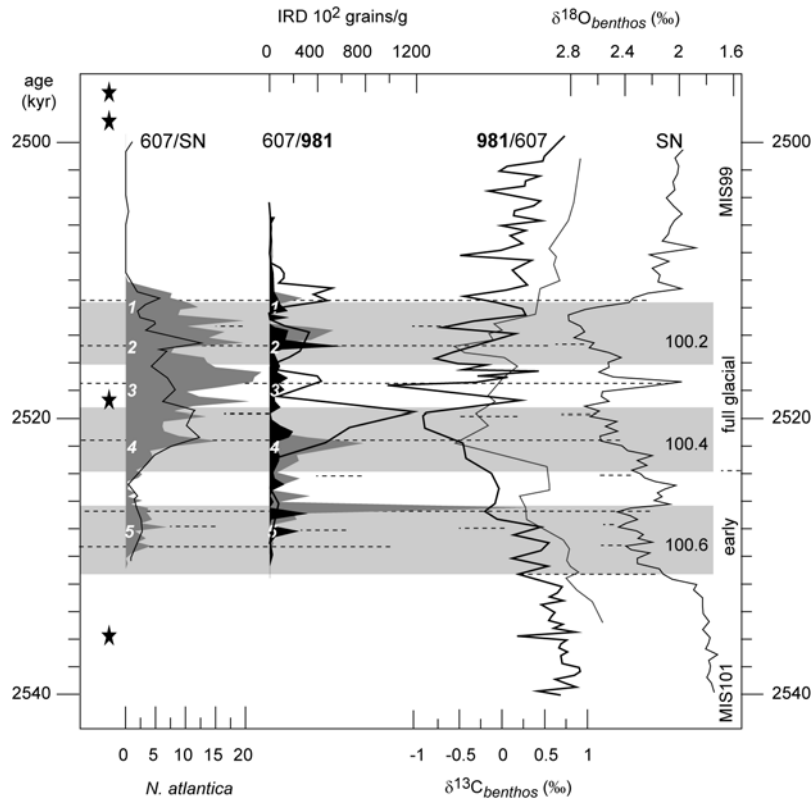


Figure 3.5: *Neogloboquadrina atlantica* percentages of Site 607 (black line) and SN (shaded), IRD of Site 607 (dark particles are shaded dark-gray, light particles are shaded light-gray, respectively) and Site 981 (thick line),  $\delta^{13}\text{C}_{\text{benthos}}$  Site 981 (thick line) and Site 607 and  $\delta^{18}\text{O}_{\text{benthos}}$  of San Nicola versus age (kyr). The IRD record of Site 607 is stretched by a factor 2 to match the IRD record of Site 981. Stippled lines and numbers indicate spacing of the events. Shaded areas and even labels indicate stadials. Early and full glacial are indicated on the left age axis. Stars on the left axis indicate the occurrence of *Globorotalia menardii*.

corresponding to IRD peaks and  $\delta^{13}\text{C}_{\text{benthos}}$  minima in both North Atlantic sites (Figure 3.5). Although *N. atlantica* was counted at lower resolution in Site 607, major *N. atlantica* peaks (1-5 including multiple peaks during 4a,b and 2a,b) are reflected in both records. The spacing of events is in the order of 3-4 kyr for major events 1-5 and approximately 1.5-2 kyr for the less distinct events 5a,b, 4a,b and 2a,b. IRD events 1-5 occur at the MIS100/MIS99 transition and within the stadials and interstadial MIS100.3, respectively. This short-term pulsating character of the IRD events in the North Atlantic cores is less evident during MIS100.5, although the IRD record of Site 607 shows some minor IRD peaks within this period. During MIS100.3, *N. atlantica* reached highest percentages in the Mediterranean corresponding with the most depleted  $\delta^{13}\text{C}_{\text{benthos}}$  values at Site 981, but with a less marked IRD event and with the temporal occurrence of *Globorotalia menardii* at Site 607 (Figure 3.5).

### 3.4. Discussion

#### 3.4.1. Sub-Milankovitch climate variability during MIS100

Millennial-scale changes in IRD abundance, *N. atlantica* percentages and  $\delta^{13}\text{C}_{\text{benthos}}$  values within MIS100 indicate that North Atlantic climate was not stable, but underwent brief reorganizations in SST, ice distribution and THC. The 1.5 to 4-kyr spacing between these rapid changes is very similar in nature and duration to the Pleistocene D-O cycles. Peak abundance of *N. atlantica* at Site 607 during MIS100 are, therefore, considered to reflect similar climatic conditions as those of *N. pachyderma* (s) during the early and late Pleistocene, which have been unambiguously correlated to the cold phase of the D-O oscillations and H events [Bond 1992; Bond et al., 1993; Raymo et al., 1998; Bond et al., 1999]. In addition, the concomitant peak occurrences of *N. atlantica* in both SN and Site 607 indicate that Mediterranean surface waters varied on the same D-O scale. This resembles the pattern of the late Pleistocene, where peak abundances of *N. pachyderma* (s) in the western Mediterranean are related to the D-O cycles and H events [Rohling et al., 1998; Cacho et al., 2000].

In addition, the stadial-interstadial  $\delta^{18}\text{O}_{\text{benthos}}$  changes during MIS100 indicate that the climate conditions in the Mediterranean and adjacent Atlantic have changed on a time scale in between the D-O and Milankovitch periods. Stadial-interstadial alternations in the  $\delta^{18}\text{O}_{\text{benthos}}$  of SN were shown to vary in parallel to SST changes with slow cooling during stadials followed by abrupt warming at the stadial/interstadial boundary (Chapter 2). Hence, the correlation between these abrupt warming events in the SN record and the major IRD events 1, 3 and 5 in the North Atlantic in combination with an average spacing of these events of 6 to 8 kyr strongly suggests that these stadial-interstadial alternations represent climate changes similar to the so-called late Pleistocene Bond-cycles. The IRD events 1, 3 and 5 are then related to the terminal phases of these cycles and would be equivalent to the Heinrich events.

### 3.4.2. North Atlantic – Mediterranean climate linkages

Today, the relatively warm water masses of the North Atlantic Current (NAC) and the North Atlantic Drift Current (NADC) (Figure 3.1a) are responsible for the mild climate in Europe by bringing warm moist air across the European continent [Otterman *et al.*, 2002]. This mechanism has probably been activated by the initiation of the Labrador current during Middle Pliocene [Spaak 1983]. Since this time changes in the position of the NADC may have caused significant latitudinal alteration in the climate zones of Western Europe on all time scales [Otterman *et al.*, 2002]. During the last glacial maximum (LGM), the frontal systems were displaced southwards in the presence of glaciers and sea ice (Figure 3.1b), leading to a North Atlantic surface circulation pattern, which consisted of two main gyre systems (Figure 3.1b, redrawn after Robinson *et al.*, [1995]): the warm, sluggish Central North Atlantic Gyre (CNAG) north of  $\sim 40^\circ\text{N}$  and the Glacial Subtropical Gyre (GSG) south of  $\sim 40^\circ\text{N}$  [Robinson *et al.*, 1995; Seidov and Maslin 1999]. This configuration resulted into large-scale cooling of the European continent [Samthein *et al.*, 1995; Cortijo *et al.*, 1997], delivery of IRD to the Gulf of Cadiz [Bard *et al.*, 2000], inflow of cold Atlantic surface water into the Mediterranean [Asioli *et al.*, 1999; Cacho *et al.*, 1999] and D-O-related SST and THC changes in the Alboran and Ligurian Seas [Rohling *et al.*, 1998; Cacho *et al.*, 2000; Cacho *et al.*, 2001; Combourieu-Nebout *et al.*, 2002].

It has been well documented that Mediterranean SST conditions varied in phase with the obliquity-controlled global ice volume changes and North Atlantic climate throughout the late Pliocene and early Pleistocene [Zachariasse *et al.*, 1990; Lourens *et al.*, 1992; Versteegh 1997]. The strongest evidence is given by the synchronous occurrence of *N. atlantica* and *Neogloboquadrina pachyderma* (s) in the Mediterranean and the Atlantic Site 607 during glacial stages 110–96 and 64–34, respectively [Zachariasse *et al.*, 1990; Lourens *et al.*, 1992; Lourens *et al.*, 1996; Lourens and Hilgen 1997; Lourens *et al.*, 1998]. The appearance of these species in the Mediterranean was linked to the inflow of cold (high-latitude) Atlantic surface waters through the Strait of Gibraltar [Spaak 1983]. Pollen data further indicate that with the extension of glaciers and sea ice in the Northern Hemisphere, polar air masses expanded southward and cooled the European continent during MIS100 [Willis *et al.*, 1999] and subsequent glacial stages [Combourieu-Nebout 1991]. A more southerly position of the polar front during MIS100 is also evidenced by perennial sea ice cover in the Norwegian Greenland Sea (NGS) [Henrich *et al.*, 2002]. The very depleted  $\delta^{13}\text{C}_{\text{benthos}}$  values at Site 981 during MIS100 may confirm episodes of extensive sea ice formation in the NGS since depleted  $\delta^{13}\text{C}_{\text{benthos}}$  values have been related to increased influxes of WTRO, which is formed in the NGS by brine formation under sea ice [Dokken and Jansen 1999; Raymo *et al.*, 2004].

The synchrony between peak occurrences of *N. atlantica* in the Mediterranean and adjacent North Atlantic suggests that short-term recurrent pulses on millennial time scales superimposed the southward extension of Atlantic polar waters during MIS100.

In addition to the direct inflow of colder Atlantic surface waters, a strengthening and northward displacement of the north-westerlies may have favored prolonged winter anticyclone stability over central and northern Europe. This would have resulted in a strong southward flow over the Mediterranean region and very cold and dry Mediterranean winters [Cacho *et al.*, 2000; Cacho *et al.*, 2001; Combourieu-Nebout *et al.*, 2002; Sanchez-Goni *et al.*, 2002; Moreno *et al.*, 2004]. The inferred cold air outbreaks from the European continent during winter should have enhanced surface water cooling and vertical convection and facilitated the peak occurrences of *N. atlantica* and

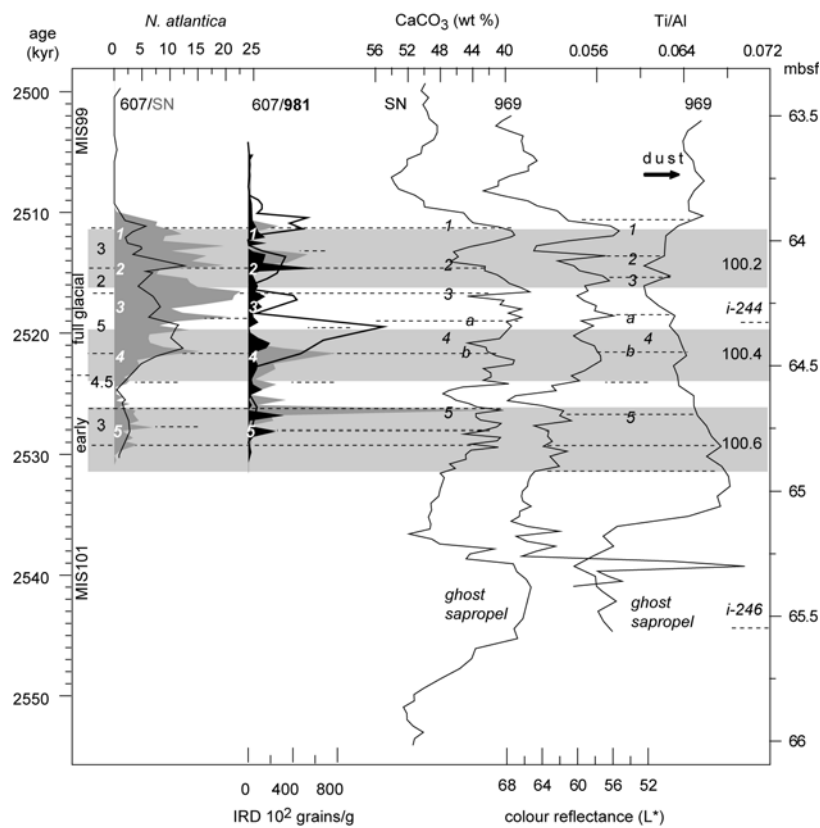


**Figure 3.6:** *Neogloboquadrina atlantica* percentages of Site 607 (black line) and SN (shaded), IRD of Site 981 (thick line) and Site 607 (dark particles are shaded dark-gray, light particles are shaded light-gray, respectively) and  $\text{CaCO}_3$  weight percentages of SN versus age (kyr). The IRD record of Site 607 is stretched by a factor 2 to match the IRD record of Site 981. The IRD event 1-5 are plotted in italics. Stippled lines and numbers on the left axis indicate the spacing of IRD events. Further labeling according to Figure 3.4. Color reflectance ( $L^*$ ) and Ti/Al of Site 969 (data Wehausen, 1999) versus meter below seafloor (mbsf). Dotted lines and italic numbers indicate IRD events 1-5 and related  $\text{CaCO}_3$  minima in SN. High Ti/Al values indicate high amounts of African dust (Chapter 2).



the cold water benthic species *Cibicides cf. ungerianus* and *Trifarina angulosa* at SN (*Chapter 2*).

A comparison between the abundance patterns of *N. atlantica* and IRD, and the northern African dust signal recorded by the bulk sediment composition of SN and Ti/Al record at ODP Site 969 in the central Mediterranean (*Chapter 2*) reveals that the cold episodes of the D-O-like cycles in the North Atlantic and Mediterranean coincide with enhanced dust supply from the African continent to the central Mediterranean (low CaCO<sub>3</sub> wt% and high Ti/Al values; Figure 3.6). This suggests that during these periods northern African climate was much drier and/or that the storm tracks responsible for the dust supply were intensified, which is in accordance with observations from the Alboran Sea during the last glacial [Moreno *et al.*, 2002]. There, intervals of high dust delivery from the African continent into the western Mediterranean are evidenced, which are contemporary to the high dust fluxes observed in the Greenland ice cores during cold D-O episodes. The similarity of both records suggests a strong atmospheric cross-latitudinal linkage and it was proposed that the pronounced equator-ward expansion of the polar regime during cold D-O and H episodes would have reduced the transfer of heat to the high latitudes, increased the meridional temperature gradient and hence affected the latitudinal trajectory of westerlies crossing the North Atlantic. Further to the south, channeling of the storm pathways and the strengthening of the high-pressure cell above the subtropical Atlantic may have caused an increase in the dust transport from the Saharan desert to the Mediterranean [Moreno *et al.*, 2002]. Such a scenario could also have been valid for MIS100.

### 3.4.3. Changes in thermohaline circulation

The waxing and waning of the Greenland-Arctic ice sheets could explain the strong climate linkages between the North Atlantic and Mediterranean regions on both Milankovitch (obliquity) and millennial (D-O) time scales of MIS100. To a high extent, such a mechanism could also explain the stadial-interstadial variability reflected in both the Mediterranean and the Atlantic  $\delta^{18}\text{O}_{\text{benthos}}$  records. For instance, the 0.3–0.6‰ drop during MIS100.3 could indicate that besides local changes in temperature and/or salinity a significant change in global ice volume may have occurred. Moreover, the asymmetric  $\delta^{18}\text{O}_{\text{benthos}}$  pattern associated with MIS100.3 is in good agreement with a fast waning and slower waxing of ice masses as predicted by ice sheet models [MacAyeal 1993]. The amplitude of the  $\delta^{18}\text{O}_{\text{benthos}}$  change during MIS100.3, however, is one-third to one-half the magnitude of the assumed  $\delta^{18}\text{O}_{\text{benthos}}$  G-I variation during MIS100, which would imply melting of large parts of the land-based ice-sheets within a few hundred years if this variability is attributed to ice volume changes alone.

Evidence that changes in ice sheet volume were probably not the only mechanism causing the stadial-interstadial variability in the  $\delta^{18}\text{O}_{\text{benthos}}$  records comes from the

$\delta^{18}\text{O}_{\text{G.rubber}}$  record of Site 607. This record reflects pervasive high-frequency variability also during MIS99 and MIS101 with similar amplitude as during MIS100. This may imply that changes in SST and SSS could have played a crucial role in changing the isotopic composition of the deep waters in the North Atlantic during full glacial conditions, probably through changes in the THC. Such a scenario is in agreement with the good correspondence between the stadial-interstadial variability and the  $\delta^{13}\text{C}_{\text{benthos}}$  record of Site 607. Low glacial  $\delta^{13}\text{C}_{\text{benthos}}$  values at Site 607 were interpreted to indicate the increased influence of Southern Ocean Water (SOW) [Raymo *et al.*, 1992], which has very depleted  $\delta^{13}\text{C}_{\text{benthos}}$  values, and the suppression of NADW, although the advection of waters from a northern source of which the  $\delta^{13}\text{C}$  composition is indistinguishable from SOW cannot be totally excluded [see also Raymo *et al.*, 2004]. Additional evidence for stadial-interstadial changes in THC may come from the  $\delta^{13}\text{C}_{\text{benthos}}$  record of ODP Site 658 (off northwest Africa) where despite the low sample resolution a  $\sim 0.6\%$  increase in the  $\delta^{13}\text{C}_{\text{benthos}}$  record is recorded approximately halfway through MIS100 [Tiedemann 1991]. This  $\delta^{13}\text{C}_{\text{benthos}}$  increase points towards a short interval of enhanced THC within MIS100, which is probably equivalent to the one observed during MIS100.3 at Site 607.

#### 3.4.4. On the origin of stadial-interstadial variability during MIS100

In contrast to Site 607, MIS100.3 at Site 981 is characterized by high abundances of IRD and minimum  $\delta^{13}\text{C}_{\text{benthos}}$  values, which were probably related to maximum influxes of WTRO, indicating extensive ice rafting and deep water formation in the NGS, and hence extremely cold climate conditions. This remarkable difference between Sites 981 and 607 is on the one hand related to the more complex oceanographically position of Site 981 and on the other hand to the time scale on which climate changes in these regions were fluctuating. At Site 607,  $\delta^{13}\text{C}_{\text{benthos}}$  primarily changed on stadial-interstadial time scales, whereas that of Site 981 is dominated by the D-O-type of climate variability. In the Mediterranean both types of climate variations interfere during MIS100.3 (Chapter 2). In conjunction with Site 981, a short interval of severe winter mixing in the central Mediterranean, indicated by the highest abundances of *N. atlantica* in the SN section, occurred within MIS100.3. This signal was linked to a cold phase of the D-O-type of climate variability, which interrupted a more humid period of precession-bound climate conditions in the Mediterranean, thereby transferring lowered SSS and  $^{18}\text{O}$  conditions to deeper waters and causing the characteristically depleted  $\delta^{18}\text{O}_{\text{benthos}}$  values at SN during MIS 100.3 (Chapter 2).

Additional evidence that the wetter climate conditions in the Mediterranean were coincident with warmer climate conditions at Site 607 during MIS100.3 comes from the appearance of *Globorotalia menardii* (Figure 3.4). This tropical-subtropical species [Hilbrecht 1996] also occurred during MIS99 and MIS101 and is an important marker species of the modern Azores Current (AC) [Ottens 1991]. The presence of *G. menardii*

at Site 607, therefore, suggests short influxes of tropical-subtropical waters during MIS100.3. At the same time the abundance of *N. atlantica* indicates cold (polar) water masses at Site 607, which seems to be at odds with the presence of *G. menardii*. Assuming a LGM-like surface water circulation in the North Atlantic, Site 607 would be positioned on the boundary between the relatively cold waters of the CNAG and the relatively warm waters of the GSC gyre system (Figure 3.1b). Therefore, the peak occurrence of *G. menardii* at Site 607 can be interpreted to present small changes in the position of the two gyre systems. Apparently, peak influxes of *G. menardii* at Site 607 indicate intervals of enhanced northward heat transport, which are accompanied by a rejuvenation of the THC during MIS100.3 as evidenced by the elevated  $\delta^{13}\text{C}_{\text{benthos}}$  values.

The peak influxes of *G. menardii* during MIS101-99 closely match the positions of precession minima taking into account the uncertainty of the age calibration at Site 607. Little is known about the positioning and strength of past North Atlantic surface currents in relation to precession forcing. *Spaak* [1983] indicated that the strength of the Canary current might have varied on a precession-scale during the late Pliocene, possibly related to the strength of the trade-winds. Direct evidence for variation in trade wind strength during MIS100 may come from the pollen data and terrigenous grain size measurements of ODP leg Site 658 [*Leroy and Dupont* 1994]. These records reveal that the observed increase in the  $\delta^{13}\text{C}_{\text{benthos}}$  record associated with MIS100.3 is accompanied by wetter climate conditions in Northwest Africa and decreased trade wind strength. Further evidence that the precession cycle may have played a critical role on the strength of the trade-winds during MIS100.3 comes from the n-alkane  $\delta^{13}\text{C}$  record of the South Atlantic ODP Site 1083 [*Denison et al.*, 2005]. This Southern Hemisphere mid-latitude record reflects relatively dry climate conditions (i.e., high contributions of C<sub>4</sub> plants and a high water stress of C<sub>3</sub> plants) during insolation cycle 244, which clearly point to an opposite precession-related signal on during insolation cycle 244 as observed in Northwest Africa. It was suggested that these climate conditions are triggered by reduced monsoonal precipitation in South West Africa and are independent of glacial-interglacial variability [*Denison et al.*, 2005]. Although the seasonal migration of the ITCZ may have had an important effect on African precipitation and the Atlantic atmospheric system on a precession scale, a causal link between the position of the ITCZ and Northern Hemisphere climate has yet not been made. We hypothesize that an increase in heat transport to the north during the precession minimum associated with MIS100.3 may have caused a sudden rejuvenation of the Atlantic's conveyor by bringing warm salty water to the north. Subsequently, melting of large ice sheets may have triggered massive iceberg discharge, which in turn reduced surface salinity conditions in the regions of deep-water formation, thereby shutting down or reducing the THC. Such an important feedback mechanism could be responsible for the cold (D-O) climate conditions observed at Site 981 and the central Mediterranean during MIS100.3.

Although minimum precession values may have played a critical role in triggering MIS100.3, a similar mechanism cannot have triggered MIS100.5. During MIS100.5, THC was most likely resumed after the first phase (MIS100.6) of ice sheet build-up during MIS100. Apparently, ice sheets were still not large enough to trigger massive iceberg discharge and hence North Atlantic and Mediterranean climate conditions returned to almost interglacial values. The apparent  $\sim 8$ kyr spacing between MIS100.5 and MIS100.3 may point to a possible influence of astronomically modulated zonal wind-driven divergence in the eastern equatorial Atlantic [McIntyre and Molino 1996] on THC changes during MIS100. McIntyre and Molino [1996] propose a mechanism analogous to a long-period El Niño when the tropical easterlies diminish, surface waters are released from the Caribbean and Gulf of Mexico warm pool into the western boundary current of the North Atlantic subtropical gyre and, subsequently, into the sub-polar Atlantic thereby producing the rapid melting of ice and hence Heinrich events. This modulation, which occurred on a period of 8.4 kyr over the past 45,000 years, is thought to be caused by the nonlinear response of climate to low-latitude insolation/precession forcing during minimum eccentricity, although it remains unclear why a periodicity of  $\sim 8.4$  kyr, which would require a rather unusual precession period, should be important during the past 45 kyr [Berger and Loutre 1997]. Nevertheless, the  $\sim 8$  kyr time spacing between MIS100.5 and MIS100.3, the apparent  $\sim 8$  kyr period in the  $\delta^{18}\text{O}_{\text{G.rubber}}$  record of Site 607, the minimum eccentricity values during MIS100 and the coincidence of MIS100.3 with a precession minimum are not in disagreement with such a hypothesis. Data from piston core SU90-03 [Chapman and Shackleton 1998] close to Site 607, indicate that during the past 45 kyr episodes of cold iceberg-laden waters alternate with the supply of warm saline waters from the sub-tropics. These changes that are similar to our data from MIS100 occur on a semi-precession to H-scale (5-8 kyr) and it was concluded that cross-equatorial heat transport is a major factor controlling surface oceanography of the mid-latitude North Atlantic [Chapman and Shackleton 1998].

In summary, our results unambiguously demonstrate that the Bond cycles and associated Heinrich events are an intrinsic part of the climate system throughout the late Pliocene and Pleistocene notwithstanding the transition from dominated 41-kyr to 100-kyr controlled glacial cycles. At the moment it remains unclear, whether part of the observed sub-Milankovitch climate variability is related to primary Milankovitch forcing and, especially, to precession forcing. A detailed comparison of our records with climate proxy records derived from equatorial regions or the Southern Hemisphere is needed to test further whether a nonlinear response to low latitude insolation/precession forcing could indeed explain the stadial-interstadial variability. This may give important constraints on current ideas about low-latitude versus high-latitude climate forcing of sub-Milankovitch climate cycles.

## **CHAPTER 4**

### **Redox conditions and dust deposition at San Nicola during MIS100: results from trace element and grain size analysis**

#### **Abstract**

High-resolution (350-500 yr) geochemical and grain size data is presented from Monte San Nicola (Sicily/Italy) during MIS101-99. Organic carbon mass accumulation rates and concentrations of redox-sensitive trace elements indicate increased primary productivity during precession minima, probably caused by the presence of a seasonal deep chlorophyll maximum. Grain size analysis and concentrations of lithogenic elements indicate intervals of large dust transport from the African continent to the Mediterranean that are linked to intensive ice rafting in the North Atlantic. These episodes vary on a Dansgaard-Oeschger scale superimposed on the primary Milankovitch frequencies.

## 4.1. Introduction

Late Neogene marine sediments of the Mediterranean have a characteristic chemical signature due to the cyclic occurrence of organic carbon ( $C_{\text{org}}$ )-rich layers in overall carbonate-rich marls and oozes. These  $C_{\text{org}}$ -rich layers called sapropel, sapropelics or sapropelites have in general high concentrations of organic carbon (between 0.5–10 weight %) and redox-sensitive and chalcophilic trace elements [e.g., *Nijenhuis, 1999*]. These high concentrations are usually assigned to intensified primary productivity in combination with enhanced preservation of organic material in a reducing water column or anoxic bottom water conditions. The formation of sapropels is associated with periods of enhanced river-runoff and circum-Mediterranean humidity [*Rohling and Hilgen, 1991*]. These conditions are generally linked to an intensified African monsoon circulation during precession minima [*Rosignol-Strick, 1983; 1985*], causing both a low salinity surface water lens in the eastern Mediterranean, surface water stratification and, consequently, the development of a (seasonal) deep chlorophyll maximum (DCM), which in turn stimulates enhanced primary productivity and stagnant bottom water conditions [*Rohling and Hilgen, 1991*].

The occurrence of sapropels increases during the short (~100 kyr) and long (~400 kyr) eccentricity maxima due to the orbital modulation of the precession cycle [*Hilgen, 1991a*]. Vice versa, there are several intervals in the sedimentary record without (distinct) sapropels, so-called thick homogenous intervals. These intervals are found in between the large-scale sapropel clusters and correspond to periods of low amplitude precession minima during 400-kyr eccentricity minima (*Chapter 1*). During these periods, precession forcing was not strong enough to initiate climate conditions favourable for sapropel formation. Nevertheless, precession-related changes in primary productivity [*Chapter 2; Lourens, et al., 1992*] and circum Mediterranean humidity [*Wehausen, 1999; Lourens, et al., 2001*] are recorded in these homogenous intervals indicating that these intervals may contain climate proxy records sensitive enough to trace minute changes in the climate state.

Here, we present the results of geochemical and grain size investigations of one of these thick homogenous intervals in the land-based marine succession of Monte San Nicola (SN) on Sicily in Italy. The interval studied comprises the obliquity-driven glacial-interglacial-glacial alternation of marine oxygen isotope stages 101–99 (MIS101–99) and is characterised by changes in sediment colour on both obliquity and sub-Milankovitch time scales (*Chapter 1*). In particular, the  $\text{CaCO}_3$  record of SN indicates episodes with low  $\text{CaCO}_3$  during MIS100 that are associated with cold (Dansgaard-Oeschger-like) intervals in the Mediterranean and ice rafting debris (IRD) events in the North Atlantic (*Chapter 3*). These rapid variations in sedimentary composition during MIS100 can be traced across the whole Mediterranean suggesting a climatic origin (*Chapter 1*). Comparison with the Ti/Al record of eastern Mediterranean ODP Site 969 proposes that these  $\text{CaCO}_3$  variations are related to episodes of enhanced African dust deposition

(Chapter 2). Notwithstanding the dominant imprint of the obliquity cycle on most of the proxy records investigated so far, a few planktonic and benthic foraminiferal species as well as the difference between the stable oxygen isotope composition of planktonic and benthic foraminifera points to a precession-controlled freshwater pulse, the development of a (seasonal) DCM and low low-oxygen bottom water conditions during MIS100 (Chapter 2).

First, we investigated the changes in organic carbon contents and concentrations of redox-sensitive major and minor trace elements to evaluate the importance of precession-related climate changes on the redox-state of the sediment during deposition of MIS101-99. Secondly, we further unravelled the relationship between low  $\text{CaCO}_3$  episodes in SN and African dust influxes on the obliquity and sub-Milankovitch time scales by investigating the element concentrations of lithogenic origin and grain size analysis. Finally, we compared both grain size and geochemical data with time-equivalent data of eastern Mediterranean ODP Site 969 and Site 967 (data of Wehausen, 1999; Chapter 2, 3) and the ice rafting debris record of North Atlantic DSDP Site 607 (Chapter 3) to advance our understanding of climate variability during MIS101-99.

## 4.2. Section

Monte San Nicola is situated 10 km north of the coastal town Gela in southern Sicily (Italy). A succession of ~160 m of rhythmically bedded marly limestones and marls from the Trubi and Monte Narbone Formation are well exposed. The sapropels of the O, A, B and C clusters [Verhallen, 1987; Zijdeveld, et al., 1991] are visible in the section. The sedimentary sequence was estimated to be deposited in an 800-1000 m deep piggyback basin on the Gela-nappe [Bonaduce and Sprovieri, 1984; Argnani, 1987; Rio, et al., 1994]. The section presents the Gelasian stratotype with the base of the Gelasian being defined at the top of the A5 sapropel (San Nicola bed) [Rio, et al., 1994].

Monte San Nicola has been used to establish the astronomically calibrated (polarity) timescale by Hilgen [1991a; 1991b]. The position of MIS96-100 is well constrained in this section [Sprovieri, 1993]. These stages are visible as grey-white alternations on a metre scale in-between the A5 sapropel and the B sapropel group with grey layers reflecting glacial stages 100, 98 and 96. Light-coloured centimetre thick bands are visible within the dark glacial stages. The base of MIS101 is characterised by a dark sapropelitic layer corresponding to i-cycle 246 [Lourens, et al., 1996].

The age assessment for the studied interval of San Nicola has been achieved by correlating the benthic  $\delta^{18}\text{O}_{\text{benthos}}$  of San Nicola to the  $\delta^{18}\text{O}_{\text{benthos}}$  of the astronomically calibrated timescale of Site 967 (Chapter 2; Lourens et al., 2001). This resulted in average time resolution of 0.45 kyr with a lowest resolution of 2.6 kyr during the sapropelitic layer.

### 4.3. Materials and Methods

MIS101 to MIS99 were sampled ~2 m above the San Nicola bed (A5) every 3 cm being 123 samples in total. The sampling transect was chosen carefully to ensure a continuous and undisturbed record. The weathered surface was cleaned and only 'fresh' material was sampled using an electric water-cooled drill. All samples packed in aluminium foil to prevent salt precipitation on the surface by drying.

Carbon and nitrogen weight percentages were measured before and after removal of carbonates with 1 M HCl on a NCS1500 analyser (Fisons Instruments) using dry-combustion at 1030°C. International (BCR71, solf acid, acetanilide and atropine) and in house powder standards (f-turbidite) were used for calibration. Relative standard deviations ( $2\sigma$ ) in duplicate measurements are below 0.27 for carbon and 2.3 for nitrogen. Calcium carbonate weight percentages were calculated by converting all inorganic carbon into carbonate.

Samples for geochemical analysis were dried at 50°C in an oven and homogenised in an agate mortar. For ICP-AES chemical measurements total digestions were made using a 6.5:2.5:1 mixture of HClO<sub>4</sub> (60%), HNO<sub>3</sub> (65%) and H<sub>2</sub>O and 2.5 ml of HF (40%). The solutions were heated to 90°C during 24 hours in closed teflon valves and subsequently dried at 160°C. The dried residual was taken up in a 1 M HCl matrix and analysed on a Perkin Elmer Optima 3000 ICP-AES. Analytical precision was determined with replicate analyses and by calibration to international (SO1 and SO3) and in house (mmm91) powder standards. Replicate analyses showed relative standard deviations <5% for all elements.

Grain size analyses were carried out on a Malvern Instruments Mastersizer S equipped with a 300-mm lens. Grain sizes are resolved in the range 0.05-754.23 μm resulting in 64 grain size classes. A Mie-based model using 3OGD parameters was used for conversion of diffraction measurements into grain size classes. For sample preparation about 5 g of sample was treated repeatedly with excess buffered acetic acid (HAc) (pH=4 at room temperature). Subsequently, the carbonate-free samples were neutralised and treated with 3% H<sub>2</sub>O<sub>2</sub> at ~85°C for 2-3 hours under continuous stirring. It was unnecessary to remove silicate as visual inspection of sieved sediments showed no biogenic opal in the sediment. Prior to analysis on the Mastersizer samples were peptised using ~2 ml of a mixture of 44.6 g Na<sub>4</sub>P<sub>2</sub>O<sub>5</sub>\*10H<sub>2</sub>O and 4.24 g Na<sub>2</sub>CO<sub>3</sub> on one litre of demi water. The dispersed samples were then added under continuous stirring to the Particle Analyser by the pipette method until an obscuration of ~15% was reached and subsequently homogenised by ultrasonic vibration for ~2 min.



## 4.4. Results

### 4.4.1. Chemical analyses

The most important element concentrations are plotted as element to aluminium ratios (element/Al) in order to correct for dilution by carbonate and are given in weight percent (%) (Figure 1.1 and Figure 1.2). The sapropelitic layer (or ghost sapropel coded i-246) just below MIS100 is characterised by slightly elevated (0.6 %) organic carbon ( $C_{org}$ ), Ni/Al ( $10 \cdot 10^{-4}$ ), Cu/Al ( $5 \cdot 10^{-4}$ ) and V/Al ( $18 \cdot 10^{-4}$ ) concentrations (Figure 1.1). Concentrations of Ni/Al, Cu/Al and V/Al are also slightly enhanced around i-244. Mn/Al concentrations, on the contrary, are slightly lower within and enhanced above the ghost sapropel. Ba/Al and Zn/Al (both not shown) vary around background concentrations of  $\sim 40 \cdot 10^{-4}$  and  $\sim 13 \cdot 10^{-4}$ , respectively with peak concentrations rising during short intervals up to  $160 \cdot 10^{-4}$  and  $30 \cdot 10^{-4}$ , respectively.  $CaCO_3$ -weight percentages and Ca correlate inversely to the Al content ( $r = -0.94$  and  $r = -0.92$ , respectively) with low  $CaCO_3$  (36%) being associated with high Al (6%) contents in the glacial and the sapropelitic layer and high  $CaCO_3$  (52%) being associated with low Al (4%) contents in the interglacials and within MIS100 (Figure 4.2). Episodes of low  $CaCO_3$  and high Al during MIS100 are labelled 1 to 5 (see Chapter 2). The distribution patterns of the terrestrial element/Al ratios (K/Al,  $Mg_{tot}/Al$ ,  $Mg_{detr}/Al$ <sup>7</sup>, Y/Al and Ti/Al) are not consistent: in the

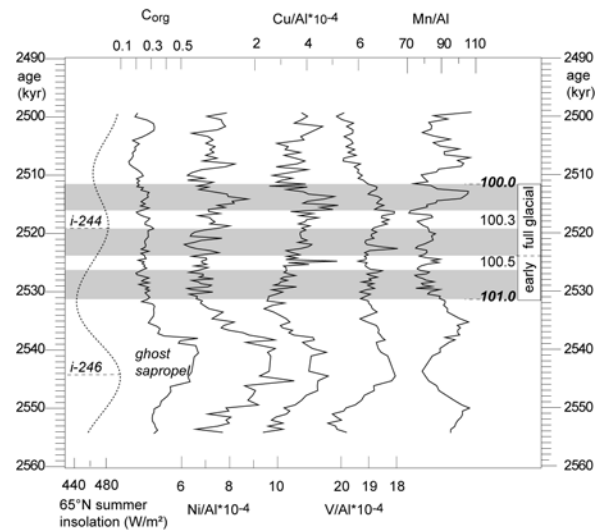


**Figure 4.1:**  $C_{org}$ , V/Al $\cdot 10^{-4}$ , Mn/Al $\cdot 10^{-4}$ , Ni/Al $\cdot 10^{-4}$  and Cu/Al $\cdot 10^{-4}$  weight percentages and  $La_{(1,1)04}$  65°N summer insolation ( $W/m^2$ ) versus age (kyr). The positions of i-cycles i-246 and i-244 [after Lourens, *et al.*, 1996] and minimum obliquity are indicated on the right y-axis. Marine oxygen isotope stages MIS101 and MIS99 and early and full glacial intervals during MIS100 are indicated on the left y-axis. The horizontal shaded intervals indicate stadials MIS100.2, 100.4 and 100.6, respectively, as defined in Chapter 2.

<sup>7</sup> The Mg/Al signal may be composed of a terrigenous ( $Mg_{detr}$ ) and a carbonate-bound ( $Mg_{CaCO_3}$ ) magnesium fraction. The  $Mg_{detr}$  can be calculated by subtracting the  $Mg_{CaCO_3}$  from the total Mg ( $Mg_{tot}$ ) content. Leaching experiments indicate that the average Mg/Ca ratio in time-equivalent Pliocene Mediterranean bulk sediment is

sapropelitic layer (i-246) K/Al,  $Mg_{detr}/Al$  and Y/Al show slightly enhanced values, whereas Ti/Al has especially low values during that interval.

All terrestrial element/Al ratios (with the exception of K/Al) are low during insolation maximum i-244 and elevated during insolation minima.

#### 4.4.2. Grain size analyses

Grain size distributions show typical bimodal distributions with modes at  $0.31 \mu m$  and around  $4.7 \mu m$  (Figure 4.3), the first being considered an artefact of the Malvern Mie

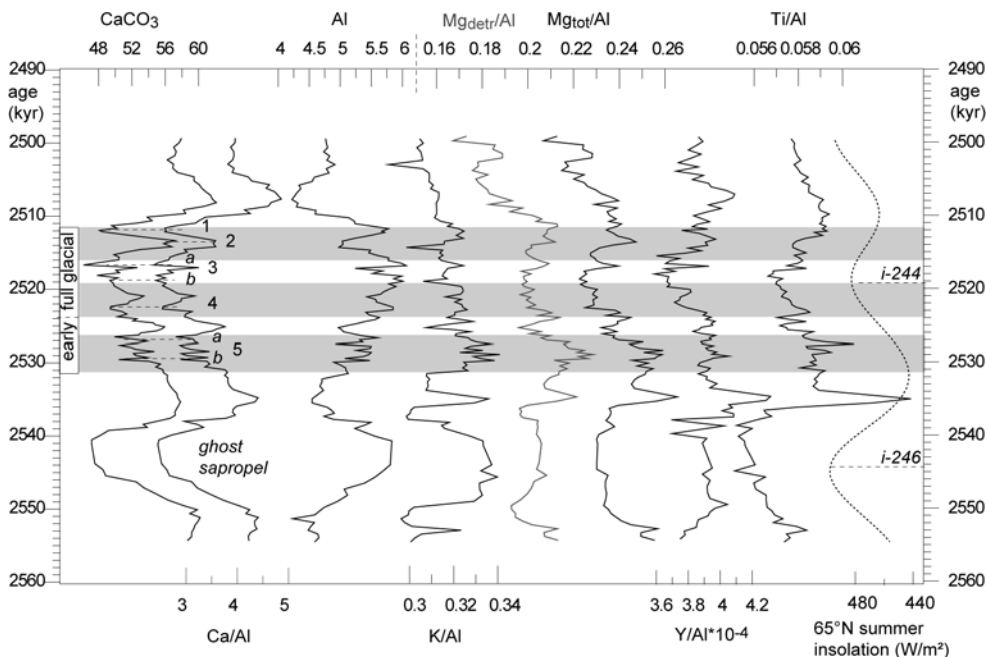


Figure 4.2:  $CaCO_3$ , Ca/Al, Al, K/Al,  $Mg_{tot}/Al$ ,  $Mg_{detr}/Al$  (grey line),  $Y/Al \cdot 10^{-4}$  and Ti/Al weight percentages versus age (kyr). Labelling according to Figure 4.1. Horizontal stippled lines indicate intervals with low  $CaCO_3$  according to Chapter 2.

model and disappearing when the refraction parameter is adjusted to 1.54, which is normally assumed for pure quartz grains. The second mode, which is the modal grain size, varies between  $3.4\text{--}6 \mu m$  in the range of fine silt indicating variations in the normal hemipelagic background sediment. Additionally, most samples show a pronounced shoulder at  $\sim 22 \mu m$  and an increase in the coarser grain sizes (medium silt to fine sand with a maximum of  $100 \mu m$ ). This fraction is of particular interest because it lies in the range of wind transported material: the percentage of the sediment in the

about 0.01 [Wehausen and Brumsack, 2000]. Assuming a similar Mg/Ca ratio for San Nicola carbonate,  $Mg_{detr}/Al$  values are  $\sim 0.3\%$  lower than  $Mg_{tot}/Al$  values but show the same distribution pattern.

7–63  $\mu\text{m}$  size range has been defined as the eolian sortable silt [EES; *McCave, et al.*, 1995] and has been used as indicator for wind-transported sediment in the western Mediterranean [*Moreno, et al.*, 2002]. In order to classify the complex grain size distributions a principal component analysis (PCA; Matlab 6.5, statistical toolbox) was carried out on all samples.

The first principal component (PCA1) explains about 85% of the variance in the grain size distribution with grain size classes of  $\sim 2\text{--}6\ \mu\text{m}$  (C1) loading on the negative and  $\sim 12\text{--}56\ \mu\text{m}$  (C2+3) on the positive axis, respectively (Figure 4.3). The PCA1 thus discriminates between the fine silt fraction (C1) and the medium to coarse silt component (C2+3), probably of either fluvial or aeolian origin. The PCA1 reveals a similar distribution ( $r=0.92$ ) as the 7–63  $\mu\text{m}$  fraction, both indicating coarsening of the sediment across time, with exceptionally lower values during i-246 and i-244 (Figure 4.4).

The second principal component (PCA2) explains  $\sim 8\%$  of the variability in the grain size distribution. Positive scores on the second component are recorded for grain size classes  $\sim 0.3\ \mu\text{m}$  (C0), negative scores for classes  $\sim 12\text{--}56\ \mu\text{m}$  (C2+3) (Figure 4.3). The PCA2 component thus indicates the relative contribution of medium to coarse silt (C2+3) to the grain size distribution and may give a measure for sorting of the sediment, although correlation with the median grain size (D50) is only modest ( $r=0.6$ ) (Figure 4.4).

The third principal component (PCA3) explains  $\sim 3\%$  of the variability in the grain size distribution. Positive scores on the third component are recorded for grain size classes  $\sim 6\text{--}16\ \mu\text{m}$  (C2) and negative scores for classes  $\sim 30\text{--}76\ \mu\text{m}$  (C3), respectively (Figure 4.3), thus splitting the C2+3 component into a medium silt and a coarse silt/fine sand component. The PCA3 thus distinguishes between a fine fluvial or aeolian (C2) component and a coarser (C3) fraction, most likely of aeolian origin. If both fractions C2 and C3 are of aeolian origin, the PCA3, presents the ratio of coarse aeolian over the total aeolian fraction ( $C3/(C3+C2)$ ) and is thus indicative for variation in wind strength. The PCA3 correlates ( $r=-0.54$ ) to the distribution of the fine sand (63–100

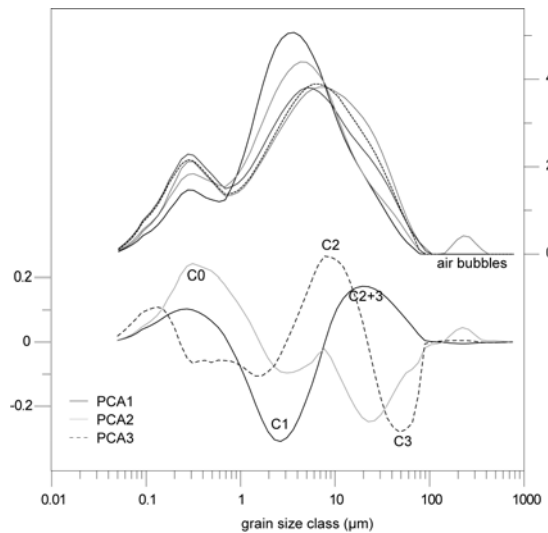


**Figure 4.3: Grain size variations in SN (random samples from MIS100, 99 and 101) and principal components (PCA) 1-3.**

$\mu\text{m}$ ) fraction, both indicating high relative contributions of coarser material during precession maxima (Figure 4.4).

## 4.5. Discussion

### 4.5.1. Changes in $C_{\text{org}}$ and redox conditions

The precise mechanism behind sapropel formation in the Mediterranean is not yet fully understood. Clearly, sapropel formation is the result from the interplay of several processes of varying importance. An ongoing point of discussion is whether the high  $C_{\text{org}}$  concentrations observed in sapropels are primarily caused by enhanced preservation of organic matter during anoxic bottom water conditions or by increased surface water productivity and subsequent export of organic material to the deep sea at times of precession minimum. Since the eastern Mediterranean is a nutrient desert rather than a concentration basin, several mechanisms have been proposed to explain the

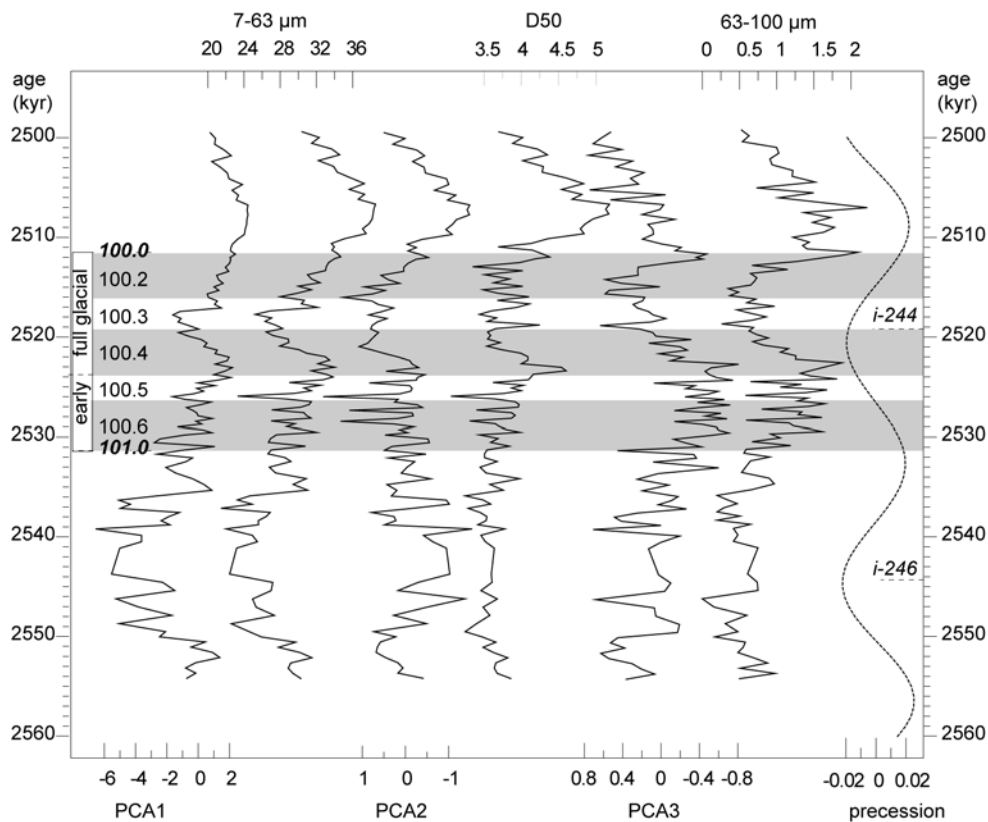


Figure 4.4: Grain size distribution versus age (kyr). PCA1, fraction 7-63  $\mu\text{m}$ , PCA2, D50, PCA3, 63-100  $\mu\text{m}$  fraction and  $\text{La04}_{(1,1)}$  65°N summer insolation ( $\text{W}/\text{m}^2$ ) versus age (kyr). Labelling according to Figure 4.1.

extraordinary high concentrations of  $C_{\text{org}}$  and trace metals associated with sapropels. Most extreme scenarios include a complete reversal of the Mediterranean hydrology from an anti-estuarine to an estuarine circulation due to a positive net precipitation over evaporation balance in the eastern Mediterranean caused by the increased freshwater inflow of the Nile-river during precession minimum [Calvert, 1983]. As a result, the eastern Mediterranean may act as a nutrient trap, which has led to anoxic bottom waters. Alternatively, nutrient recycling in a deep chlorophyll maximum (DCM) was proposed as efficient mechanism for enhancing primary productivity under normal anti-estuarine conditions [Rohling and Gieskes, 1989]. These authors show that a freshening of the surface water during minimum precession could initiate a shoaling of the pycnocline into the nutricline and, subsequently, the development of a (seasonal) deep chlorophyll maximum (DCM) [Rohling and Hilgen, 1991]. The development of a seasonal DCM would need only small amounts of freshwater to the surface water [Bethoux and Pierre, 1999] to result in short periods of stagnation and thus could explain the enhanced primary productivity without the essential of enhanced preservation due to anoxic bottom waters. Evidence of the presence of a (seasonal) DCM and enhanced primary productivity in the studied interval of SN may come from the increased abundances of *Neogloboquadrina* spp (dex) during the more depleted  $\delta^{18}\text{O}_{\text{G.ruber}}$  values of i-244 (Chapter 2). The presence of epibenthic foraminifers throughout the SN record (Chapter 2) indicates however that bottom water conditions were never anoxic during MIS101-99 at this site.

The average  $C_{\text{org}}$  weight percentages of San Nicola are in the range of background concentrations observed in other deep marine eastern Mediterranean ODP Leg 160 sediments [Wehausen, 1999]. The maximum  $C_{\text{org}}$  values in the sapropelitic layer is in agreement with  $C_{\text{org}}$  contents of badly developed or diagenetic altered sapropels in Plio-Pleistocene sediments of Site 967 and Site 964 [data Wehausen, 1999]. However,  $C_{\text{org}}$  contents in land-based marine sections can be lower because of desiccation and subsurface weathering, which may decrease organic components to a certain degree [Van Os, et al., 1994; Nijenhuis, et al., 2001]. Although we removed the upper 2 m of the weathered surface this effect cannot be excluded. On the other hand, sedimentation is much higher in the San Nicola section than in equivalent deep marine cores of Site 967 and Site 964 [data Wehausen, 1999] and may have diluted the organic matter signal. One way to compare  $C_{\text{org}}$  fluxes at such different setting is to back-calculate primary productivity from the organic carbon mass accumulation rates (MAR).

The SN  $C_{\text{org}}$  mass accumulation rate ( $\text{MAR}_{C_{\text{org}}}$ ) calculates to 0.64 g/m<sup>2</sup>yr during i-246 and 0.32 g/m<sup>2</sup>yr during i-244 with the average sedimentation rate being 6.25 cm/kyr and the average density being 1.7 g/cm<sup>3</sup>. These values are comparable to  $\text{MAR}_{C_{\text{org}}}$  values at ODP Site 964 and Site 967 during the same time intervals [Wehausen, 1999], although it should be realised that the  $\text{MAR}_{C_{\text{org}}}$  are not only a function of the primary productivity export flux ( $\text{PP}_{\text{exp}}$ ), but strongly depend on other factors such as the

amount of terrigenous organic detritus, water depth, sedimentation rate, and oxygen conditions within the water column and sediment. To overcome these problems, barium (Ba) is commonly used as proxy for palaeo-productivity calculations in sapropels, as it has been proven to be independent of the redox state of the water column and sediment [van Santvoort, *et al.*, 1996]. However, in a relatively shallow water environment such as San Nicola, Ba has been proven useless as  $PP_{exp}$  indicator [von Breyman, *et al.*, 1992]. Hence we could only rely on  $MAR_{C_{org}}$  to get some idea about changes in  $PP_{exp}$  notwithstanding the uncertainties in this estimate as mentioned above.

The  $MAR_{C_{org}}$  of SN calculates to a  $PP_{exp}$  of 400 gC/m<sup>2</sup>yr during i-246 and 200 gC/m<sup>2</sup>yr during i-244, respectively, by using a preservation factor of 0.16% that is proposed for pelagic oxic environments [Nijenhuis, 1999]. These values are in the range of  $PP_{exp}$  observed in modern upwelling areas [Suess, 1980]. Using a preservation factor of 2.5% that was assumed by Wehausen [1999] for anoxic bottom water conditions and sapropel intervals in deep marine eastern Mediterranean ODP sites, the  $PP_{exp}$  of SN calculates to 25.6 gC/m<sup>2</sup>yr during i-246 and 12.8 gC/m<sup>2</sup>yr during i-244, respectively. These  $PP_{exp}$  values are comparable to present day  $PP_{exp}$  rates in the Mediterranean, which are in the order of 26 gC/m<sup>2</sup>yr [Bethoux and Pierre, 1999]. For pre-anthropogenic times  $PP_{exp}$  values might have been lower [Bethoux and Pierre, 1999], probably matching  $PP_{exp}$  values recorded during i-244 at San Nicola. A lower background productivity would leave slightly enhanced  $PP_{exp}$  rates during i-246, which is probably realistic. Furthermore, this indicates that using a higher preservation factor for SN might be realistic to account for the higher sedimentation rate at San Nicola rather than suggesting (partly) anoxic bottom waters.

The redox-sensitive trace elements in SN are not significantly enriched as is typically observed in sapropel environments but are in the range of lithogenic background concentrations of Pliocene ODP Leg 160 sediments [Wehausen, 1999] and average shale [Wedepohl, 1995] thus pointing again against severe oxygen depletion in the bottom water. Only Cu/Al and Ni/Al are slightly higher during i-246 and around i-244, with Ni/Al showing a moderate correlation with  $C_{org}$  ( $r=0.75$ ). In seawater these elements are scavenged by organic matter [Calvert, *et al.*, 1985] or co-precipitate with sulphides [Jacobs and Emerson, 1985] under anoxic conditions. Scavenging by organic material may be explaining the enrichment in these elements during the sapropel but there is no indication of changes in sulphide concentrations or organic matter content during i-244. The enhanced Cu/Al and Ni/Al values during i-244 could be related to co-precipitation with Mn-oxihydroxide [Klinkhammer, 1980; Hem, 1989]. Usually, V/Al and Mn/Al are good indicators for the redox state of the bottom water: V in the form of metavanadate is dissolved in seawater and forms complexes with organic ligands under anoxic conditions, on the contrary, Mn is soluble under anoxic conditions and precipitates as Mn-oxihydroxide under oxic conditions. The concentration profile of

Mn/Al indicates some mobilisation within the sapropelitic layer and precipitation on top, suggesting slightly anoxic conditions, probably only in the pore water and more related to the fast sedimentation rather than pointing towards anoxia in the water column.

In summary, the chemical data indicate that environmental conditions during formation

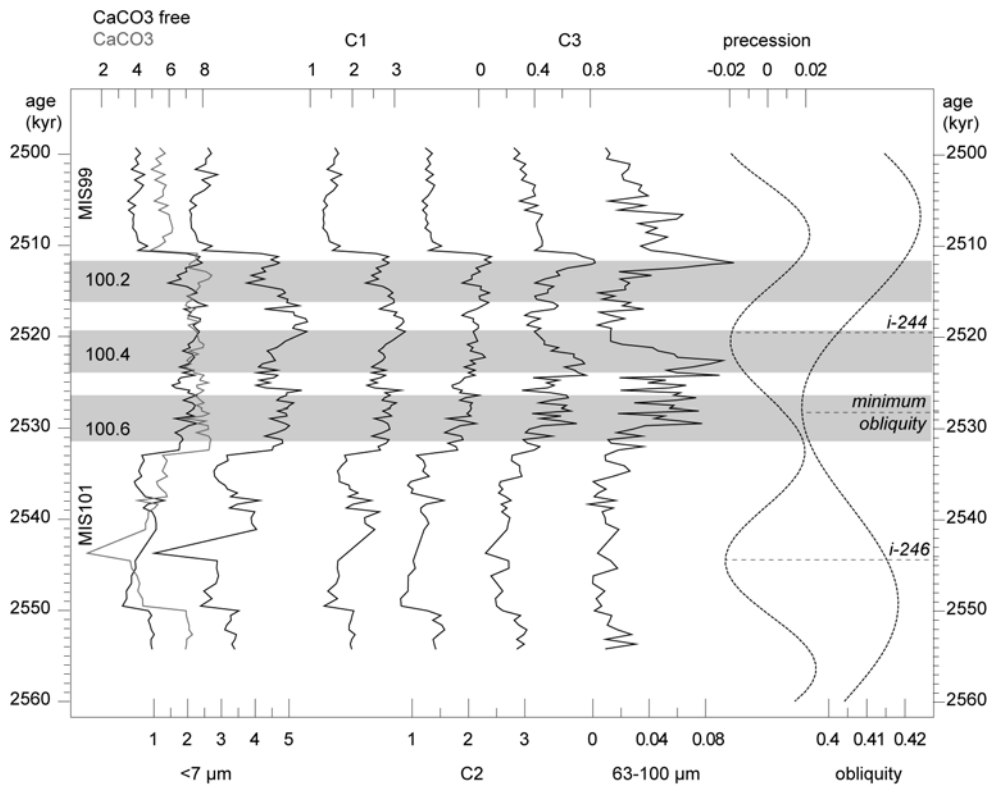


**Figure 4.5:** MAR (in  $\text{g}/\text{cm}^2\text{kyr}$ ) of carbonate (grey) and the carbonate-free sediment, MAR (in  $\text{g}/\text{cm}^2\text{kyr}$ ) of the carbonate free sediment fractions  $<7 \mu\text{m}$ , C1-3 and  $63\text{-}100 \mu\text{m}$  and precession and obliquity of the  $\text{La04}_{(1,1)}$  astronomical solution versus age. Labelling according to Figure 4.1.

of the ghost sapropel were not very different from conditions leading to sapropel formation. Both, primary productivity and surface water stratification (DCM conditions) were just not intense enough to produce conditions favourable for sapropel formation during i-246 and were probably just outside normal conditions during i-244.

## 4.5.2. Changes in CaCO<sub>3</sub> and terrestrial components

### 4.5.3. Obliquity-scale changes

The bulk carbonate record of the San Nicola sediment reflects the main character of the Narbone sediments, namely the cyclic alterations of carbonates and marls with light-coloured layers (interglacials, homogenous intervals) being carbonate-rich and dark-coloured layers (glacials, sapropels, sapropelitic layers) being carbonate-poor (*Chapter 1*). The good correlation ( $r=0.95$ ) of Ca with CaCO<sub>3</sub> (Figure 4.2) and its opposite behaviour to Al shows that all Ca is bound to CaCO<sub>3</sub> rather than to Ca-bearing aluminosilicates. In addition, the good correlation between Sr/Al and CaCO<sub>3</sub> ( $r=0.83$ ) and P/Al and CaCO<sub>3</sub> ( $r=0.82$ ) indicates that both elements are bound to carbonates and suggest that most calcium carbonate is of biogenic origin. This interpretation is emphasised by the Sr/Ca value being  $\sim 51$  on average, which is in agreement with Sr/Ca value of nannofossil and foraminiferal oozes [*Morse and MacKenzie, 1990*]. Furthermore, smear slide analysis on seven samples disapproved the presence of biogenic silica in the form of diatoms so that the SN sediment indeed presents a two-component mixing system with biogenic carbonate and aluminosilicates as mixing end-members. Preliminary XRF data confirms that sediments of SN lie on the mixing line of average shale and calcium carbonate.

## 4.6. Precession-scale changes

Dilution of carbonates by terrigenous material is an important mechanism in controlling the Mediterranean precession-related carbonate-marl and sapropel-marl sequences. It has been observed, that Mediterranean sediments have a characteristic detrital matter chemistry, which depends on the source of the terrigenous detrital fraction [*Venkatarathnam and Ryan, 1971; Dominik and Stoffers, 1978*]. Subsequently, it has been shown, that the clay mineral composition and the element/Al ratios of typical lithogenic origin (K/Al, Mg/Al, Si/Al, Zr/Al and Ti/Al) at different eastern Mediterranean locations vary at precession-scale indicating changes in the relative contribution of terrigenous material from different source regions (aeolian from the Sahara and fluvial from adjacent river drainage), which are related to changes in circum-Mediterranean humidity [*Foucault and Mélières, 1995; Wehausen, 1999*]. Especially, the K/Al and Ti/Al profiles of Eastern Mediterranean ODP leg 160 records show high correlation and an in phase relationship with northern hemisphere summer insolation, so that a detailed age model could be generated for these records by correlating the K/Al and Ti/Al to the astronomical solution [*Wehausen, 1999; Wehausen and Brumsack, 2000; Lourens, et al., 2001*]. The advantage of using the Ti/Al and K/Al for age calibration is that precession-forced variations in the Ti/Al and to a lesser degree in the K/Al are also recorded in the homogenous intervals, allowing an age calibration that is independent from the occurrence of sapropels.



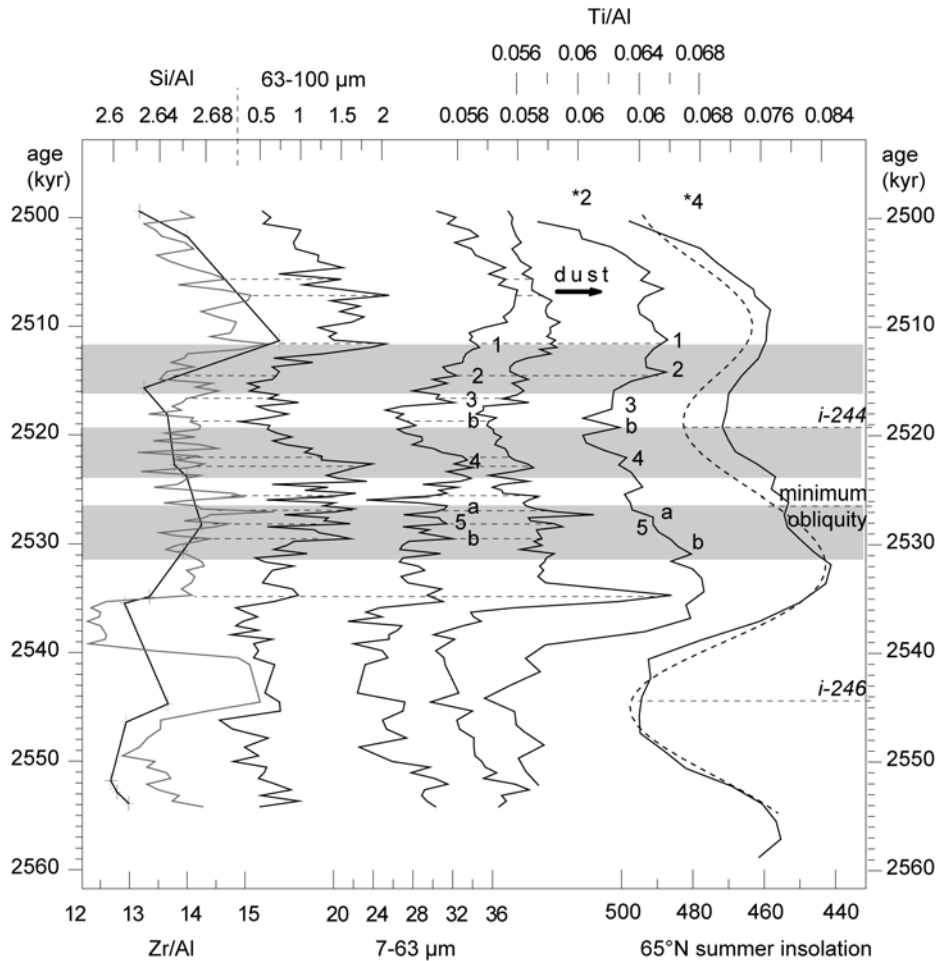


**Figure 4.6:** Relative contribution of Zr/Al (grey line), Si/Al, 63-100  $\mu\text{m}$  fraction, 7-63  $\mu\text{m}$  and Ti/Al versus age. Si/Al are from preliminary XRF data, Zr/Al profile from the second series of ICP measurements on the same samples (see text). Ti/Al of ODP Site 969 [data *Wehausen, 1999*] and Site 967 [data *Lourens, et al., 2001*] and  $\text{La04}_{(1,1)}$  65°N summer insolation (stippled line; notice inverted x-axis) versus age. Notice that Ti/Al amplitudes of Site 969 and Site 967 are respectively twice and four times larger than the Ti/Al amplitude of SN. Further labelling according to Figure 4.1.

The distribution patterns of the lithogenic element/Al ratios Si/Al, Zr/Al<sup>8</sup>, Y/Al<sup>9</sup> and Ti/Al of San Nicola evidence precession-related variability (Figure 4.2, Figure

<sup>8</sup> The Zr/Al profile (unpublished data) comes from a second series of ICP measurements on the same samples of SN following the same procedure but unfortunately no standards were used for this series. However,

4.6). The Ti/Al profile of SN is very similar to that of Site 969 and Site 967 and although average values and variations are much smaller than at Site 969 and 967 (~one half the amplitude of Site 969 and ~one fourth the amplitude of Site 967, respectively; Figure 4.6), it is reasonable to infer that variations in the Ti/Al of San Nicola reflect

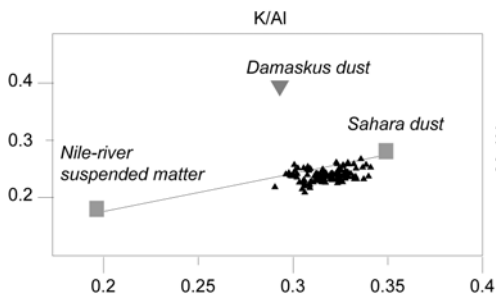


**Figure 4.7: Mg/Al versus K/Al of San Nicola (triangles). Squares indicate the average composition of Nile suspended material and Saharan dust, with thin black line indicating the mixing line between these two end members. Triangle indicates the composition of dust from the Damascus area [figure after Wehausen and Brumsack, 2000]**

similar changes in dry/wet periods associated with changes in the precession index. Furthermore, the values of the lithogenic element/Al ratios are similar to those of African desert sand and Mediterranean aerosols [Guerzoni, 1996; Guieu and Thomas, 1996] and, therefore, are likely to be attributed to the input of aeolian transported material, mainly from the Saharan desert [Shimmiel, 1992; Nijenhuis, 1999]. This interpretation is confirmed by the aeolian sortable silt fraction, which varies in parallel to the Ti/Al and indicates an increase in the wind-transported material during precession maximum and an increase of finer (more clayey) material during precession minima (Figure 4.6), which is probably associated with fine river-transported material at times of enhanced Mediterranean humidity. On the contrary, PCA<sub>3</sub> indicates a coarsening of the (wind-transported) material, possibly related to an increase in the wind strength and an intensification of the dust supply to the Mediterranean during maximum precession. The high Zr/Al values around the precession maxima could indicate an increase in wind strength since Zr is included in the heavy mineral zircon, which is extremely resistant to chemical weathering and, like Si, enriched in desert sand. Larger or heavier particles are difficult to mobilise, so that only very strong dust storms can transport these particles over a longer distance. Examination of the MAR of the carbonate free sediment fractions indicates a doubling of the accumulation of coarse material (C<sub>2+3</sub>) during precession maxima (Figure 4.5). This is in accordance with observations at ODP

---

distribution patterns of all element concentrations and element/Al ratios from this second series are similar to our ICP data although absolute values are slightly lower in this series.

<sup>9</sup> We included Y/Al in Figure 4.6 because the distribution pattern is very similar to the Ti/Al ( $r=0.98$ ). Normally, Y is investigated together with rare earth elements (REE) as it behaves like a lanthanoid in seawater [Nozaki and al, 1997] and complexation with organic ligands is important in the distribution of Y [Byrne and Lee, 1993]. However, Y/Al does not show any relation with the C<sub>org</sub> profile of San Nicola and was earlier used as dust indicator [Nijenhuis, 1999]. The small peak enrichment of Y/Al above the sapropelitic layer, which correlates with peak enrichments of the other lithogenic element/Al justifies this interpretation.

Site 969 and Site 967 [Wehausen, 1999]. At SN, the precession component in the coarse fraction is clearly superimposed on the obliquity-related glacial-interglacial variability.

#### 4.6.1. Sub-Milankovitch scale variation in CaCO<sub>3</sub> and terrestrial components

The K/Al and Mg/Al values of San Nicola are in good agreement with those of the Plio-Pleistocene marine sediments of ODP leg 160 [Nijenhuis, 1999; Wehausen, 1999] and plot on the mixing line between average Nile-river suspended material and Sahara dust (Figure 4.7). The San Nicola Mg/Al and K/Al profiles, however, do not show a prominent aeolian or fluvial phase nor do these element/Al ratios vary on precession scale. Instead, Mg/Al and K/Al seem to be associated with the rapid fluctuations of Al and CaCO<sub>3</sub> during MIS100. Such a discrepancy is evidenced in the nearby ODP Site 964 and the more easterly Site 969 [data Wehausen, 1999]: In contrast to the older and younger sapropel containing intervals, where K/Al and Mg/Al values varying at precession scale, K/Al and Mg/Al profiles during MIS101-95 vary in parallel to the Ca/Al at a glacial-interglacial (obliquity) scale with superimposed higher-frequency (sub-Milankovitch) variability. This may indicate that precession forcing (and possible river runoff) was not strong enough to trigger the typical sedimentary expression of precession cycles during this time interval.

The basin-wide recognition of high-frequency variations in the CaCO<sub>3</sub> and K/Al, Mg/Al content during MIS100 suggests a common mechanism, most likely dilution of carbonates by aluminosilicates. The absence of CaCO<sub>3</sub> variability during interglacial MIS101 and MIS99 indicates that the climate mechanism(s) behind these variations were either amplified in the glacial or solely active during glacial periods. The relatively low CaCO<sub>3</sub> fluxes during MIS100 could have increased the sensitivity of the sedimentary system to record small fluctuations in terrestrial derived material. The correlation between rapid variations in CaCO<sub>3</sub>, EES, and Ti/Al in Site 969 and SN (Figure 4.6) suggests that these fast (2-4 kyr) variations are caused by changes in dust deposition (see also *Chapter 2*). In addition, the Zr/Al and coarse aeolian fraction indicate short episodes (~1.5-4.5 kyr) of heavy dust delivery to SN, which are most pronounced during the first precession maximum and early glacial (obliquity minimum). During these episodes MAR of the coarse 63-100 μm fraction increase by up to 4 times to ~0.08 g/cm<sup>2</sup>kyr (Figure 4.5). These values are much lower than those recorded in the finer fractions, indicating that this fraction probably captures only the most severe (dust) episodes.

The absence of variations in the Ti/Al of Site 967 (Figure 4.6) has been noticed earlier (*Chapters 2 and 3*) and it has been argued, that the easternmost Mediterranean was probably not affected by high-frequency climate changes. This would imply that the dust storms recorded in SN and Site 967 probably did not reach Site 967. In the present day Mediterranean, there are two different dust deposition systems: in the eastern

Mediterranean, maximum dust deposition takes place during spring and is related to the *sharav* cyclones, originating between Egypt and Tunisia or to the *sharki* with origin from the Sinai and Niger [Yaalon and Ganor, 1979; Kubilay, et al., 1997]. In the western and central Mediterranean, dust is transported at the end of summer by cyclones originating from the Balearics travelling towards Corsica and Italy. Additionally dust is transported from the south by the *sirocco*, *ghibli* or *chamsin* storms, the latter being responsible for the present day precipitation of Saharan dust in central Europe and Scandinavia [Littmann, et al., 1990]. The absence of high-frequency dust episodes at Site 967 suggests that the dust source area lies in the north-west Sahara and a dust transport path from west to east, so that dust is more likely to be deposited in the central and western part of the eastern Mediterranean compared to Site 967. As shown earlier, concentrations of lithogenic element/Al ratios at SN are comparable to those from the Sahara, so that a Saharan origin of dust deposited at SN is likely. Furthermore, SN K/Al values are not in agreement with K/Al values of Damaskus dust (Figure 4.7).

On the other hand, the colour reflectance and CaCO<sub>3</sub> of Site 967 indicates changes similar to those of Site 969 and SN (Chapter 2, Chapter 4) and the absence of high-frequency variations in the Ti/Al of Site 967 could be due to dilution of the Ti/Al signal by Ti/Al-rich suspended material. The Ti/Al ratios increase from the central to the eastern Mediterranean, being lowest at San Nicola and highest at Site 967. This is explained by the additional input Ti/Al-rich material from ultramafic source rocks in the eastern Mediterranean borderland [Ophiolith complexes at Cyprus and Turkey, Wehausen, 1999].

#### 4.6.2. Relationship between Mediterranean dust episodes and North Atlantic IRD-events

It was stated, that dust episodes in the Mediterranean are associated with cold (Dansgaard-Oeschger-type) stadials evidenced in the Mediterranean benthic oxygen isotope record (Chapter 2). This relationship is confirmed by the good ( $r=0.85$ ) and modest ( $r=0.50$ ) correlation between the EES and coarse (63–100  $\mu\text{m}$ ) fraction and the  $\delta^{18}\text{O}_{\text{benthos}}$  of SN (Figure 4.8). It was further assumed, that low sea surface temperatures (SST) in the Mediterranean during MIS100 are associated with low SST and ice rafting (IRD) events in the North Atlantic (Chapter 3). If this relationship is valid, this implies that periods of intensive dust transport from the African continent to the Mediterranean are linked to periods of intensive ice rafting in the North Atlantic. The agreement between Mediterranean dust episodes and the IRD record of the North Atlantic Site 607 (Figure 4.8) is indeed striking, although small differences occur. For example the second and third peak in the Mediterranean dust and Al record are slightly different to the equivalent IRD peak of Site 607.

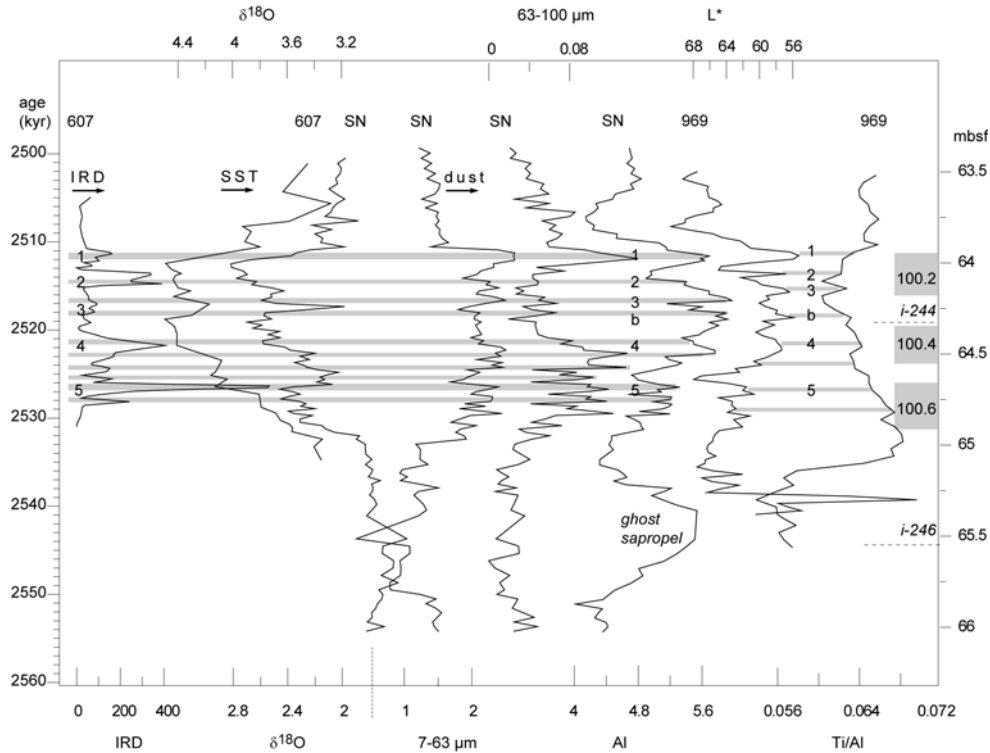


**Figure 4.8:** IRD and  $\delta^{18}\text{O}_{\text{benthos}}$  of DSDP Site 607 (*Chapter 3*),  $\delta^{18}\text{O}_{\text{benthos}}$ , MAR ( $\text{g}/\text{cm}^2\text{kyr}$ ) of the 7-63  $\mu\text{m}$  and 63-100  $\mu\text{m}$  fractions and Al wt% of SN versus age (kyr) in comparison with the colour reflectance ( $L^*$ ) and Ti/Al [data *Wehausen, 1999*] of Site 969 (versus metres below surface; mbsf). Thin shaded intervals indicate episodes of high IRD (1-5), low SST and high dust (1-5). Further labelling according to Figure 4.1.

The most likely link between Saharan dust outbreaks and IRD-events is via the atmospheric moisture content. During IRD episodes it is generally colder and drier, resulting in more frequent dust storms and an increase in the dust transport from the Saharan desert to the Mediterranean (see *Chapter 2* and *3*). This is analogous to what was observed from the last glacial maximum in the western Mediterranean Alboran Sea [*Moreno, et al., 2002*] and in the Greenland ice core record. From our data it becomes evident, that dust export is operating on different timescales. Strongest variability occurs during maximum precession and minimum obliquity, this is also when climate modellers see strongest variability in sea ice formation and thermohaline overturning events [*Tuenter, 2004*].

## 4.7. Conclusions

Mass accumulation rates of organic carbon during i-244 and i-246 are similar to  $MAR_{C_{org}}$  in coeval ODP sediments (data Wehausen, 1999) but primary productivity (PP) rates are difficult to estimate because of uncertainties in the redox state of the sediment and bottom water. Trace metal enrichments are modest, most likely because scavenging by organic matter was not effective in a relatively shallow oxic water column. Only Cu/Al and Ni/Al contents are slightly enhanced during i-244 and i-246, possibly through co-precipitation with Mn-oxihydroxides. The presence of epibenthic foraminifers throughout the record (*Chapter 2*) indicates that bottom waters never became anoxic. It is therefore suggested that the deposition of the sapropelitic layer i-246 and sapropel-related signatures during i-244 are related to enhanced primary productivity and nutrient recycling within a deep chlorophyll maximum.

The bulk composition of the San Nicola sediment during MIS100 is comparable to the bulk chemistry of Pliocene Mediterranean deep marine sediments of ODP Leg 160 sites. The San Nicola sedimentary system is a two-component system with biogenic carbonate and aluminosilicate as mixing end-members. The relative contribution of these two components changes predominantly at obliquity-driven glacial-interglacial scale. Superimposed on the glacial-interglacial variability, basin-wide short-term (1.5-4.5 kyr) changes are observed, which are related to episodes of strong dust delivery from the African continent seemingly time equivalent to north Atlantic IRD events. Episodes of intensive dust supply are persistent in the record but amplified during maximum precession and minimum obliquity. Additionally, low carbonate background concentrations during the glacial could have increased the sensitivity of the sedimentary system to record fast changes in the terrigenous detrital input.

# CHAPTER 5

## Cycle geometry of MIS100-96 in relation to orbital forcing

### Abstract

Benthic oxygen isotope data from eastern Mediterranean ODP Leg 160 Site 967 are used in combination with the coupled model of Northern Hemisphere ice sheets and ocean temperatures recently presented by *Bintanja et al.* [2005a; 2005b] to generate global ice volume and northern Hemisphere annual air temperature data during late Pliocene marine oxygen isotope stages (MIS) 101-95 (~2.56-2.4 Ma). Since the age model of Site 967 is independent from glacial-interglacial cycles [*Lourens et al.*, 2001], these data allow a detailed evaluation of the response times of the different climate components with respect to obliquity forcing.

Response times between optimum glacial conditions (i.e., maximum  $\delta^{18}\text{O}$  values, maximum ice) and minimum obliquity are in the order of 5-7 kyr for the 41 kyr filter components, but increase and decrease by ~5 kyr during the long MIS100 and MIS96, and respectively the shorter MIS98 in the presence of 80- and 28-kyr components. The presence of spectral density at 80 and 28 kyr indicates that nonlinear interactions between obliquity and eccentricity may have played an important role in determining the frequency characteristics and shape of the glacial/interglacial succession. This finding has considerable implications for dating late Pliocene benthic isotope records by tuning them to either a combined obliquity-precession target curve or a simple ice sheet model assuming fixed time lags.

## 5.1. Introduction

The Milankovitch theory of the ice ages that holds that astronomical perturbations in the Earth's orbit and axis influence climate by changing the seasonal and latitudinal distribution of incoming solar radiation is generally accepted by the geological community. In particular, the consistency of spectral peaks in benthic foraminifera oxygen isotope ( $\delta^{18}\text{O}$ ) records with Milankovitch frequencies has indicated that there is a clear relationship between glacial-interglacial driven ice volume changes and astronomical perturbations [Hays *et al.*, 1976]. Hence, emphasis has been taken on establishing chronologies of sedimentary records by tuning benthic isotope records to astronomical-forced patterns of climate change.

In the widely applied astronomical tuning procedure of Imbrie and Imbrie [1980], it is assumed that the ice sheets have a fixed response time ( $T_m$ ), which results in different time lags with respect to orbital forcing in the various Milankovitch frequency bands and a fixed non-linearity coefficient ( $b$ ), which represents the slow build-up and fast termination of the ice sheets. For the late Pleistocene a  $T_m$  of 17 kyr has been estimated, which results in a 3-kyr and a 5-kyr time lags of global ice volume (i.e., benthic  $\delta^{18}\text{O}$  records) with respect to orbital precession and obliquity, respectively. This tuning procedure has subsequently been used to obtain time scales for the early Pleistocene and late Pliocene [Imbrie *et al.*, 1984; Shackleton *et al.*, 1990]. These constants are usually assumed to be independent of time whereas in reality accumulation rate and size of the ice sheet vary continuously in time. The smaller ice sheets during the late Pliocene for example would have resulted in a smaller time constant and hence in a reduction of the time lag between the perturbing astronomical cycle and the ice volume response [Chen *et al.*, 1995].

Recently, a new global stacked benthic oxygen isotope record and chronology has been constructed (LR04; [Lisiecki and Raymo 2005]) for the past 5.3 million years in which changes in ice sheet volume in time have been taken into account. For this purpose, the Imbrie and Imbrie [1980] ice sheet model was used, including different time constants for different time intervals. The LR04 chronology used a  $T_m$  of 15 kyr for the Pleistocene, a  $T_m$  of 5 kyr for the early Pliocene, when no ice was present on the Northern Hemisphere, and a linearly increasing  $T_m$  (5-15) in the time interval 3-1.5 Ma, during Northern Hemisphere ice sheets built up. This includes different physical mechanisms like isostatic rebound, different ice growth rates or calving, which act on different timescales and might be operating more effectively on larger ice sheets. Additionally, the uncertainty in the size-prediction of ice sheets is increased by the fact, that benthic foraminiferal  $\delta^{18}\text{O}$  records contain an additional deep water temperature component. Therefore, the evaluation of phase relations between orbital forcing and climate requires two assumptions: Firstly, a global ice sheet model that is able to model the ice volume component accurately for any given time interval, and secondly an age scale that is independent of glacial-interglacial ice volume changes.



*Bintanja et al.* [2005a], developed a thermo-mechanical ice-sheet/ice-shelf/bedrock model in conjunction with an inverse method, which allowed to decompose the  $\delta^{18}\text{O}_{\text{benthos}}$  into an ice volume and a mean NH surface air temperature component which determines the deep water temperature of the ocean. It is assumed that precipitation north of  $40^\circ\text{N}$  controlling ice volume growth and decay is largely (westerly amplification factor) related to the moisture holding capacity of the troposphere, and hence to tropospheric temperature. According to *Sidall* [2005] the largest assumption is the linear relation between air temperature and deep water temperature. In each model step the modelled ice volume (in sea level equivalents) is compared with the observed sea level change (derived from  $\delta^{18}\text{O}$ ) of the next step (i.e. 100 yr later in our case) and the difference between modelled and observed global sea level is translated into a perturbation in northern hemisphere atmospheric temperature. Temperature is continuously adjusted so that the modelled ice volume changes in the desired direction. The model has recently been used to reconstruct Northern Hemisphere temperatures and sea level variations over the last million years [*Bintanja et al.*, 2005b].

Here we apply this inverse forward modelling approach to evaluate changes in ice volume and temperature associated with the severe obliquity-dominated late Pliocene glacial stages 100, 98 and 96 (2.5-2.4 Ma). As input series we use the benthic foraminiferal  $\delta^{18}\text{O}$  record of ODP leg 160 Site 967 (eastern Mediterranean), which resolve marine oxygen isotope stage (MIS) 101-95 at a high temporal (350-500 yr) resolution. Moreover, the chronology of Site 967 is entirely based on correlating circum-Mediterranean humidity (indicated by the Ti/Al) to the  $\text{La2004}_{(1,1)}$  summer insolation curve at  $65^\circ\text{N}$  [*Lourens et al.*, 2001; *Laskar et al.*, 2004], which enables us to precisely estimate the astronomical phase relations for the different components of the  $\delta^{18}\text{O}$  record independent of assumptions about the response time of the ice sheets itself. For this purpose, we carried out frequency analysis and band-pass filtering on the  $\delta^{18}\text{O}$  and the modelled ice volume/temperature components and calculated the response times with respect to the forcing frequency, i.e. orbital obliquity in this time interval by applying cross-correlation.

## 5.2. Materials and methods

ODP leg 160 Site 967 ( $34^\circ 04'\text{N}$ ,  $32^\circ 43'\text{E}$ ) was drilled in the eastern Mediterranean near the Eratosthenes seamount at a water depth of 2554 m. Three holes were drilled in order to gain a continuous succession. A composite depth profile was constructed by correlating colour reflectance records between different holes [*Sakamoto et al.*, 1998]. The studied interval of ODP Site 967 has been astronomically dated by correlating the Ti/Al to the  $\text{La90-93}_{(1,0.5)}$   $65^\circ\text{N}$  summer insolation curve [*Lourens et al.*, 2001], which has been interpreted in terms of changes in the relative contribution of aeolian versus fluvial material. For statistical purposes *Lourens et al.*, [2001] assumed an in-phase relationship between Ti/Al and  $65^\circ\text{N}$  summer insolation, which differ by 3 kyr from

the lagged ages given by *Lourens et al.*, [1996]. Here, we apply a new astronomical solution, La2004 including present-day values for the Earth's tidal dissipation and dynamical ellipticity [*Laskar et al.*, 2004], in stead of the older La90-93 solution [*Laskar et al.*, 1993], although both solutions reveal the same ages within the studied interval.

Samples for foraminiferal stable isotope analysis were freeze-dried and washed through 63, 125 and 600  $\mu\text{m}$  sieves. For benthic stable isotope analysis 3-5 specimens of *Cibicides kullenbergi* were hand picked in a narrow size range from the  $>212 \mu\text{m}$  fraction. Measurements were carried out at Bremen University stable isotope facilities where a CARBO-KIEL automated carbonate preparation device linked on-line to a FINNIGAN MAT 251 mass spectrometer is operated. Replicate analyses and calibration to the international carbonate standard NBS19 and in-house standard (shk\_br; carrara) revealed an analytical precision better than 0.05‰. The  $\delta^{18}\text{O}$  results of *Cibicides kullenbergi* were adjusted by adding 0.64‰ to be in equilibrium with ambient sea water [*Shackleton* 1974].

Since the ice sheet model and ocean routine have large response times (3-5 kyr), shorter-term climatic fluctuations were ignored [*Bintanja et al.*, 2005b;2005a]. For this purpose the original  $\delta^{18}\text{O}_{\text{benthos}}$  was smoothed applying a moving average and interpolated at 100 kyr intervals (a more detailed description of the methodology is provided by *Bintanja et al.*, 2005a, b). The procedure was run for the time interval between 2.4 and 2.56 Myr. The model is forced by the La2004<sub>(1,1)</sub> summer insolation at 65N, which is applied uniformly throughout the grid and thus independent of the season. It is assumed that the majority (85%) of the land-based ice are the Fennoscandian ice sheet in Northern Eurasia and the Laurentide-Corderillian ice sheet complex in North America.

Frequency analysis is carried out using the MC\_CLEAN (version 2.0) frequency analysis program of *Heslop and Dekkers* [2002]. MC\_CLEAN is based on the CLEAN algorithm of *Roberts et al.*, [1987], which allows to extract frequency information directly from an unevenly-spaced time series. In addition to CLEAN, Monte Carlo methods for different types of noise (here red noise) allow to generate a set of slightly different spectra from the (single) input signal. The difference between these spectra give the confidence interval around the mean spectrum. Furthermore, the application of an Inverse Fourier Transform on the mean spectrum allows to reconstruct a noise free (or cleaned) version of the input series. Additionally, we apply band pass filtering (AnalySeries, [*Paillard et al.*, 1996]) using a Gaussian filter with central frequency.

## 5.3. Results

### 5.3.1. Oxygen isotopes

The oxygen isotope values for *C. kullenbergi* ( $\delta^{18}\text{O}$ ) vary from  $\sim 2.0\text{‰}$  in the interglacials to  $\sim 3.1\text{‰}$  in the glacials, resulting in glacial/interglacial amplitudes of  $\sim 1.1\text{‰}$  (Figure

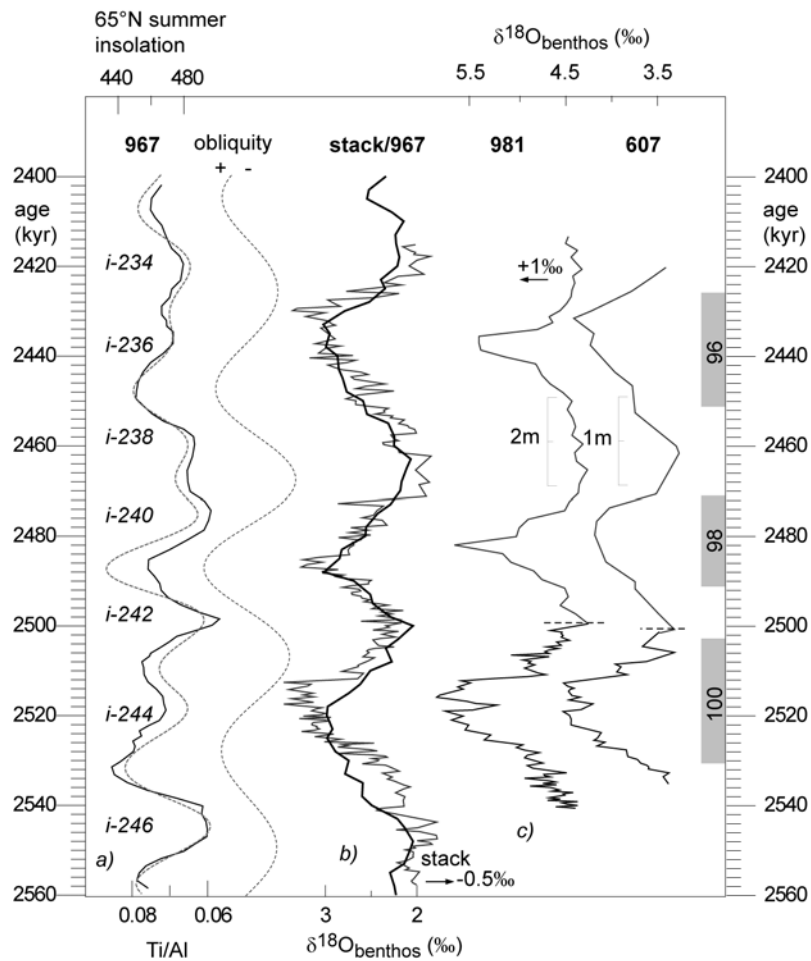
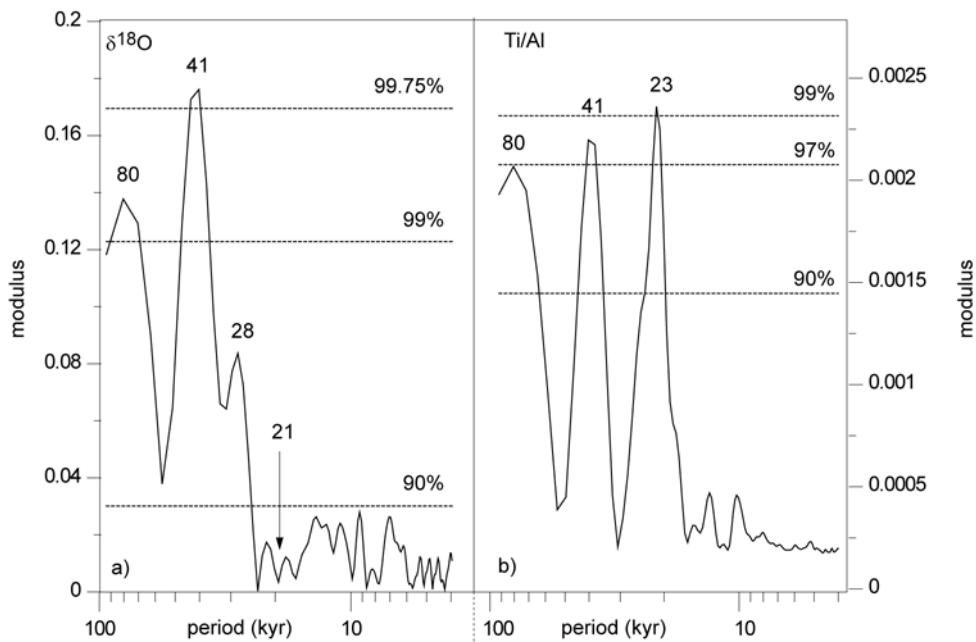


Figure 5.1: a) Ti/Al of Site 967 and La04<sub>(1,1)</sub> 65°N summer insolation and obliquity (stippled lines) versus age. I-cycles (after Lourens et al. [1996]) are labelled *i-246* through *i-234*. b)  $\delta^{18}\text{O}_{\text{benthos}}$  of Site 967 overlain by the stacked  $\delta^{18}\text{O}_{\text{benthos}}$  of Lisiecky and Raymo, [2005] (thick black line). Notice that  $\delta^{18}\text{O}_{\text{benthos}}$  of the stack is shifted to the right by 0.5‰ for clarity. c)  $\delta^{18}\text{O}_{\text{benthos}}$  of ODP Site 981 and DSDP Site 607. Notice that the  $\delta^{18}\text{O}_{\text{benthos}}$  of Site 981 is shifted to the left by 1‰ for clarity.  $\delta^{18}\text{O}_{\text{benthos}}$  of MIS100 (Chapter 3) is plotted versus age (kyr),  $\delta^{18}\text{O}_{\text{benthos}}$  of MIS98-95 (Site 981: data Draut et al. [2003]; Site 607 Raymo et al., [1989]) is plotted versus metre composite depth. All  $\delta^{18}\text{O}$  are in ‰ PDB and plotted on an inverse axis.

5.1). These  $\delta^{18}\text{O}$  amplitudes of Mediterranean Site 967 are similar to those from the North Atlantic ODP Leg 162 Site 981 (data of MIS100 see *Chapter 3*; MIS98-96 data of *Draut et al.* [2003]) and DSDP Leg 94 Site 607 (data of MIS100 see *Chapter 3*; MIS98-96 data of *Raymo et al.*, [1989]). All  $\delta^{18}\text{O}_{\text{benthos}}$  records reveal an overall distinct asymmetric pattern characterised by a gradual increase during the early glacial toward maximum values during full glacial conditions and a sudden decrease at the termination. This implies that both the ice volume and temperature contributions to the  $\delta^{18}\text{O}$  signal of the Mediterranean and open ocean Atlantic records are of the same magnitude, considering that salinity-related changes of the isotopic composition are negligible. This is in agreement with the LR04 global stacked benthic oxygen isotope record [*Lisiecki and Raymo 2005*], which exhibit a similar geometry and amplitude of the glacial-interglacial variability (Figure 5.1).

In all  $\delta^{18}\text{O}$  records, MIS98 is outstanding as it lacks the extreme asymmetry or saw tooth shape of MIS100 and MIS96. Instead MIS98 is almost symmetric with maximum  $\delta^{18}\text{O}$  values being centred in the middle of the glacial. Remarkably, the  $\delta^{18}\text{O}$  of MIS98 is in phase with orbital obliquity with maximum  $\delta^{18}\text{O}$  values (midpoint of glacial) being



**Figure 5.2: CLEAN spectrum of the  $\delta^{18}\text{O}$  (a) and Ti/Al (b) of Site 967. Horizontal stipple lines indicate significance levels.**

associated with minimum obliquity and minimum  $\delta^{18}\text{O}$  values (midpoints of interglacial MIS99 and MIS97) being associated with maximum obliquity. This is in contrast to MIS100 and MIS96 where maximum  $\delta^{18}\text{O}$  values (midpoints of glacial) lag

minimum obliquity by 8–9 kyr. Additionally, MIS98 seems to be thinner compared to the other glacials and has a  $\sim 2$  kyr shorter duration than MIS100 and a  $\sim 4$  kyr shorter duration than MIS96, respectively.

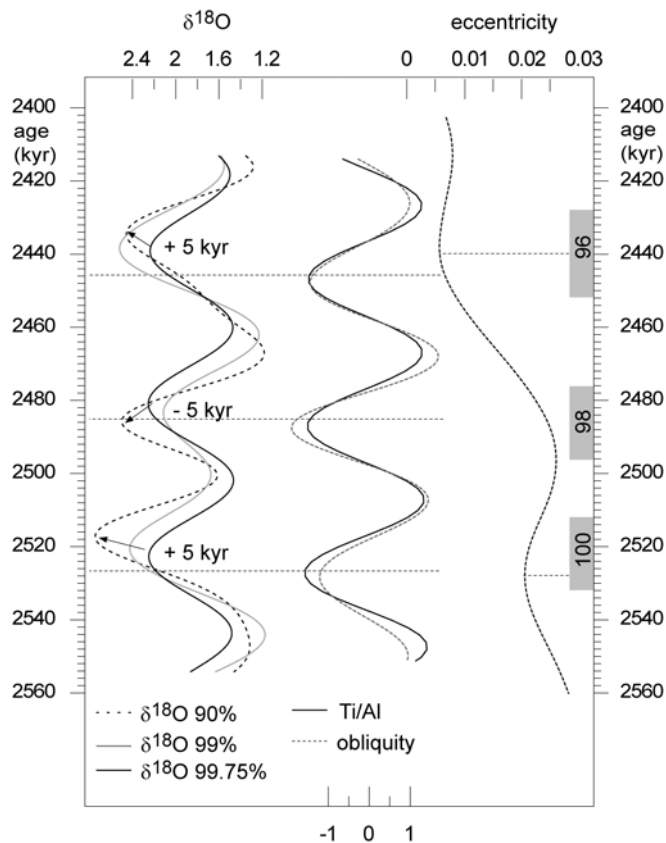


**Figure 5.3:** Cleaned signals of the  $\delta^{18}\text{O}$  time series of Site 967 at the 90% (stipple line), 99% (grey line) and 99.75% (black line) significance level in comparison with the 41-kyr component of the Ti/Al (black line) orbital obliquity (grey dashed line) and eccentricity (black dashed line). Horizontal stipple lines indicate obliquity and eccentricity minima, respectively. Arrows and numbers indicate the shift in the time lag of  $\delta^{18}\text{O}$  with respect to obliquity minima. Shaded areas indicate marine isotope stages.

A comparison between the  $\delta^{18}\text{O}$  records with the  $\text{La04}_{(1,1)}$  June21 summer insolation at  $65^\circ\text{N}$  indicates that the interval of MIS98 is associated with a relatively narrow insolation minimum with summer insolation values being twice as low as during the preceding (i-243) and following (i-241) insolation minimum (Figure 5.1). This exceptional insolation configuration results from the coincidence of a minimum in obliquity with a maximum in precession. In addition, precession minima i-242 and i-240 fall on the glacial-interglacial transitions. Low  $\delta^{18}\text{O}$  values coincide with precession minima, resulting either in a prolongation of interglacial  $\delta^{18}\text{O}$  values (MIS99 or MIS97), a narrow glacial (MIS98) or an interruption of glacial maximum  $\delta^{18}\text{O}$  values (MIS100, MIS96).

The CLEAN spectrum of the  $\delta^{18}\text{O}$  indicates maximum concentration of variance above the 99.75% significance level at 41 kyr (Figure 5.2). Furthermore, concentration

of variance above the 99% and 90% significance level is observed at 80 kyr and 28 kyr but absent in the precession-band. The cleaned (or filtered)  $\delta^{18}\text{O}$  signal above the 99.75%, 99% and 90% significance level results in three curves that are composed of a) a sole 41-kyr period, b) combination of the 41-kyr and 80-kyr periods and c) combination of 41-kyr, 80-kyr and 28-kyr components of the  $\delta^{18}\text{O}$  record (Figure 5.3). Maximum values in the 41-kyr component of the  $\delta^{18}\text{O}$  record are offset with respect to their correlative obliquity minima by 5.2 kyr for MIS100, 5.8 kyr for MIS98 and 7.5 kyr for MIS96 (Table 5.1).

**Table 5.1: Phase lags and cross correlation of with orbital obliquity.**

|                                 | MIS100    |                | MIS98     |                   | MIS96     |                |
|---------------------------------|-----------|----------------|-----------|-------------------|-----------|----------------|
|                                 | Age (kyr) | Time lag (kyr) | Age (kyr) | Time lag (kyr)    | Age (kyr) | Time lag (kyr) |
| Obliquity-minimum               | 2528.0    |                | 2487.0    |                   | 2447.0    |                |
|                                 |           | 41.0           |           | 40.0              |           |                |
| <b>41kyr</b>                    |           |                |           |                   |           |                |
| $\delta^{18}\text{O}$ (max)     | 2522.8    | 5.2            | 2481.2    | 5.8               | 2439.5    | 7.5            |
| Ice <sub>tot</sub> (max)        | 2520.4    | 7.6            | 2479.5    | 7.5               | 2438.5    | 8.5            |
| NAM (max)                       | 2521.0    | 7.0            | 2480.5    | 6.5               | 2440.0    | 7.0            |
| EAS (max)                       | 2519.7    | 8.3            | 2478.5    | 8.5               | 2437.2    | 9.8            |
| T <sub>air</sub> (min)          | 2526.2    | 1.8            | 2484.1    | 2.9               | 2442.0    | 5.0            |
| Ti/Al (max)                     | 2527.7    | 0.3            | 2486.8    | 0.2               | 2445.9    | 1.1            |
| <b>41kyr, 80kyr &amp; 28kyr</b> |           |                |           |                   |           |                |
| $\delta^{18}\text{O}$ (max)     | 2517.5    | 10.5           | 2486.0    | 1.0               | 2434.8    | 12.3           |
| Ice <sub>tot</sub> (max)        | 2516.3    | 11.7           | 2484.4    | 2.6               | 2434.5    | 12.5           |
| NAM (max)                       | 2517.3    | 10.7           | 2484.9    | 2.1               | 2434.9    | 12.1           |
| EAS (max)                       | 2515.4    | 12.6           | 2484.0    | 3.0               | 2433.8    | 13.2           |
| T <sub>air</sub> (min)          | 2522.1    | 5.9            | 2488.8    | -1.8              | 2439.3    | 7.7            |
|                                 |           | Average        |           | Cross-correlation |           |                |
| <b>41kyr</b>                    |           | Time lag (kyr) |           | Time lag (kyr)    |           |                |
| $\delta^{18}\text{O}$ (max)     |           | 6.2            |           | 6.4               |           |                |
| Ice <sub>tot</sub> (max)        |           | 7.9            |           | 8.1               |           |                |
| NAM (max)                       |           | 6.8            |           | 7.1               |           |                |
| EAS (max)                       |           | 8.9            |           | 9.1               |           |                |
| T <sub>air</sub> (min)          |           | 3.2            |           | 3.6               |           |                |
| Ti/Al (max)                     |           | 0.5            |           | 0.5               |           |                |

These offsets with respect to obliquity increases to 10.5 kyr and 12.3 kyr for MIS100 and MIS96, respectively, and decreases to 1.0 kyr during MIS98, when including the 80-kyr and 28-kyr components in the reconstructed  $\delta^{18}\text{O}$  (Table 5.1).

### 5.3.2. Inverse forward modelling

Decomposition of the  $\delta^{18}\text{O}$  using the inverse forward modelling approach indicates that both ice volume and NH surface air temperature contribute almost evenly with  $\sim 0.5$ -

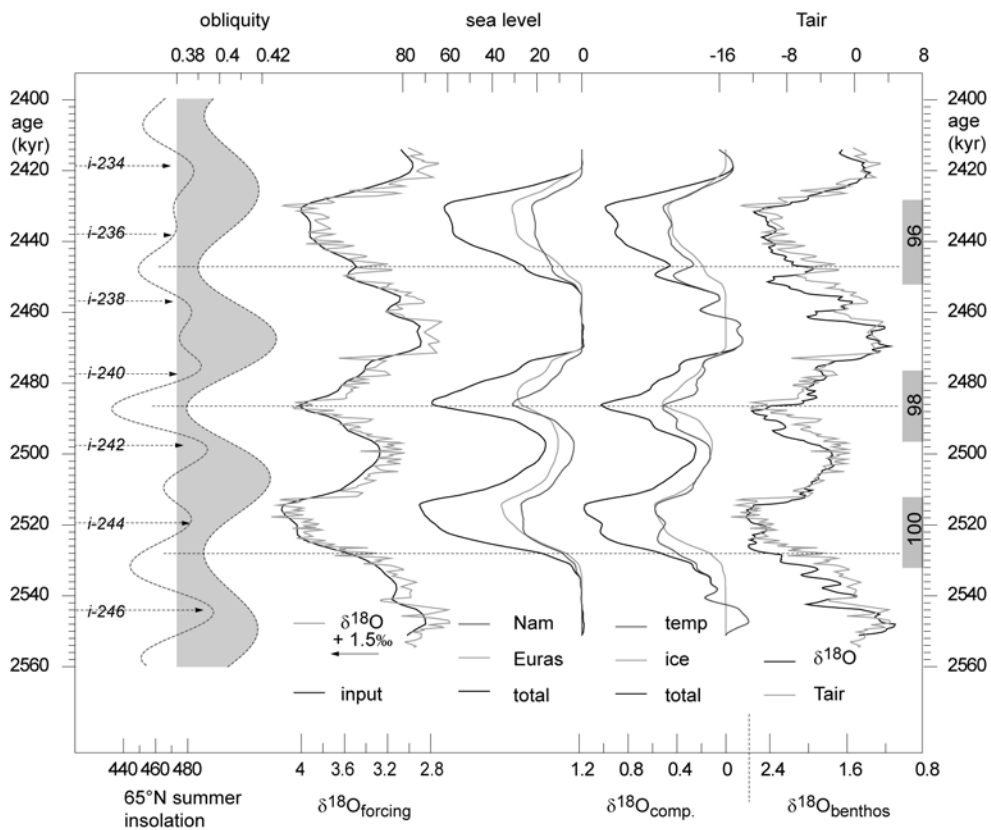
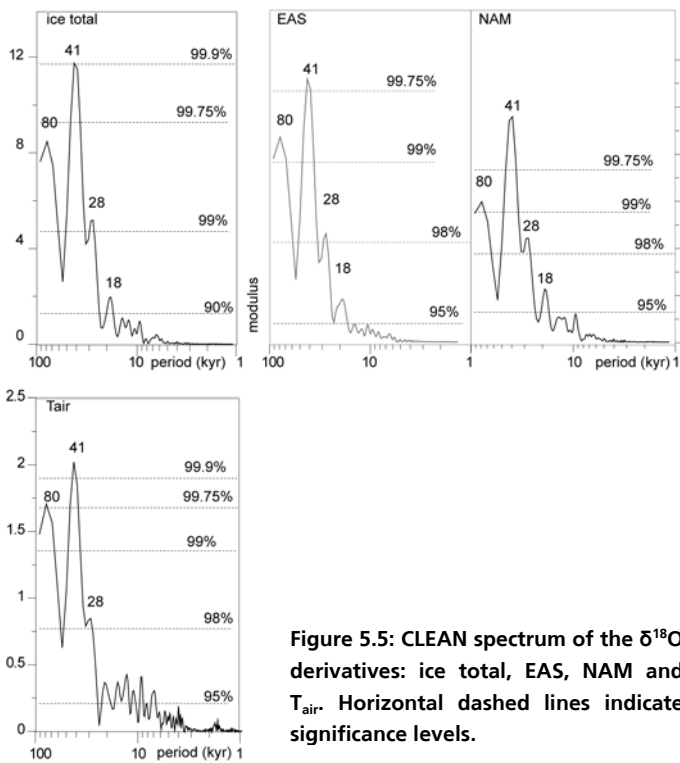


Figure 5.4: Results of the inverse forward modelling: a) 21 June summer insolation of 65°N and orbital obliquity of the La04<sub>(1,1)</sub> astronomical solution versus age (kyr). Insolation maxima are numbered with the i-cycle coding after *Lourens et al.* [1996]. Maxima in obliquity are grey shaded, minima indicated by thin horizontal stipple lines. b) Input data. Original  $\delta^{18}\text{O}_{\text{benthos}}$  of Site 967 (thin grey line) moved to the left by 1.5‰ for clarity and smoothed  $\delta^{18}\text{O}_{\text{benthos}}$  of Site 967 (black line) similarly adjusted. c) Output data: Global ice volume in metre sea level equivalents (black line), split up in contribution of Eurasian ice sheets (grey line) and North American ice sheets (thin black line). d) smoothed  $\delta^{18}\text{O}_{\text{benthos}}$  of Site 967 (black line) decomposed into a global ice volume component (grey line) and a temperature component (thin black line). e) Annual mean air temperature (black line) averaged over continents north of 40°N in comparison with  $\delta^{18}\text{O}_{\text{benthos}}$  of Site 967 (grey line).

0.6‰ to the glacial-interglacial  $\Delta\delta^{18}\text{O}$  changes recorded at Site 967 (Figure 5.4). This results in an absolute sea level change of 60-70 m during MIS101-95, with a maximum low stand (71 m) during MIS100. Maximum ice volume and minimum temperatures associated with MIS100 and MIS96 are largely out of phase with respect to obliquity, but are almost in phase with obliquity during MIS98. In addition, the build-up of the North American (NAM) and Eurasian (EAS) ice sheets show saw-tooth asymmetry during MIS100 and MIS96, but not during MIS98 (Figure 5.4c). The annual mean air temperature ( $T_{\text{air}}$ ) averaged over the continents north of 40°N is very similar to the  $\delta^{18}\text{O}$ . Small-scale variations as observed in the  $\delta^{18}\text{O}$  are amplified in the  $T_{\text{air}}$  (Figure 5.4d). The glacial-interglacial change of  $T_{\text{air}}$  is 12-14°C with superimposed variations in the order of 4-8°C at irregular spacing. Generally,  $T_{\text{air}}$  leads changes in the  $\delta^{18}\text{O}$ .

Spectral analysis of the modelled individual ice sheet and temperature components indicates concentration of power at 80 kyr, 41 kyr and 28 kyr above the 99% significance level (Figure 5.5) and are thus very similar to that obtained from the  $\delta^{18}\text{O}$  record (Figure 5.6). Additional peaks (being significant above the 90% significance level) in the ice volume spectrum are resolved at 18 kyr, 16 kyr and 10 kyr periods. Spectral power in the precession-band (23-19 kyr) is very weak to absent and is only



**Figure 5.5: CLEAN spectrum of the  $\delta^{18}\text{O}$  derivatives: ice total, EAS, NAM and  $T_{\text{air}}$ . Horizontal dashed lines indicate significance levels.**

significant (above the 90% significance level) for  $T_{\text{air}}$ . Maxima in the 41-kyr component of the modelled total ice volume signal lag minima in the obliquity cycle with 7.6 kyr (MIS100), 7.5 kyr (MIS98) and 8.5 kyr (MIS96). In case the 80-kyr and 28-kyr components are included in the reconstruction, time lags related to MIS100 and 96 increases with  $\sim 4$  kyr and decreases with  $\sim 5$  kyr during MIS98 (Table 1). With reference to total ice volume, changes in NAM lead and EAS lag with  $\sim 0.6$ -1.5 kyr.



The maxima in the 41-kyr component of  $T_{\text{air}}$  lag obliquity with 1.8 kyr, 2.9 kyr and 5.0 kyr during MIS100, MIS98 and MIS96, respectively. The lag increases to 5.9 kyr and 7.7 kyr during MIS100 and MIS96, respectively, and decreases to a lead of 1.8 kyr during MIS96, when including the 80-kyr and 28-kyr component in the reconstructions.

## 5.4. Discussion

### 5.4.1. Late Pliocene glacial-interglacial temperature and ice volume changes

The outcome of the inverse forward modelling experiment indicates that the benthic  $\delta^{18}\text{O}$  changes during the late Pliocene were composed of an equally large temperature and ice volume component of which the first is leading. The estimated sea level changes of 60–70 m for MIS100–96 are smaller than considered by *Raymo et al.*, [1989], who assumed that change in the benthic  $\delta^{18}\text{O}$  record of North Atlantic DSDP Site 607 were composed to two-thirds by ice volume and to one-third by temperature. Using this ratio, which has been established for the late Pleistocene record at the same site, largest  $\delta^{18}\text{O}$  values during glacial stages MIS100 and MIS96 would present ice growth events equivalent to a  $\sim 80$  m sea level change. Hence the ice model results suggest that this is an overestimation. Our results differ even more from the sea-level constraints derived from the shallow-marine successions of New Zealand, which revealed changes in the order of  $110 \pm 20$  m for MIS100–99,  $100 \pm 20$  m for MIS98–97, and  $78 \pm 20$  m for MIS96–95 [Naish 1997]. This would imply that either 1) the

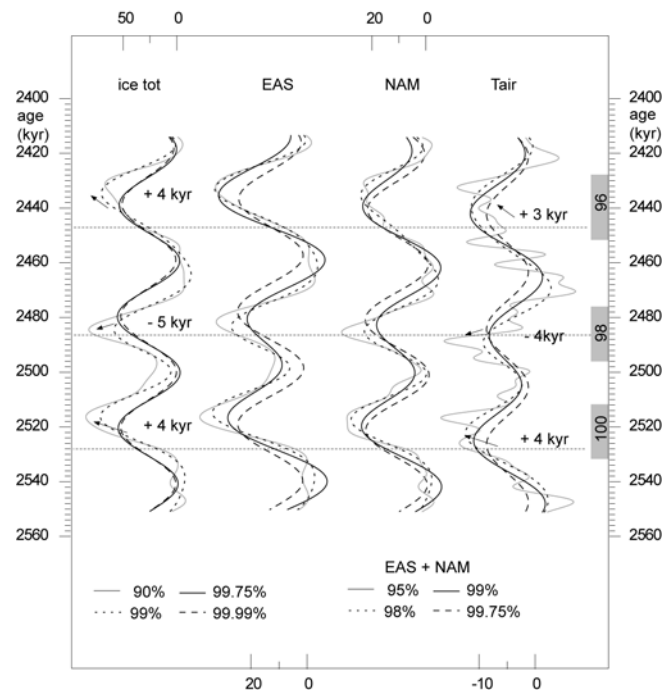


**Figure 5.6: Cleaned signals of the  $\delta^{18}\text{O}$  derivatives: ice total, EAS, NAM and  $T_{\text{air}}$  at the 90% (grey line), 99% (thin dashed line), 99.75% (black line) and 99.9% (thick dashed line) significance level. Horizontal stipple lines indicate obliquity minima. Arrows and numbers indicate the shift in the time lag with respect to obliquity minima.**

Mediterranean  $\delta^{18}\text{O}$  signal is not representative for global sea-level changes and NH surface air temperatures alone, but is strongly influenced by regional changes in bottom water temperature and salinity, 2) almost the entire  $\delta^{18}\text{O}$  signal associated with MIS100-96 should be attributed to ice volume changes and not present an equal amount of NH surface air temperature as indicated in our model, or 3) the eustatic sea-level constraints based on the shallow marine successions of New Zealand are highly overestimated.

Mediterranean deep water is generally warmer than that of the open ocean, but the similarity in glacial/interglacial amplitude and shape of the Mediterranean and Atlantic benthic  $\delta^{18}\text{O}$  records strongly points to a comparable deep water temperature and ice volume component in both oceans. In addition, the outcome of the same inverse modelling experiment on the LR04 global oxygen isotope stack revealed a  $\sim 60$  m of sea-level change during the glacial/interglacial transitions of MIS100-96 [Bintanja and van de Wal in prep.], indicating that a regional salinity and/or temperature component would account for maximal 15% of the total  $\delta^{18}\text{O}$  signal in the Mediterranean, therefore excluding option 1. The excellent agreement between model results and independent proxy data over the past 400 kyr [Bintanja et al., 2005a] indicates that the model is capable of correctly extracting the temperature component from the  $\delta^{18}\text{O}$  signal over that time interval. An overestimation of the temperature contribution by the model for the late Pliocene time interval seems unlikely, but uncertainties related to the isotopic composition and volume of the Antarctic and Greenland ice sheets - which were excluded from our simulations -, temperature to  $\delta^{18}\text{O}$  relationship in precipitation, and atmosphere to deep water temperature relationships [Bintanja et al., 2005b] may explain part of the discrepancy. On the other hand, this discrepancy can also be partly attributed to the large uncertainty estimates derived for the eustatic sea-level reconstructions.

#### 5.4.2. Astronomical forcing: linear and nonlinear systems

Notwithstanding the relatively short time series, the CLEAN algorithm clearly unravels dominant power in the  $\delta^{18}\text{O}_{\text{benthos}}$  record and its modelled derivatives (ice volume and NH surface air temperature) at 41, 80 and 28 kyr periods. Evidently, all these records are controlled by the 41 kyr cycle of obliquity, whereas a direct influence of the precession cycle is notably absent. This is in contrast to the spectral characteristics of the Ti/Al record for the same time interval that exhibit strong power at 21, 41 and 80 kyr (Figure 2b). The changes in Ti/Al on both precession and obliquity time scales were interpreted to reflect the direct influence of astronomical-induced insolation changes on circum-Mediterranean climate (aridity) conditions through African monsoon intensity [Lourens et al., 2001; Tuenter et al., 2005]. The absence of a clear precession signal in the  $\delta^{18}\text{O}_{\text{benthos}}$  record of Site 967 confirms that this record is not significantly altered by regional aridity or temperature changes, but dominated by global-scale glacial/interglacial variations.

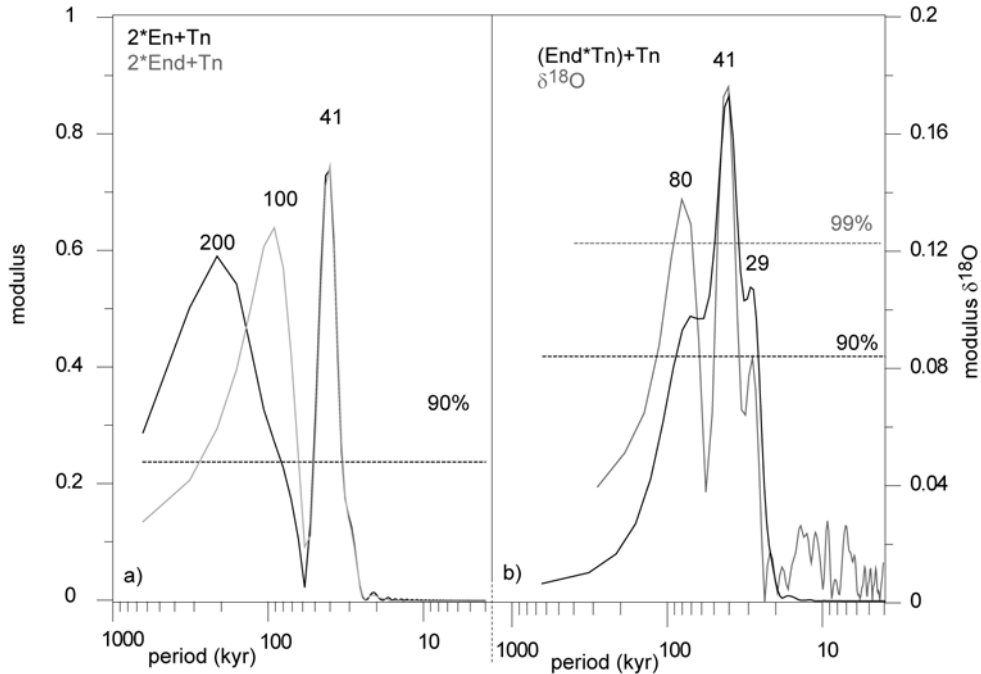


**Figure 5.7: CLEAN spectrum of a)  $2E_n+T_n$  (black line) and  $2E_{nd}+T_n$  (grey line) and b)  $T_n+(E_{nd}*T_n)_n$  (black line) and  $\delta^{18}O$  (grey line). Horizontal stipple lines indicate significance levels.**

At first sight, the strong 80 kyr period seems to mark the characteristic difference between MIS100 and MIS96 on the one hand and MIS98 on the other hand. From the combined filter of the 80 and 41 kyr cycles it seems that the 80-kyr component reflects the alternating high-low-high amplitude maximum in the  $\delta^{18}O_{\text{benthos}}$  record, where 80 kyr maxima are associated with the severe and long MIS100 and MIS96 and the minimum in the 80 kyr cycle with the intervening weaker and relatively short MIS98 (Figure 5.3). Remarkably, this alternating pattern coincides with a short-term ( $\sim 80$  kyr) eccentricity cycle, where MIS100 and MIS96 occur during a local minimum and MIS98 during a local maximum. To test the possible imprint of an 80-kyr eccentricity cycle on the spectrum of the  $\delta^{18}O_{\text{benthos}}$  record we have run the clean algorithm for the combined eccentricity (E) and obliquity (T) time series in the time interval 2.4–2.56 Ma. For this purpose the sum was taken for both normalized astronomical parameters ( $E_n$  and  $T_n$ , respectively) of which  $E_n$  was multiplied by 2 (i.e.  $2E_n+T_n$ ). The CLEAN spectrum of this time series clearly reveals a strong 41 kyr peak, but almost all variance in the eccentricity band is concentrated at low frequencies with a mean period of  $\sim 200$  kyr (Figure 5.7a). This long period has been attributed to the trend in eccentricity related to its 400-kyr component (Figure 5.3). We therefore detrended the eccentricity time series ( $E_{nd}$ ) and followed the same procedure again. The resulting  $2E_{nd}+T_n$

spectrum reflects a strong peak at  $\sim 100$  kyr, which is still significantly offset from the strong 80 kyr cycle observed in the  $\delta^{18}\text{O}$  record (Figure 5.7b). This discrepancy is confirmed by the very low correlation ( $r^2 = .009$ ,  $n = 157$ ) between the filtered 60-110-kyr components of the  $\delta^{18}\text{O}$  and  $2E_{\text{nd}} + T_n$  series (Figure 5.8). Hence, a linear response of the ice sheets to eccentricity forcing seems unlikely, but in view of the short time series we readily acknowledge that eccentricity modulation of these three stages is difficult to prove objectively. It is, however, interesting to note that the encompassing weak MIS94 and MIS102 [i.e. *Zachariasse et al.*, 1990; *Lourens et al.*, 1996] are close to short-term eccentricity maxima as well and that the direct influence of the eccentricity on late Pliocene climates has been well considered [*Clemens and Tiedemann* 1997].

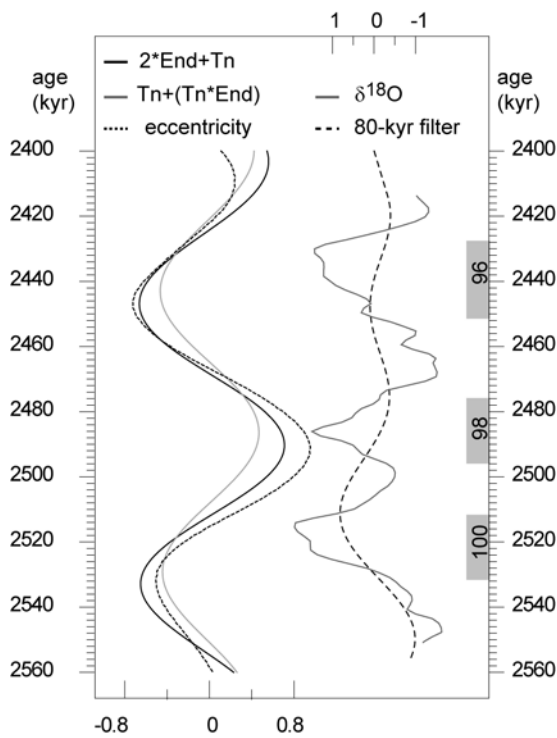


**Figure 5.8: Comparison between the normalised 80-kyr components of  $2E_{\text{nd}} + T_n$  (black),  $T_n + (E_{\text{nd}} * T_n)_n$  (grey, inverted),  $E_{\text{nd}}$  (dashed line) and the normalised  $\delta^{18}\text{O}$  (grey) of Site 967 overlain by the filtered 80-kyr component (dashed line, inverted). Filters were obtained by applying a Gaussian band-pass filter centred at frequency 0.0125 and bandwidth 0.002.**

In the  $\delta^{18}\text{O}_{\text{benthos}}$  spectrum, and that of its derivatives ice volume and NH surface air temperature, another strong peak, besides the one at  $\sim 80$  kyr, was observed at  $\sim 28$  kyr, suggesting that nonlinear interactions between obliquity and eccentricity may have played an important role in determining the frequency characteristics and shape of the glacial/interglacial succession. Such a (weak) nonlinear interaction could generate a peak in the frequency spectrum at  $\sim 70$  kyr, resulting from difference frequency ( $1/41 + 1/100 = 1/70$ ) and a secondary peak at  $\sim 29$  kyr resulting from the sum frequency ( $1/100 + 1/41 = 1/29$ ) [*Pisias and Rea* 1988]. The imprint of the  $\sim 70$  kyr and  $\sim 29$  kyr cycle is a common feature in late Pleistocene  $\delta^{18}\text{O}_{\text{benthos}}$  records [e.g. *Huybers and Wunsch* 2004; *Lisiecki and Raymo* 2005]. This is in agreement with the findings of *Rial and Anaclerio* [2000], who found evidence for strong spectral density at  $\sim 69$  kyr and  $\sim 29$  kyr in climate data of the Vostock ice core, which they interpreted accordingly to present sidebands of the frequency modulated obliquity

signal. According to them, frequency modulation should occur if the 413-kyr eccentricity signal and its harmonics and sub-harmonics frequency-modulate the 100-kyr eccentricity, obliquity and possibly the precession signals. This will result in a nonlinear interband interaction, where energy is transferred from one band into the other thereby creating combination tones (sidebands) of the primary forcing (carrier).

In addition, *Pisias and Rea* [1988] and *Beaufort et al.* [2001] extensively discussed a 30–31 kyr period found in late Pleistocene productivity and wind intensity records from the tropical Pacific and tropical Indian oceans. By applying cross spectral analyses *Beaufort et al.* [2001] showed that these productivity series are highly coherent with the CO<sub>2</sub> record of Antarctica at the 30- and 23-ky periods, indicating that biological production in the equatorial Indo-Pacific may act as an important mechanism in controlling atmospheric CO<sub>2</sub> concentrations. Hence this would imply that the ~29 kyr cycle observed in Vostok are primarily related to non-linear processes driven by the precession cycle. Indeed, the difference frequency between eccentricity and 23 kyr precession component could also produce a peak at 30 kyr ( $1/23 - 1/100 = 1/30$ ). In the  $\delta^{18}\text{O}_{\text{benthos}}$  spectrum of Site 967, however, no significant variance is observed at the primary precession frequencies in, which makes such a nonlinear scenario in our case unlikely.

Since our  $\delta^{18}\text{O}_{\text{benthos}}$  record of Site 967 is too short to apply higher order statistics we use a different approach in order to further test if nonlinear interactions between eccentricity and tilt could produce a period of 29 kyr in the studied time interval. For this purpose, we introduce a weak nonlinearity into the combined  $E_{\text{nd}}$  and  $T_{\text{n}}$  time series by simply adding  $T_{\text{n}}$  to the normalised product of  $E_{\text{nd}} \star T_{\text{n}}$  (i.e.  $T_{\text{n}} + (E_{\text{nd}} \star T_{\text{n}})_{\text{n}}$ ) and, subsequently, applied spectral analysis on the  $T_{\text{n}} + (E_{\text{nd}} \star T_{\text{n}})_{\text{n}}$  signal (Figure 5.7b). Evidently, the spectrum reveals strong peaks at 70, 41 and 29 kyr, approximating the observed power spectrum of the  $\delta^{18}\text{O}_{\text{benthos}}$  record. Hence, a combination of linear obliquity forcing and nonlinear interactions between obliquity and eccentricity forcing could account for most of the variance observed in the  $\delta^{18}\text{O}_{\text{benthos}}$  time series between 2.4 and 2.56 Ma. Nevertheless, the correlation coefficient calculated between the filtered 60–110 kyr components of the  $\delta^{18}\text{O}_{\text{benthos}}$  and the  $T_{\text{n}} + (E_{\text{nd}} \star T_{\text{n}})_{\text{n}}$  series is even lower ( $r^2=0.074$ ,  $n=157$ ) than in case of a linear eccentricity response ( $2E_{\text{nd}}+T_{\text{n}}$ ). Hence, such a nonlinear system cannot unambiguously explain the lower frequencies in the spectra observed.

Taking a closer look at Figure 5.8 shows that the 80-kyr component in the  $\delta^{18}\text{O}_{\text{benthos}}$  record seems to differentiate between a strong maximum in the filtered record associated with MIS100 and part of MIS98 and a smaller maximum during MIS96. The modelled ice volume ( $\text{ice}_{\text{total}}$ , NAM and EAS) records indicate that there were still significant ice caps left during interglacial MIS99, in particular at EAS (Figure 5.4). In contrast, during MIS101, MIS97 and MIS95 sea level returned to zero values. Apparently, ice caps developed during MIS100 became large enough to survive

insolation maxima during MIS99. Hence, merging of these two glacial periods due to this nonlinear response of the ice sheets to obliquity forcing could explain the  $\sim 80$  kyr. In addition, the sum frequency between this 80 kyr (secondary) and the 41 kyr (primary) components may also explain the strong secondary peak at 28 kyr.

### 5.4.3. Late Pliocene obliquity-related response times of global ice volume

Cross-correlation analyses between the 41-kyr components of the various proxy records and the obliquity time series of the studied time interval revealed that changes in circum-Mediterranean climate conditions (Ti/Al) preceded changes in NH surface air temperature and total ice volume by  $\sim 3$  kyr and  $\sim 7.5$  kyr, respectively, whereas there are almost in phase ( $+0.5$  kyr) with obliquity (Figure 5.9). The latter is not surprising since an almost in phase relationship between obliquity and the 41-kyr component in Ti/Al has been used to constrain the optimum values for the tidal dissipation and dynamical ellipticity terms incorporated in the astronomical solution [Lourens *et al.*, 2001]. Considering the accuracy of our age model, largest uncertainties in the obliquity-related lag for the Ti/Al series in our time interval do not arise from the optimum tidal dissipation and dynamical ellipticity values, but from the adopted in phase relationship between Ti/Al and insolation forcing. Including a 3 kyr lag as assumed by Lourens *et al.*, [1996; 2004] for the (Ti/Al-related) sapropel chronology of the Mediterranean would increase all obliquity-related lags displayed in Figure 5.9 with

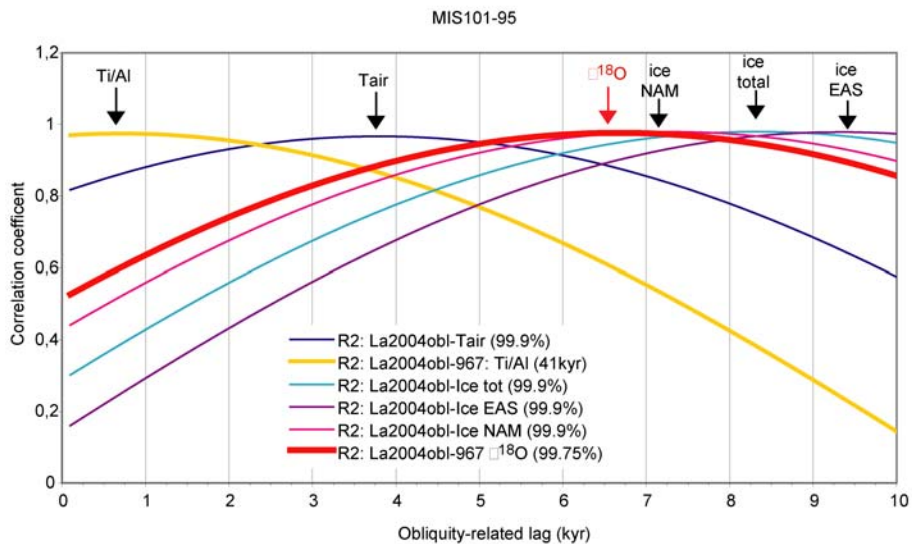


Figure 5.9: Cross correlation of the 41-kyr components of Ti/Al,  $\delta^{18}O$ , ice tot, NAM, EAS and  $T_{air}$  with orbital obliquity.

3 kyr, but will leave their internal phase relations unchanged. This would imply that the average obliquity-related lag for the  $\delta^{18}\text{O}_{\text{benthos}}$  time series (Table 5.1) should have been 9.4 kyr. A 9.4 kyr lag is even larger than the 8 kyr estimated for the late Pleistocene by SPECMAP [Imbrie *et al.*, 1984]. In contrast, a 6.4 kyr response time for the benthic isotope curve is in much better agreement with a  $T_m$  value of  $\sim 8.5$  adopted for the late Pliocene time interval of the LR04 stack [Lisiecki and Raymo 2005]. On this basis, we consider the lower response time of 6.4 kyr for the  $\delta^{18}\text{O}_{\text{benthos}}$  record as the most likely.

The  $\sim 4.5$  kyr lag of ice volume with respect to NH surface air temperature is slightly less than the 6 kyr derived from the LR04 stack at 2.5 Ma [Bintanja and van de Wal in prep.]. This discrepancy is possibly due to the longer (500 kyr) time interval used by Bintanja and van de Wal for cross-spectral analysis, thereby, including also the on average less severe late Pliocene glacial stages. In this respect, the ice volume to NH surface air temperature response during MIS100, MIS98 and MIS96 resembles the glacial/interglacial conditions during the Mid-Pleistocene climate transition at  $\sim 1.5$  Ma, when the 100-kyr glacial cycles started to emerge [Bintanja and van de Wal in prep.]. The EAS ice sheets have relatively the largest response time due to the colder and drier climate conditions, which resulted in average accumulation rates being roughly half of its NAM counterpart [Bintanja and van de Wal in prep.].

In general, the observed differences between the primary obliquity-related lags associated with the individual stages are small (Table 5.1). Largest response times with respect to the obliquity minima are observed for MIS96, including that of the Ti/Al record. Probably this increase is linked to uncertainties in the age model derived from either the tuning target or position of the calibration points. More interestingly is the observation that the timing of optimum glacial conditions in both temperature and ice volume components changes differently for the three stages by incorporating the 80- and 28 kyr periods. This observation has considerable implications for dating late Pliocene benthic isotope records since tuning them to either a combined obliquity-precession target curve or a simple ice sheet model assuming fixed time lags [i.e. Raymo *et al.*, 1989; Shackleton *et al.*, 1990; Lisiecki and Raymo 2005] will suppress nonlinearities as discussed above and lead to artificial changes in sedimentation rates (see also Huybers and Wunsch [2004]).

## 5.5. Conclusions

We have decomposed the benthic  $\delta^{18}\text{O}$  of ODP Site 967 (eastern Mediterranean) encompassing MIS101-MIS95 ( $\sim 2.5$  Ma) into an ice volume and a Northern Hemisphere surface air temperature component using a recently developed inverse modelling approach. Our results indicate a significant larger temperature component in the benthic  $\delta^{18}\text{O}$  records during the late Pliocene than thus far assumed. Consequently,

sea-level changes during MIS100-96 based on benthic  $\delta^{18}\text{O}$  estimates have been overestimated by approximately 20-50 m.

Spectral analysis of the  $\delta^{18}\text{O}$  record (and of its derivatives ice volume and a Northern Hemisphere surface air temperature indices) reveals significant concentration of variance at 80, 41 and 28 kyr, similar to that found in late Pleistocene deep sea  $\delta^{18}\text{O}$  records. The 41 kyr cycle is interpreted as reflecting the dominance of the astronomical obliquity cycle, whereas the 80 and 28 kyr components are related to nonlinear behaviour of the ice sheets to this primary forcing mechanism. Evidence for (non)linear interactions between eccentricity and obliquity was not found.

The 41-kyr component of the  $\delta^{18}\text{O}$  record lags astronomical obliquity by  $\sim 6.4$  kyr in accordance to that adopted in the recently established global  $\delta^{18}\text{O}$  stack for this time interval. However, the time lags between optimum glacial conditions (i.e., maximum  $\delta^{18}\text{O}$  values) and the minimum of their corresponding obliquity cycle increase and decrease with  $\sim 5$  kyr for MIS100 and MIS96, and MIS98 respectively, and are related to the presence of the 80- and 28-kyr components.



# CHAPTER 6

## Evaluation of African aridity and North Atlantic Dansgaard-Oeschger cycles during Pliocene MIS101-95

### Abstract

High-resolution planktonic and benthic oxygen isotope data of the Mediterranean marine land-based section of San Nicola (Sicily/Italy) and eastern Mediterranean ODP Leg 160 Site 967 are presented together with colour reflectance (CR) and magnetic susceptibility (MS) data of the same sites and of DSDP Leg 94 Site 607 and ODP Leg 162 Site 981 (North Atlantic) throughout marine oxygen isotope stages (MIS) 101-95. Visual inspection of the climate records indicates a relationship between Mediterranean temperature and aridity with North Atlantic temperature and ice rafting history both on a glacial-interglacial (41 kyr) as well as a stadial-interstadial (6-7 kyr) scale and possibly millennial (3.5 kyr) scale. Spectral analysis of the Mediterranean  $\delta^{18}\text{O}$  records indicates high variance at periodicities similar to those observed in the ice volume record (i.e. 80 kyr, 41 kyr, and 28 kyr; *Chapter 5*), whereas spectra of the Mediterranean sediment property (CR and MS) records indicate additional variance within the precession band and at periodicities equal to harmonics and combination tones of primary precession, suggesting a low latitude forcing component. On the contrary, frequency-modulation may explain the 8-12 kyr periodicities in  $\delta^{18}\text{O}$  and the non-stationary character of this signal in the sub-Milankovitch range, the modulator being probably the ~80 kyr (ice volume) component.

## 6.1. Introduction

Mediterranean climate during late Pliocene marine oxygen isotope stage 100 (MIS100) underwent rapid fluctuations similar to those associated with the Dansgaard-Oeschger (D-O) and Heinrich events (HE) of the late Pleistocene (*Chapter 2*). Distinct changes in Mediterranean sea surface temperature (SST) and deep convection occurred in conjunction with changes in SST, thermohaline circulation (THC) and ice rafting in the North Atlantic. This concurrence points to the coupling of Mediterranean and North Atlantic climate on millennial to Milankovitch time scales, either directly through the inflow of Atlantic surface waters into the Mediterranean or, more importantly, indirectly through an atmospheric connection with the North Atlantic climate system. Both these couplings are controlled by rapid oscillations in the Arctic-Greenland ice cap, where in particular severe (winter) winds from the Alps, similar to the present-day *bora* and *mistral* winds, during cold European climate conditions (cold D-O phases) resulted in downwelling of Mediterranean surface waters due to intensified cooling.

In addition to the strong winter cooling and the vigorous deep convection in the central Mediterranean during cold D-O and stadial intervals, grain size data and geochemical proxies point to an increase in aeolian dust supply of Saharan origin to the Mediterranean during these intervals. Maximum dust supply from the Sahara occurs during intervals of maximum ice rafting in the North Atlantic (*Chapters 3 and 4*) indicating a linkage between low-latitude African aridity/wind strength and North Atlantic cooling during MIS100 (*Chapters 3 and 4*). Such a relationship has been observed in the Mediterranean record of the past 50 kyr [Allen *et al.*, 1999; Moreno *et al.*, 2001; Combourieu-Nebout *et al.*, 2002; Sanchez-Goni *et al.*, 2002; Moreno *et al.*, 2004] and a strong atmospheric cross-latitudinal linkage between mid and high latitude has been suggested.

In order to further evaluate the relationship between low-latitude and high-latitude climate changes on sub-Milankovitch time scales during the major phase of Northern Hemisphere glaciation in the late Pliocene, we extended the benthic and planktonic foraminiferal  $\delta^{18}\text{O}$  records of San Nicola and ODP Site 967 (*Chapters 2 and 3*) up to MIS95. The new isotope data were subsequently compared with high-resolution magnetic susceptibility and colour reflectance records of the same sites as well as those of ODP Site 969 (Mediterranean) and ODP Site 981 and DSDP Site 607 in the North Atlantic. The Mediterranean oxygen isotope data suggest SST and deep water changes during MIS98 and MIS96 that are similar to the D-O and H-like climate variations observed during MIS100 (*Chapters 2 and 3*). The colour reflectance data of the North Atlantic sites suggest ice rafting episodes during MIS100, 98 and 96 on a D-O to Heinrich timescale (*Chapter 3*), whereas the magnetic susceptibility and colour reflectance records in the Mediterranean are probably controlled by changes in dust supply from the African continent (*Chapter 4*). To test for cyclicity in the observed

climate variability records we applied spectral analysis and band-pass filtering in the time as well as in the frequency domain on the long time series.

## 6.2. Materials and Methods

### 6.2.1. Sections and sampling

Samples have been derived from the Mediterranean land-based marine section of Monte San Nicola (Sicily/Italy) and ODP Leg 160 Site 967 Hole A (Figure 6.1). Monte San Nicola is situated 10 km north of the coastal town of Gela in southern Sicily (Italy) (for detailed location map and description see [Rio *et al.*, 1994]). San Nicola (SN) consists of a succession of ~160 m of rhythmically bedded marly limestones and marls from the Trubi and Monte Narbone Formation. Sapropels of the O, A, B

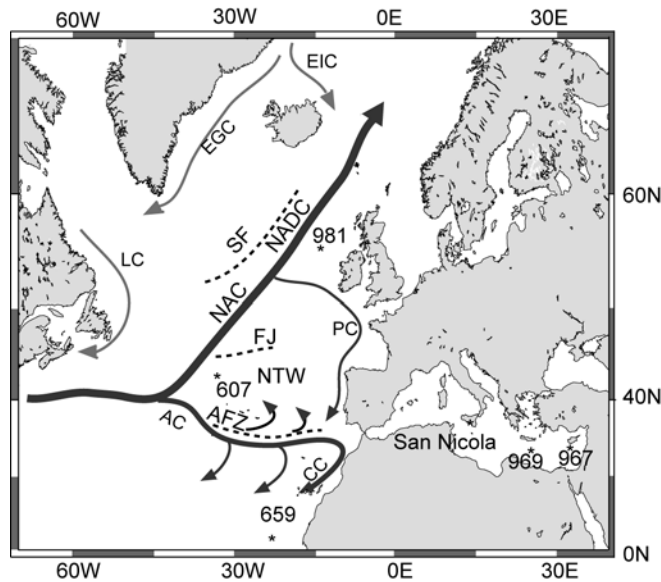


Figure 6.1: Location map of ODP Site 981, DSDP Site 607, Monte San Nicola section, ODP Site 967 and ODP Site 969. Arrows indicate North Atlantic surface water masses: AC – Azores current; CC – Canary current; NTW – North Atlantic transitional waters; NAC – North Atlantic current; PC – Portuguese current; EIC – East Iceland current; EGC – East Greenland current; LC – Labrador current. Dashed lines indicate frontal zones: AFZ – Azores Frontal Zone; SF – Subpolar Front; FJ – Frontal Jets.

and C clusters [Verhallen 1987; Zijderveld *et al.*, 1991] can easily be recognised in the section. Depth of deposition was estimated to be 800–1000 m [Bonaduce and Sprovieri 1984; Rio *et al.*, 1994] and the average sedimentation rate is ~8 cm/kyr [Sprovieri *et al.*, 1986]. The Gelasian GSSP (Global boundary Stratotype Section and Point) is formally defined in the San Nicola section at the top of the A<sub>5</sub> sapropel, also termed the SN marker bed [Rio *et al.*, 1994].

Marine oxygen isotope stages (MIS) 96–100 are well defined in the central Mediterranean by prominent incursions of the cold water planktonic foraminifer *Neogloboquadrina atlantica* [Zachariasse *et al.*, 1990]. At San Nicola, these stages are visible in the field as meter-scale grey-white alternations in between sapropel A<sub>5</sub> and the B

sapropel group with grey layers reflecting glacial stages 100, 98 and 96. Light-coloured decimetre thick bands are visible within the dark glacial stages. The base of MIS101 is characterised by a dark layer which represents the ghost sapropel that corresponds to insolation cycle i- 246 [Lourens *et al.*, 1996].

The interval of MIS101 to MIS95 was sampled in two trajectories with the top part of MIS100 being sampled twice in stratigraphic overlap. Sampling of the older part (MIS101-99) started ~2 m above the San Nicola bed (*Chapter 2*), while the younger part (MIS100-95) was sampled in the other trajectory starting ~5 m above the SN marker bed. The sampling trajectory was carefully chosen as to ensure a continuous and undisturbed succession. The weathered surface was cleaned and only 'fresh' sediment was sampled using an electric water-cooled drill. Generally, two cores of 2.5 cm diameter were drilled per sample level (every 3 cm) resulting in 123 and 341 sample levels for the lower and upper trajectory, respectively. The magnetic susceptibility of the samples was measured on a Kly-2 magnetic facility at the paleomagnetic laboratory Fort Hoofdijk, Utrecht University, to check continuity of the section and build a composite depth profile. Three specimens of each drilled sample were measured in duplicate and results were averaged.

ODP Leg 160 Site 967 (34°04'N, 32°43'E) was drilled in the eastern Mediterranean near the Eratosthenes seamount at a water depth of 2554 m. Three holes were drilled to recover a continuous succession. A composite depth profile was constructed by correlating colour reflectance records between different holes [Sakamoto *et al.*, 1998]. The top 125 m consists of lower Pliocene to Holocene hemipelagic sediments containing 80 sapropels. The sapropels occur in clusters and correlate with the large-scale O, A, B and C sapropel groups as found in the land-based marine successions of the Vrica, Singa, Punta Piccola and San Nicola sections [Kroon *et al.*, 1998; Lourens *et al.*, 1998]. The interval between sapropel A5 and the B sapropel group is marked by a reddish colour. Glacial stages 100, 98 and 96 can be recognised as dark layers in the core. Hole A on Site 967 was sampled every centimetre in the interval 8H4-6 (hereafter referred to as Site 967). The continuity of the section was checked using core photographs and colour reflectance data of all holes (A-C). Additionally, colour reflectance was measured on the half core every centimetre and on the individual samples using a hand-held Minolta CM 503i spectrophotometer.

For stable isotope analysis of the San Nicola samples about 20 specimens of the benthic foraminifer *Uvigerina peregrina* and 50 specimens of the planktonic foraminifer *Globigerinoides ruber* were hand picked from a split of the >212 µm size fraction. The analysis was carried out at Utrecht University stable isotope facility where an ISOCARB common bath carbonate preparation device linked on-line to a VG SIRA24 mass spectrometer is operated. Isotope values were calibrated to the PeeDeeBelemnite (PDB) scale. Analytical precision was determined by replicate analyses and by comparison to the international (IAEA-CO1) and in house carbonate

standard (NAXOS). Replicate analyses showed standard deviations of  $< 0.06\text{‰}$  and  $< 0.1\text{‰}$  for  $\delta^{13}\text{C}$  and  $\delta^{18}\text{O}$ , respectively.

### 6.2.2. Age model

The studied interval at ODP Site 967 has been astronomically dated by correlating the Ti/Al record interpreted in terms of the relative contribution of aeolian versus fluvial material to the  $65^\circ\text{N}$  summer insolation curve of solution La93 [Lourens *et al.*, 2001]. Lourens *et al.* [2001] assumed an in-phase relationship between Ti/Al and  $65^\circ\text{N}$  summer insolation, resulting in 3-kyr younger ages for the i-cycles than the lagged ages of Lourens *et al.* [1996]. Here, the La04<sub>(1,1)</sub> astronomical solution with present-day values for the Earth's tidal dissipation and dynamical ellipticity [Laskar *et al.*, 2004] is used, in stead of the older La90-93 solution [Laskar *et al.*, 1993], although both solutions reveal essentially the same ages for the studied interval. Sedimentation rate at Site 967 is on average 2.5 cm/kyr, resulting in a sample resolution of  $\sim 400$  yr.

The age model for SN is based on graphical correlation between the benthic oxygen isotope records of SN and Site 967 (Figure 6.2). Tie-points are based on the recognition of glacial-interglacial transitions and stadial-interstadial variability in both benthic  $\delta^{18}\text{O}$  records. Graphical correlation yields a correlation of  $r=0.88$  and  $r=0.87$ , respectively, between the benthic and planktonic  $\delta^{18}\text{O}$  of both locations. Linear interpolation between tie-points results in a duration of  $\sim 20$  kyr for MIS100, 18 kyr for MIS98 and 26 kyr for MIS96, respectively. At SN, average sedimentation rates are  $\sim 6$  cm/kyr in the interglacials and  $\sim 8$  cm/kyr in glacials resulting in an average temporal resolution of  $\sim 500$  yr and  $\sim 350$  yr, respectively.

The age model of Site 969 is based on correlating the Ti/Al to the  $65^\circ\text{N}$  summer insolation curve of the La93 solution [Wehausen 1999]. Here, we refine the initial age assessment of Wehausen by tying the colour reflectance data [Sakamoto *et al.*, 1998] to the new high resolution colour reflectance data of Site 967 (Figure 6.3). This results in slightly modified ages.

### 6.2.3. Spectral analysis

Spectral analysis is carried out using the MC\_CLEAN (version 2.0) frequency analysis program of Heslop and Dekkers, [2002]. MC\_CLEAN is based on the CLEAN algorithm of Roberts *et al.* [1987], which allows to extract frequency information directly from an unevenly-spaced time series. In addition to CLEAN, Monte Carlo methods for different types of noise (here red noise) allow to generate a set of slightly different spectra from the (single) input signal. The differences between these spectra give the confidence interval around the mean spectrum.

In order to test spectral results and to trace non-stationary signals, filtering in the frequency-domain was carried out by using wavelet analysis (Matlab verison 6.5,

wavelet toolbox) following the protocol of *Torrence and Compo*, [1998]. This routine applies a simple Morlet waveform on the normalised, equally-spaced (linearly interpolated) data. Maximum power at the 95% significance level is scaled to 1. For filtering in the time domain, we applied band-pass filters (*AnalySeries*, *Paillard et al.*, [1996]), using a Gaussian filter with central frequency.

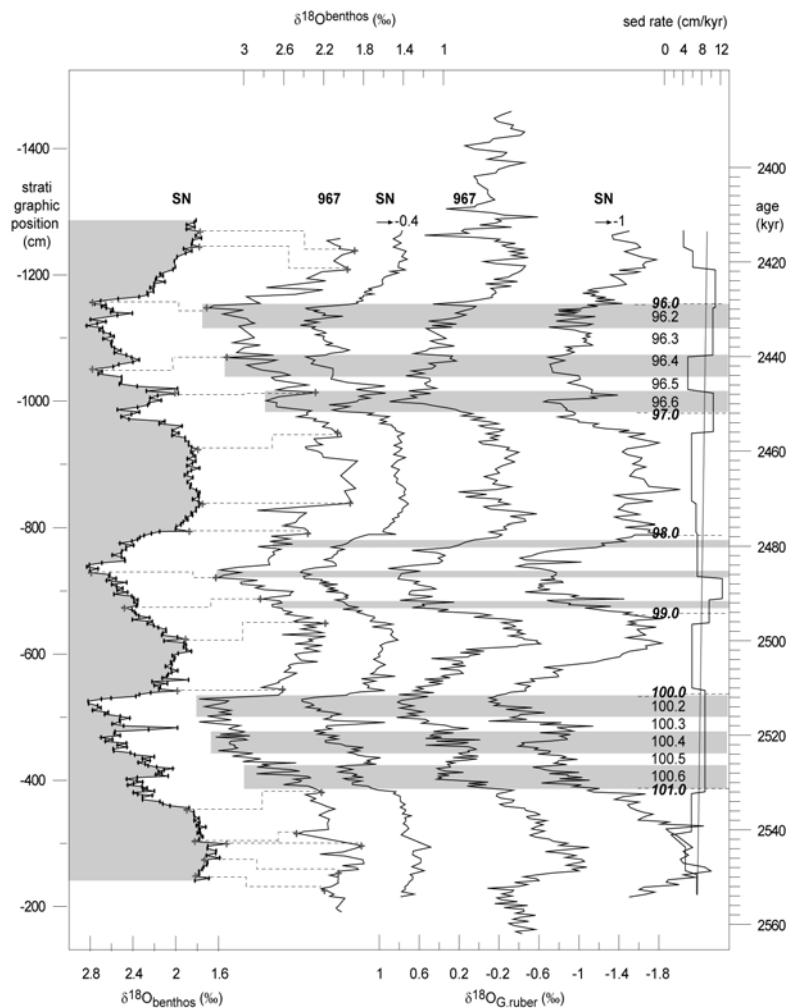


**Figure 6.2:** Depth-age correlation of the  $\delta^{18}\text{O}_{\text{benthos}}$  of SN (versus depth (cm)) with the  $\delta^{18}\text{O}_{\text{benthos}}$  of Site 967 (versus age (kyr)). Crosses indicate age-calibration points and horizontal dashed lines illustrate graphical correlation.  $\delta^{18}\text{O}_{\text{benthos}}$  of SN,  $\delta^{18}\text{O}_{\text{G.ruber}}$  of Site 967 and SN and sedimentation rates (overlain by average) of SN plotted versus age (kyr). Notice that all  $\delta^{18}\text{O}$  records are plotted on the same horizontal scale (inversed) and that benthic and planktonic  $\delta^{18}\text{O}$  records of SN have been shifted for clarity by respectively 0.4‰ and 1‰ towards lighter values. Labelling of stadials (grey shaded) and interstadials according to *Martinson et al.* [1987].

### 6.3. Results

#### 6.3.1. Stable isotopes of SN and ODP Site 967

The San Nicola (SN)  $\delta^{18}\text{O}$  values for *U. peregrina* ( $\delta^{18}\text{O}_{\text{benthos}}$ ) vary from  $\sim 1.8\text{‰}$  in the interglacials to  $\sim 2.8\text{‰}$  in the glacials, resulting in a glacial-interglacial amplitude of  $\sim 1\text{‰}$ . The SN  $\delta^{18}\text{O}$  values of *G. ruber* ( $\delta^{18}\text{O}_{\text{G.ruber}}$ ) are  $\sim -0.75\text{‰}$  in the interglacials with minimum values of  $-1.2\text{‰}$  during i-246. Maximum  $\delta^{18}\text{O}_{\text{G.ruber}}$  values are  $0.8\text{‰}$  in MIS100,  $0.5\text{‰}$  in MIS98 and  $0.25\text{‰}$  in MIS96 resulting in glacial-interglacial

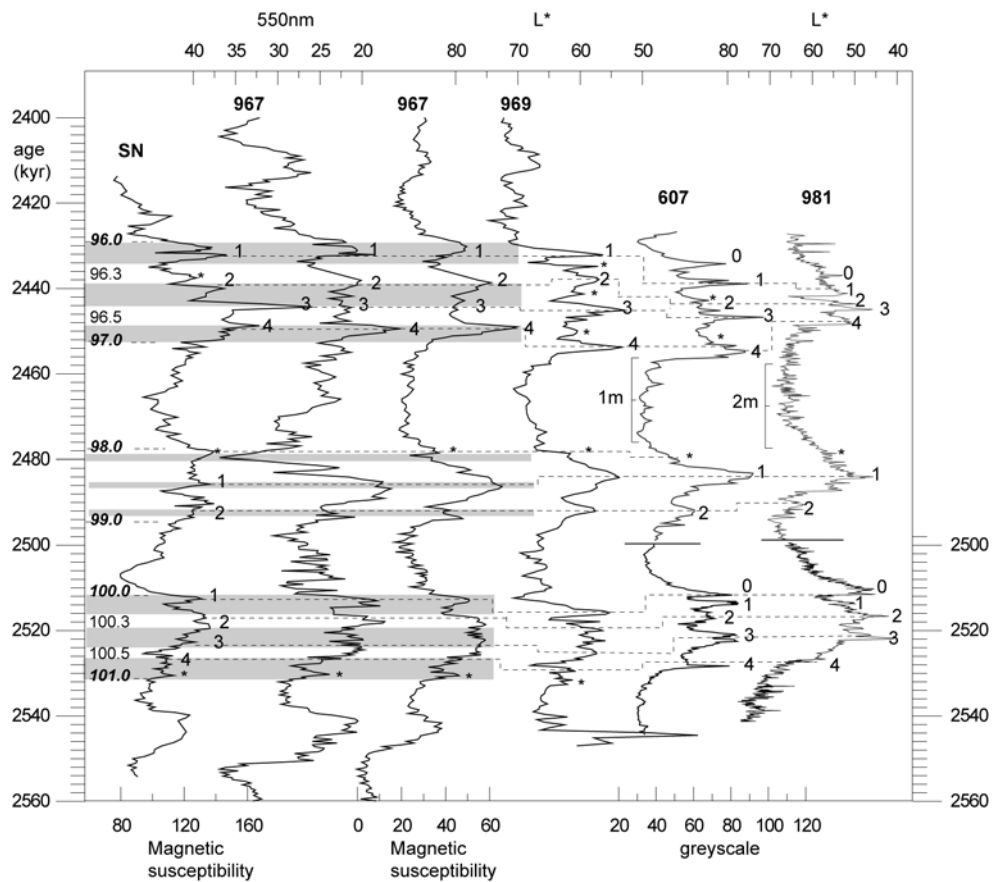


Figure 6.3: Magnetic susceptibility of San Nicola, colour reflectance of Site 967, magnetic susceptibility of Site 967 and colour reflectance of Site 969 versus age (kyr). Greyscale of Site 607 and colour reflectance of Site 981 are plotted versus age (kyr) (lower record, MIS100) and versus depth (m) (upper record; MIS99-95). Notice that all colour reflectance results are plotted on an inverse y-axis. Shaded intervals and labels indicate stadials and cold D-O episodes as defined in *Chapter 5*. Horizontal dashed lines indicate visual correlation of MS and CR peaks between sites and labels indicate numbering of peaks.

amplitudes of 1.55‰, 1.25‰ and 1‰, respectively. Glacial-interglacial amplitudes in  $\delta^{18}\text{O}_{\text{G.rubber}}$  of Site 967 are constant  $\sim 1.25\text{‰}$  with values being  $\sim -0.5\text{‰}$  (slightly lower than SN) in the interglacials and  $\sim 0.75\text{‰}$  in the glacials respectively. Similar to San Nicola, minimum  $\delta^{18}\text{O}_{\text{G.rubber}}$  values ( $-1\text{‰}$ ) are associated with i-246.

Benthic oxygen isotope records both reveal an overall distinct saw-tooth pattern characterised by a gradual increase during the early glacial toward maximum values during full glacial conditions and a sudden decrease at the termination. This saw-tooth pattern is less obvious in the  $\delta^{18}\text{O}_{\text{G.rubber}}$  during MIS98 and MIS96 and seems even reversed during MIS96 at Site 967. Sub-stages as defined in the  $\delta^{18}\text{O}_{\text{benthos}}$  record of SN during MIS100 (*Chapter 2*) can be recognised in MIS96 and are labelled according to the nomenclature established for late Pleistocene glacials where even numbers refer to stadial phases and odd numbers refer to interstadial phases [Imbrie *et al.*, 1984; Martinson *et al.*, 1987]. Each sub-cycle shows a saw-tooth pattern, starting with a gradual increase in isotope values that takes about 4-5 kyr followed by a sudden decrease to lighter values (with amplitudes of  $\sim 0.4\text{--}0.5\text{‰}$ ). Values remain low for another 2-3 kyr so that the average duration of each sub-cycle is 6-8 kyr. It has been shown that the sub-cycles depicted in the  $\delta^{18}\text{O}_{\text{benthos}}$  of SN during MIS100 are associated with major ice rafting episodes in the North Atlantic and, therefore, present climate variability equivalent to the Pleistocene Bond-cycles (*Chapter 3*). These Bond-type cycles are also observed in the  $\delta^{18}\text{O}_{\text{G.rubber}}$  of SN but are less pronounced in the  $\delta^{18}\text{O}$  of Site 967. No such stadial-interstadial variations are observed in the  $\delta^{18}\text{O}$  during MIS98, although  $\delta^{18}\text{O}$  decrease for short episodes ( $\sim 2$  kyr), similar to the short decreases observed during the gradual increase in  $\delta^{18}\text{O}$  of each Bond-cycle. Again, these short episodes in MIS100 have been shown to be equivalent to Pleistocene Dansgaard-Oeschger warm phases (*Chapter 3*).

### 6.3.2. Magnetic susceptibility and colour reflectance

The San Nicola magnetic susceptibility (MS) record generally matches the weathered and fresh sediment colour changes as observed in the field (*Chapter 1*). High MS values ( $\sim 160 \text{ SI} \cdot 10^{-4}$ ) are associated with the darker-coloured glacial sediments and the ghost sapropel (i-246) and low MS values ( $\sim 80 \text{ SI} \cdot 10^{-4}$ ) with the lighter sediments. During glacials, MS values vary with high amplitude ( $\sim 20\text{--}40 \text{ SI} \cdot 10^{-4}$ ) showing distinct maxima with a spacing of 3-6 kyr: four extremes (1-4) can be labelled in MIS100, three in MIS98 and four in MIS96 (Figure 6.3). Given the duration of the glacials this results in a spacing of the extremes of  $\sim 5$  kyr in MIS100,  $\sim 6$  kyr in MIS98 and  $\sim 6.5$  kyr in MIS96, respectively. Furthermore, the 1<sup>st</sup> and 2<sup>nd</sup> peak in MIS96 and the 3<sup>rd</sup> and 4<sup>th</sup> peak in MIS100 represent double peaks with a shorter spacing of  $\sim 3$  kyr. Major peaks in MS correspond to maximum  $\delta^{18}\text{O}_{\text{benthos}}$  values of SN (Figure 6.4) and thus stadial and D-O cold intervals (shaded). Lower amplitude variations with irregular spacing occur during interglacial stages.



The colour reflectance (CR) and MS records of ODP Site 967 reveal a similar variability as the MS record of SN with low CR values (dark coloured sediment) being associated with glacials and the ghost sapropel and high values with interglacials (Figure 6.3). High-amplitude variations in CR are found throughout the entire interval. Distinct peaks during glacial intervals can be correlated to the MS of SN and have been labelled accordingly. Small differences are found between the two sites: in MIS100, the 3<sup>rd</sup> peak is more pronounced in Site 967 than at SN and better separated from the 2<sup>nd</sup>

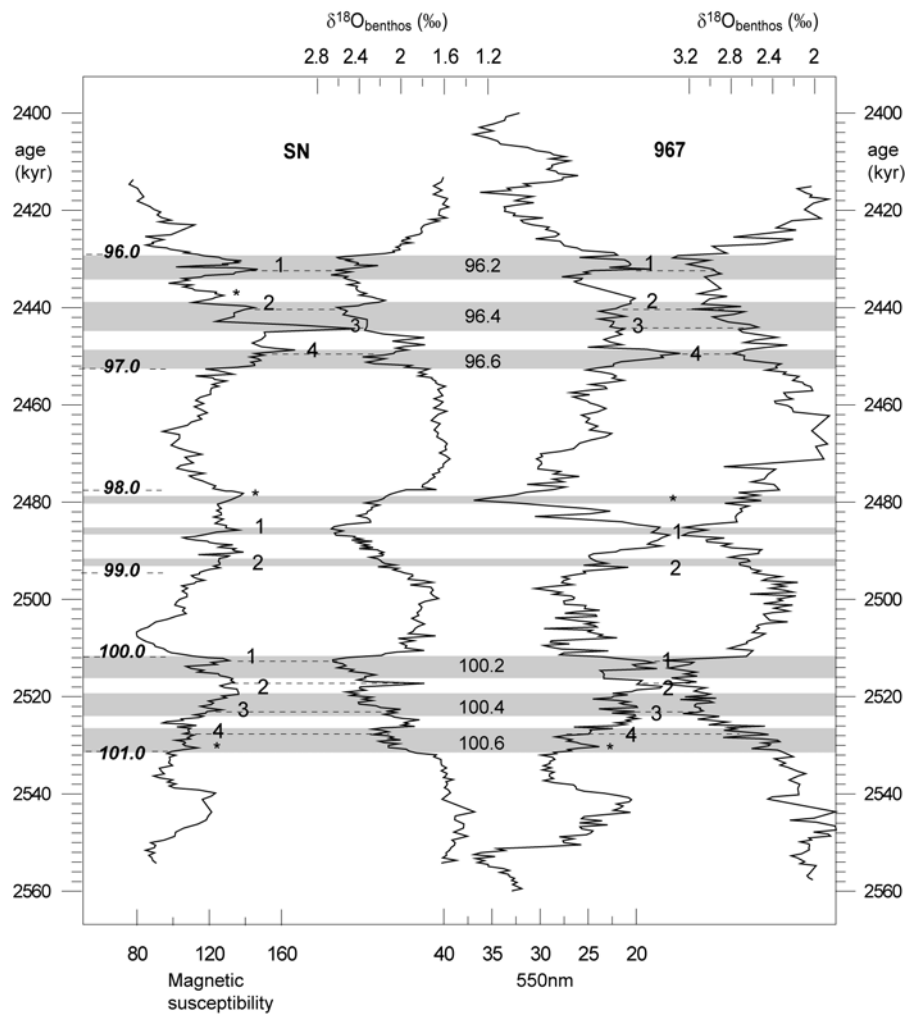


Figure 6.4: Magnetic susceptibility of San Nicola,  $\delta^{18}\text{O}_{\text{benthos}}$  of SN, colour reflectance of Site 967 and  $\delta^{18}\text{O}_{\text{benthos}}$  of Site 967 versus age. Notice that  $\delta^{18}\text{O}_{\text{benthos}}$  and colour reflectance results are plotted on an inverse y-axis. Shaded intervals and labels indicate stadials and cold D-O episodes as defined in Chapter 5. Horizontal stipple lines and labels indicate correlative peaks.

peak. In MIS96.3, part of the additional peak (\*) is missing at Site 967 because an interstitial water sample has been taken at this position in core 967A-8H-4 (Site 967 core photographs). In the parallel hole B of Site 967, both peaks (\* and 2) are resolved (Shipboard data), indicating that two peaks are associated with this interval. In addition, the 3<sup>rd</sup> peak in MIS96 has lower amplitude than at SN and is less distinct. Similar to SN high CR values are related to maximum  $\delta^{18}\text{O}_{\text{benthos}}$  with the exception of those peaks in interstadial MIS100.3 and MIS96.3 (Figure 6.5). Comparison with the colour reflectance record of Site 969 (scientific shipboard party) shows that all peaks can be correlated basin-wide (Figure 6.3).

At Sites 607 and 981, high grey-scale values and low CR values (*Chapter 3*) are

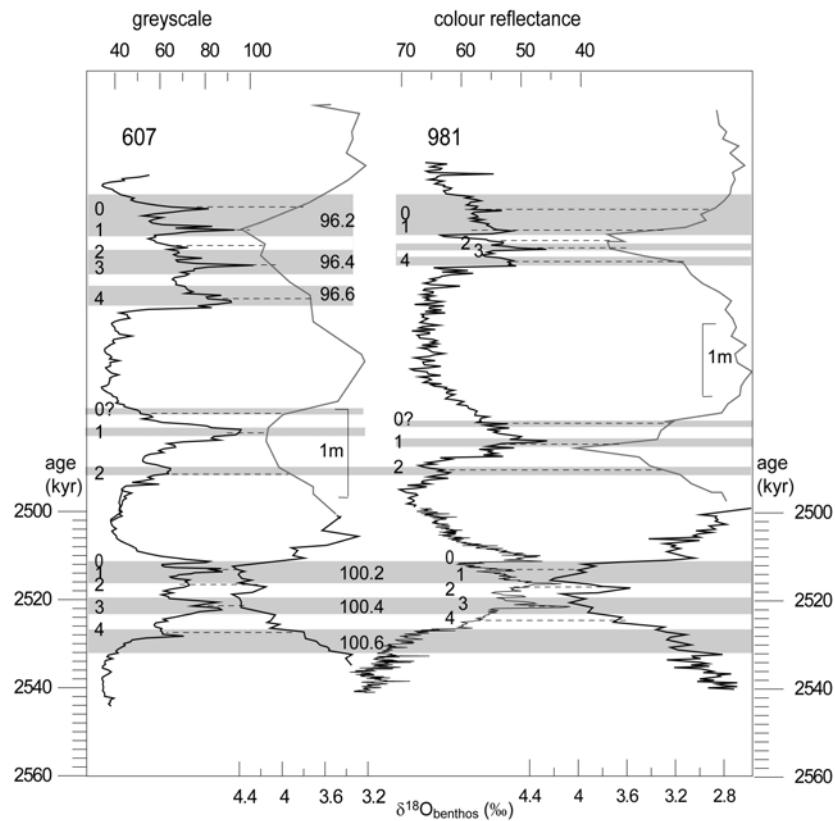


Figure 6.5: Greyscale record of Site 607,  $\delta^{18}\text{O}_{\text{benthos}}$  of Site 607, colour reflectance of Site 981 and  $\delta^{18}\text{O}_{\text{benthos}}$  of Site 981. Lower part of record (MIS100) is plotted versus age (kyr) (*Chapter 3*) and upper part (MIS99-95) of the record is plotted versus depth (m) (Site 981: data of *Draut et al.* [2003]; Site 607: data of *Raymo et al.*, [1989]). Notice that  $\delta^{18}\text{O}_{\text{benthos}}$  and colour reflectance results are plotted on an inverse y-axis. Shaded intervals and labels indicate stadials and cold D-O phases as defined in the Mediterranean record. Dashed lines and labels indicate correlative peaks.

associated with dark glacial sediments in MIS100, 98 and 96 (Figure 6.3). Four dark intervals (1-4) are recorded within the glacial stages MIS100 and MIS96 and three with MIS98, which correspond to or are close to maximum  $\delta^{18}\text{O}_{\text{benthos}}$  values ( $\delta^{18}\text{O}_{\text{benthos}}$  of Site 607: *Raymo et al.*, [1989];  $\delta^{18}\text{O}_{\text{benthos}}$  of Site 981: *Draut et al.* [2003]) (Figure 6.5). In contrast, the uppermost dark interval of each glacial cycle (0) does not correspond with a  $\delta^{18}\text{O}_{\text{benthos}}$  maximum but with decreasing  $\delta^{18}\text{O}_{\text{benthos}}$  values marking the glacial-interglacial transition.

### 6.3.3. Spectral results

*Oxygen isotopes.* The spectra of the  $\delta^{18}\text{O}_{\text{benthos}}$  records reveal maximum concentration of power at or near periodicities of 80 kyr, 41 kyr and 28 kyr (Figure 6.6). This is in agreement with results as discussed in *Chapter 5*. No significant concentration of

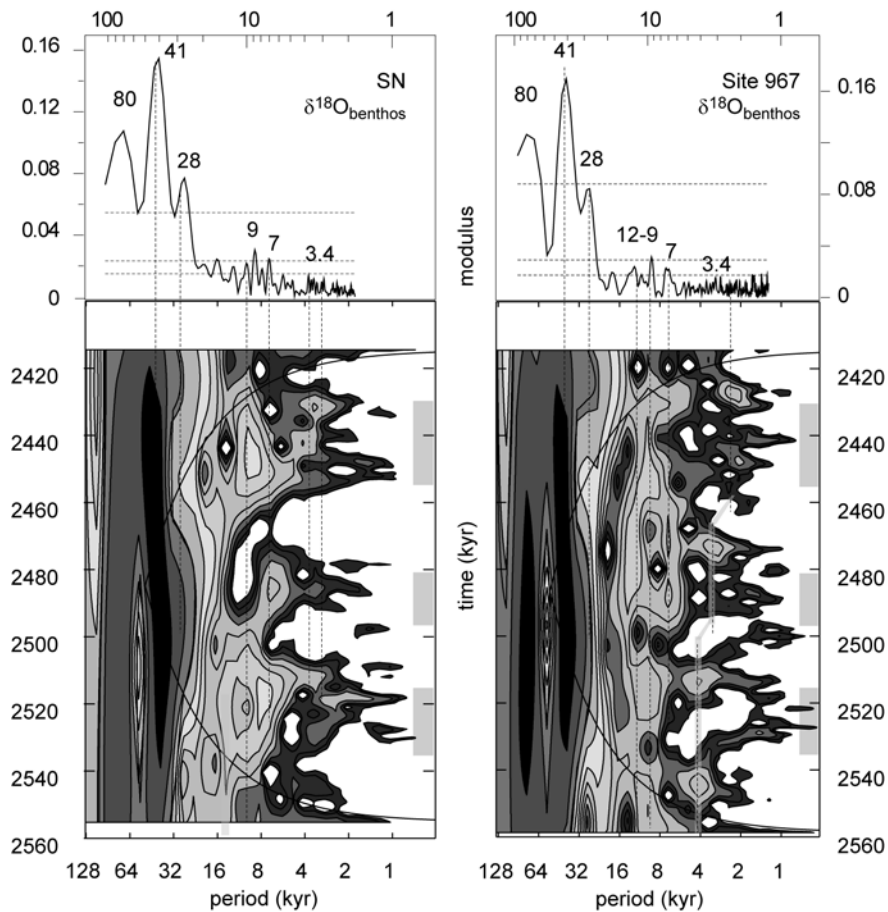
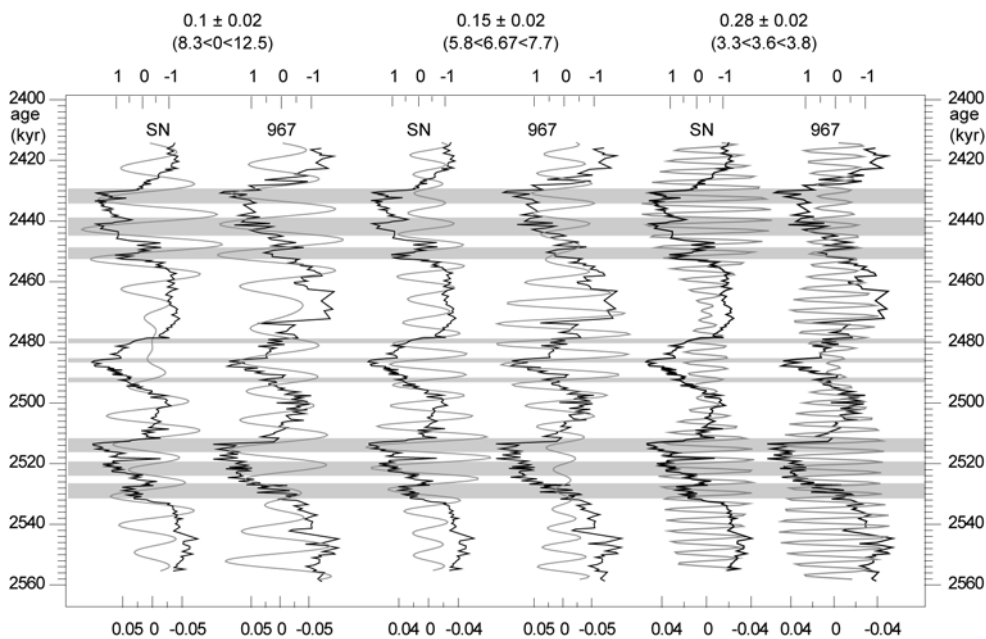


Figure 6.6: Power spectrum (versus period in kyr) of  $\delta^{18}\text{O}_{\text{benthos}}$  of Site 967 and SN in relation to the 80-95% significance levels (dark grey stipple lines) and corresponding wavelet maps. Important periodicities are highlighted by horizontal grey bars. Grey intervals on the right axis of the wavelet map indicate positions of MIS100, 98 and 96

variance is resolved in the precession-band. Additionally, peaks are resolved at or near sub-Milankovitch periodicities of 12 kyr, 9 kyr, 7-6 kyr and 4-3 kyr. These are considered to be significant above the 85-90% confidence level. Results of wavelet analysis indicate that concentration of variance is spread over a relatively broad range of periodicities and not uniformly distributed throughout the time series, which explains the rather low significance levels. To pinpoint these differences in the time domain,



**Figure 6.7: Normalised  $\delta^{18}\text{O}_{\text{benthos}}$  of Site 967 and SN with superimposed Gaussian filters (grey lines) centred at  $0.1 \pm 0.02$  cycles/kyr,  $0.15 \pm 0.02$  cycles/kyr and  $0.28 \pm 0.02$  cycles/kyr versus age. Shaded intervals and labels indicate stadials and cold D-O episodes.**

filters with a relatively broad band were used. To evaluate the 7-9 kyr periodicity range different filters were selected to trace the signal around the upper ( $8.3 \text{ kyr} < 10 \text{ kyr} < 12 \text{ kyr}$ ) and lower ( $5.8 \text{ kyr} < 6.7 \text{ kyr} < 7.7 \text{ kyr}$ ) margins of the frequency band (Figure 6.7). The long 10 kyr filter picks up the subcycles in the benthic  $\delta^{18}\text{O}$  during MIS96, while the 6 kyr filter picks up the  $\delta^{18}\text{O}_{\text{benthos}}$  subcycles during MIS100 (SN) and MIS98. This is in agreement with *a priori* observations in the time domain (see results section  $\delta^{18}\text{O}$ ). Higher frequency (low amplitude) variations within subcycles are picked up by fixing the filter at  $3.3 \text{ kyr} < 3.6 \text{ kyr} < 3.8 \text{ kyr}$ .

The power spectra of the  $\delta^{18}\text{O}_{\text{G.ruber}}$  reveal maximum concentration of power at or near periodicities of 80 kyr and 41 kyr in agreement with those of the  $\delta^{18}\text{O}_{\text{benthos}}$  (Figure 6.8). Variance at 28 kyr is observed in the spectrum of SN but absent in Site 967.

Additionally, concentration of variance around the precession-band is observed in both records, although concentrated occurs in a rather broad 28-22 kyr band, with maximum concentration during MIS98. Concentration of variance in the sub-Milankovitch band is observed at or near periodicities of 11-8 kyr, 7-5 kyr, 3-4 kyr, 2.5 kyr and 1.7 kyr. Again, variance is concentrated in rather broad bands and is not uniformly distributed throughout the time series causing rather low significance levels at Site 967. Results of wavelet analysis (Figure 6.8) and Gaussian filters (Figure 6.9) of SN indicate that variations around 10-8 kyr are important in MIS98-96, and

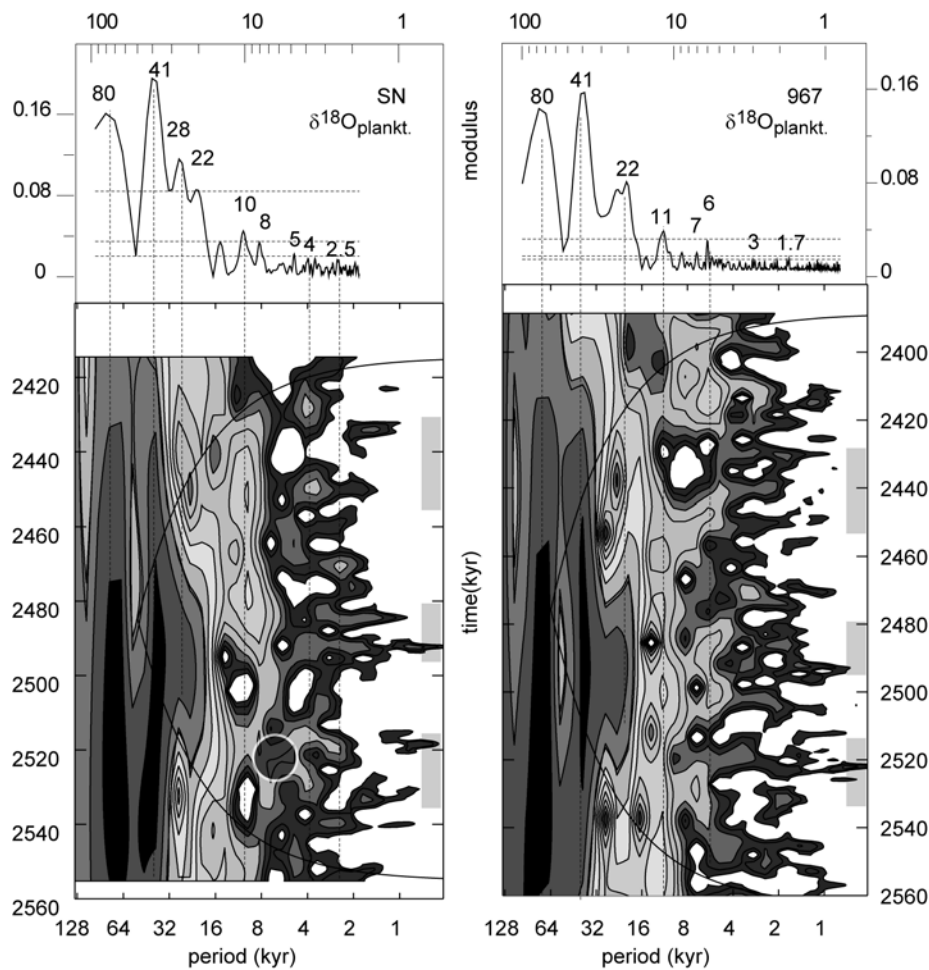


**Figure 6.8:** Power spectrum (versus period) of  $\delta^{18}\text{O}_{\text{G.ruber}}$  of Site 967 and SN in relation to the 80-95% significance levels (dark grey stipple lines) and corresponding wavelet maps (lower panel versus age (kyr)). Important periodicities are highlighted by horizontal grey bars. Grey intervals on the right axis of the wavelet map indicate positions of MIS100, 98 and 96.

correspond to the sub-cycles in MIS96. On the contrary, variations  $\sim 7$  kyr are more important during MIS100 (highlighted in Figure 6.6). This is similar to observations in the  $\delta^{18}\text{O}_{\text{benthos}}$  where shorter cycles were observed during MIS100 compared to MIS96. In contrast to the SN  $\delta^{18}\text{O}_{\text{benthos}}$ , cycles in both these ranges are also detected in

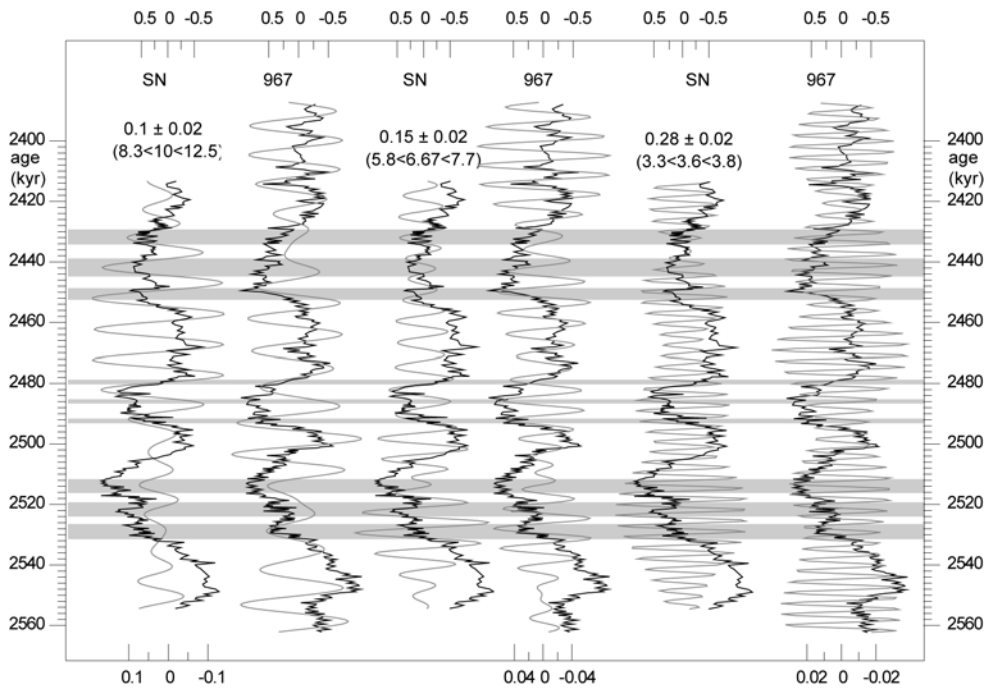


**Figure 6.9: Normalised  $\delta^{18}\text{O}_{\text{G.ruber}}$  of Site 967 and SN with superimposed Gaussian filters (grey lines) centred at  $0.1 \pm 0.02$  cycles/kyr,  $0.15 \pm 0.02$  cycles/kyr and  $0.28 \pm 0.02$  cycles/kyr versus age. Shaded intervals and labels indicate stadials and cold D-O episodes.**

interglacials. This is even more evident in the filtered records of Site 967  $\delta^{18}\text{O}_{\text{G.ruber}}$ , where the long period  $\sim 10$  kyr is strongly related to interglacials and MIS98 (Figure 6.9). The shorter (6–7 kyr) is strong in the entire record except during the late stage of MIS100 and MIS96. Periodicities  $\sim 3$ –4 kyr in the  $\delta^{18}\text{O}_{\text{G.ruber}}$  are related to the shorter low amplitude fluctuations in the glacials (except MIS96 at SN) and in the interglacials of Site 967.

*Magnetic susceptibility and Colour reflectance:* Spectra of the CR (Site 967 and Site 969) and MS (SN) are very different in the Milankovitch-range (Figure 6.10). At SN and Site 967 maximum concentration of variance is centred at 41 kyr with additional variance occurring around 66 kyr (Site 969) and 70 kyr (SN). Variance at 28 kyr is reduced at Site 969 and hidden in the flank of the large 41 kyr peak at SN. Variance at 23 kyr is present at SN. At Site 967 concentration of variance at 41 kyr is reduced compared to the large peaks observed at 80 kyr, 28 kyr and 21 kyr, possible due to the larger

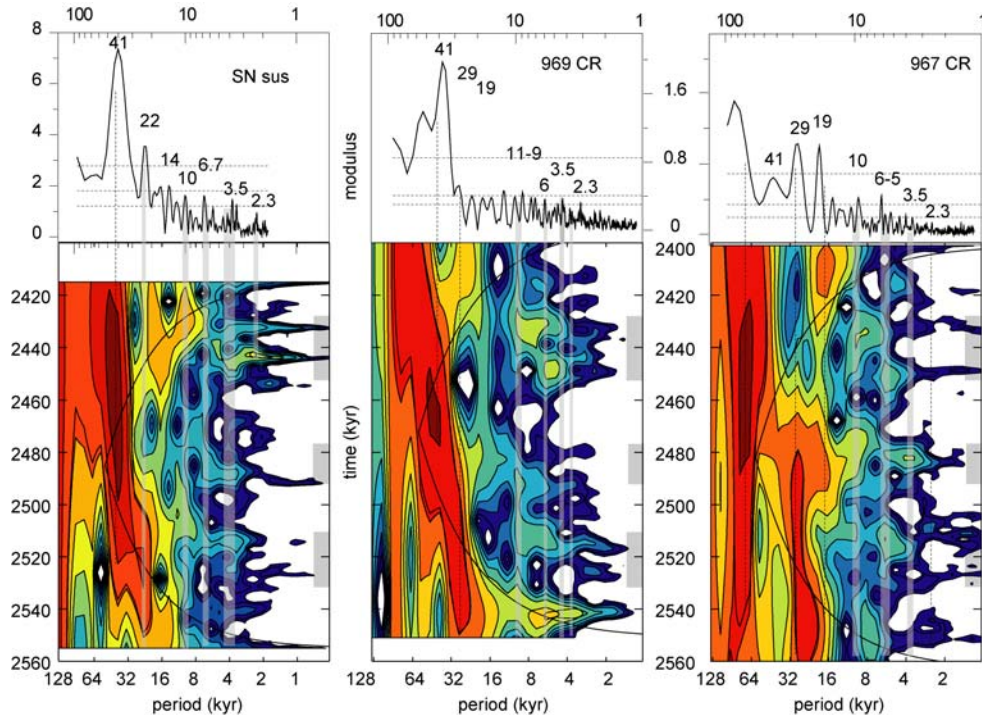


**Figure 6.10:** Spectral results of Site 969 (colour reflectance), Site 967 (greyscale) and San Nicola (magnetic susceptibility) in relation to the 80-95% significance levels (dashed lines). Wavelet maps (lower panel) of magnetic susceptibility and colour reflectance data of San Nicola and Site 969 and Site 967, respectively. Important periodicities are highlighted by horizontal grey bars. Grey intervals on the right axis of the wavelet map indicate positions of MIS100, 98 and 96.

precession signal at this site. Results of wavelet analysis indicate, that variance at 29-19 kyr is clearly related to MIS101-98 in all records.

Peaks in the sub-Milankovitch range are resolved around periodicities of 10-9 kyr, 6.7-5 kyr, ~3.5 kyr and 2.3 kyr and are significant above the 85-90% level. Distribution of variance in the time domain looks rather difficult given the variety of peaks in the spectrum (Figure 6.11). Variance around 10 kyr seems to be related to the ghost sapropel and the upper part of MIS100-MIS99 in all records and during MIS96 in Site 967, picking up the three darkest intervals in that interval. Concentration of variance at ~6-7 kyr is related to the glacial stages, although not very clear in the lower part of SN, and to the interglacials MIS99 (Site 969 and Site 967) and MIS97 (Site 967). This observation is in agreement with observations in the depth domain and the labelling of the dark intervals accordingly (*Chapter 1*, i.e. during MIS96, four peaks were labelled at all sites and this results in an average spacing of 6 kyr given the duration of that glacial

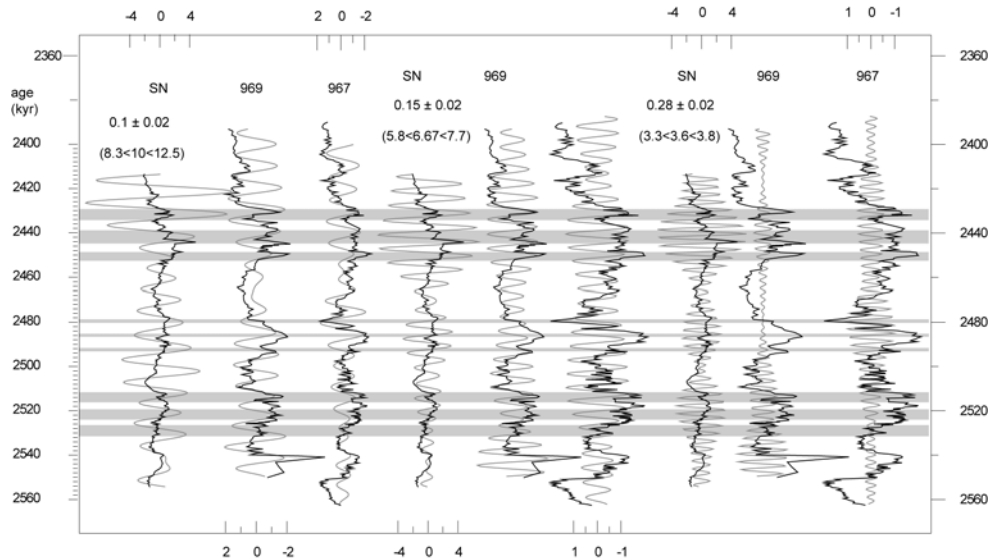


**Figure 6.11:** Normalised magnetic susceptibility (San Nicola), and colour reflectance (Site 969 and 967) data (black lines) with superimposed Gaussian filters (grey lines) centred at  $0.1 \pm 0.02$  cycles/kyr,  $0.15 \pm 0.02$  cycles/kyr and  $0.28 \pm 0.02$  cycles/kyr versus age (kyr). Shaded intervals and labels indicate stadials and cold D-O episodes.

(26 kyr)). Power at around 3.5 kyr is strongly related to the glacials at SN and Site 967 (MIS98 only).

## 6.4. Discussion

### 6.4.1. Dust episodes in the Mediterranean

The good agreement between magnetic susceptibility, colour reflectance and bulk carbonate content ( $r^2=0.96$ ; *Chapter 4*) at SN mirrors the typical cyclic character of the limestone-marl alternations in the Narbone Formation with light-coloured layers (interglacials, homogenous intervals) being carbonate-rich and dark-coloured layers (glacials, sapropels, sapropelitic layers) being carbonate-poor. As such, these changes in bulk sediment composition can be driven by (i) variations in the carbonate productivity, (ii) dilution of carbonates by aluminosilicates, (iii) dissolution of carbonates through oxidation of organic material or (iv) a combination of i-iii. In *Chapter 4* it was discussed that a combination of both changes in carbonate productivity and aluminosilicate input are most likely the most important mechanisms controlling bulk sediment composition. The sediments at SN may thus represent a two-component mixing system with biogenic carbonate and terrigenous clastic material as end-members (*Chapter 4*). Sediments at ODP Sites 967 and 969 [Wehausen 1999] are similar in composition and changes in CR and MS at these Sites can thus be similarly



interpreted. In addition, the basin-wide registration and correlation of these signals suggests a climatic origin.

Foraminiferal fluxes at SN indicate that carbonate production was generally lower (about twice as low) during MIS100 than during the encompassing interglacials (*Chapter 2*). Grain size analyses of the carbonate free component at SN and geochemical proxies (Ti/Al and Zr/Al) at SN, Site 967 and Site 969 further indicate that at least part of the observed fluctuations in the CaCO<sub>3</sub> and Al content (and thus MS and CR) is related to wind-transported material with high Al values (high MS values) being related to periods of increased dust input from the African continent, either by an increase in wind strength or by aridification (*Chapter 4*).

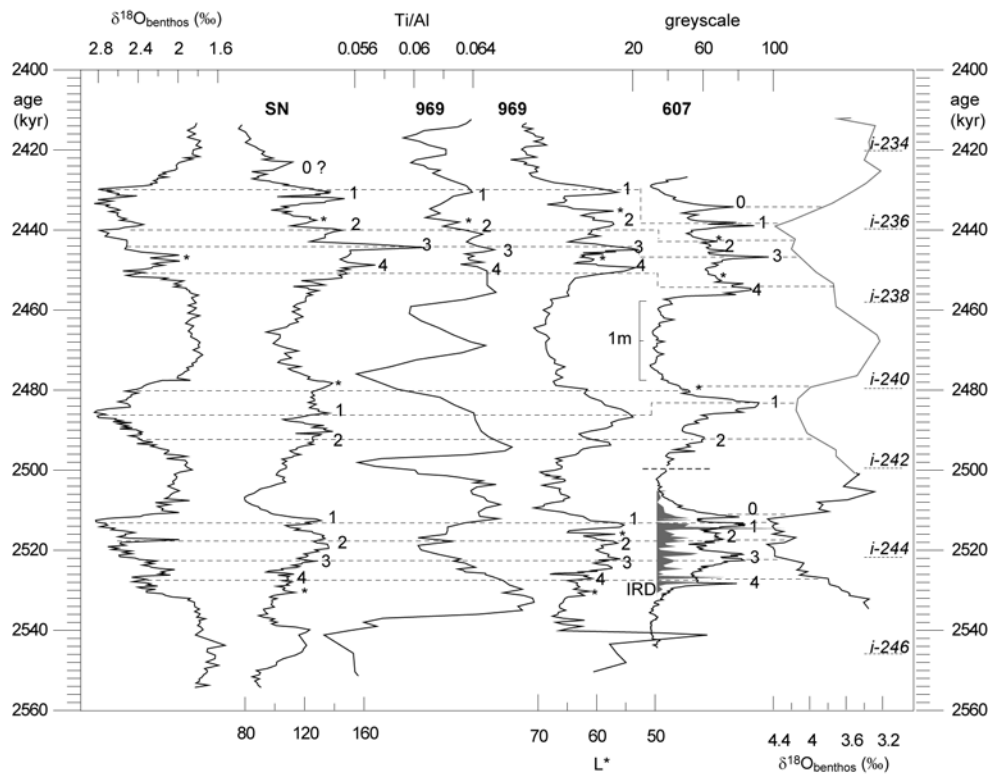


**Figure 6.12:**  $\delta^{18}\text{O}_{\text{benthos}}$  and magnetic susceptibility of SN and Ti/Al [data *Wehausen 1999*] and colour reflectance of Site 969 versus age in comparison with greyscale, IRD and  $\delta^{18}\text{O}_{\text{benthos}}$  of Site 607 versus age (kyr) (lower part (MIS100) of Site 607 and depth (m) (upper part (MIS99-95) data of *Raymo et al.*, [1989]). Horizontal stipple lines and labels indicate correlative peaks.

Comparison between the Ti/Al and CR records of Site 969, and MS and CR records of SN and Site 967 reveals that a similar relationship holds for MIS98 and MIS96 (Figure 6.2 and Figure 6.12). Evidently, MS and CR peaks at SN and Site 967 have an

equivalent peak in the CR and Ti/Al records of Site 969 (Figure 6.2 and Figure 6.12). In analogue to the long-term changes in Ti/Al, Si/Al and Zr/Al series of Sites 969 and 967 which vary in concert with summer insolation [Wehausen 1999], these rapid fluctuations have been interpreted to present dry-wet alterations of circum-Mediterranean climate conditions. The episodes of enhanced dust input correspond primarily to  $\delta^{18}\text{O}$  maxima indicating a strong link with cold D-O phases and/or stadial intervals (see also *Chapter 2*). During the two exceptions, MIS100.3 and MIS96.3, when high dust influxes occurred at times of low  $\delta^{18}\text{O}$  values at SN, the precession cycle reaches minimum values (i.e., low background Ti/Al values in Site 967 and 969). This orbital configuration may have resulted in the exceptional low  $\delta^{18}\text{O}$  values during MIS100 and MIS96 related to a surface water temperature/salinity signal similarly as at times of sapropel formation, although less intense, whereas the increased dust flux may be related to a cold D-O phase, which operates on a much shorter time scale (*Chapter 2*).

#### 6.4.2. Relation with the open ocean record

The occurrence of dark coloured layers at Sites 607 and 981 were interpreted as reflecting periods of enhanced terrigenous clastic input (ice rafted debris; IRD), which interrupt the biogenic carbonates and oozes [Carter and Raymo 1999]. Grey-scale data of different North Atlantic Sites within the IRD belt [Ruddiman *et al.*, 1989] indicates that the occurrence of these dark sediments is restricted to glacial intervals and that variations in sediment colour in MIS100-96 can be correlated basin-wide and hence sustain the notion that CR changes are associated with distinct basin-wide phases of ice rafting during MIS100, 98 and 96.

The comparison between the CR and  $\delta^{18}\text{O}_{\text{benthos}}$  records of Sites 607 and 981 further indicated that the dark sediment layers correlate with or are close to maximum  $\delta^{18}\text{O}_{\text{benthos}}$  values in the northern Atlantic (Figure 6.5), indicating a direct relation between cold episodes (maximum ice volume) and ice rafting. Taken the average spacing of  $\sim 6$  kyr between prominent dark layers suggests that these oscillations are similar in nature and spacing as the Pleistocene Heinrich events. In addition, these prominent dark layers consist of multiple advances suggesting that glacial surges appeared on even shorter time scales comparable to that of a D-O type of variability.

Despite the reduced variability in and lower resolution of the Atlantic  $\delta^{18}\text{O}_{\text{benthos}}$  records used for stratigraphic correlation, the striking similarity between the short-term Mediterranean dust episodes and dark sediment layers at Sites 607 and 981 during MIS100, MIS98 and MIS96 (Figure 6.5, *Chapter 3*), indicates a strong link between circum Mediterranean and North Atlantic climates. The discrepancy of five IRD phases versus four MS/CR peaks is probably related to the additional thick IRD peak at the glacial/interglacial transition of MIS100 and MIS96, which seems therefore not related with extreme cold glacial conditions, but to melting of ice caps at the glacial-

interglacial transition. The observed relation between dust, IRD and  $\delta^{18}\text{O}_{\text{benthos}}$  is valid for most of the cold phases (stadials).

Exceptions seem to occur at times of the precession minima when glacial CR/greyscale values at Site 607 are relatively low, suggesting a reduced IRD input. This was already observed for interstadial MIS100.3, where low IRD abundance were associated with unusual warm surface water conditions in the mid-Atlantic and an almost interglacial deep water production in the North Atlantic as a consequence of an increase in the meridional heat transport during minimum precession (i-cycle 244; *Chapter 4*). The similarity of the IRD signal during insolation cycles i-240 and i-236 with the signal during i-cycle 244 suggests that conditions are comparable during these intervals and that precession-related climate signals may suppress D-O and H-type of variability during the dominantly obliquity controlled glacials (Figure 6.5; *Chapter 3*), although this did not lead to significant ice volume changes on a precession scale (*Chapter 5*).

In conclusion, despite the different age models and temporal resolution, the visual peak to peak correlation between the proxy records suggests that African dust transport to the Mediterranean varied in harmony with the waxing and waning of the ice cap at high northern latitudes throughout MIS100-96 on sub-Milankovitch time scales. Mediterranean climate during glacial stages MIS100-96 is dominated by an alternation of relatively cold phases with surface water cooling, deep convection and enhanced aeolian dust input and more temperate, stable climate phases. Dry cold phases in the Mediterranean correspond to cold stadial phases in the mid- to high-latitude Atlantic marked by changes in meridional heat transport from low latitudes and the position of the polar front and by significant input of IRD (*Chapter 4*). The relation between Mediterranean SST, North African dust and North Atlantic IRD points to an atmospheric connection, most likely through the trade wind system.

#### 6.4.3. Forcing mechanisms of sub-Milankovitch climate variability

Contrasting ideas exist about the linkage between high-latitude climate and ice rafting, and low latitude winds. *Hughen et al.* [1996] suggested that changes in North Atlantic sea surface temperature driven by modifications in the North Atlantic thermohaline circulation influence the tropical trade wind and summer monsoon strength. By contrast, *McIntyre and Molino* [1996] proposed that changes in zonal wind-driven divergence in the eastern equatorial Atlantic control the discharge of tropical surface waters from the Caribbean and Gulf of Mexico warm pool into the western boundary current of the North Atlantic subtropical gyre and further into the sub-polar Atlantic thereby producing the rapid melting of ice and hence Heinrich events. According to the authors, these changes that occurred with a period of 8.4 kyr over the last 45,000 years are caused by a nonlinear climate response to low-latitude insolation/precession forcing during minimum eccentricity.

In his original paper, *Heinrich* [1988] proposed that North Atlantic ice rafting events are primarily a response to precession-induced variations in seasonal insolation. He related ice rafting events to times of respectively maximum summer and maximum winter insolation, thereby stating that these events occur every 11 kyr. Our data do not provide compelling evidence that late Pliocene climate fluctuations with frequencies similar to those of the much younger Heinrich events were triggered by low-latitude forcing even though we proposed that precession-induced changes in meridional heat flux may drive variations in North Atlantic deep water formation and thus thermohaline circulation during MIS100 (*Chapter 4*). On the other hand our results are also not in disagreement with the model proposed by *McIntyre and Molino* [1996] although their model requires interactions at a rather exceptional precession period [*Berger and Loutre* 1997]. Furthermore, our data are in excellent agreement with data from the late Pleistocene mid-Atlantic of *Chapman and Shackleton* [1998]. These data show a broad peak around 5-7 kyr in the  $\delta^{18}\text{O}_{\text{benthos}}$  spectrum, which might actually be composed of two separate peaks centred around 7 and 5.7 kyr. The data also show significant concentration of variance at the semi-precession cycle and *Chapman and Shackleton* [1998] state that cross-equatorial heat transfer exerts a major control on the mid-latitude Atlantic, again suggesting a low-latitude control. But what could actually cause such rapid climate fluctuations on millennial timescales?

No consensus exists about the forcing mechanism underlying sub-Milankovitch climate variability, notwithstanding the huge amount of high-resolution proxy records derived from various archives, latitudes and time intervals, which substantiate sub-Milankovitch variability at similar periodicities [e.g. *Yiou et al.*, 1994, for overview]. Different forcing mechanisms have been proposed in the literature. For example, changes in solar output [*Van Geel et al.*, 1999; *Perry and Hsu* 2000; *Bond et al.*, 2001] or tidal motion [*Keeling and Whorf* 2000] were used to explain climate variations in the decadal to millennial frequency range and, in particular, to account for the world-wide expression of D-O related cyclicity. However, these external forcing mechanisms are relatively weak and it remains therefore difficult to explain how they influenced the climate system. Modelling studies predict that small fluctuations in solar energy related to the 11-year solar (sunspot) cycle may affect atmospheric circulation patterns [*Haigh* 1994; 1996]. Also sub-harmonics of the 11-year sunspot cycle [*Gauthier* 1999] and amplifying mechanisms involving the role of UV variations and solar wind [*Van Geel et al.*, 1999] have been proposed to link millennial scale climate variability to solar activity.

Alternatively, self-sustained free oscillations [*Le Treut and Ghil* 1983; *Le Treut et al.*, 1988] and internal oscillations within the ocean-atmosphere system [*Sakai and Peltier* 1997] or the ice sheets [*MacAyeal* 1993; *Van Kreveld and al.* 2000] have been put forward to explain the D-O and H-events. Clearly northern Hemisphere ice sheets are important because high-amplitude millennial-scale climate variations occur during full glacial conditions in contrast to the relative low-amplitude variability during interglacial

times (e.g. Holocene). However, millennial-scale climate variations with similar periodicities have also been found at times that large northern Hemisphere ice sheets were absent and prior to northern Hemisphere glaciations [Ortiz *et al.*, 1999; Steenbrink *et al.*, 2003]. It was therefore suggested that northern Hemisphere ice sheets (or possibly even southern Hemisphere ice sheets) might act as amplifiers [Raymo *et al.*, 1992; McIntyre *et al.*, 2001] or resonating systems [Wara *et al.*, 2000] causing amplification or frequency-modulation rather than triggering high-frequency climate variability. Evidently, the world-wide recognition of climate variability at D-O and H frequencies over the last 100,000 years suggests that ocean and ice sheets are amplifiers operating mostly via feedback mechanisms and internal oscillations.

A widely used explanation for sub-Milankovitch climate variability with periodicities ranging between 12 and 4 kyr is a non-linear response to primary Milankovitch forcing, which will introduce harmonics and produce combination tones [Pestiaux *et al.*, 1988; Hagelberg *et al.*, 1994; Ortiz *et al.*, 1999]. Generally, the potential for such a non-linear climate response is supported by the notion that climate records contain integrated signals that hold information from more than just one season [Crowley 1992]. The presence of variations near the 2<sup>nd</sup>, 3<sup>rd</sup> and 4<sup>th</sup> harmonics of primary precession (periodicities of 12–5 kyr) was regarded evidence for non-linear climate system response to primary orbital forcing [Pokras and Mix 1987]. The delivery of the freshwater diatom *Melosira* to the equatorial Atlantic at half- and quarter precession frequencies suggested that African aridity and changes in the trade-wind system react in a non-linear way to precession forcing, although lake desiccation itself is a classic example of a nonlinear process [Crowley *et al.*, 1992]. Pestiaux *et al.*, [1988] concluded that monsoon-related processes are responsible for a nonlinear climate system response to precessional forcing in the Indian ocean. The importance of low-latitude climate forcing is strengthened by the notion that the twice-yearly overhead passage of the sun across the equator [Short and Mengel 1986; Short *et al.*, 1991] might create a climate cycle with a semi-precession frequency. Evidently, such a low-latitude climate forcing scenario is in conflict with suggestions that internal ice sheet-ocean oscillations trigger sub-Milankovitch climate variability.

#### **6.4.4. Harmonics and combination tones of primary Milankovitch cycles**

In principle, a variety of frequencies in the sub-Milankovitch range can be generated as harmonics and combination tones of the primary Milankovitch frequencies because climatic precession is not composed of a single component but is dominated by double components around 23 and 19 kyr with periods of 22.2 and 23.8 kyr, and of 18.8 kyr, respectively (see von Dobeneck and Schmieder, [1999] for an overview). As a consequence the pattern will increase in complexity with increasing frequency although the amplitude will decrease. In palaeoclimatic timeseries, the presence of additional free oscillations [Saltzman and Sutera 1984; Le Treut *et al.*, 1988] and stochastic noise

increases the difficulty in interpreting spectral results and separating internal climate system variability from external forcing. Gaining information about the underlying climate mechanisms from spectral analysis is, therefore, challenging.

Harmonics occur in narrow frequency bands and decrease in amplitude with increasing frequency. The only proof for the presence of harmonics is their detection in the time as well as in the frequency domain and by testing them against periodicities found in different environmental settings, climate proxies and time intervals using different spectral methods. Spectral results of SN, Site 967 and Site 969 are consistent with results from other palaeoclimatic studies [e.g. *Yiou et al.*, 1994 for overview] and, therefore, a similar origin might be expected. In the time domain, the  $\delta^{18}\text{O}$  and CR-MS time series indicate climate variations with average spacing of roughly  $\sim 10$  kyr,  $\sim 7$  kyr, 3-4 kyr and 1-2 kyr (see also *Chapter 2* and *Chapter 3*). In the frequency domain, variance is concentrated around these frequencies, although in relatively broad bands.

If we consider in a first attempt that these periodicities present harmonics of the primary obliquity cycle, the 2<sup>nd</sup> to 5<sup>th</sup> harmonic (treating the fundamental as the first harmonic) would be 20.5 kyr, 13.6 kyr, 10.3 kyr and 8.2 kyr. Evidently, the 2<sup>nd</sup> and 4<sup>th</sup> harmonic of 41 kyr periodicity fall into the precession- and half-precession range and, therefore, are difficult to identify. Concentration of variance  $\sim 14$  kyr is observed in the MS and CR spectra and vaguely in the  $\delta^{18}\text{O}$ . Variance at  $\sim 8$  kyr is observed in the  $\delta^{18}\text{O}$ , however, the detection of a 5<sup>th</sup> harmonic would be very unlikely to be traced in palaeoclimate records in the presence of (red) noise.

Harmonics produced by the different precession components 23.8 kyr, 22.2 kyr and 18.8 kyr cover a rather broad range [e.g. *Berger* 1988 for overview]. Variance at the 2<sup>nd</sup> (9.4-11.9 kyr) 3<sup>rd</sup> (6.3-7.9 kyr) and 4<sup>th</sup> (4.7-5.9 kyr) harmonic are observed in the spectra but their interpretation is not straightforward. For example, the observed 6.7 kyr periodicity in the MS record of SN and the 6 kyr in the CR record of Sites 969 and 967 may have a similar origin as indicated by bandpass filtering. A periodicity of 6 kyr can either be related to the 3<sup>rd</sup> or 4<sup>th</sup> harmonic, if we start from a fundamental period of either 18.8 kyr or 23.8 kyr. The 18.8 kyr precession component reaches a deep minimum at 2.5 Ma and has as a consequence a weak expression in the insolation record. At such an astronomical configuration, the 18.8 kyr cycle may even be a doublet itself [*Hinnov* 2004], thereby increasing the uncertainty in the interpretation of the spectral peaks. On the contrary, the 23.8 kyr and 22.2 kyr precession components have stable amplitudes within the time interval studied, however, the presence of a 4<sup>th</sup> harmonic, necessary to explain the observed variability at 6 kyr, is unlikely. It is more likely that the lower periodicities are related to combination tones of the primary Milankovitch (precession) periodicities.

Periodicities of 7-5 kyr and 3.4 kyr may represent sum combination tones of the primary precession couplets and their harmonics. A periodicity of 7.1 kyr can be produced by the combination tone of the 18.8 kyr cycle with the 2<sup>nd</sup> harmonic of the

23.8 kyr cycle. Similarly, the combination of the 23.8 kyr cycle with the 2<sup>nd</sup> harmonic of the 18.8 kyr cycle will produce a 6.7 kyr cycle and the combination of the 2<sup>nd</sup> harmonics of the 18.8 and 23.8 kyr cycle a 5.2 kyr cycle. A periodicity of 3.4 kyr results from combining the primary 18.8 kyr cycle with the 3<sup>rd</sup> harmonic of the 23.8 kyr cycle. In summary, spectral results of SN, Site 967 and Site 969 proxy data suggest a strong relation between sub-Milankovitch climate variability and primary Milankovitch forcing. In the next section we will deal with the question how these signals are translated into (regional) climate variability.

#### 6.4.5. Possible climate forcing mechanism at sub-Milankovitch timescales

##### *Clipped precession*

Climate oscillations at periodicities equal to precession harmonics have been predicted by a two-dimensional seasonal energy balance model, indicating a complex response of surface temperature to insolation forcing at equatorial latitudes where the sun passes twice a year overhead producing two insolation maxima in the annual cycle [Short *et al.*, 1991]. Since climate is responding to the largest possible maximum insolation, independently of the month of the year (i.e. in the season that occurs nearest to perihelion), maximum summer temperature ( $T_{\max}$ ) moves from spring to fall and vice versa as perihelion interacts with the overhead passage of the sun at either equinox [Short and Mengel 1986; Short *et al.*, 1991].

At the equator,  $T_{\max}$  shows a ‘clipped’ curve with two maxima spaced exactly half a precession cycle apart, thus potentially capable of generating a semi-precession cycle. A major drawback of this scenario is that it is only valid at the equator itself. Further away from the equator, spacing of the two  $T_{\max}$  becomes asymmetric until a single  $T_{\max}$  is reached per precession cycle at the tropics of Cancer and Capricorn. However, also the difference between  $T_{\max}$  and  $T_{\min}$  varies in a complicated way at equatorial latitudes. The difference between the strongest temperature maximum ( $T_{\max}$ ) and the strongest minimum ( $T_{\min}$ ) in the annual cycle results in a curve at the equator with maxima spaced a quarter of a precession cycle apart [Berger pers. comm.].

The difference between  $T_{\max}$  and  $T_{\min}$  (minmax curve) is shown in (Figure 6.13) for the interval between 2 and 3 Ma. This curve is dominated by eccentricity. The eccentricity detrended curve shows the typical modulation by obliquity and is very similar to the  $\text{LaO}_{4(1,1)}$  65°N summer insolation curve (lower panel) although 20 times lower in amplitude. Spectral results indicate a dominant periodicity of 5-5.8 kyr and concentration of variance at the 2<sup>nd</sup>, 3<sup>rd</sup> and 4<sup>th</sup> harmonics of the 5-6 kyr with periodicities of 2.9-2.5 kyr, 1.9-1.7 kyr and 1.5-1.4 kyr, respectively. These periodicities are also hidden in the original  $\text{LaO}_{4(1,1)}$  65°N summer insolation curve, but become statistically significant as precession is averaged out in the way described above. Although the amplitude and thus the forcing at these frequencies is small, the effect on

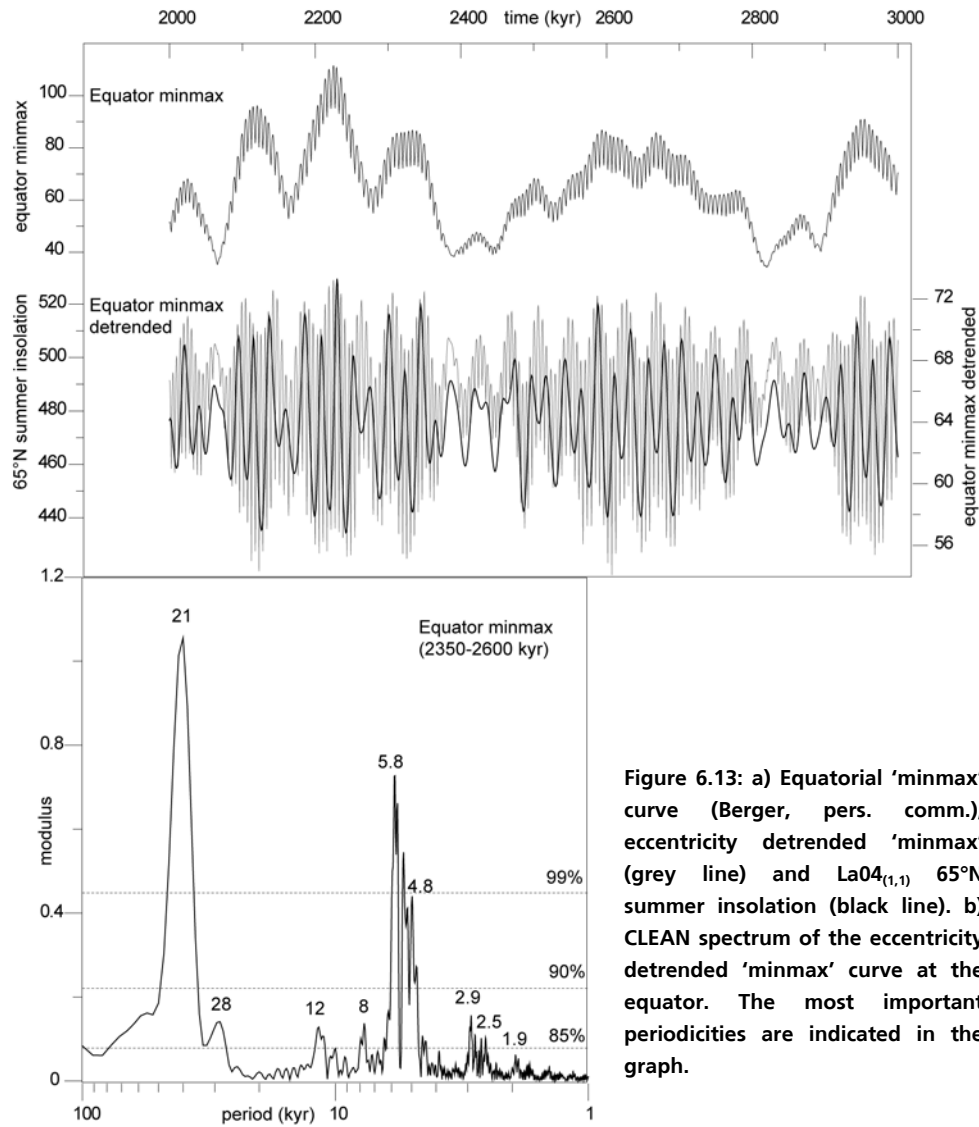


**Figure 6.13: a) Equatorial ‘minmax’ curve (Berger, pers. comm.), eccentricity detrended ‘minmax’ (grey line) and La04<sub>(1,1)</sub> 65°N summer insolation (black line). b) CLEAN spectrum of the eccentricity detrended ‘minmax’ curve at the equator. The most important periodicities are indicated in the graph.**

climate processes at low latitudes can not be ruled out and can be important in understanding sub-Milankovitch climate variability at low-latitudes and the transfer of sensible and latent heat to high-latitudes.

The ‘minmax’ curve suffers essentially from the same short-coming as  $T_{max}$  in the way that the curve starts to reveal a different pattern and spectral characteristics when moved away from the equator. Construction of a ‘minmax’ curve at latitudes between 0-23.5°N results in a target curve that is highly nonlinear (Figure 6.14). For instance the eccentricity detrended ‘minmax’ curve for 5°N varies in concert with La04<sub>(1,1)</sub> 65°N



summer insolation with the same amplitude but rectified and with variability at half-precession clearly visible. The resulting power spectrum is dominated by precession and semi-precession frequencies and clearly not significant additional peaks which

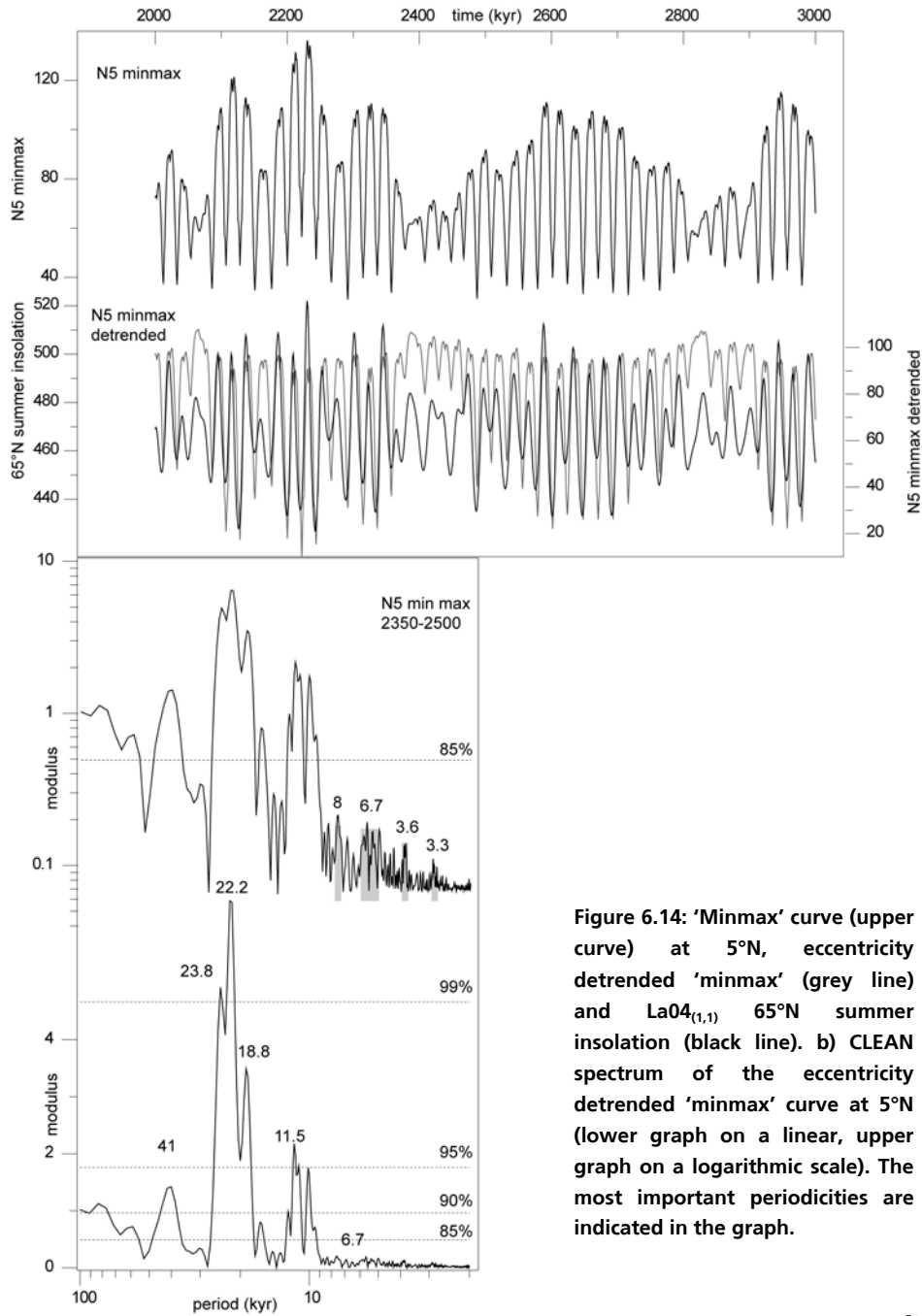


Figure 6.14: 'Minmax' curve (upper curve) at 5°N, eccentricity detrended 'minmax' (grey line) and La04<sub>(1,1)</sub> 65°N summer insolation (black line). b) CLEAN spectrum of the eccentricity detrended 'minmax' curve at 5°N (lower graph on a linear, upper graph on a logarithmic scale). The most important periodicities are indicated in the graph.

correspond to periods of 7-6.7 kyr and 3.6-3.3 kyr. The latter are very similar to those found in our data, and suggest that the 7-6.7 kyr and  $\sim 3.5$  kyr might be related to harmonics and combination tones of primary precession introduced in a nonlinear way.

Although the 'N<sub>5</sub> minmax' curve could provide an illustration of how nonlinearities are introduced in the (low-latitude) climate system, it remains unclear whether such a mechanism could affect climate physically. Preliminary climate modelling results using a coupled model of intermediate complexity (CLIMBER-2) reveal changes in thermohaline overturning at a quarter-precession cycle of 5-6 kyr if an interactive vegetation cover and feedbacks are included [Tuenter 2004]. The underlying mechanism is not yet clear but seems to include vegetation controlled changes in low-latitude runoff into the low latitude Atlantic and resultant changes in sea surface water salinity, which in turn controls deep water formation in the North Atlantic convection areas. The importance of vegetation feedbacks could explain why continental records, such as the pollen record from Florida over the last 50 kyr [Grimm *et al.*, 1993] and colour reflectance records of Pliocene lacustrine successions in Greece [Steenbrink *et al.*, 2003], often portray a more regular pacing of sub-Milankovitch climate variability around periodicities of 5-6 kyr than marine records. The example of the N<sub>5</sub> minmax could present one way to explain why Northern Hemisphere Heinrich events do not occur regularly at a quarter precession cycle but have a the longer quasi periodic pacing of  $\sim 7$  kyr.

#### **6.4.6. Sub-Milankovitch climate variability in relation to nonlinearities in the ice sheet-ocean system**

Another way to explain differences between continental and marine records is by taking nonlinearities within the ice-sheet ocean system and (nonlinear) interactions with this system into account. Different temporal responses of the various climate components to orbital forcing, diverse feedback mechanisms as well as internal oscillations indicate that the ice-sheet ocean system is highly complex.

The response times for the different climate components during MIS100-96 were evaluated in *Chapter 5*. The response times of the  $\delta^{18}\text{O}_{\text{benthos}}$  of Site 967 and its derivative ice volume show a large lag with respect to orbital obliquity while Northern Hemisphere annual air temperature ( $T_{\text{air}}$ ) is leading ice volume by only a few kyr. More importantly, it was shown that response times were not constant through time for all the components and may have been altered in the presence of sum and difference frequencies to the main orbital forcing. By contrast, the Ti/Al record of Site 967 does show a constant in phase relationship with orbital obliquity, which was the basic assumption in creating the age model of Site 967 [Lourens *et al.*, 2001]. Similarly, the 41-kyr components of the MS and CR indicate constant phase leads/lags with respect to obliquity throughout MIS101-95 indicating that these climate systems were probably independent of (nonlinear) ice-sheet (ocean) dynamics.

Additionally, spectral results indicate a more regular pacing of MS and CR variations on a sub-Milankovitch scale as compared to the  $\delta^{18}\text{O}$ . Especially, the  $\delta^{18}\text{O}_{\text{benthos}}$  of SN reveals a broad range of spectral peaks, which might, however, be related to the same climate signal. Wavelet analysis and band-pass filtering of the SN  $\delta^{18}\text{O}_{\text{benthos}}$  record indicate that the spacing between sub-cycles (stadial-interstadial variations) varies through time pointing to a non-stationary behaviour. This suggests that either the time series on which the climate system acts has varied through time or that the primary signal is constant but has been frequency-modulated.

Evaluation of the  $\delta^{18}\text{O}_{\text{benthos}}$  of SN in the time domain indicates that the spacing of the subcycles might be controlled by the duration of the glacial, with longer spacing being associated with a longer duration of the glacial.

Frequency-modulation (FM) of the obliquity (and eccentricity) cycle caused by the  $\sim 413$  kyr eccentricity has been discussed in *Chapter 5*. It was argued that the strong peaks at the 28 and 80 kyr observed in the  $\delta^{18}\text{O}_{\text{benthos}}$  of Site 967 and its derivatives, ice volume and  $T_{\text{air}}$ , may represent sidebands of a 41 kyr carrier (*Chapter 5*), although these periodicities are slightly offset from those predicted in theory [*Rial and Anaclerio*

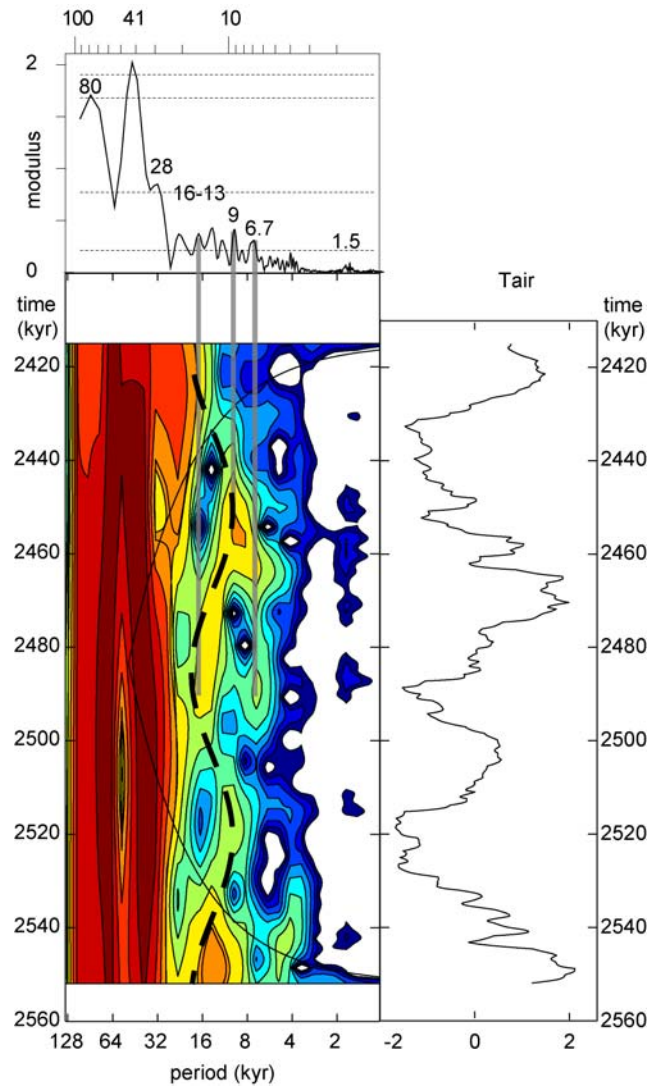


**Figure 6.15:** CLEAN spectrum and wavelet map of  $T_{\text{air}}$  Site 967 versus period (kyr) and  $T_{\text{air}}$  of San Nicola versus age. Shaded intervals in the CLEAN spectrum indicate significant periodicities. The thick stipple line indicates the modulation.

2000]. But how does this observation relate to the observed variations in cycle length of the  $\delta^{18}\text{O}_{\text{benthos}}$  sub-cycles of SN? Could indeed frequency-modulation alter the cycle duration?

The Northern Hemisphere surface air temperature ( $T_{\text{air}}$ ), which has been derived from the  $\delta^{18}\text{O}_{\text{benthos}}$  of Site 967, reveals high-frequency variability superimposed on the obliquity dominated glacial interglacial variation like the  $\delta^{18}\text{O}_{\text{benthos}}$  of Site 967 itself (*Chapter 5*). In the spectrum of  $T_{\text{air}}$ , peaks are observed at or near periodicities of 7, 9, 13 and 16 kyr, but the power distribution is non-stationary through time (Figure 6.15). Maximum concentration of power at a periodicity of  $\sim 9$  kyr occurs during late MIS100 – early MIS99 and MIS96 while concentration of power at or near 13 and 16 kyr and around 7 kyr (or 4–5 in case of MIS101) is observed during MIS101, 98 and 95. Bifurcations of the signal from a strong signal around 9 kyr into two signals centred around a longer (13–16 kyr) and a shorter (7 kyr) periodicity occurs every 70 kyr (dotted line in Figure 6.15). This example shows that nonlinear behaviour within the climate system, cannot be excluded. However, higher order statistics (i.e. bispectral analysis) are required to substantiate such a mechanism by determining phase and frequency locking of the components. Unfortunately our record is too short to adequately resolve variance in the Milankovitch range. Preliminary results of bicoherence analysis (not shown) of the global benthic stacked record of *Lisiecki and Raymo* [2005] shows evidence for phase coupling as would be expected if frequency-modulation of the obliquity signal plays a role. However, these preliminary results also show that precession might have an influence although it should be realised that the stacked record has been tuned to precession and obliquity.

Getting back to our data, a  $\sim 8$ –9 kyr periodicity seems to play an important role in the  $\delta^{18}\text{O}_{\text{benthos}}$  records of SN and Site 967, and in the derivative  $T_{\text{air}}$  record. This periodicity brings us back to the model proposed by *McIntyre and Molino* [1996], who stated that the 8.4 kyr periodicity observed in the zonal wind-driven divergence in eastern tropical Atlantic over the past 40 kyr represents the 2<sup>nd</sup> harmonic of 16.4 kyr, which is the difference tone of a short eccentricity cycle (of 72 kyr) and primary precession (22 kyr). The anomalous short eccentricity cycle should then be related to a minimum in the 400 kyr eccentricity. *Berger and Loutre* [1997] showed that a set of anomalous short (80–76 kyr) eccentricity cycles may produce a range of periodicities between 9.3 and 8.1 kyr. Alternatively, the 8.4 kyr cycle can be related to the difference tone between the 2<sup>nd</sup> harmonic of 28 kyr and the 80 kyr cycle ( $2/28 \text{ kyr} - 1/80 \text{ kyr} = 1/16.9 \text{ kyr}$ ) and thus probably to (internal) ice sheet oscillations (*Chapter 5*).

## 6.5. Conclusions

Oxygen isotope and sediment property data of San Nicola and Site 967 record climate relationships during MIS98 and MIS96 that are comparable to those observed during MIS100 (*Chapters 2, 3 and 4*), i.e. low latitude dust episodes as recorded by the colour

reflectance (CR) and magnetic susceptibility (MS) can be linked with cooling cycles in the Mediterranean and the North Atlantic, and with North Atlantic ice rafting history. Spectral analysis indicates however, that these climate systems might have operated on slightly different time scales: On a Milankovitch-scale, spectra of the oxygen isotope records are dominated by 80, 41 and 28 kyr periodicities, which is in agreement with global ice volume and Northern Hemisphere annual air temperature in that interval (*Chapter 5*). Only the spectra of  $\delta^{18}\text{O}_{\text{G.rubber}}$  indicate variance at the precession period, reflecting a local sea surface salinity/temperature component. The CR and MS spectra indicate a much stronger precession component but they differ significantly from one site to the other. These differences may be explained by the shortness of the records and, probably more importantly, differences in the glacial-interglacial signature of the individual sites and the strength of the precessional signal. Spectra of these records are more similar in the sub-Milankovitch range, showing concentration of variance around 6–7 kyr close to periodicities resulting from harmonics and combinations tones of the primary precession components. Comparison with the power spectrum of a curve constructed by taking the difference between the strongest temperature maximum ( $T_{\text{max}}$ ) and the strongest minimum ( $T_{\text{min}}$ ) in the annual cycle at the equator indicates that differential heating related to the orbital configuration may explain the observed climate variability recorded by the MS and CR at SN and Site 967. Such a model would be in agreement with a (stationary) periodic climate signal as observed in the sediment property records of SN and Site 967. However, a link with primary precession may be considered less likely in view of the reduced precessional amplitude as a consequence of minimum eccentricity at that time.

On the contrary, spacing of  $\delta^{18}\text{O}$  subcycles, which represent the most prominent feature on a sub-Milankovitch scale in the  $\delta^{18}\text{O}$  record of the investigated time interval (see also *Chapter 2*), vary from one glacial to the other between 7 and 9 kyr, with the length of the cycles being related to the length of the glacial. Wavelet analysis indicates that both intensities and frequencies of the climate signal change through time, explaining the relatively broad peak in the power spectrum around 7–9 kyr. Such a non-stationary behaviour points towards nonlinear components either in the recording mechanism, the climate response or the forcing itself. Such nonlinear components could arise from frequency modulation of the primary eccentricity, obliquity and precession cycle or from internal ice sheet dynamics. An example of frequency modulation is presented for the Northern Hemisphere annual air temperature ( $T_{\text{air}}$ ), a derivative of the  $\delta^{18}\text{O}_{\text{benthos}}$  of Site 967, which shows the presence of a 8 kyr or  $\sim 12$  kyr component being modulated by a  $\sim 70$  kyr periodicity. This example is more in agreement with the model proposed by *McIntyre and Molino* [1996], who related zonal wind-driven divergence in the equatorial Atlantic with a periodicity of  $\sim 8.4$  kyr to nonlinear interaction between precession and an anomalous short eccentricity periodicity. However, our data also clearly indicate that more work has to be done to unravel the enigmas of sub-Milankovitch variability in the climate system.

## References

- Adhémar, J. A. (1842), *Révolutions de la mer*, privately published, Paris.
- Agassiz, L. (1838), Upon glaciers, moraines and erratic blocks: Address delivered at the opening of the Helvetic Natural History Society at Neuchatel, *New Philosophy Journal Edinburgh*, *24*, 864-883.
- Allen, J. R. M., U. Brandt, A. Brauer, H. W. Hubberten, B. Huntley, J. Keller, M. Kraml, A. Mackensen, J. Mingram, J. F. W. Negendank, N. R. Nowaczyk, H. Oberhansli, W. A. Watts, S. Wulf and B. Zolitschka (1999), Rapid environmental changes in southern Europe during the last glacial period, *Nature*, *400*, 740-743.
- Alley, R. B. and D. R. MacAyeal (1994), Ice rafted debris associated with binge/purge oscillations of the Laurentide Ice Sheet, *Paleoceanography*, *9*, 503-511.
- Argnani, A. (1987), The Gela nappe: evidence of accretionary melange in the Maghrebian foredeep of Sicily, *Mem. Soc. Geol. Ital.*, *38*, 419-428.
- Asioli, A., F. Trincardi, J. J. Lowe and F. Oldfield (1999), Short-term climate changes during the Last Glacial-Holocene transition: comparison between Mediterranean records and the GRIP event stratigraphy, *J. Quat. Sci.*, *14*, 373-381.
- Bar-Matthews, M., A. Ayalon and A. Kaufman (2000), Timing and hydrological conditions of Sapropel events in the Eastern Mediterranean, as evidenced from speleothems, Soreq cave, Israel, *Chemical Geology*, *169*, 145-156.
- Bard, E., F. Rostek, J.-L. Turon and S. Gendreau (2000), Hydrological Impact of Heinrich Events in the Subtropical Northeast Atlantic, *Science*, *289*, 1321-1324.
- Bé, A. W. H. and W. H. Hutson (1977), Ecology of planktonic foraminifera and biogeographic patterns of life and fossil assemblages in the Indian Ocean, *Micropaleontology*, *23*, 369-414.
- Beaufort, L., T. de Garide-Thoron, A. C. Mix and N. G. Pisias (2001), ENSO-like forcing on oceanic primary production during the late Pleistocene, *Science*, *293*, 2440-2444.
- Berger, A. (1988), Milankovitch theory and climate, *Rev. Geophys.*, *26*, 624-657.
- Berger, A. and M.-F. Loutre (1997), Intertropical latitudes and precessional and half-precessional cycles, *Science*, *278*, 1476-1478.
- Berger, A., X. S. Li and M.-F. Loutre (1999), Modelling Northern Hemisphere ice volume over the last 3 Ma, *Quat. Sci. Rev.*, *18*, 1-11.
- Bethoux, J.-P. and C. Pierre (1999), Mediterranean functioning and sapropel formation: respective influences of climate and hydrological changes in the Atlantic and the Mediterranean, *Mar. Geol.*, *153*, 29-39.
- Bigg, G. R. (1995), Aridity of the Mediterranean Sea at the last glacial maximum: A reinterpretation of the  $\delta^{18}\text{O}$  record, *Paleoceanography*, *10*, 283-290.
- Bintanja, R., R. S. W. van de Wal and J. Oerlemans (2005a), A new method to estimate ice age temperatures, *Clim. Dyn.*, *24*, 197-211.
- Bintanja, R., R. S. W. van de Wal and J. Oerlemans (2005b), Modelled atmospheric temperatures and global sea levels over the past million years, *Nature*, *437*, 125-128.
- Bintanja, R. and R. S. W. van de Wal (in prep.).

R E F E R E N C E S

- Bonaduce, G. and R. Sprovieri (1984), The appearance of *Cyteropteron testudo* Sars (Crustacea: Ostracoda) is a Pliocene event. Evidence from the south-central Mediterranean, *Boll. Soc. Paleont. Ital.*, *23*, 131-136.
- Bond, G. C. (1992), Evidence for massive discharges of icebergs into the North Atlantic ocean during the last glacial period, *Nature*, *360*, 245-249.
- Bond, G. C., W. Broecker, S. Johnsen, J. McManus, L. Labeyrie, J. Jouzel and G. Bonani (1993), Correlations between climate records from North Atlantic sediments and Greenland ice., *Nature*, *365*, 143-147.
- Bond, G. C. and R. Lotti (1995), Iceberg discharges into the North Atlantic on millennial time scales during the last glaciation, *Science*, *267*, 1005-1010.
- Bond, G. C., W. Showers, M. Elliot, M. Evans, R. Lotti, I. Hadjas, G. Bonani and S. Johnson (1999), The North Atlantic's 1-2 kyr climate rhythm: Relation to Heinrich events, Dansgaard/Oeschger cycles and the Little Ice Age, in *Mechanisms of Global Climate Change at Millennial Time Scales*, edited, pp. 35-58.
- Bond, G. C., B. Kromer, J. Beer, R. Muscheler, M. Evans, N., W. Showers, S. Hoffmann, R. Lotti-Bond and G. Bonani (2001), Persistent solar influence on North Atlantic climate during the Holocene, *Science*, *294*, 2130-2136.
- Broecker, W. (1992), Origin of the northern Atlantic's Heinrich events, *Clim. Dyn.*, *6*, 265-273.
- Broecker, W. (1997), Thermohaline circulation, the Achilles Heel of our climate system: Will man-made CO<sub>2</sub> upset the current balance? *Science*, *278*, 1582-1588.
- Byrne and Lee (1993).
- Cacho, I., J. O. Grimalt, C. Pelejero, M. Canals, F. J. Sierro, J.-A. Flores and N. J. Shackleton (1999), Dansgaard-Oeschger and Heinrich event imprints in Alboran sea paleotemperatures, *Paleoceanography*, *14*, 698-705.
- Cacho, I., J. O. Grimalt, F. J. Sierro, N. Shackleton and M. Canals (2000), Evidence for enhanced Mediterranean thermohaline circulation during rapid climatic coolings, *Earth Planet. Sci. Lett.*, *183*, 417-429.
- Cacho, I., J. O. Grimalt, M. Canals and L. Sbaiffi (2001), Variability of the western Mediterranean Sea surface temperature during the last 25,000 years and its connection with the Northern Hemisphere climatic changes, *Paleoceanography*, *16*, 40.
- Cacho, I., J. O. Grimalt and M. Canals (2002), Response of Western Mediterranean Sea to rapid climatic variability during the last 50,000 years: a molecular biomarker approach, *J.Mar. Syst.*, *33-34*, 253-272.
- Calvert, S. E. (1983), Geochemistry of Pleistocene sapropels and associated sediments from the Eastern Mediterranean, *Oceanol. Acta*, *6*, 255-267.
- Calvert, S. E., S. Mukherjee and R. Morris (1985), Trace metals in fluvic and hunic acids from modern organic-rich sediments, *Oceanol. Acta*, *8*, 167-173.
- Carter, S. J. and M. E. Raymo (1999), Sedimentological and mineralogical control of multisensor track data at Sites 981 and 984, in *Proceedings of the Ocean Drilling Program, Scientific Results*, edited by M. E. Raymo, E. Jansen, P. Blum and T. D. Herbert, pp. 247-256, ODP, College Station, Texas.
- Channell, J. E. T. and B. Lehman (1999), Magnetic stratigraphy of North Atlantic sites 980-984, in *Proceedings of the Ocean Drilling Program, Scientific Results*, edited by M. E. Raymo, E. Jansen, P. Blum and T. D. Herbert, pp. 113-130, ODP, College Station, Texas.
- Chapman, M. R. and N. J. Shackleton (1998), Millennial-scale fluctuations in North Atlantic heat flux during the last 150,000 years, *Earth Planet. Sci. Lett.*, *159*, 57-70.

## REFERENCES

- Chen, J., J. W. Farrell, D. W. Murray and W. L. Prell (1995), Time scale and paleoceanographic implications of a 3.6 m.y. oxygen isotope record from the north east Indian Ocean (Ocean Drilling Program site 758), *Paleoceanography*, *10*, 21-47.
- Cita, M. B., C. Vergnaud-Grazzini, C. Robert, H. Chamley, N. Ciaranfi and S. D'Onofrio (1977), Paleoclimatic record of a long deep-sea core from the eastern Mediterranean, *Quat. Res.*, *8*, 205-235.
- Clemens, S., C. and R. Tiedemann (1997a), Eccentricity forcing of Pliocene-Early Pleistocene climate revealed in a marine oxygen isotope record, *Nature*, *385*, 801-804.
- Clemens, S. C., D. W. Murray and W. L. Prell (1996), Nonstationary phase of the Plio-Pleistocene Asian Monsoon, *Science*, *274*, 943-948.
- Clemens, S. C. and R. Tiedemann (1997b), Eccentricity forcing of Pliocene-Early Pleistocene climate revealed in a oxygen-isotope record, *Nature*, *385*, 801-804.
- Clement, A. C., R. Seager and M. A. Cane (1999), Orbital controls on the El Nino/ Southern Oscillation and the tropical climate, *Paleoceanography*, *14*, 441-456.
- Combourieu-Nebout, N. (1991), Late Pliocene northern Hemisphere glaciations: the continental and marine responses in the central Mediterranean, *Quat. Sci. Rev.*, *10*, 319-334.
- Combourieu-Nebout, N., J. L. Touron, R. Zahn, L. Capotondi, L. Londeix and K. Pahnke (2002), Enhanced aridity and atmospheric high-pressure stability over the western Mediterranean during the North Atlantic cold events of the past 50 k.y., *Geology*, *30*, 863-866.
- Corliss, B. H. (1985), Microhabitats of benthic foraminifera within deep-sea sediments, *Nature*, *314*, 435-438.
- Cortijo, E., L. Labeyrie, L. Vidal, M. Vautravers, M. Chapman, J.-C. Duplessy, M. Elliot, M. Arnold, J.-L. Touron and G. Auffret (1997), Changes in sea surface hydrology associated with Heinrich event 4 in the North Atlantic Ocean between 40 and 60°N, *Earth Planet. Sci. Lett.*, *146*, 29-45.
- Croll, J. (1864), On the physical cause of the change of climate during geological epochs, *Philosophical Magazine*, *28*, 121-137.
- Crowley, T., J. (1992), North Atlantic Deep Water cools the Southern Hemisphere, *Paleoceanography*, *7*, 489-497.
- Crowley, T. J., K.-Y. Kim, J. G. Mengel and D. A. Short (1992), Modelling 100,000 year climate fluctuations in pre-Pleistocene time series, *Science*, *255*, 705-707.
- Curry, W. B. and D. W. Oppo (1997), Synchronous, high-frequency oscillations in tropical sea surface temperatures and North Atlantic Deep Water production during the last glacial cycle, *Paleoceanography*, *12*, 1-14.
- Dannenmann, S., B. K. Linseley, D. W. Oppo, Y. Rosenthal and L. Beaufort (2003), East Asian monsoon forcing of suborbital variability in the Sulu Sea during Marine Isotope Stage 3: Link to Northern Hemisphere climate, *Geochem., Geophys., Geosyst.*, *4*, 1-13.
- Dansgaard, W., S. J. Johnsen, H. B. Clausen, D. Dahl-Jensen, N. Gundestrup, C. U. Hammer and H. Oeschger (1984), North Atlantic climatic oscillations revealed by deep Greenland ice cores, *Geophys. Monogr.*, *29*, 288-298.
- Dansgaard, W., S. J. Johnsen, H. B. Clausen, D. Dahl-Jensen, N. S. Gundestrup, C. U. Hammer, C. S. Hvidberg, J. P. Steffensen, A. E. Sveinbjörnsdottir, J. Jouzel and G. Bond (1993), Evidence for general instability of past climate from a 250-kyr ice-core record, *Nature*, *364*, 218-220.
- de Rijk, S., A. Hayes and E. J. Rohling (Eds.) (1999), *Eastern Mediterranean sapropel S1 interruption: an expression of the onset of climatic deterioration around 7 ka BP*, 337-343 pp., Elsevier, Amsterdam.



R E F E R E N C E S

- deMenocal, P. B. and D. Rind (1993), Sensitivity of Asian and African monsoon climate to variations in seasonal insolation, glacial ice cover, sea surface temperature and Asian orography, *J. Geophys. Res.*
- Denison, S. M., M. A. Maslin, C. Boot, R. D. Pancost and V. J. Ettwein (2005), Precession-forced changes in South West African vegetation during Marine Isotope Stages 101-100 (~2.56-2.51 Ma), *Palaeogeog., Palaeoclimatol., Palaeoecol.*, *220*, 375-386.
- Dokken, T. M. and E. Jansen (1999), Rapid changes in the mechanism of ocean convection during the last glacial period, *Nature*, *401*, 458-461.
- Dominik, J. and P. Stoffers (1978), The influence of late Quaternary Stagnations on Clay Sedimentation in the Eastern Mediterranean Sea, *Geologische Rundschau*, *68*, 302-317.
- Draut, A., M. E. Raymo, J. F. McManus and D. W. Oppo (2003), Climate stability during the Pliocene warm period, *Paleoceanography*, *18*, 1078.
- Dulac, F., C. Moulin, C. E. Lambert, F. Guillard, J. Poitou, W. Guelle, C. R. Quétel, X. Schneider and U. Ezat (1996), Quantitative remote sensing of African dust transport to the Mediterranean, in *The Impact of Desert Dusts Across the Mediterranean*, edited by S. G. a. R. Chester, pp. 25-49, Kluwer Academic Publishers, Dordrecht.
- Emeis, K.-C., A. H. F. Robertson and C. Richter (1998), Preliminary Report Mediterranean I, *Ocean Drilling Program Leg 160*.
- Emeis, K.-C., H. Schulz, U. Struck, M. Rossignol-Strick, H. Erlenkeuser, M. W. Howell, D. Kroon, A. Mackensen, S. Ishizuka, T. Oba, T. Sakamoto and I. Koizumi (2003), Eastern Mediterranean surface water temperatures and  $\delta^{18}\text{O}$  composition during sapropel formation in the late Quaternary, *Paleoceanography*, *18*, 1-18.
- Fariduddin, M. and P. Loubere (1997), The surface ocean productivity response of deeper water benthic foraminifera in the Atlantic Ocean., *Mar. Micropaleontol.*, *32*, 289-310.
- Flower, B. P. (1999), *Data report*. Planktonic foraminifera from the subpolar North Atlantic and Nordic Seas, sites 980-987 and 907, in *Proceedings of the Ocean Drilling Program, Scientific Results*, edited by M. E. Raymo, E. Jansen, P. Blum and T. D. Herbert, pp. 19-34, ODP, College Station, Texas.
- Foucault, A. and F. Mélières (1995), Nature et origine des cycles sédimentaires métriques du Pliocène de l'Ouest méditerranéen d'après l'étude du contenu terrigène de la Formation Narbone (Punta Piccola, Sicile, Italie), *C. R. Acad. Sci. Paris t.*, *321*, 869-876.
- Foucault, A. and F. Mélières (2000), Palaeoclimatic cyclicity in central Mediterranean Pliocene sediments: the mineralogical signal, *Palaeogeog., Palaeoclimatol., Palaeoecol.*, *158*, 311-323.
- Gauthier, J. H. (1999), Unified structure in Quaternary climate, *Geophys. Res. Lett.*, *26*, 763-766.
- Giorgi, F. (1996), Climate modelling over the Mediterranean region, in *The impact of desert dust across the Mediterranean*, edited by S. Guerzoni and C. Roy, pp. 1-14, Kluwer, Dordrecht.
- Grimm, E. C., G. L. J. Jacobson, W. A. Watts, B. C. S. Hansen and K. A. Maasch (1993), A 50,000-year record of climate oscillations from Florida and its temporal correlation with the Heinrich events, *Science*, *261*, 198-200.
- Guerzoni, S. (1996), Chemical data from aerosols, in *The impact of desert dust across the Mediterranean*, edited by S. Guerzoni and R. Chester, pp. 333-339, Kluwer, Dordrecht.
- Guerzoni, S. and C. Roy (1996), *The impact of desert dust across the Mediterranean*, ISSN 1382-3124 ed., 389 pp., Kluwer, Dordrecht.
- Guiou, C. and A. J. Thomas (1996), Saharan Aerosols: from the soil to the ocean, in *The impact of desert dust across the Mediterranean*, edited by S. Guerzoni and C. Roy, pp. 207-275, Kluwer, Dordrecht.

## REFERENCES

- Gupta, A. K. (1997), Paleoceanographic and paleoclimatic history of the Somali Basin during the Pliocene-Pleistocene: Multivariate analyses of benthic foraminifera from DSDP Site 241 (Leg 25), *J. Foram. Res.*, *27*, 196-208.
- Hagelberg, T., N. Pisias and S. Elgar (1991), Linear and nonlinear couplings between orbital forcing and the marine  $\delta^{18}O$  record during the late Neogene, *Paleoceanography*, *6*, 729-746.
- Hagelberg, T. K., G. Bond and P. deMenocal (1994), Milankovitch band forcing of sub-Milankovitch climate variability during the Pleistocene, *Paleoceanography*, *9*, 545-558.
- Haigh, J. D. (1994), The role of stratospheric ozone in modulating the solar radiative forcing of climate, *Nature*, *370*, 544-546.
- Haigh, J. D. (1996), The impact of solar variability on climate, *Science*, *272*, 981-984.
- Harloff, J. and A. Mackensen (1997), Recent benthic foraminiferal associations and ecology of the Scotia Sea and Argentine Basin, *Mar. Micropaleontol.*, *31*, 1-29.
- Hays, J. D., J. Imbrie and N. J. Shackleton (1976), Variations in the Earth's orbit: pacemaker of the ice ages, *Science*, *194*, 1121-1132.
- Hayward, B. W., H. Neil, R. Carter, H. R. Grenfell and J. Hayward (2002), Factors influencing the distribution patterns of Recent deep-sea benthic foraminifera, east of New Zealand, Southwest Pacific Ocean, *Mar. Micropaleontol.*, *46*, 139-176.
- Heinrich, H. (1988), Origin and consequences of cyclic ice rafting in the NE Atlantic Ocean during the past 130,000 years, *Quat. Res.*, *29*, 142-152.
- Hem, J. D. (1989), Coprecipitation and redox reactions of manganese oxides with copper and nickel, *Geochim. Cosmochim. Acta*, *53*, 2811-2822.
- Hemleben, C., M. Spindler and O. R. Anderson (1989), *Modern Planktonic Foraminifera*, Springer Verlag, New York.
- Henrich, R., K.-H. Baumann, R. Huber and H. Meggers (2002), Carbonate preservation records of the past 3 Myr in the Norwegian-Greenland Sea and the northern North Atlantic: implications for the history of NADW production, *Mar. Geol.*, *184*, 17-39.
- Heslop, D. and M. J. Dekkers (2002), Spectral analysis of unevenly spaced climatic time series using CLEAN: signal recovery and derivation of significance levels using a Monte Carlo simulation, *Physics of the Earth and Planetary Interiors*, *130*, 103-116.
- Hilbrecht, H. (1996), Extant planktic foraminifera and the physical environment in the Atlantic and Indian Oceans, *Mitteilungen aus dem Geologischen Institut der Eidgen. Technischen Hochschule und der Universität Zürich*, *300*, 93pp.
- Hilgen, F. J. (1991a), Extension of the astronomically calibrated (polarity) time scale to the Miocene/Pliocene boundary, *Earth Planet. Sci. Lett.*, *107*, 349-368.
- Hilgen, F. J. (1991b), Astronomical calibration of Gauss to Matuyama sapropels in the Mediterranean and implication for the geomagnetic polarity time scale, *Earth Planet. Sci. Lett.*, *104*, 226-244.
- Hilgen, F. J., L. J. Lourens, A. Berger and M. F. Loutre (1993), Evaluation of the astronomically calibrated time scale for the late Pliocene and earliest Pleistocene, *Paleoceanography*, *8*, 549-565.
- Hilgen, F. J., W. Krijgsman, C. G. Langereis, L. J. Lourens, A. Santarelli and W. J. Zachariasse (1995), Extending the astronomical (polarity) time scale into the Miocene, *Earth Planet. Sci. Lett.*, *136*, 495-510.
- Hinnov, L. (2004), in *The geological timescale. Recent developments and global correlations*, edited, Cambridge University Press.

R E F E R E N C E S

- Hughen, K., J. T. Overpeck, L. C. Peterson and S. Trumbore (1996), Rapid climate changes in the tropical Atlantic region during the last deglaciation, *Nature*, *380*, 51-54.
- Huybers, P. and C. Wunsch (2004), A depth-derived Pleistocene age model: Uncertainty estimates, sedimentation variability, and nonlinear climate change, *Paleoceanography*, *19*, PA 1028.
- Imbrie, J. and J. Z. Imbrie (1980), Modelling the climatic response to orbital variations, *Science*, *207*, 943-952.
- Imbrie, J., J. D. Hays, D. G. Martinson, A. McIntyre, A. C. Mix, J. J. Morley, N. G. Pisias, W. L. Prell and N. J. Shackleton (1984), The orbital theory of Pleistocene climate: support from a revised chronology of the marine  $\delta^{18}O$  record, in *Milankovitch and Climate, understanding the response to astronomical forcing*, edited by A. Berger, J. Imbrie, J. Hays, G. Kukla and B. Saltzman, p. 510, D. Reidel Publishing Company, Dordrecht / Boston / Lancaster.
- Imbrie, J., E. A. Boyle, S. C. Clemens, A. Duffy, W. R. Howard, G. Kukla, J. Kutzbach, D. G. Martinson, A. McIntyre, A. Mix, B. Molino, J. Morley, N. Pisias, W. L. Prell, M. E. Raymo, N. J. Shackleton and J. R. Toggweiler (1992), On the structure and origin of major glaciation cycles 1. Linear response to Milankovitch forcing, *Paleoceanography*, *7*, 701-738.
- Imbrie, J., A. C. Mix and D. G. Martinson (1993), Milankovitch theory viewed from Devils Hole, *Nature*, *363*, 531-533.
- Jacobs, L. and S. Emerson (1985), Partitioning and transport of metals across the O<sub>2</sub>/H<sub>2</sub>O interphase in a permanently anoxic basin: Framvaren Fjord, Norway, *Geochim. Cosmochim. Acta*, *49*, 1433-1434.
- Jannink, N. T., W. J. Zachariasse and G. J. Van der Zwaan (1998), Living (Rose Bengal stained) benthic foraminifera from the Pakistan continental margin (northern Arabian Sea), *Deep-Sea Research I*, *45*, 1483-1513.
- Jansen, E., M. E. Raymo, P. Blum and T. D. Herbert (1996a), Sites 980/981, *Proceedings of the Ocean Drilling Program, Init. Rep.*, *162*, 81-138.
- Jansen, E., M. E. Raymo, P. Blum and T. D. Herbert (1996b), Explanatory notes, *Proceedings of the Ocean Drilling Program, Init. Rep.*, *162*, 49-90.
- Jian, Z., L. Wang, M. Kienast, M. Sarnthein, W. Kuhnt, H. Lin and P. Wang (1999), Benthic foraminiferal paleoceanography of the South China Sea over the last 40,000 years, *Mar. Geol.*, *156*, 159-186.
- Jorissen, F. J., D. M. Barmawidjaja, S. Puskaric and G. J. Van der Zwaan (1992), Vertical distribution of benthic foraminifera in the northern Adriatic Sea: The relation with the organic flux, *Mar. Micropaleontol.*, *19*, 131-146.
- Kallel, N., M. Paterne, J.-C. Duplessy, C. Vergnaud-Grazzini, C. Pujol, L. Labeyrie, M. Arnold, M. Fontugne and C. Pierre (1997a), Enhanced rainfall in the Mediterranean region during the last sapropel event, *Oceanol. Acta*, *20*, 697-712.
- Kallel, N., M. Paterne, L. Labeyrie, J.-C. Duplessy and M. Arnold (1997b), Temperature and salinity records in the Tyrrhenian Sea during the last 18,000 years, *Palaeogeog., Palaeoclimatol., Palaeoecol.*, *135*, 97-108.
- Kallel, N., J. C. Duplessy, L. Labeyrie, M. Fontugne, M. Paterne and M. Montacer (2000), Mediterranean pluvial periods and sapropel formation over the last 200 000 years, *Palaeogeog., Palaeoclimatol., Palaeoecol.*, *157*, 45-58.
- Keeling, C. D. and T. P. Whorf (2000), The 1,800-year oceanic tidal cycle: A possible cause of rapid climate change, *PNAS*, *97*, 3814-3819.

## REFERENCES

- Kennett, J. P. and M. S. Srinivasan (1983), *Neogene planktonic foraminifera*, 263 pp., Hutchinson Ross Publishing, Pennsylvania.
- Kleiven, H. F., E. Jansen, T. Fronval and T. M. Smith (2002), Intensification of Northern Hemisphere glaciations in the circum Atlantic region (3.5-2.4 Ma) - Ice-rafted detritus evidence, *Palaeogeog., Palaeoclimatol., Palaeoecol.*, *184*, 213-223.
- Klinkhammer, G. P. (1980), Early diagenesis in sediments from the eastern equatorial Pacific - II: Pore water metal results, *Earth Planet. Sci. Lett.*, *49*, 81-101.
- Köppen, W. and A. Wegener (1924), *Die Klimate der geologischen Vorzeit*, 255 pp., Bornträger, Berlin.
- Kroon, D., I. Alexander, M. Little, L. J. Lourens, A. Matthewson, A. H. F. Robertson and T. Sakamoto (1998), Oxygen isotope and sapropel stratigraphy in the Eastern Mediterranean during the last 3.2 million years, in *Proceedings of the Ocean Drilling Program, Scientific Results*, edited by A. H. F. Robertson, K.-C. Emeis, C. Richter and A. Camerlenghi, pp. 181-190, Ocean Drilling Program, College Station, TX.
- Kubilay, N. N., A. C. Saydam, S. Yemenicioglu, G. Kelling, S. Kapur, C. Karaman and E. Akca (1997), Seasonal chemical and mineralogical variability of atmospheric particles in the coastal region of the Northeast Mediterranean, *Catena*, *28*, 313-328.
- Kuhnt, W., S. Hess and Z. Jian (1999), Quantitative composition of benthic foraminiferal assemblages as a proxy indicator for carbon flux rates in the South China Sea, *Mar. Geol.*, *156*, 123-158.
- Laskar, J., F. Joutel and F. Boudin (1993), Orbital, precessional, and insolation quantities for the Earth from -20 Myr to +10 Myr, *Astronomy and Astrophysics*, *270*, 522-533.
- Laskar, J., P. Robutel, F. Joutel, M. Gastineau, A. C. M. Correia and B. Levrard (2004), A long term numerical solution for the insolation quantities of the Earth, *Astronomy and Astrophysics*, *428*, 261-285.
- Le Treut, H. and M. Ghil (1983), Orbital forcing, climatic interactions, and glaciation cycles, *J. Geophys. Res.*, *93*, 9365-9383.
- Le Treut, H., J. Portes, J. Jouzel and M. Ghil (1988), Isotopic modelling of climatic oscillations: implications for a comparative study of marine and ice core records, *J. Geophys. Res.*, *93*, 9365-9383.
- Leroy, S. and L. Dupont (1994), Development of vegetation and continental aridity in northwestern Africa during the Late Pliocene: the pollen record of ODP Site 658, *Palaeogeog., Palaeoclimatol., Palaeoecol.*, *109*, 295-316.
- Leuschner, D. C. and F. Sirocko (2000), The low-latitude monsoon climate during Dansgaard-Oeschger cycles and Heinrich events, *Quat. Sci. Rev.*, *19*, 243-254.
- Lisiecki, L. E. and M. E. Raymo (2005), A Pliocene-Pleistocene stack of 57 globally distributed benthic  $\delta^{18}O$  records, *Paleoceanography*, *20*, 1003.
- Littmann, T., J. Steinrücke and F. Gasse (1990), African mineral aerosol deposition on west Germany 1987-1989: characteristics, origin and transport mechanisms, *Geoökodynamik*, *XI*, 163-189.
- Liu, H.-S. (1992), Frequency variations of the Earth's obliquity and the 100-kyr ice-age cycles, *Nature*, *358*, 397-399.
- Liu, H.-S. (1995), A new driving mechanism of Milankovitch glaciation cycles, *Earth Planet. Sci. Lett.*, *131*, 17-26.
- Loubere, P. and K. Moss (1986), Late Pliocene climatic change and the onset of Northern Hemisphere glaciation as recorded in the northeast Atlantic Ocean, *Geol. Soc. Amer. Bull.*, *77*, 818-828.

REFERENCES

- Lourens, L. J., F. J. Hilgen, J. Gudjonsson and W. J. Zachariasse (1992), Late Pliocene to early Pleistocene astronomically-forced sea surface productivity and temperature variations in the Mediterranean, *Mar. Micropaleontol.*, *19*, 49-78.
- Lourens, L. J. (1994), Astronomical forcing of Mediterranean climate during the last 5.3 million years, 247 thesis, Utrecht.
- Lourens, L. J., A. Antonarakou, F. J. Hilgen, A. A. M. Van Hoof, C. Vergnaud-Grazzini and W. J. Zachariasse (1996), Evaluation of the Plio-Pleistocene astronomical timescale, *Paleoceanography*, *11*, 391-413.
- Lourens, L. J. and F. J. Hilgen (1997), Long-periodic variations in the Earth's obliquity and their relation to third-order eustatic cycles and Late Neogene glaciations, *Quat. Intern.*, *40*, 43-52.
- Lourens, L. J., F. J. Hilgen and I. Raffi (1998), Base of large Gephyrocapsa and astronomical calibration of Early Pleistocene sapropels in site 967 and hole 969D: solving the chronology of the Vrica section (Calabria, Italy), *Proceedings of the Ocean Drilling Program, Scientific Results*, *160*, 191-197.
- Lourens, L. J., R. Wehausen and H. J. Brumsack (2001), Geological constraints on tidal dissipation and dynamical ellipticity of the Earth over the past three million years, *Nature*, *409*, 1029-1032.
- Lourens, L. J., F. J. Hilgen, N. J. Shackleton, J. Laskar and D. Wilson (2004), The Neogene Period, in *A Geological Timescale 2004*, edited by F. Gradstein, I. Ogg and A. Smith, Cambridge Univ. Press, UK.
- Lutze, G. F. and W. T. Colbourn (1984), Recent benthic foraminifera from the continental margin of Northwest Africa: community structure and distribution, *Mar. Micropaleontol.*, *8*, 361-401.
- MacAyeal, D. R. (1993), Binge/purge oscillations of the Laurentide ice sheet as a cause of the North Atlantic's Heinrich events, *Paleoceanography*, *8*, 775-784.
- Mackensen, A., H. P. Sejrup and E. Jansen (1985), The distribution of benthic foraminifera on the continental slope and rise off Norway, *Mar. Micropaleontol.*, *9*, 275-306.
- Mackensen, A., D. K. Füttere, H. Grobe and G. Schmiedl (1993), Benthic foraminiferal assemblages from the eastern South Atlantic Polar Front region between 35 and 57°S: Distribution, ecology and fossilization potential, *Mar. Micropaleontol.*, *22*, 33-69.
- Mackensen, A., G. Schmiedl, J. Harloff and M. Giese (1995), Deep-sea foraminifera in the South Atlantic Ocean: Ecology and assemblage generation, *Micropaleontology*, *41*, 342-358.
- Marchitto, T. M., W. B. Curry and D. W. Oppo (1998), Millennial-scale changes in North Atlantic circulation since the last glaciation, *Nature*, *393*, 557-561.
- Martinson, D. G., N. G. Pisias, J. D. Hays, J. Imbrie, T. C. Moore and N. J. Shackleton (1987), Age dating and the orbital theory of the Ice Ages: development of a high-resolution 0 to 300,000-year chronostratigraphy, *Quat. Res.*, *27*, 1-29.
- McCave, I. N., B. Manighetti and S. G. Robinson (1995), Sortable silt and fine sediment size/composition slicing: Parameters for palaeocurrent speed and palaeoceanography, *Paleoceanography*, *10*, 593-610.
- McIntyre, A. and B. Molino (1996), Forcing of Atlantic Equatorial and Subpolar Millennial Cycles by Precession, *Science*, *274*, 1867-1870.
- McIntyre, K., M. Delaney, L. and A. C. Ravelo (2001), Millennial-scale climate change and oceanic processes in the late Pliocene and early Pleistocene, *Paleoceanography*, *16*, 535-543.
- Meggers, H. and K.-H. Baumann (1997), Contributions to the Micropaleontology and Paleoceanography of the Northern North Atlantic, in *Grzybowski Foundation Special Publication*, edited by H. C. Hass and M. A. Kaminski, pp. 39-50.
- Miao, Q. and R. C. Thunell (1996), Late Pleistocene-Holocene distribution of deep-sea benthic foraminifera in the South China Sea and Sulu Sea: paleoceanographic implications, *J. Foram. Res.*, *26*, 9-23.

R E F E R E N C E S

- Milankovitch, M. (1941), Kanon der Erdbestrahlung und seine Anwendung auf das Eiszeitenproblem, *Royal Serb. Acad. Spec. Publ.*, *133*, 1-633.
- Moreno, A., J. Targarona, J. Henderiks, M. Canals, T. Freudenthal and H. Meggers (2001), Orbital forcing of dust supply to the North Canary Basin over the last 250 kyr, *Quat. Sci. Rev.*, *20*, 1327-1339.
- Moreno, A., I. Cacho, M. Canals, M. A. Prins, M. F. Sanchez-Goni, J. O. Grimalt and G.-J. Weltje (2002), Saharan dust transport and high-latitude glacial climate variability: the Alboran Sea record, *Quat. Res.*, *58*, 318-328.
- Moreno, A., I. Cacho, M. Canals, J. O. Grimalt and A. Sanchez-Vidal (2004), Millennial-scale variability in the productivity signal from the Alboran Sea record, Western Mediterranean Sea, *Palaeogeog., Palaeoclimatol., Palaeoecol.*, *211*, 205-219.
- Morse, J. W. and F. T. MacKenzie (1990), *Geochem. of Sed. Carbonates*, 707 pp., Elsevier, Amsterdam.
- Muller, R. A. and G. J. MacDonald (1995), Glacial cycles and orbital inclination, *Nature*, *377*, 107-108.
- Murray, J. W. (1991), *Ecology and Palaeoecology of Benthic Foraminifera*, 397 pp., Longman Scientific & Technical.
- Naish, T. (1997), Constraints on the amplitude of late Pliocene eustatic sea-level fluctuations: New evidence from the New Zealand shallow-marine sediment record, *Geology*, *25*, 1139-1142.
- Negri, A., L. Capotondi and J. Keller (1999), Calcareous nannofossils, planktonic foraminifera and oxygen isotopes in the late Quaternary sapropels of the Ionian Sea, *Mar. Geol.*, *157*, 89-103.
- Nijenhuis, I. A. (1999), Geochemistry of eastern Mediterranean sedimentary cycles, *Geologica Ultraiectina*, *167*, 168.
- Nijenhuis, I. A., J. Becker and G. J. de Lange (2001), Geochemistry of coeval marine sediments in Mediterranean ODP cores and a land section: implications for sapropel formation models, *Palaeogeog., Palaeoclimatol., Palaeoecol.*, *165*, 97-112.
- Nozaki and et al. (1997).
- O'Neil, J. R., R. N. Clayton and T. K. Mayeda (1969), Oxygen isotope fractionation in divalent metal carbonates, *J. Chem. Phys.*, *52*, 5547-5558.
- Oerlemans, J. and C. J. van der Veen (1984), *Ice Sheets and Climate*, 217 pp., Kluwer Academic, Hingham, Mass.
- Ortiz, J., A. Mix, S. Harris and S. O'Connell (1999), Diffuse spectral reflectance as a proxy for percent carbonate content in the North Atlantic sediments, *Palaeoceanography*, *14*, 171-186.
- Ottens, J. J. (1991), Planktic foraminifera as North Atlantic water mass indicators, *Oceanol. Acta*, *14*, 123-140.
- Otterman, J., J. K. Angell, J. Ardizzone, R. Atlas, S. Schubert and D. Starr (2002), North-Atlantic surface winds examined as the source of winter warming in Europe, *Geophys. Res. Lett.*, *29*, 18.
- Paillard, D., L. Labeyrie and P. Yiou (1996), Macintosh Program Performs Time-Series Analysis, *Eos Trans. AGU*, *77*, 379.
- Paterne, M., N. Kallel, L. Labeyrie, M. Vautravers, J.-C. Duplessy, M. Rossignol-Strick, E. Cortijo, M. Arnold and M. Fontugne (1999), Hydrological relationship between the North Atlantic Ocean and the Mediterranean Sea during the past 15-75 kyr, *Paleoceanography*, *14*, 626-638.
- Perry, C. A. and K. J. Hsu (2000), Geophysical, archaeological, and historical evidence support a solar-output model for climate change, *PNAS*, *97*, 12433-12438.

R E F E R E N C E S

- Pestiaux, P., I. v. d. Mersch, A. Berger and J. C. Duplessy (1988), Paleoclimatic variability at frequencies ranging from 1 cycle per 10,000 years to 1 cycle per 1000 years: evidence for nonlinear behaviour of the climate system, *Clim. change*, *12*, 9-37.
- Peterson, L. C., G. H. Haug, K. A. Hughen and U. Röhl (2000), Rapid changes in the hydrologic cycle of the tropical Atlantic during the last glacial, *Science*, *290*, 1947-1951.
- Pinardi, N. and E. Masetti (2000), Variability of the large scale general circulation of the Mediterranean Sea from observations and modelling: a review, *Palaeogeog., Palaeoclimatol., Palaeoecol.*, *158*, 153-173.
- Pisias, N. G. and D. K. Rea (1988), Late Pleistocene paleoclimatology of the central equatorial pacific: Sea surface response to the southeast trade winds, *Paleoceanography*, *3*, 21-37.
- Pokras, E. M. and A. C. Mix (1987), Earth's precession cycle and Quaternary climatic change in tropical Africa, *Nature*, *326*, 486-487.
- Poore, R. Z. and W. A. Berggren (1975), The morphology and classification of *Neogloboquadrina atlantica* (Berggren), *J. Foram. Res.*, *5*, 692-694.
- Prospero, J. M. (1996), Saharan dust transport over the North Atlantic Ocean and Mediterranean, in *The impact of desert dust across the Mediterranean*, edited by S. Guerzoni and C. Roy, pp. 133-152, Kluwer, Dordrecht.
- Qvale, G. (1986), Distribution of benthic foraminifera in surface sediments along the Norwegian continental slope shelf between 62 and 72°N, *Nor. Geol. Tidsskr.*, *66*, 209-221.
- Rathburn, A. E. and B. H. Corliss (1994), The ecology of living (stained) benthic foraminifera from the Sulu Sea, *Paleoceanography*, *9*, 87-150.
- Raymo, M. E., W. F. Ruddiman and B. M. Clement (1986), Pliocene-Pleistocene Paleoceanography of the North Atlantic at Deep Sea Drilling Project Site 609, in *Init. Repts. DSDP*, edited by W. F. Ruddiman, R. B. Kidd, E. Thomas and e. al., pp. 895-901, U.S. Govt. Printing Office, Washington.
- Raymo, M. E., W. F. Ruddiman, J. Backman, B. M. Clement and D. G. Martinson (1989), Late Pliocene variation in Northern Hemisphere ice sheets and North Atlantic deep water circulation, *Paleoceanography*, *4*, 413-446.
- Raymo, M. E. (1992), Global climate change: a three million year perspective, in *Start of a Glacial, Proceedings of the Mallorca NATO ARW*, edited by G. Kukla and E. Went, pp. 207-223, Springer-Verlag, Heidelberg.
- Raymo, M. E., D. Hodell and E. Jansen (1992), Response of deep ocean circulation to initiation of Northern Hemisphere glaciation (3-2 Ma), *Paleoceanography*, *7*, 645-672.
- Raymo, M. E., K. Ganley, S. Carter, D. W. Oppo and J. McManus (1998), Millennial-scale climate instability during the early Pleistocene epoch, *Nature*, *392*, 699-702.
- Raymo, M. E. and K. Nisancioglu (2003), The 41 kyr world: Milankovitch's other unsolved mystery, *Paleoceanography*, *18*, 1011.
- Raymo, M. E., D. W. Oppo, B. P. Flower, D. A. Hodell, J. F. McManus, K. A. Venz, H. F. Kleiven and K. McIntyre (2004), Stability of North Atlantic water masses in face of pronounced climate variability during the Pleistocene, *Paleoceanography*, *19*, PA2008.
- Rial, J. A. (1999), Pacemaking of the Ice Ages by Frequency Modulation of Earth's Orbital Eccentricity, *Science*, *285*, 564-571.
- Rial, J. A. and C. A. Anaclerio (2000), Understanding nonlinear responses of the climate system to orbital forcing, *Quat. Sci. Rev.*, *19*, 1709-1722.

R E F E R E N C E S

- Rio, D., R. Sprovieri and E. Di Stefano (1994), The Gelasian Stage: a proposal of a new chronostratigraphic unit of the Pliocene Series, *Riv. It. Paleont. Strat.*, *100*, 103-124.
- Roberts, D. G. and et al. (1987), Time series analysis with CLEAN. I. Derivation of a spectrum, *The astronomical journal*, *93*, 968-989.
- Robinson, S. G., M. A. Maslin and N. McCave (1995), Magnetic susceptibility variations in Upper Pleistocene deep-sea sediments of the NE Atlantic: Implications for ice rafting and paleocirculation at the last glacial maximum, *Paleoceanography*, *10*, 221-250.
- Rohling, E. J. and W. W. C. Gieskes (1989), Late Quaternary changes in Mediterranean Intermediate Water density and formation rate, *Paleoceanography*, *5*, 531-545.
- Rohling, E. J. and F. J. Hilgen (1991), The eastern Mediterranean climate at times of sapropel formation: a review, *Geologie en Mijnbouw*, *70*, 252-264.
- Rohling, E. J., F. J. Jorissen, C. Vergnaud-Grazzini and W. J. Zachariasse (1993), Northern Levantine and Adriatic Quaternary planktic foraminifera: Reconstruction of paleoenvironmental gradients, *Mar. Micropaleontol.*, *21*, 191-218.
- Rohling, E. J., A. Hayes, S. De Rijk, D. Kroon, W. J. Zachariasse and D. Eisma (1998), Abrupt cold spells in the northwest Mediterranean, *Paleoceanography*, *13*, 316-322.
- Rohling, E. J., R. Sprovieri, T. Cane, J. S. L. Casford, S. Cooke, I. Bouloubassi, K.-C. Emeis, R. Schiebel, M. Rogerson, A. Hayes, F. J. Jorissen and D. Kroon (2004), Reconstructing past planktic foraminiferal habitats using stable isotope data: a case history for Mediterranean sapropel S5, *Mar. Micropaleontol.*, *50*, 89-123.
- Rossignol-Strick, M., W. Nesteroff, P. Olive and C. Vergnaud-Grazzini (1982), After the deluge: Mediterranean stagnation and sapropel formation, *Nature*, *295*, 105-110.
- Rossignol-Strick, M. (1983), African monsoons, an immediate climate response to orbital insolation, *Nature*, *304*, 46-49.
- Rossignol-Strick, M. (1985), Mediterranean Quaternary sapropels, an immediate response of the African monsoon to variation of insolation, *Palaeogeog., Palaeoclimatol., Palaeoecol.*, *49*, 237-263.
- Ruddiman, W. F., A. McIntyre and M. Raymo (1986a), Matuyama 41,000-year cycles: North Atlantic Ocean and northern hemisphere ice sheets, *Earth Planet. Sci. Lett.*, *80*, 117-129.
- Ruddiman, W. F., A. McIntyre and M. Raymo (1986b), Paleoenvironmental results from North Atlantic sites 607 and 609, in *Initial Report Deep Sea Drilling Project*, edited by W. F. Ruddiman, R. Kidd and e. al., pp. 855-878, U.S. Gov. Print. Off., Washington D.C.
- Ruddiman, W. F., M. E. Raymo, D. G. Martinson, B. M. Clement and J. Backman (1989), Pleistocene evolution of Northern Hemisphere climate, *Paleoceanography*, *4*, 353-412.
- Sakai, K. and W. R. Peltier (1997), Dansgaard-Oeschger oscillations in a coupled atmosphere-ocean climate model, *J. Clim.*, *10*, 949-970.
- Sakamoto, T., T. Janecek and K.-C. Emeis (1998), Continuous sedimentary sequences from the eastern Mediterranean Sea: composite depth sections, in *Proceedings of the Ocean Drilling Program, Scientific Results*, edited by A. H. F. Robertson, K.-C. Emeis, C. Richter and A. Camerlenghi, pp. 37-51, ODP, College Station, Texas.
- Saltzman, B. and A. Sutera (1984), A model of the internal feedback system involved in late Quaternary climatic variations, *J. Atmosphere. Sci.*, *41*, 736-745.



R E F E R E N C E S

- Sanchez-Goni, M. F., I. Cacho, J. L. Turon, J. Guiot, F. J. Sierro, J.-P. Peypouquet, J. O. Grimalt and N. J. Shackleton (2002), Synchronicity between marine and terrestrial responses to millennial scale climatic variability during the last glacial period in the Mediterranean region, *Clim. Dyn.*, *19*, 95-105.
- Sarnthein, M. and A. V. Altenbach (1995), Late Quaternary changes in surface and deep water masses of the Nordic Seas and north-eastern North Atlantic: a review, *Geologische Rundschau*, *84*, 89-107.
- Sarnthein, M., E. Jansen, M. Weinelt, M. Arnold, J. C. Duplessy, H. Erlenkeuser, A. Flatoy, G. Johannessen, T. Johannessen, S. Jung, N. Koc, L. Labeyrie, M. A. Maslin, U. Pflaumann and H. Schulz (1995), Variations in Atlantic surface ocean paleoceanography, 50°-80°N: A time-slice record of the last 30,000 years, *Paleoceanography*, *10*, 1063-1094.
- Schiebel, R., J. Waniek, M. Bork and C. Hemleben (2001), Planktic foraminiferal production stimulated by chlorophyll redistribution and entrainment of nutrients, *Deep-Sea Research I*, *48*, 721-740.
- Schmidt, G. A. and S. Mulitza (2002), Global calibration of ecological models for planktic foraminifera from coretop carbonate oxygen-18, *Mar. Micropaleontol.*, *44*, 125-140.
- Schmiedl, G., A. Mackensen and P. J. Müller (1997), Recent benthic foraminifera from the eastern South Atlantic Ocean: dependence on food supply and water masses, *Mar. Micropaleontol.*, *32*, 249-287.
- Schmiedl, G., A. Mitsuhele, S. Bec, K.-C. Emeis, C. Hemleben, H. Schulz, M. Sperling and S. Weldeab (2003), Benthic foraminiferal record of ecosystem variability in the eastern Mediterranean Sea during times of sapropel S5 and S6 deposition, *Palaeogeog., Palaeoclimatol., Palaeoecol.*, *190*, 139-164.
- Schmittner, A. and A. C. Clement (2002), Sensitivity of the thermohaline circulation to tropical and high latitude freshwater forcing during the last glacial-interglacial cycle, *Paleoceanography*, *17*, 1017.
- Schmitz and McCartney (1993), On the North Atlantic circulation, *Rev. Geophys.*, *31*, 29-49.
- Schulz, M. and M. Mudelsee (2002), REDFIT: estimating red-noise spectra directly from unevenly spaced paleoclimatic time series, *Computer and Geosciences*, *28*, 421-426.
- Seidenkrantz, M.-S., T. J. Kouwenhoven, F. J. Jorissen, N. J. Shackleton and G. J. Van der Zwaan (2000), Benthic foraminifers as indicators of changing Mediterranean-Atlantic water exchange in the late Miocene, *Mar. Geol.*, *163*, 387-407.
- Seidov, D. and M. A. Maslin (1999), North Atlantic deep water circulation collapse during Heinrich events, *Geology*, *27*, 23-26.
- Shackleton, N. J. (1967), Oxygen isotope analyses and Pleistocene temperatures reassessed, *Nature*, *215*, 15-17.
- Shackleton, N. J. (1974), Attainment of isotopic equilibrium between ocean water and the benthonic foraminifera genus *Uvigerina*: isotopic changes in the ocean during the last glacial., *Les Meth. Quant. d'étude Var. Clim. au Cour du Pleist., Coll. Int. C.N.R.S.*, *219*, 203-209.
- Shackleton, N. J. and N. D. Opdyke (1976), Oxygen isotope and paleomagnetic stratigraphy of Pacific core V28-238 Late Pliocene to Latest Pleistocene, *GSA Memoir*, *145*, 449-464.
- Shackleton, N. J., J. Backman, H. Zimmerman, D. V. Kent, M. A. Hall, D. G. Roberts, D. Schitker and J. Baldauf (1984), Oxygen isotope calibration of the onset of ice-rafting and history of glaciation in the North Atlantic region, *Nature*, *307*, 620-623.
- Shackleton, N. J. and M. A. Hall (1984), Oxygen and carbon isotope stratigraphy of Deep Sea Drilling Project Hole 552A: Plio-Pleistocene glacial history, in *Init. Repts. DSDP*, edited by D. G. Roberts, D. Schnitker and others, pp. 599-609, U.S. Govt. Printing Office, Washington.

## REFERENCES

- Shackleton, N. J., A. Berger and W. R. Peltier (1990), An alternative astronomical calibration of the lower Pleistocene timescale based on ODP Site 677, *Transactions of the Royal Society of Edinburgh: Earth Sciences*, *81*, 251-261.
- Shackleton, N. J., M. A. Hall and D. Pate (1995), Pliocene stable isotope stratigraphy of ODP Site 846, *Proc. Ocean Drill. Prog., Sci. Results*, *138*, 337-355.
- Shackleton, N. J. (2000), The 100,000-year Ice-age cycle identified and found to lag temperature, carbon dioxide, and orbital eccentricity, *Science*, *289*, 1897-1902.
- Shimmield, G. B. (1992), Can sediment geochemistry record changes in coastal upwelling palaeoproductivity? Evidence from northwest Africa and the Arabian Sea, in *Upwelling systems: Evolution since the Early Miocene*, edited by C. P. Summerhayes, W. L. Prell and K.-C. Emeis, pp. 29-64, Geol. Soc. Spec. Publ.
- Short, D. A. and J. G. Mengel (1986), Tropical climatic phase lags and Earth's precession cycle, *Nature*, *323*, 48-50.
- Short, D. A., J. G. Mengel, T. J. Crowley, W. T. Hyde and G. R. North (1991), Filtering of Milankovitch cycles by Earth's geography, *Quat. Res.*, *35*, 157-173.
- Siddall, M. (2005), The riddle of the sediments, *Nature*, *437*, 39-41.
- Spaak, P. (1983), Accuracy in correlation and ecological aspects of the planktonic foraminiferal zonation of the Mediterranean Pliocene, *Utrecht Micropaleontol. Bull.*, *28*, 160.
- Sprovieri, R., R. Thunell and M. Howell (1986), Paleontological and geochemical analysis of three laminated sedimentary units of Late Pliocene-Early Pleistocene age from the Monte San Nicola section in Sicily, *Riv. It. Paleont. Strat.*, *92*, 401-434.
- Sprovieri, R. and S. Hasegawa (1990), Plio-Pleistocene benthic foraminifer stratigraphic distribution in the deep-sea record of the Tyrrhenian Sea (OPD Leg 107), in *Proceedings of the Ocean Drilling Program, Scientific Results*, edited by K. A. Kastens, J. Mosle and et al., pp. 529-459, Ocean Drilling Program, College Station, TX.
- Sprovieri, R. (1993), Pliocene-Early Pleistocene astronomically forced planktonic foraminifera abundance fluctuations and chronology of Mediterranean calcareous plankton bio-events., *Riv. It. Paleont. Strat.*, *99*, 371-414.
- Steenbrink, J., M. L. Kloosterboer van Hoeve and F. J. Hilgen (2003), Millennial-scale climate variations recorded in early Pliocene colour reflectance time series from the lacustrine Ptolemais Basin (NW Greece), *Global and Planetary Change*, *36*, 47-75.
- Stott, L., C. Poulsen, S. Lund and R. Thunell (2002), Super ENSO and global climate oscillations at millennial time scales, *Science*, *297*, 2345-2348.
- Suess, E. (1980), Particulate organic carbon flux in the oceans - surface productivity and oxygen utilization, *Nature*, *288*, 260-263.
- Thunell, R. and D. F. Williams (1989), Glacial-Holocene salinity changes in the Mediterranean Sea: Hydrographic and depositional effects, *Nature*, *338*, 493-496.
- Tiedemann, R. (1991), Acht Millionen Jahre Klimageschichte von Nordwest Afrika und Paläozeanographie des angrenzenden Atlantiks: Hochoflösende Zeitreihen von ODP Sites 658-661, Ber. 46, 190 pp, Universität Kiel, Germany, Kiel.
- Torrence, C. and G. P. Compo (1998), A practical guide to wavelet analysis, *Bull. of the Am. Meteorol. Soc.*, *79*, 61-78.

R E F E R E N C E S

- Tuenter, E., S. L. Weber, F. J. Hilgen and L. J. Lourens (2003a), The response of the African summer monsoon to remote and local forcing due to precession and obliquity, *Global and Planet. Change*, *36*, 219-235.
- Tuenter, E., S. L. Weber, F. J. Hilgen, L. J. Lourens and A. Ganopolski (2003b), Simulation of climate phase lags in response to precession and obliquity forcing, *Clim. Dyn.*, *submitted*.
- Tuenter, E. (2004), Modeling orbital induced variations in circum-Mediterranean climate, 144 pp, Utrecht University, Utrecht.
- Tuenter, E., S. L. Weber, F. J. Hilgen, L. J. Lourens and A. Ganopolski (2005), Simulation of climate phase lags in the response to precession and obliquity forcing and the role of vegetation, *Clim. Dyn.*, *24*, 279-295.
- Van Geel, B., O. M. Raspopov, H. Renssen, J. van der Plicht, V. A. Dergachev and H. A. J. Meijer (1999), The role of solar forcing upon climate change, *Quat. Sci. Rev.*, *18*, 331-338.
- Van Krevelend, S. and e. al. (2000), Potential links between surging ice sheets, circulation changes, and the Dansgaard-Oeschger cycles in the Irminger Sea, 60-18 kyr, *Paleoceanography*, *15*, 425-442.
- Van Os, B. J. H., L. J. Lourens, L. Beaufort, F. J. Hilgen and G. J. de Lange (1994), The formation of Pliocene sapropels and carbonate cycles in the Mediterranean: diagenesis, dilution and productivity, *Paleoceanography*, *9*, 601-617.
- van Santvoort, P. J. M., G. J. de Lange, J. Thomson, H. Cussen and T. R. S. Wilson (1996), Active post-depositional oxidation of the most recent sapropel (S1) in sediments of the eastern Mediterranean Sea, *Geochim. and Cosmochim. Acta*, *21*, 4007-4024.
- Venkatarathnam, K. and B. F. Ryan (1971), Dispersal patterns of clay minerals in the sediments of the eastern Mediterranean Sea, *Mar. Geol.*, *11*, 261-282.
- Vergnaud-Grazzini, C., W. B. F. Ryan and M. B. Cita (1977), Stable isotope fractionation, climatic change and episodic stagnation in the eastern Mediterranean during the late Quaternary., *Mar. Micropaleont.*, *2*, 353-370.
- Verhallen, P. J. J. M. (1987), Early development of *Bulimina marginata* in relation to paleo-environmental changes in the Mediterranean Pliocene, *Kon. Ned. Akad. Wet., B*, 161-180.
- Verhallen, P. J. J. M. (1991), Late Pliocene to early Pleistocene Mediterranean mud-dwelling foraminifera: influence of a changing environment on community structure and evolution, *Utrecht Micropaleontol. Bull.*, *40*, 220pp.
- Versteegh, G. J. M. (1997), The onset of major Northern Hemisphere glaciations and their impact on dinoflagellate cysts and acritarchs from the Singa section, Calabria (southern Italy) and DSDP Holes 607/607A (North Atlantic), *Mar. Micropaleontol.*, *30*, 319-343.
- Voelker, A., workshop and participants (2002), Global distribution of centennial-scale records during Marine Isotope Stage (MIS) 3: a database, *Quat. Sci. Rev.*, *21*, 1185-1212.
- von Breyman, M. T., K.-C. Emeis and E. Suess (1992), Water depth and diagenetic constraints on the use of barium as a palaeoproductivity indicator, in *Upwelling systems: Evolution since the Early Miocene*, edited by C. P. Summerhayes, W. L. Prell and K.-C. Emeis, pp. 273-284, Geol. Soc. Spec. Publ.
- von Dobeneck, T. and F. Schmieder (1999), Using rock magnetic proxy records for orbital tuning and extended time series analyses into the super- and sub-Milankovitch bands, in *Use of proxies in paleoceanography: examples from the South Atlantic*, edited by W. Fischer and G. Wefer, pp. 601-633, Springer, Berlin Heidelberg.

R E F E R E N C E S

- Wara, M. W., A. C. Ravelo and J. S. Revenaugh (2000), The pacemaker always rings twice, *Paleoceanography*, *15*, 616-624.
- Wedepohl, K. H. (1995), The composition of the continental crust, *Geochimica et Cosmochimica Acta*, *59*, 1217-1232.
- Wehausen, R. (1999), Anorganische Geochemie zyklischer Sedimente aus dem östlichen Mittelmeer: Rekonstruktion der Paläoumweltbedingungen, Dissertation thesis, 162 pp, Carl-von-Ossietzky-Universität, Oldenburg.
- Wehausen, R. and H.-H. Brumsack (1999), Cyclic variations in the chemical composition of eastern Mediterranean Pliocene sediments: a key for understanding sapropel formation, *Mar. Geol.*, *153*, 161-176.
- Wehausen, R. and H. J. Brumsack (2000), Chemical cycles in Pliocene sapropel-bearing and sapropel-barren eastern Mediterranean sediments, *Palaeogeog., Palaeoclimatol., Palaeoecol.*, *158*, 325-352.
- Willis, K. J., A. Kleckowski and S. J. Crowhurst (1999a), 124,000-year periodicity in terrestrial vegetation change during the late Pliocene epoch, *Nature*, *397*, 685-688.
- Willis, K. J., A. Kleckowski, K. M. Briggs and C. A. Gilligan (1999b), The Role of sub-Milankovitch Climatic Forcing in the Initiation of the Northern Hemisphere Glaciation, *Science*, *285*, 568-571.
- Yaalon, D. H. and E. Ganor (1979), East Mediterranean trajectories of dust-carrying storms from the Sahara and Sinai, in *Saharan Dust*, edited by C. Morales, pp. 187-193, Wiley & Sons, New York.
- Yiou, P., M. Ghil, J. Jouzel, D. Paillard and R. R. Vautard (1994), Nonlinear variability of the climatic system from singular and power spectra of Late Quaternary records, *Clim. Dyn.*, *9*, 371-389.
- Zachariasse, W. J., L. Gudjonsson, F. J. Hilgen, L. J. Lourens, P. J. J. M. Verhallen, C. G. Langereis and J. D. A. Zijderveld (1990), Late Gauss to early Matuyama invasions of *Neogloboquadrina atlantica* in the Mediterranean and associated record of climatic change, *Paleoceanography*, *5*, 239-252.
- Zijderveld, J. D. A., F. J. Hilgen, C. G. Langereis, P. J. J. M. Verhallen and W. J. Zachariasse (1991), Integrated magnetostratigraphy and biostratigraphy of the upper Pliocene-lower Pleistocene from the Monte Singa and Crotona areas Calabria (Italy), *Earth Planet. Sci. Lett.*, *107*, 697-714.

## Samenvatting

### De Milankovitchtheorie van de ijstijden

De Milankovitchtheorie van de ijstijden houdt in dat astronomische veranderingen in de baan van de Aarde en de stand van de aardas verantwoordelijk zijn voor de ijstijden doordat ze het klimaat beïnvloeden door veranderingen in de seizoensale en latitudinale verdeling van de instraling van de Zon: deze theorie is nu algemeen geaccepteerd door de wetenschappelijke gemeenschap. Het was *Adh mar* [1842] die als eerste suggereerde dat de ijstijden astronomisch gestuurd zijn, dus slechts 5 jaar nadat *Agassiz* zijn theorie van de ijstijden had gepresenteerd in [1837]. In [1864] werkte *Croll* de oorspronkelijke theorie uit en stelde de relatie op tussen de astronomische parameters en de ijstijden. Met behulp van de formules van de Franse astronoom *Le Verrier* berekende hij de reeksen voor de veranderingen in de excentriciteit<sup>10</sup> en precessie<sup>11</sup> en suggereerde dat koude winters van doorslaggevend belang zijn voor het ontstaan van een ijstijd. Maar hij merkte ook op dat de astronomisch gestuurde veranderingen in de instraling te klein zijn om de ijstijden alleen te veroorzaken en suggereerde dat een intern mechanisme van versterking van het oorspronkelijke signaal binnen het klimaatsysteem nodig is als positieve terugkoppeling. *Milankovitch* [1941] werkte de astronomische theorie van de ijstijden verder uit en berekende de instraling van de zon zoals die op de top van de atmosfeer op verschillende breedtegraden ontvangen wordt waarbij hij rekening hield met de veranderingen in precessie, obliquiteit<sup>12</sup> en excentriciteit. In tegenstelling tot *Croll*, die aannam dat winterinstraling doorslaggevend is, stelde hij dat de zomerinstraling op 65° noorderbreedte verantwoordelijk is voor het optreden van een ijstijd en voorspelde dat de ijstijden gedomineerd zouden worden door de 41.000 jaar cyclus van de obliquiteit.

Met de opkomst van de magnetostratigrafie, en de analyse van radioactieve en stabiele isotopen, kreeg de Milankovitchtheorie de wind in de rug. Nieuwe boortechnieken resulteerden in het naar boven halen van lange en continue sedimentkernen uit de diepzee. De echte doorbraak in de acceptatie van de Milankovitchtheorie kwam met de ontdekking dat pieken in de spectra van (proxy) reeksen voor ijsvolume ( $\delta^{18}\text{O}$ ) precies overeenkwamen met de door Milankovitch voorspelde periodes. Dit werd algemeen gezien als een duidelijk bewijs voor de samenhang tussen de ijstijden en de

<sup>10</sup> Excentriciteit is een maat voor de uitrekking van de aardbaan en varieert tussen nul (een cirkelvormige aardbaan) en 0.06 (enigszins elliptisch) met als voornaamste periodes die van 400.000 en 100.000 jaar.

<sup>11</sup> Astronomische precessie is de langzame beweging van de aardas rond een cirkelvormig pad met  en omwenteling in de 26.000 jaar. Door de tegengestelde beweging van de excentrische aardbaan zelf, heeft de precessie van de equinoxen, die ook wel de klimatologische precessie wordt genoemd, een kortere periode van ongeveer 21.000 jaar. De sterkte of amplitude van deze klimatologische precessie wordt bepaald door de excentriciteit.

<sup>12</sup> De obliquiteit beschrijft de hoek tussen de aardas en het baanvlak van de Aarde en varieert tussen de 22° en 25° met een belangrijkste periode van 41.000 jaar.

astronomische baanparameters van de Aarde [Hays, *et al.*, 1976]. Ook de uitkomsten van een eenvoudig model voor ijsvolume lieten zien dat er een duidelijk verband bestaat met precessie en obliquiteit. Daarmee werd bevestigd dat glaciaal-interglaciaal afwisselingen veroorzaakt worden door veranderingen in de baanparameters van de Aarde en de stand van de aardas, dus met een orbitaal-forcing, met vaste ‘leads’ en ‘lags’ [Imbrie and Imbrie, 1980; Imbrie, *et al.*, 1984]. Dit inzicht leidde tot het opstellen van een astronomisch gedateerde tijdschaal (SPECMAP) voor de laatste ~800 kyr. Deze tijdschaal is sindsdien gebruikt als een mal voor het dateren van diepzee-afzettingen van laat Pleistocene ouderdom [Imbrie, *et al.*, 1984].

In tegenstelling met de voorspelling van *Milankovitch* werden de  $\delta^{18}\text{O}$  reeksen van het laat Pleistoceen echter gedomineerd door een ijstijdcyclus met een periode van 100.000 jaar; deze periode suggereert een verband tussen globale klimaatveranderingen en excentriciteit. Het is algemeen geaccepteerd dat de verandering in de totale hoeveelheid instraling die jaarlijks door de Aarde ontvangen wordt en met excentriciteit samenhangt te klein is om klimaatveranderingen op de schaal van de ijstijden te veroorzaken. Het is daarom waarschijnlijker dat de sterke 100.000 jaar cyclus in het  $\delta^{18}\text{O}$  spectrum samenhangt met een niet-lineaire overdracht van energie vanuit het precessie bereik [Imbrie, *et al.*, 1984; Hagelberg, *et al.*, 1991]. Alternatieve modellen suggereren dat de glaciaal-interglaciaal afwisselingen een gevolg zijn van niet-lineaire interne wisselwerkingen binnen een in hoge mate complex systeem [Saltzman and Sutter, 1984] en dat ijsvolume veranderingen veeleer worden gemoduleerd dan bepaald door de veranderingen in de baanparameters. Tenslotte hebben Muller and McDonald [1997] voorgesteld dat de 100.000 jaar cyclus samenhangt met veranderingen in de hellingshoek van het Aardse baanvlak in plaats van met veranderingen in de excentriciteit van de aardbaan [see also Raymo, 1997; Ridgwell, *et al.*, 1999]. Duidelijk is echter dat de quasi-periodieke fluctuaties binnen de verschillende componenten van het klimaatsysteem, zoals veranderingen in atmosferische kooldioxideconcentraties, in de circulatie van de oceanen en in de temperatuur van het oppervlakte- en diepe water een vaste faserelatie vertonen met de veranderingen in instraling die het gevolg zijn van de 100.000 jaar cyclus .

In tegenstelling tot de laatste 800.000 jaar van het Laat Pleistoceen worden de klimaatreeksen van het Laat Pliocene en Vroeg Pleistoceen veelal gedomineerd door een 41.000 jarige cyclus en het is nu algemeen geaccepteerd dat de ijstijden van 3 tot 1 miljoen jaar geleden vooral bepaald werden door de cyclus van de obliquiteit [Shackleton, *et al.*, 1984; Ruddiman, *et al.*, 1986; Raymo, *et al.*, 1989], in overeenstemming met de oorspronkelijke voorspellingen van *Milankovitch*. Men moet zich echter wel realiseren dat de instralingsreeksen van *Milankovitch* berekend werden voor het calorisch halfjaar; dit versterkt het signaal van de obliquiteit ten opzichte van het signaal in de instraling voor de zomerpiek (21 juni – juni/juli) in de instralingsreeksen [Berger, *et al.*, 1999; Raymo and Nisancioglu, 2003].

### Sapropelen in de Middellandse Zee

Hoewel de Milankovitchtheorie vooral van toepassing is op de ijstijden, en de daarmee samenhangende veranderingen in het klimaat op middenbare en hoge breedtegraden, werd overtuigend aangetoond dat de verstoringen in de aardbaan en de aardas ook een sterke invloed uitoefenen op het klimaat op lage breedten. De instraling op lage breedten wordt echter gedomineerd door precessie terwijl die op hoge breedten door de obliquiteit gedomineerd wordt. Klimaatssystemen op lage breedtegraden zoals bijvoorbeeld de moesson worden gestuurd door de seizoensale verdeling van de binnenkomende instraling op lage breedtegradenname tijdens de zomer.

Een klassiek voorbeeld van klimaatveranderingen die door precessie gestuurd worden is vastgelegd in het (sediment)archief van sapropelen in de Middellandse Zee [Hilgen, 1991]. Het regelmatige en cyclische voorkomen van deze sapropelen (donkere, organisch-rijke lagen) wordt in verband gebracht met veranderingen in de uitstroom van rivieren en de vochtigheid van het klimaat rondom de Middellandse Zee [Rohling and Hilgen, 1991], die het gevolg zijn van een intensivering van de circulatie van de Afrikaanse moesson ten tijde van precessieminima wanneer de noordelijke zomer in perihelion valt [Rossignol-Strick, 1983; 1985]. Gegevens van microfossielen, pollen en stabiele isotopen laten zien dat de voornaamste klimaatveranderingen in het precessiebereik van warm-nat naar koud-droog gaan en terug [Cita, et al., 1977; Vergnaud-Grazzini, et al., 1977; Rossignol-Strick, 1983; 1997; Kallel, et al., 2000]. Desondanks is het precieze mechanisme achter het ontstaan van de sapropelen in de Middellandse Zee niet volledig bekend. Een doorlopend punt van discussie is daarbij of de hoge concentraties van organisch materiaal in sapropelen veroorzaakt wordt door een betere preservatie van het organisch materiaal door het ontbreken van zuurstof in het bodemwater of door een hogere productiviteit in het oppervlaktewater waardoor meer organisch materiaal naar de bodem van de diepzee geëxporteerd wordt. Duidelijk is wel dat de vorming van sapropelen het resultaat is van een samenspel van verschillende processen.

Het optreden van sapropelen hangt samen met perioden van versterkte moesson circulatie die optreedt tijdens een grote sterkte (amplitude) van de precessie (minima). Omdat de amplitude van precessie gemoduleerd wordt door de excentriciteit, komen sapropelen voor in groepen die geassocieerd zijn met maxima in de excentriciteit. Daarnaast komt nog een afwisseling voor van dikke en dunnere sapropelen die wijst op de extra invloed van de obliquiteit [Lourens, et al., 1996]. Deze invloed is nog steeds niet helemaal begrepen maar de voorlopige uitkomsten van onderzoek met behulp van klimaatmodellen laat zien dat de obliquiteit de Afrikaanse moesson en dus (indirect) de rivierafvoer naar de Middellandse Zee kan beïnvloeden [Tuenter, pers. comm.].

Naast het aan de precessiecyclus gerelateerd optreden van de sapropelen worden in de Middellandse Zee veranderingen in de temperatuur van het oppervlaktewater waargenomen in de tijdreeksen van planktonische foraminiferen (gaatjesdragers) en zuurstof isotopen ( $\delta^{18}\text{O}$ ) van 3 tot 1 miljoen jaar geleden die vooral samenhangen met de obliquiteit. Deze veranderingen kunnen gekoppeld worden aan veranderingen in het ijsvolume en de temperatuur zoals die bekend zijn uit kernen van de Noord-Atlantische Oceaan [Zachariasse, *et al.*, 1990; Lourens, *et al.*, 1992]. Dit laatste houdt in dat er een nauw verband bestaat tussen het klimaat rond de Middellandse Zee en in het Noord-Atlantische gebied op glaciaal-interglaciaal tijdschalen gedurende het Laat Pliocen en Vroeg Pleistoceen. De klimaatreeksen van de Middellandse Zee laten dus cyclische veranderingen zien die aan twee verschillende klimaatsystemen toegeschreven kunnen worden, namelijk de Noord-Atlantische gebied op hoge breedtegraad en het Afrikaanse moessonsysteem op lage breedtegraad. De verschillen in het ritme van deze veranderingen geven aan dat deze klimaatsystemen in elk geval gedeeltelijk ontkoppeld waren van elkaar.

### Faseverschuiving

Er wordt algemeen vanuit gegaan dat sapropelen in het Middellandse-Zeegebied 3.000 jaar na het bijbehorende precessieminimum optreden. Deze faseverschuiving is gebaseerd op het verschil in ouderdom tussen het midden van de jongste Holocene sapropel S1, die met behulp van de radiometrische koolstofdatering (AMS  $^{14}\text{C}$ ) methode op  $\sim 8.500$  jaar gedateerd is, en het bijbehorende precessieminimum en zomerinstralingsmaximum op 11.500 jaar. Lourens *et al.* [1996] suggereerden dat deze verschuiving te maken hebben met een  $\sim 3.000$  jaar verschuiving die optreedt tussen de precessieparameter en de maximale zomertemperatuur respons ( $T_{\text{max}}$ ) in Noord Afrika; deze laatste bleek uit de resultaten van een EBM (“Energy Balance Model”) klimaatmodel [Short and Mengel, 1986]. Meer recent uitgevoerd onderzoek met behulp van klimaatmodellen liet zien dat  $T_{\text{max}}$  op lage breedtegraden ( $15^\circ\text{N}$ ) inderdaad achterloopt op de precessieparameter, maar dat er geen sprake is van een faseverschuiving tussen de neerslag van de Afrikaanse en Indische moesson en precessie [Tuenter, *et al.*, 2003]. Dit houdt in dat de afzetting van sapropelen in de Middellandse Zee niet uitsluitend samenhangt met veranderingen in de neerslag van het moessonsysteem, ofwel dat de schatting voor de fase verschuiving van de S1 een uitzondering is die mede beïnvloed wordt door de deglaciatie die optreedt na de Jonge Dryas periode.

Door ervan uit te gaan dat de instraling en de aanwezigheid van vocht in het circum-Mediterrane gebied in fase zijn lieten Lourens *et al.* [2001] zien dat de obliquiteit-gerelateerde faseverschuiving voor de Mediterrane Ti/Al proxy voor droogte vergelijkbaar is met de verschuiving voor precessie, namelijk  $150 \pm 300$  jaar. Deze waarneming is in overeenstemming met de uitkomsten van het modelleeronderzoek van Tuenter *et al.* [2005], die een in-fase relatie vonden tussen de jaarlijkse hoeveelheid



neerslag in de Afrikaans-Indische moesson en de obliquiteitparameter. Deze uitkomsten verschillen aanzienlijk van de resultaten van *Clemens et al.* [1996], die faseverschuivingen vonden tussen de Aziatische moesson en de precessie- en obliquiteitparameters van 6.000 en 13.400 jaar, respectievelijk, gedurende het laat Pleistoceen. De faserelaties verschillen verder geheel van de fasevertragingen die uit het onderzoek naar de veranderingen in het ijsvolume naar voren zijn gekomen [*Imbrie and Imbrie*, 1980]; dit laatste maakt aannemelijk dat delen van het klimaatsysteem op lage breedtegraden ontkoppeld zijn van de glaciële ontwikkeling op hoge breedtegraden. Tenslotte suggereren de modelresultaten dat deze faserelaties niet constant zijn geweest maar door de tijd heen gevarieerd hebben in antwoord op veranderingen in de globale verdeling van de ijskappen op de polen.

### **Sub-Milankovitch variaties**

Onderzoek aan de lange ijskernen van de ijskap op Groenland heeft laten zien dat het klimaatsysteem op Aarde extreem instabiel is geweest over de laatste 150.000 jaar en snelle veranderingen heeft ondergaan op tijdschalen van duizenden jaren [*Dansgaard, et al.*, 1984]. Sterke schommelingen in de luchttemperatuur boven Groenland, Dansgaard-Oeschger (D-O) cycli genoemd, culmineerden in armada's van ijsbergen over de Noord-Atlantische Oceaan. De nagelaten sporen van deze armada's in de vorm van puin op de zeebodem staan bekend als Heinrich (H) gebeurtenissen [*Heinrich*, 1988; *Bond*, 1992; *Broecker*, 1992; *Bond, et al.*, 1993; *Dansgaard, et al.*, 1993; *Bond, et al.*, 1999]. Deze schommelingen gaan gepaard met grootschalige reorganisaties van de verdeling van de temperatuur van het oppervlaktewater in de Noord-Atlantische Oceaan en van de globale thermohaline (oceaan)circulatie. Deze veranderingen zijn vastgelegd in diepzeekernen afkomstig uit de hele Noordelijke Atlantische Oceaan en de voornaamste hypothese relateert de koude fasen van de D-O cycli en de H gebeurtenissen aan het instorten van de ijskappen, wat op zijn beurt resulteert in de injectie van grote volumes smeltwater in de richting van de brongebieden van het Noord Atlantisch Diep Water (NADW). De daaruit volgende verlaging van de saliniteit van het oppervlaktewater leidde tot een afname van de diepe convectie en dus een vertraging in de globale thermohaline circulatie (THC) [*Broecker*, 1997].

Fluctuaties in het klimaat die geassocieerd zijn met de D-O cycli en de H gebeurtenissen blijven echter niet beperkt tot het Noord-Atlantische gebied maar zijn terug gevonden in de archieven van het klimaat over de hele wereld [*Leuschner and Sirocko*, 2000; *Voelker, et al.*, 2002]. Het mechanisme achter deze hoog-frequente klimaatveranderingen is onzeker en in de discussie daarover wordt in het algemeen onderscheid gemaakt tussen interne mechanismen, zoals oscillaties in de ijskap die veroorzaakt worden door de interactie tussen de grote ijskappen en het onderliggende vaste gesteente [*MacAyeal*, 1993; *Alley and MacAyeal*, 1994], en externe mechanismen zoals variaties in de activiteit van de Zon [*Van Geel, et al.*, 1999; *Perry and Hsu*, 2000;

*Bond, et al., 2001*], periodieke getijdebewegingen van de Aarde en de Maan [*Keeling and Whorf, 2000*] die versterkt worden in de aanwezigheid van grote ijskappen, een niet-lineaire respons als boventoon of combinatie van de primaire orbitaalcycli [*Pestiaux, et al., 1988; Hagelberg, et al., 1994; Ortiz, et al., 1999*], of eenvoudig de tweejaarlijkse passage van de Zon over de equator [*Short and Mengel, 1986; Short, et al., 1991*]. Vooral de twee laatste mechanismen suggereren dat de klimaatvariaties op tijdschalen van duizenden jaren eerder gestuurd worden door het klimaat op lage dan op hoge breedtegraden; de processen die daarbij betrokken zijn omvatten sterke terugkoppelingen tussen de atmosfeer en de oceaan, zoals veranderingen in het equatoriale windsysteem die het equivalent zijn van veranderingen op lange termijn in de El Niño - Southern Oscillation (ENSO), veranderingen in de intensiteit van de Intertropische Convergence Zone (ITCZ) of de moessonvariabiliteit [*Stott, et al., 2002*].

### **De klimaatreeksen van het Pliocen en Pleistoceen**

De meeste van deze onderzoeken richtten zich op het tijdsinterval waarin de ijstijden gedomineerd werden door de 100.000 jaar cyclus, en dan nog met name op de laatste 150.000 jaar. Aangezien er over de achterliggende oorzaak van deze ijstijden nog steeds heftig gediscussieerd wordt, is het meer voor de hand liggend de relaties tussen klimaatvariabiliteit op tijdschalen van duizenden jaren en de primaire Milankovitchforcering te onderzoeken in het Laat Pliocen of Vroeg Pleistoceen toen de ijstijden bepaald werden door de obliquiteit. De aanwezigheid van D-O en H-achtige veranderingen in het klimaat ten tijde van de kleinere door de obliquiteit gestuurde glacialen in het Laat Pliocen tot Midden Pleistoceen [*Raymo, et al., 1998; McIntyre, et al., 2001*], of zelfs 2.7 miljoen jaar geleden (dus voor het ontstaan van de enorme ijskappen op het Noordelijk Halfrond) [*Ortiz, et al., 1999; Kleiven, et al., 2002; Steenbrink, et al., 2003*] met een vergelijkbare frequentie als de D-O and H-oscillaties laat zien dat dergelijke fluctuaties in het klimaat met een hoge frequentie herhaaldelijk optreden tijdens de geschiedenis van het klimaat op Aarde. Toch is de interpretatie van deze oudere klimaatsreeksen niet altijd eenvoudig door het ontbreken van de noodzakelijke stratigrafische controle of van gedetailleerde correlaties met de reeksen van open oceaan.

Opeenvolgingen van Laat Pliocene tot Vroeg Pleistocene ouderdom in het Middellandse Zeegebied zijn echter zeer geschikt voor onderzoek naar klimaatsveranderingen op tijdschalen van duizenden jaren aangezien ze zowel informatie bevatten over de door de obliquiteit gestuurde glacialen als over de door precessie gestuurde sapropelen; deze sapropelen kunnen astronomisch gedateerd worden en geven dus een uitstekende tijdscontrole. Verder komen veranderingen op de schaal van de D-O cycli en de H-gebeurtenissen voor in de glaciaal-interglaciale afwisselingen in diep mariene afzettingen zoals die tegenwoordig op land ontsloten zijn

in het centraal Mediterane gebied (field observations) en in de kernen van ODP Leg 160 uit het oostelijke deel van de Middellandse Zee over de laatste 2-3 miljoen jaar [Shipboard data *Sakamoto, et al.*, 1998] (Figuur 1.1). Snelle veranderingen in de sedimentologische eigenschappen<sup>13</sup> kunnen over het hele bekken gecorreleerd worden; dit laatste suggereert een gemeenschappelijk achterliggend (klimaat) mechanisme dat opereert op Milankovitch tot sub-Milankovitch tijdschalen (Figuur 1.2). Voorlopige resultaten van spectraalanalyse<sup>14</sup> van de lange kleurreeks van Site 967 (69.64-89.73 rmc; Shipboard data) laten cyclische veranderingen met golflengtes van ~60 cm, 27-30 cm, 17-15 cm en ~10 cm zien, die boven het 90% significantie niveau uitkomen (Figuur 1.3a). Duidelijk is dat de veranderingen in kleur met een golflengte van 60 cm samenhangen met het voorkomen van sapropelen in Site 967 (Figuur 1.1) en dus corresponderen met de precessie cyclus. Vervolgens kunnen de frequenties in het diepte domein vertaald worden naar frequenties in het tijdsdomein die overeenkomen met de periodes van half-precessie (30 cm), kwart-precessie (15 cm) en een periode van ~3.500 jaar (10 cm). Gefilterde componenten<sup>15</sup> van deze frequenties laten over het algemeen een grotere amplitude zien in de sapropel intervallen (Figuur 1.4). Variaties met een periode van de helft van de precessie cyclus zijn niet overtuigend aanwezig in deze intervallen en vertegenwoordigen mogelijk een artefact. Variaties met een golflengte van 15 cm (overeenkomend met een kwart precessie cyclus) en 10 cm zijn in de gehele reeks aanwezig. Deze 10 en 15 cm cycli bepalen tevens voor een groot deel de veranderingen in kleur op sub-Milankovitch schaal in de glacialen. In de sapropelen intervallen vallen er steeds twee 15 cm of drie 10 cm cycli binnen een enkele sapropel. Frequentie analyse in het tijdsbereik van de kleurreeks van Site 967 [ouderdomsmodel van *Lourens, et al.*, 2001] bevestigt dat veranderingen in de kleur van het sediment optreden met periodes van 21.000, (10.000), 5-6.000 en 3.500 jaar die uitsteken boven de 80% betrouwbaarheidslimiet (Figuur 1.3b).

Een eerste frequentie-analyse van de magnetische susceptibiliteitreeks van San Nicola laat een concentratie van de variantie zien op golflengtes van 357, 175, 102, 45, 30 en 26 cm, boven het 80% significantieniveau (Figuur 1.5). Het extraheren van het laagfrequente signaal met behulp van een filter dat gecentreerd is op 0.0028 cycli/cm (een golflengte van 357 cm) laat zien dat deze frequentie overeenkomt met de obliquiteitscyclus (Figuur 1.6). Vervolgens kunnen de waargenomen variaties in het dieptebereik vertaald worden naar het tijdsbereik met periodes van 41, 19, 11, 5, 3.4 en 2.9 duizend jaar; golflengtes rond de 30 cm (~3 kyr) vertegenwoordigen daarbij de veranderingen op de kleinste schaal (met een lage amplitude) in de magnetische susceptibiliteitreeks van San Nicola.

<sup>13</sup> ODP Site 967 scheepsboord kleurreflectie gegevens en voorlopige magnetische susceptibiliteit gegevens van San Nicola en Singa. Zie *Hoofdstuk 6* voor een meer gedetailleerde beschrijving van methoden en gegevens.

<sup>14</sup> Frequentie analyse uitgevoerd met behulp van het REDFIT programma van [*Schulz and Mudelsee*, 2002].

<sup>15</sup> Filtering uitgevoerd met behulp van een Gaussisch filter met een centrale frequentie [*Paillard et al.*, 1996].

### MIS 101-95

Op het oog inspectie van Monte San Nicola (SN) en Site 967 laat zien dat het interval tussen de sapropelgroepen A en B (rond ~2.5 miljoen jaar geleden) bij uitstek geschikt is voor onderzoek met een hoog oplossend vermogen naar veranderingen in het klimaat op Milankovitch tot sub-Milankovitch tijdschalen (Figuur 1.1). In dit tijdsinterval is de amplitude van precessie gering vanwege het minimum in de 400.000 jaar cyclus van de excentriciteit en dus laten de diep mariene sedimenten in het centrale en oostelijke deel van de Middellandse Zee vooral door de obliquiteit-gestuurde glaciaal-interglaciaal afwisselingen zien. Eerder onderzoek had al laten zien dat de donkere banden, die tussen de A5 sapropel (basis van het Gelasien) en de B-sapropelgroep op meterschaal voorkomen, de glaciële cycli MIS100, MIS98 en MIS96 vertegenwoordigen [Zachariasse, *et al.*, 1990]. Dit zijn drie van de meest uitgesproken glaciëlen die kort na het begin van de grootschalige glaciaties op het Noordelijk halfrond optraden [Ruddiman, *et al.*, 1986; Raymo, *et al.*, 1989]. Binnen de grenzen van deze donkere glaciële intervallen zijn dm-dikke lichtgekleurde lagen zichtbaar. Deze lagen wijzen op klimaatvariabiliteit op sub-Milankovitch schaal bovenop de obliquiteit-gestuurde glaciële veranderingen. Aanwijzingen voor het optreden van ijsbergen tijdens deze eerste volledige glaciële cycli zijn afkomstig van de kleurveranderingen op de foto's van diepzee kernen (DSDP Leg 94 sites) (Figuur 1.7) en de 'ice rafted debris' (IRD) reeksen van de Noord-Atlantische boorkernen [Raymo, *et al.*, 1992; Carter and Raymo, 1999]. Deze foto's laten variaties in IRD zien met een spaciëring die vergelijkbaar is met die van de veranderingen in de Mediterrane kleurreeksen. Snelle veranderingen in de grootte van de continentale ijskappen in die tijd worden verder bevestigd door verschuivingen in de zuurstof isotopen reeksen van benthonische foraminiferen [Raymo, *et al.*, 1989; Raymo, *et al.*, 1992]. De kleurreeksen van ODP Site 967 laten verder zien dat MIS100, 98 en 96 niet even dik zijn maar dat ze een patroon van afwisselend dik, dun, dik vertonen. Een dergelijke afwisseling wijst op een modulatie van de obliquiteit gestuurde glaciële cycli, mogelijk door de (400.000 jaar) excentriciteitscyclus. Daarnaast zijn de sub-Milankovitch variaties duidelijker zichtbaar in de relatief dikke MIS100 en MIS96.

### Samenvatting van het onderzoek

Het in dit proefschrift gepresenteerde onderzoek heeft tot doel licht te werpen op de volgende fundamentele vragen: Zijn er sub-Milankovitch veranderingen in het Laat Pliocene aanwezig met dezelfde frequenties als in het Laat Pleistoceen en, zo ja, is het klimaatmechanisme vergelijkbaar (*Hoofdstuk 2*)? Wat is de relatie van deze veranderingen met het klimaat op hoge en op lage breedtegraden (*Hoofdstukken 3 en 4*)? Zijn de faserelaties van de verschillende klimaatcomponenten met betrekking tot de

primaire Milankovitchfrequenties (obliquiteit en precessie) constant binnen het bestudeerde interval en zijn ze vergelijkbaar met de faserelaties in het Pleistoceen (*Hoofdstuk 5*)? Wat is de rol van sub-Milankovitchvariabiliteit op de fasevertragingen in het klimaatsysteem op Milankovitchtijdschalen? Ten slotte, is het mogelijk om de waargenomen veranderingen in het sub-Milankovitchbereik te koppelen aan de primaire Milankovitchfrequenties (*Hoofdstuk 6*)?

Om deze vragen te kunnen beantwoorden werd in het in dit proefschrift gepresenteerde onderzoek het interval van MIS101-99 in de op het land ontsloten mariene sectie van Monte San Nicola (Sicilië/Italië) en in ODP Leg 160 Site 967 onderzocht met een hoog oplossend vermogen (~400 jaar). Hierbij werd gekozen voor een multi-proxy benadering met, onder andere, onderzoek naar foraminiferenassociaties, stabiele isotopen (i.e., ijsvolume) en calciumcarbonaatgehaltes (CaCO<sub>3</sub>). Dit onderzoek werd uitgevoerd om een eerste inzicht te krijgen in de klimaatvariabiliteit op Milankovitch- tot sub-Milankovitchtijdschalen zoals die aanwezig was in het Mediterrane gebied tijdens het laat Pliocceen (*Hoofdstuk 2*). Obliquiteit-gestuurde glaciale veranderingen zijn duidelijk zichtbaar in de zuurstofisotopenreeksen van zowel planktonische als benthonische foraminiferen; deze laten een zaagtandpatroon zien met stadiaal-interstediaal variabiliteit gesuperponeerd op het glaciale signaal in MIS100: in total worden twee stadialen (100.3 en 100.5) en drie interstadialen (100.2, 100.4 en 100.6) herkend. Zowel de  $\delta^{18}\text{O}$  als de temperatuur van het oppervlaktewater (SST) laten een fasevertraging van ongeveer zesduizend jaar zien ten opzichte van de obliquiteit. Schattingen van de SST, gebaseerd op veranderingen in de samenstelling van de planktonische foraminiferenfaunas, laten ook cycli van afkoeling zien met een zaagtandpatroon; deze cycli bevestigen het voorkomen van een stadiaal-interstediaal type van klimaatvariabiliteit met een duur en aard die vergelijkbaar is met de Bond-cycli van de open oceaan in het laat Pleistoceen. Daarnaast laten veranderingen in de talrijkheid van *Neogloboquadrina atlantica*, een koud-watersoort van planktonische foraminifeer, intervallen van lage SST zien met een even kortere periode (1.5-3 duizend jaar) ten tijde van MIS100. Koude intervallen vallen ook samen met hoge percentages van de benthonische foraminifeer *Trifarina angulosa*. Dit wijst erop dat deze intervallen gekenmerkt werden door een toename in de ventilatie van het diepe water die veroorzaakt wordt door intensieve mixing en diepe convection. Dit scenario is analoog aan dat voor het westelijke Mediterrane gebied tijdens het laatste Pleistocene [Cacho, et al., 1999; Cacho, et al., 2001] waarvoor een zelfde mechanisme opgesteld is: Lage SST-waarden geassocieerd met een toename in diepwatervorming tijdens stadialen zijn gerelateerd aan a) een directe invloed van koud Atlantisch oppervlaktewater dat de Middellandse Zee binnenkomt, en b) een meer indirecte verbinding met het Atlantische systeem, dat zich waarschijnlijk verder uitbreidde in het gebied van de Middellandse Zee door een zwakkere moesson ten tijde van een minimum (400.000-jaar) in excentriciteit. Afwijkende omstandigheden werden gevonden voor cyclus i-244, toen een oppervlakte laag met een lage saliniteit en

geassocieerd met een diep chlorofyl maximum (DCM) wijst op de sterke invloed van precessie-gestuurde veranderingen in het klimaat.

De afwezigheid van hoog-frequente variaties in de  $\delta^{18}\text{O}$  van Site 967 suggereert dat het oostelijk deel van de Middellandse Zee ofwel ontkoppeld was van of niet gevoelig was voor de klimaatforcering vanuit de Noord-Atlantische Oceaan. Kleurreeksen laten echter wel vergelijkbare veranderingen zien op sub-Milankovitch tijdschaal in het oostelijke en centrale deel van de Middellandse Zee. Een vergelijking van deze veranderingen met de Ti/Al (een proxy voor de humiditeit/ariditeit in het circum-Mediterrane gebied) reeks van ODP Site 969 [gegevens van *Wehausen*, 1999] laten een relatie zien tussen de sedimentaire kenmerken (kleur,  $\text{CaCO}_3$ ), eolisch stof uit Afrika (Ti/Al) en koude intervallen ( $\delta^{18}\text{O}$ ) van de D-O en H-achtige gebeurtenissen, die een koppeling suggereren tussen het klimaat op hoge en lage breedtegraden. De proxygegevens van de Middellandse Zee laten zien dat klimaatveranderingen met een hoge frequentie erg gecompliceerd kunnen zijn door de interferentie van variaties in het klimaat op verschillende tijdschalen.

De relatie tussen klimaatsveranderingen met een hoge frequentie in het Middellandse Zeegebied gedurende MIS101-95 en de variabiliteit in het klimaat op hoge breedtegraden wordt onderzocht in **Hoofdstuk 3**. Dit wordt gedaan door de Mediterrane  $\delta^{18}\text{O}$  en *N. atlantica* reeksen te vergelijken met de hoge-resolutie  $\delta^{18}\text{O}$ ,  $\delta^{13}\text{C}$ , *N. atlantica* en 'ice rafted debris' (IRD) reeksen van de Atlantische DSDP Leg 94 Site 607 en ODP Leg 162 Site 981. Voor dit doel werd de zeer nauwkeurige tijdschaal van Site 967 geëxporteerd naar de Atlantische Oceaan waarbij de benthonische zuurstofisotopenreeks werd gebruikt voor de correlatie. Deze vergelijking laat zien dat cycli van afkoeling op tijdschalen van duizenden jaren ook voorkomen in de Atlantische Oceaan waar ze geassocieerd zijn met episoden van ijsbergvorming. Lagere  $\delta^{13}\text{C}$  waarden in IRD-rijke lagen wijzen op een koppeling tussen veranderingen in de wereldwijde thermohaline circulatie en ijs transport het voorkomen van grote hoeveelheden ijsbergen in de Noord-Atlantische Oceaan, zoals ook het geval was tijdens de laat Pleistocene Heinrich en Dansgaard-Oeschger gebeurtenissen.

Opnieuw treedt er een uitzondering op tijdens MIS100.3 (i-244): de aanwezigheid van de planktonische foraminifeer *Globorotalia menardii* wijst op een opwarming van het oppervlaktewater die gepaard gaat met een herstart van de diepwatercirculatie. Het blijft onzeker of de afname in het benthonisch  $\delta^{18}\text{O}$  wijst op een gelijktijdige opwarming van het diepe water. In het onderzochte interval hangen twee andere voorkomens van de subtropische soort *G. menardii* eveneens nauw samen met precessieminima; dit wijst op de interferentie van precessie-gestuurde (lage breedtegraad?) klimaatvariabiliteit en obliquiteit-gestuurde glaciaal-interglaciaal afwisselingen. Nochtans tonen de resultaten ondubbelzinnig aan dat de Bondcycli en de daarmee samenhangende Heinrichgebeurtenissen een intrinsiek onderdeel van het

klimaatstelsel uitmaken gedurende het hele laat Pliocen en Pleistoceen ondanks de overgang van glaciale cycli met een dominante periode van 41 naar 100 duizend jaar.

De rol van precessie-gestuurde variabiliteit van het klimaat in de Middellandse Zee en het mogelijke verband tussen een klimaatcomponent van lage breedtegraden (stof) en klimaatveranderingen op hoge breedtegraad gedurende MIS100 worden verder uitgewerkt in **Hoofdstuk 4**. Voor dit doel zijn de bulk geochemie van het sediment en de korrelgrootte van de terrigene component gemeten met hetzelfde oplossend vermogen als de SST en  $\delta^{18}\text{O}$  reeksen.

De chemische gegevens laten zien dat de milieu-omstandigheden ten tijde van MIS100 te zwak waren voor de vorming van een sapropel, wat in overeenstemming is met de afgenomen amplitude van precessie in dit tijdsinterval ten gevolge van een minimum in de excentriciteit. De ontwikkeling van een DCM in i-244 zoals voorgesteld in **Hoofdstuk 2** kan echter verwacht worden. De chemische gegevens laten verder zien dat de sedimenten van San Nicola bestaan uit een twee componenten mengstelsel met biogeen carbonaat en aluminiumsilicaten als eindleden. De relatieve bijdrage van deze componenten verandert vooral op glaciaal-interglaciale (obliquiteit) schaal. Bovenop deze glaciaal-interglaciale variabiliteit komen precessiegestuurde veranderingen in de afzetting van het stof en korte-termijnveranderingen (1.5-4.5 duizend jaar) in stof en  $\text{CaCO}_3$  voor, die waarschijnlijk het gevolg zijn van een toename in de aanvoer van eolisch stof vanaf het Afrikaanse continent tijdens precessiemaxima en obliquiteitminima. Deze stofepisodes in de Middellandse Zee treden op hetzelfde moment op als de IRD gebeurtenissen in de Noord-Atlantische Oceaan; dit wijst op een verband tussen de aanwezigheid van stof op lage breedtegraden en ijstransport op hoge breedtegraden ten tijde van MIS100.

In **Hoofdstuk 5** worden de faserelaties tussen de benthonische  $\delta^{18}\text{O}$  en obliquiteit afzonderlijk bekeken voor de MIS100, MIS98 en MIS96 glacialen. Hiertoe werd de  $\delta^{18}\text{O}_{\text{benthos}}$  van Site 967 ontleed in twee componenten van enerzijds het ijsvolume en anderzijds de jaarlijkse luchttemperatuur voor het Noordelijk halfrond. Deze ontleding vond plaats op grond van een gekoppeld model voor ijsplaten op het Noordelijk Halfrond en oceaantemperaturen ontwikkeld door *Bintanja et al.* [2005]. Dit model staat toe om nauwkeurig de ijsvolume- en de temperatuurcomponent te extraheren uit de  $\delta^{18}\text{O}$  in een gegeven tijdsinterval. Belangrijk voordeel van het gebruik van Site 967 is dat zijn tijdschaal onafhankelijk is van de glaciaal-interglaciale variabiliteit; dit model voor de ouderdom van de Site is ontwikkeld door de Ti/Al reeks te calibreren aan de tijdreeks voor de zomerinstraling op  $65^\circ\text{N}$ , die uitgerekend is met behulp van de astronomische oplossing  $\text{LaO}_{4(t,1)}$ , onder de aanname van een in-fase relatie [*Lourens, et al.*, 2001].

De uitkomsten van het model laten veranderingen in de zeespiegel zien in de orde van 60-70 m gedurende MIS101-95, wat aangeeft dat de diepwatertemperatuur-component onderschat is tijdens eerder onderzoek naar zeespiegelschommelingen tijdens het laat Pliocene. In vergelijking met de interglacialen daalde de jaarlijkse luchttemperatuur op het Noordelijk Halfrond tijdens glacialen met  $\sim 12$  °C; daarop gesuperponeerd kwamen (stadaal-interstadaal) variaties voor tot 4-6°C (MIS96). Spectraalanalyse van de  $\delta^{18}\text{O}$  reeks en zijn afgeleiden, globaal ijsvolume en jaarlijkse luchttemperatuur op het Noordelijk Halfrond, laten sterke pieken zien met periodes van  $\sim 80$ , 41 en 28 duizend jaar en, opvallend genoeg, geen variantie in het precessiebereik. De gefilterde 41 duizend jaar componenten van de verschillende proxies laten een fase vertraging van 5-8 duizend jaar ten opzichte van de obliquiteit. Deze fase vertraging neemt echter toe tijdens MIS100 en MIS96, en af tijdens MIS98 met  $\sim 5$  duizend jaar, als de 80 en 28 duizend jaar componenten meegenomen worden bij de reconstructie van het signaal. Aanwijzingen dat de 80 en 28 duizend jaar componenten het gevolg zijn van een niet-lineaire interactie tussen de obliquiteit en de excentriciteit zijn onduidelijk. In plaats daarvan wordt de 80 duizend jaar (en de 28 duizend jaar) waarschijnlijk veroorzaakt door een niet-lineaire respons van de ijskappen op de forcering door de obliquiteit ten gevolge van de interne dynamiek van deze platen. In het bijzonder kan het bestaan van een aanzienlijke ijskap tijdens MIS99 het optreden van deze frequenties als 'sidebands' verklaren.

In *Hoofdstuk 6* wordt spectraalanalyse toegepast op de verschillende componenten (SST, ijsvolume en stof uit Afrika) van het Mediterrane klimaat. Gegevens van de zuurstofisotopen en de sedimentkarakteristieken van San Nicola en Site 967 laten klimaatrelaties zien tijdens MIS98 en MIS96 die sterk vergelijkbaar zijn met die gedurende MIS100 (*Hoofdstukken 2, 3 en 4*); stof episodes afkomstig van lage breedtegraden en vastgelegd in de kleurreflectiefactor (CR) en de magnetische susceptibiliteit (MS) kunnen gekoppeld worden aan cycli van afkoeling in de Middellandse Zee en de Noord-Atlantische Oceaan, en aan de geschiedenis van ijstransport in de laatste. De uitkomsten van de spectraalanalyse laten echter zien dat deze klimaat systemen mogelijk op iets andere tijdschalen geopereerd hebben: op Milankovitch tijdschalen worden de spectra van de zuurstofisotopenreeksen gedomineerd door pieken die corresponderen met periodes van 80, 41 en 28 duizend jaar, wat in overeenstemming is met het globale ijsvolume en de jaarlijkse luchttemperatuur op het Noordelijk Halfrond in dit tijdsinterval (*Hoofdstuk 5*). Alleen de spectra van  $\delta^{18}\text{O}$  van planktonische foraminiferen laten variantie in het precessiebereik zien; dit signaal geeft de lokale component in de saliniteit/temperatuur van het oppervlaktewater weer. De CR en MS spectra laten een veel sterkere precessiecomponent zien maar deze component verschilt tussen de sites. Deze verschillen kunnen verklaard worden door de korte duur van de tijdreeksen en,



waarschijnlijk belangrijker, verschillen in de glaciaal-interglaciale signatuur van de individuele sites in combinatie met de sterkte van het precessiesignaal. Spectra van deze reeksen lijken meer op elkaar in het sub-Milankovitch bereik, waar ze een concentratie van de variantie laten zien rond een periode van 6-7 duizend jaar; deze periode ligt dicht tegen periodes aan die het gevolg zijn van boventonen ('harmonics') en combinatietonen van de primaire precessiecomponenten. Een vergelijking met het spectrum van een reeks die het verschil weergeeft tussen het sterkste temperatuur maximum ( $T_{\max}$ ) en het sterkste minimum ( $T_{\min}$ ) in de jaarlijkse temperatuurcyclus op de evenaar laat zien dat differentiële opwarming gekoppeld aan de configuratie van de aardbaan de klimaatvariabiliteit in de MS en CR reeksen van SN en Site 967 kan verklaren. Een dergelijke verklaring zou in overeenstemming zijn met een (stationair) periodiek klimaat signaal zoals aanwezig in de sedimentreeksen van SN en Site 967. Een verband met de primaire precessiecyclus kan echter als minder waarschijnlijk worden bestempeld gezien de geringe amplitude van de precessie ten gevolge van het minimum in de excentriciteit in die tijd.

De spatiering van de subcycli in  $\delta^{18}\text{O}$ , die het meest opvallende kenmerk in de  $\delta^{18}\text{O}$  reeks van het onderzochte interval op een sub-Milankovitch tijdschaal vormen (zie ook *Hoofdstuk 2*), varieert daarentegen van het ene glaciaal naar het andere tussen de 7 en 9 duizend jaar; de duur van de cycli is daarbij gekoppeld aan de duur van het glaciaal. 'Wavelet'-analyse laat zien dat zowel de intensiteit als de frequenties van het klimaatsignaal veranderden door de tijd heen; dit geeft een verklaring voor de relatief brede piek in het spectrum rond de 7-9 duizend jaar. Een dergelijk niet-stationair gedrag wijst op niet-lineaire componenten in het mechanisme van het vastleggen van het signaal, in de klimaatrespons of in de forcering zelf. Dergelijke niet-lineaire componenten kunnen optreden als gevolg van een frequentiemodulatie van de primaire cycli van de excentriciteit, obliquiteit en precessie of als gevolg van de interne dynamiek van de ijskappen. Een voorbeeld van frequentiemodulatie wordt gepresenteerd voor de jaarlijkse luchttemperatuur ( $T_{\text{air}}$ ) op het Noordelijk Halfrond, een afgeleide van de  $\delta^{18}\text{O}_{\text{benthos}}$  reeks van Site 967, die de aanwezigheid van een 8 of  $\sim 12$  duizend jaar component laat zien die gemoduleerd wordt door een  $\sim 70$  duizend jaar periode. Dit voorbeeld is meer in overeenstemming met het model dat door *McIntyre and Molino* [1996] is voorgesteld; zij koppelden veranderingen in de door de wind aangedreven divergentie in de equatoriale Atlantische Oceaan met een periode van  $\sim 8.4$  duizend jaar aan een niet-lineaire interactie tussen de precessie en een afwijkende korte periode van de excentriciteit. Onze gegevens laten echter duidelijk zien dat nog veel onderzoek gedaan moet worden om de enigma's van de sub-Milankovitch variabiliteit in het klimaat systeem te ontraadselen.

## Acknowledgements

Many people supported my work scientifically and non-scientifically and I would like to thank them all.

First of all, I would like to thank my promotor Johan Meulenkamp for accepting me as a PhD student and supporting me throughout the time being in Utrecht. Thanks for being such a warm-hearted authority.

In particular, I would like to thank my co-promoters Frits Hilgen and Lucas Lourens for all the support, patience, understanding, and for giving me the opportunity to finish this thesis. Thank you for introducing me into the 'Milankovitch-world' and for providing the chance to work on the amazing sections of Sicily and Calabria. Although I often returned into the safe havens of high-resolution palaeoceanography, I learned a lot on Mediterranean cyclostratigraphy. I am convinced that one day we will completely unravel the complex relationship between sub-Milankovitch climate variability in the Mediterranean and primary Milankovitch forcing.

I am grateful for all technical assistance I got in order to produce high-quality data. I appreciate this assistance even more, now working as a technician myself. Geert Ittman and Gerrit van't Veld are thanked for sample preparation and logistics. I very much enjoyed coming into the lab for a chat. Arnold van Dijk is acknowledged for running the stable isotope analyses at Utrecht University. Many thanks to Hubert Vonhof and Gerald Ganssen who made it possible for me to run samples in their stable isotope facility at Amsterdam Free University. Thanks also to the EU Project 'Paleostudies' (contract No.: HPRI-CT-2001-0124) for providing funding for additional stable isotope analysis at Bremen University and to Monika Segl for sharing her laboratory resources. Marjan Reith and Jan-Berend Stuut are thanked for assistance with grain size analysis; Helen de Waart and Gijs Nobbe are acknowledged for ICP-AES analyses. Hanneke Tjibbosch, Wouter Kuipers and Frits Hilgen helped with foraminifera and IRD data and Erwin van der Laan provided stable isotope and foraminiferal data of his master thesis. Tanja Kouwenhoven and Lucas Lourens are thanked for checking the benthic and planktonic foraminiferal countings. Anja Reitz and Diana Menzel are acknowledged for labwork when I was not allowed to work in the lab during pregnancy. Marjolein Boonstra is thanked for assistance with bureaucracy and the porters lodge for assistance with lost keys and a good chat.

For scientific contribution I would like to thank Gert-Jan Reichert for his everlasting patience in preparing manuscripts or presentations. The discussions and suggestions

motivated and encouraged me. Furthermore, I would like to thank Jan-Willem Zachariasse for reading through manuscripts and Dave Heslop for providing MC\_CLEAN and working with me on bispectral analysis. This last issue remains difficult and maybe we should get another try on that. I am quite happy that Richard Bintanja and Roderik van de Wal agreed to work together with Lucas and me. Thanks for analysing our Mediterranean data and providing valuable comments on the manuscript. I hope that our cooperation will continue. I am grateful to Maureen Raymo for providing data and sample material and contributing to our joint manuscript. Thanks for reading my thesis and the overall positive feedback. I also would like to thank the other members of the reading committee (Dick Kroon, Henk Dijkstra, Gert de Lange, and Rainer Zahn) for evaluating this thesis and contributing with their comments.

I want to thank all my old and new colleagues and room mates in Utrecht and Cardiff, who contributed in one way or the other to this work, most of it being company, chats, baby-sitting (Frank and Vicky, Vicky, Vicky you are both excellent), provision with coffee or scientific discussions. I realised how much I appreciated working within the 'Strat-Pal' group by leaving Utrecht. Many thanks also to the 'Pal-en-Pal' group for their company and hospitality. Luckily, there is one of your lot in Cardiff: thanks Karin for making my start in Cardiff much easier ;- ) and a million thanks for doing the layout of this thesis!

Finally, cheers to all my friends in Utrecht and Aachen. Wim, thank you for your company and all the laughing especially in the early time in Utrecht. Although I tend to forget your birthday I won't forget you. Gesa and Gera thanks for unforgettable times at Brederoplein. Rike and Wolfram huge thanks for all the evenings with good food, Doko, football or Tatort and the early morning coffees at the institute. Anja, Diana and Anke thanks for cheering me up in difficult times. See you all in Cardiff (Kike, Dan, Buc and Sabine made already a start!). Thanks also to my old and new neighbours, especially to Maria and Eddy, Hans and Ursula Schlüsener, Bob and Mary and the Barthelmes 'clan', for distracting me after a long days work or on a Sunday afternoon, for providing me with company, coffee and looking after Ronja.

Last and most importantly, I want to thank my family for being there.

## ACKNOWLEDGEMENTS

### Curriculum vitae

Julia Becker was born on the 14<sup>th</sup> of November 1973 in München/D. She successfully completed the Martin-Luther Gymnasium in Marburg in 1993 and started studying geology at the Christian-Albrecht University in Kiel the same year. In 1996 she spent 9 months as an ERASMUS-student at the department of marine geochemistry (Earth Sciences) of Utrecht University, where she carried out a small research project under the supervision of Ivar Nijenhuis and Gert de Lange. This research resulted into a joined master thesis supervised by Gert de Lange (Utrecht University) and Rainer Zahn (Geomar/Kiel). Julia Becker graduated from Kiel University in 1999 with specialities in marine geology, oceanography and petrology. In the same year she was appointed as a PhD student at Utrecht University, at the department of Stratigraphy/Paleontology. In 2002 she gave birth to a daughter and worked part time at Utrecht University from this time on. Since July 2005 she is working as a research technician (IRMS) at the School of Earth, Ocean and Planetary Sciences, Cardiff University/UK.

